Towards a Proper Understanding of Fatigue Crack Growth and Crack Closure

Can Vacuum Invalidate ΔK as Similitude Parameter and Explain the R-Effect by means of Strain Energy Release?

Name: Joël Jacco Hogeveen

Supervisor: Dr. Ir. R.C. Alderliesten

Faculty of Aerospace Engineering

Master of Science Thesis

TUDelft

Towards a Proper Understanding of Fatigue Crack Growth and Crack Closure

Can Vacuum Invalidate ΔK as Similitude Parameter and Explain the R-effect by means of Strain Energy Release?

MASTER OF SCIENCE THESIS

For obtaining the degree of Master of Science in Aerospace Engineering at Delft University of Technology

J.J. Hogeveen

October 2016

Faculty of Aerospace Engineering · Delft University of Technology

DELFT UNIVERSITY OF TECHNOLOGY
FACULTY OF AEROSPACE ENGINEERING
DEPARTMENT OF AEROSPACE STRUCTURES AND MATERIALS

The undersigned hereby certify that they have read and recommend to the Faculty of Aerospace Engineering for acceptance of thesis entitled "**Towards a Proper Understanding of Fatigue Crack Growth and Crack Closure**" by **J.J. Hogeveen** in partial fulfilment of the requirements for the degree of **Master of Science**.

Date: October 2016

Supervisor: _____
                                               Dr. Ir. R.C. Alderliesten

Committee Members: _____
                                               Dr. Ir. S.R. Turteltaub

                                               _____
                                               Ir. J. Sinke

                                               _____
                                               PhD. J.A. Pascoe

Summary

Fatigue is the weakening of a material or structure due to cyclic loading and unloading. As such fatigue is very important in engineering fields like aerospace, where structures are exposed to cyclic loads. Therefore theories on the initiation and propagation of fatigue have been extensively researched In the past century. The main Fatigue Crack Growth (FCG) prediction models are based on a Stress Intensity Factor (SIF), ΔK. Representing FCG data as a function of this SIF causes a stress ratio (R-)effect, which is accounted for by means of plasticity induced crack closure. Crack closure causes the crack to close before a zero tensile load is applied, as such influencing the effective SIF. If FCG data is presented as a function of the effective SIF ΔK_{eff} instead of ΔK, the data correlates very well and the R-effect disappears.

However, the theories based on a SIF and crack closure have recently been subject of discussion. The prediction models using ΔK for similitude are empirically derived and thus do not have any physical explanation. Furthermore ΔK has been derived for quasi-static loading conditions and as such it cannot be blindly adopted for fatigue loading conditions. Besides there is a lot of confusion about the phenomenon (plasticity induced) crack closure, load-displacement observations attributed to crack closure could for instance also be attributed to residual compressive stresses. Especially early test results in vacuum environment do not agree with theories based on SIF and crack closure.

An alternative proposed in literature is to approach fatigue from a Strain Energy Release (SER) perspective. This theory approaches fatigue conform the laws of thermodynamics, and claims that not the amount of energy released under quasi-static load conditions should be considered, but the energy released during a complete fatigue load cycle. It also claims that the R-effect is only an artefact of choosing ΔK for similitude. Treating fatigue as a SER dominated phenomenon instead of a SIF dominated phenomenon, might result in a proper description, prediction and understanding of fatigue.

As such the first goal of this research was to investigate if ΔK is a correct similitude parameter for FCG. This was investigated by comparing experimental results in air and vacuum. According to conventional fatigue theories based on SIF, there should be no difference between air and vacuum. Experiments were designed and similar test conditions were applied with the only difference the environment tested in. Experimental results in air showed -as expected- a clear R-effect that could be accounted for by the plasticity induced crack closure corrections proposed in literature. However, the results in vacuum did not show this R-effect, while the results of crack opening experiments and plasticity did not differ compared to results of experiments in air. It was therefore concluded that ΔK is improper to use as similitude parameter for FCG prediction.

The second goal of this research was to investigate if fatigue is SER dominated, again by comparing experimental results in both air and vacuum environment. First a numerical analysis was done to predict the strain energy released per cycle at a certain FCG rate. Apart from that, the strain energy released after a complete fatigue load cycle was measured during the experiments. Conform expectations, a similar behaviour was observed in terms of energy dissipation between experiments in air and vacuum environment. Furthermore the experimental results showed a similar trend as

observed in the results from the numerical analysis. The observed differences in energy dissipation between the two environments, could be largely correlated by taking into account the crack surface roughness. As the SER-theory still holds in vacuum, it was concluded that fatigue is a SER dominated phenomenon, especially as proposed crack closure corrections could also be explained from an energy perspective.

The last goal of this research was to investigate if the R-effect is caused by (plasticity induced) crack closure. The experimental results showed similar load-displacement behaviour around the crack in both environments, and also the plastic behaviour of the material was equal in both environments. However, as the R-effect using ΔK for similitude disappeared in vacuum, it was concluded that plasticity induced crack closure is not responsible for the R-effect. It is unknown what mechanism exactly causes the non-linear behaviour. Furthermore the experimentally determined 'opening stresses' were considerably lower than prescribed by conventional crack closure corrections. It was shown that these crack closure corrections are actually a cyclic energy correction, hence the R-effect largely disappears if fatigue is approached from an energy perspective. Therewith it could be concluded that the R-effect is not caused by plasticity induced crack closure and that it actually is an artefact of choosing ΔK for similitude.

As such the main conclusions of this Master thesis are that ΔK is an improper similitude parameter for FCG prediction, that the R-effect is an artefact of choosing ΔK for similitude and that fatigue actually is a SER dominated phenomenon instead of a SIF dominated phenomenon. The R-effect in air environment is not caused by crack closure, but the 'crack closure' corrections proposed in literature are actually a cyclic energy correction. Hence FCG data correlates very well if presented in terms of energy dissipation. Differences in energy dissipation trends observed in the test results could be largely correlated by including a crack surface roughness analysis. It is assumed that further correlation should be obtained by quantifying other energy dissipation mechanisms such as plasticity.

Therefore it is recommended to accurately quantify energy dissipation due to plasticity and other energy dissipating mechanisms in order to research if observed differences in experimental SER data can be further correlated. Next to that further research is required to determine what causes the non-linear load-displacement behaviour around the crack, as it is unknown if this load-displacement behaviour is actually due to (plasticity induced) crack closure or due to other mechanisms such as residual compressive stresses. Lastly, once the physics behind fatigue is fully understood, it is proposed to develop a proper FCG prediction model based on SER.

Acknowledgements

It would have been impossible to successfully complete this Master thesis without the help and support I have received from many people.

First all I would like to thank my supervisor, Dr. Ir. René Alderliesten, for his valuable feedback and advice and for his positivity that kept me motivated at hard times throughout my thesis.

A major part of this thesis consisted of experimental research, meaning I have had a lot of support from the staff at the Delft Aerospace Structures and Materials laboratory (DASML). I would like to thank the DEMO team, in particular Kees Paalvast, for providing me with the required specimens as designed for this research. Also I would like to thank Frans van Oostrum, who taught me how to use the available microscopes for inspection of fracture surfaces.

Furthermore I would like to mention Gert-Jan Mulder and Berthil Grashof in particular, as they taught me how to use the fatigue test machines and other test equipment. I am grateful for their expertise, patience and motivation as without their help it would have been impossible to successfully complete this Master thesis.

Also I would like to thank my family and friends, for their valuable discussions and their unconditioned support and understanding, and -of course- for the necessary distraction at times needed. At last I would like to thank my girlfriend living in Vietnam, who despite the long distance has shown great understanding for being apart, and who has been a massive support throughout my research.

Joël Hogeveen
Delft, October 2016

The important thing is not to stop questioning. Curiosity has its own reason for existing.
One cannot help but be in awe when he contemplates the mysteries of eternity, of life,
of the marvellous structure of reality. It is enough if one tries merely to comprehend
a little of this mystery every day. Never lose a holy curiosity.

- Albert Einstein -

Table of Contents

Nomenclature

Acronyms and Abbreviations

Acronym	Meaning
2D	Two-Dimensional
3D	Three-Dimensional
ASTM	American Society for Testing and Materials
COD	Crack Opening Displacement
DASML	Delft Aerospace Structures and Materials Laboratory
FE	Finite Elements
FEA	Finite Element Analysis
FCG	Fatigue Crack Growth
HD	High Definition
LEFM	Linear Elastic Fracture Mechanics
LEXT OLS	Laser Next Generation Olympus Laser Scanning
LSM	Least Squares Method
MTS	Material Test System
RMSE	Root Mean Square Error
SEM	Scan Electron Microscope
SER	Strain Energy Release
SERR	Strain Energy Release Rate
SCF	Stress Concentration Factor
SIF	Stress Intensity Factor
UR	Unload Ratio
VIC	Video Image Correlation

Abbreviation	Meaning
Hz	Hertz
mJ	Millijoule
J	Joule
kg	Kilogram
µm	Micrometre
mm	Millimetre
m	Metre
MPa	Megapascal
GPa	Gigapascal
kN	Kilonewton

Roman Symbols

Symbol	Meaning	Unit	Symbol	Meaning	Unit
a	Crack Length	mm	P	Applied Load	kN
A	Area	mm^2	P	Pressure	Bar
C	Constant	-	p	Material Constant	-
d	Displacement	mm	q	Material Constant	-

Symbol	Meaning	Unit	Symbol	Meaning	Unit
E	Young's Modulus	MPa	r	Radius from Crack Tip	mm
E	Strain Energy	J	R	Crack Growth Resistance	J
f	Opening/Max Stress Ratio	-	R	Stress Ratio	-
f	Body Forces	N	r_p	Plastic Zone	mm^2
F	Ratio $U_{in,a}/U_{in,a=0}$	-	S	Stress	MPa
G	Strain Energy Release Rate	mJ/mm^2	t	Specimen Thickness	mm
H	Specimen Height	mm	U	Strain Energy	J
K	Stress Intensity Factor	MPa$\sqrt{mm}$	U_s	Total Strain Energy	J
K_c	Fracture Toughness	MPa$\sqrt{mm}$	v	Poisson Ratio	-
K_t	Stress Concentration Factor	-	V	Volume	mm^3
L	Specimen Length		W	Specimen Width	mm
m	Material Constant	mm	X	Relative to x-axis	-
n	Material Constant	-	Y	Relative to y-axis	-
N	Load Cycles	-			

Greek Symbols

Symbol	Meaning	Unit	Symbol	Meaning	Unit
Δ	Delta/Change	-	ρ	Density	kg/m^3
β	Geometry Correction Factor	-	ρ	Notch Height	mm
δ	Displacement	mm	σ	Stress	MPa
ε	Strain	-	Θ	Angle Between r and Crack Tip	°
ϒ	Surface Energy	J/mm^2	τ	Shear Stress	MPa
$ϒ_p$	Plastic Energy Dissipation	J			

Subscripts and Superscripts

Sub-Superscript	Meaning	Sub-Superscript	Meaning
*	Critical Value	m	Mean
$_0^*$	Monotonic After Load Cycle	m	Measured
↓	Applied by Specimen	max	Maximum
↑	Applied by Test Machine	min	Minimum
0	Initial	op	Open
0	Monotonic Before Load Cycle	out	Out
0,2	Yielding	pl	Plasticity
a	Amplitude	pr	Crack Propagation
a	Crack	req	Required
actual	Actual	rls	Released
c	Critical	shifted	Shifted
cod	Crack Opening Displacement	th	Threshold
cyc	Cyclic	tip	Crack Tip
eff	Effective	tot	Total
f	Final	top	Top
c	Failure	tr	Transition
i	Initial	x	x-direction
in	In	y	y-direction

1 Introduction

Fatigue is the weakening of a material or structure as a result of repeated loading and unloading. Fatigue is therefore very important in all engineering fields dealing with structures exposed to cyclic loads. A proper understanding of fatigue can improve structural designs and operations, which in turn may increase safety and economic benefits.

In the past century, the initiation and especially the propagation of fatigue cracks has been intensively researched both theoretically and experimentally. This research has led to generally accepted theories of fatigue with corresponding Fatigue Crack Growth (FCG) prediction models.

However, lately confusion raised about the scientific appropriateness of these fatigue theories and about the set-up and interpretation of the experimental results. Conclusions from previous work have been disputed and alternative FCG theories and prediction models have been proposed. This Master thesis discusses (the origin of) conventional fatigue theories to determine the sore points. Furthermore it takes alternative fatigue theories into consideration. Experiments are designed to determine which theories are in line with the experimental results and which are not. As such it is aimed for to get a better understanding of (the theories of) fatigue.

To obtain this understanding, first the literature of FCG is reviewed in Chapter 2. Based on the literature review, multiple hypotheses are formulated in Chapter 3. The chapter also covers the theories behind the hypotheses and elaborates on a research plan to test them. The experiments to obtain the required information to test the hypotheses of Chapter 3 are designed in Chapter 4. The results of a numerical pre-study of the experiments are reported in Chapter 5, and the results of the actual experiments are provided in Chapter 6.

Chapter 7 discusses the results of Chapter 6 in relation to the hypotheses and numerical analysis of Chapter 3 and Chapter 5 respectively. Based on the work from Chapter 2 until Chapter 7, conclusions are drawn and future recommendations are provided in Chapter 8.

2 Literature Review

As mentioned in the introduction, fatigue is the weakening of a material or structure due to loading and unloading, and is therefore very important in engineering fields dealing with cyclic loads such as the aerospace industry. A proper understanding of fatigue is essential. The state-of-the-art theories of FCG, deeply settled in the engineering world, are therefore discussed in Section 2.1. However, the validity of these conventional theories has been disputed by multiple researchers as discussed in Section 2.2. Section 2.3 provides a deeper historical overview to discover where the theories discussed in Section 2.1 come from and it critically reviews and emphasizes the sore points of these theories. As such it is aimed for to determine whether fatigue is actually properly understood. The chapter is concluded by a thesis proposal in Section 2.4.

2.1 The Conventional Theories of Fatigue

In this section the state-of-the-art knowledge of fatigue is discussed. The section covers the theories of fatigue as settled over the past decennia and as widely accepted and used in the engineering world. In general fatigue can be approached from two perspectives: Fatigue from a stress intensity perspective and fatigue from an energy release perspective. The total fatigue life is shortly discussed in Section 2.1.1. Then theories of fatigue from a stress intensity perspective are covered in Section 2.1.2 and fatigue from an energy release perspective in Section 2.1.3.

2.1.1 Fatigue Life

As mentioned in the introduction, fatigue is the weakening of a material or structure due to applied cyclic loads. The entire period from crack initiation to final failure, called the fatigue life of a structure, can be split in multiple phases as illustrated in the block diagram of Figure 2.1 [1]. In the crack initiation period, when the crack is called a microcrack, the crack is of grain size level and the crack growth is a surface phenomenon dependent on e.g. surface roughness and inclusions.
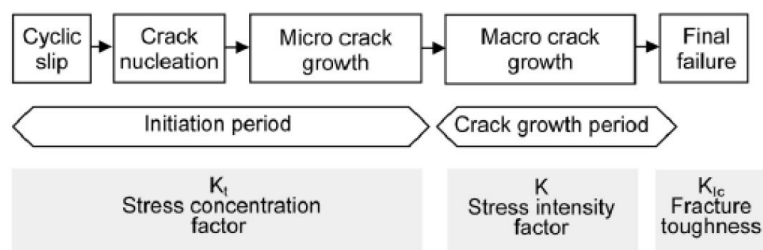

Figure 2.1: Phases of Fatigue Life [1]

When the crack has penetrated a certain amount of grains such that the crack growth becomes more or less continuous, the crack growth has become a bulk property instead of a surface phenomenon and the microcrack is now called a macrocrack. At this point the crack initiation period has been completed and the crack growth period has started. The macrocrack can propagate both as a part-

through or a through crack in various modes as illustrated in Figure 2.2. The main mode is mode I, as this is the mode where the crack is opened perpendicular to the tensile stress. Mode II and mode III cracks occur due to cyclic shear stresses, but quickly turn into a mode I crack as the tensile components open and thus propagate the crack. The remainder of this thesis will concentrate on through cracks (which are usually treated as two-dimensional (2D) cracks) with opening mode I during the crack growth period of the fatigue life.
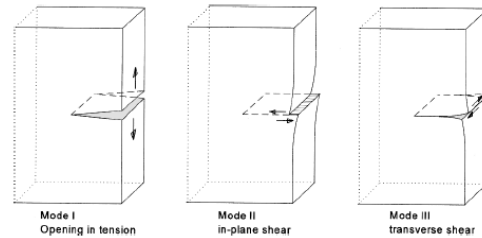
Figure 2.2: Crack Opening Modes [1]

2.1.2 Fatigue from a Stress Intensity Perspective

As mentioned in the introduction of this section, fatigue can be approached from a stress intensity perspective and from an energy release perspective. This section discusses fatigue from a stress intensity perspective. Energy considerations are covered in Section 2.1.3.

2.1.2.1 Stress Concentration Factor and Stress Intensity Factor

During the initiation period, the Stress Concentration Factor (SCF) K_t is given by Equation 2.1.

$$K_t = 1 + 2\sqrt{\frac{a}{\rho}}$$

Equation 2.1

Equation 2.1 describes the severity of stress at a notch [1,2]. In this equation a is the notch width and ρ the notch height. The SCF influences the duration of the crack initiation period, but becomes useless once a crack has initiated as ρ then goes towards zero and thus K_t towards infinity.

Therefore a new concept was introduced to describe the severity of the stresses at the crack tip by means of the so called Stress Intensity Factor (SIF) K. This parameter is extremely important in Linear Elastic Fracture Mechanics (LEFM), as it is the parameter used to present and predict FCG. The question is what K is, where it comes from and how it is used in FCG.

If an infinite sheet containing a crack is loaded in uniaxial tension and the crack opening mode is mode I, the stress components at the tip of the crack can be illustrated as in Figure 2.3.
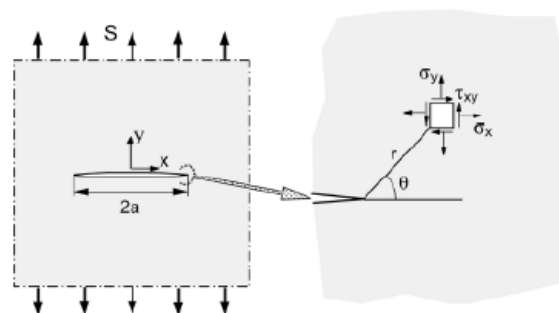

Figure 2.3: Stress Components at Crack Tip [4]

Westergaard and Irwin derived an expression given by Equation 2.2 for these stress components [1,4,42].

$$\sigma_{i,j} = \frac{K}{\sqrt{2\pi r}} f_{i,j}(\theta)$$
<div align="right">*Equation 2.2*</div>

It needs to be noted that this set of equations is valid only within a relatively small range compared to the crack length a ($r << a$) as is further discussed in Section 2.3. The parameter K in Equation 2.2 is called the SIF given by Equation 2.3.

$$K = S\sqrt{\pi a}$$
<div align="right">*Equation 2.3*</div>

For a finite sheet instead of an infinite sheet, Equation 2.3 is still valid provided that the crack stays a mode I-crack. However, the SIF for a finite sheet needs to be corrected by a dimensionless geometry correction factor β. The general expression for the SIF, describing the severity of stress around a crack tip, therefore becomes as follows:

$$K = \beta S\sqrt{\pi a}$$
<div align="right">*Equation 2.4*</div>

This equation is only valid within a relatively small range compared to the crack length. However, too close to the crack tip r goes towards zero. From Equation 2.2 it can be seen that the stresses at the crack tip in that case go to infinity, disastrous for brittle materials. Fortunately in reality most materials have some ductile properties, leading to a levelling off of the peak stresses near the crack tip due to the forming of a plastic zone. Nonetheless the equations for the SIF still give a proper estimation of the stress intensity at the crack tip as long as the crack tip is within the K-dominated zone [1].

2.1.2.2 Similarity Principle

So K defines the stress intensity around the crack tip. During a load cycle this varies between K_{min} and K_{max}. Therefore the range is ΔK, which conform Equation 2.4 can be calculated using Equation 2.5.

$$\Delta K = \beta \Delta S\sqrt{\pi a}$$
<div align="right">*Equation 2.5*</div>

This equation can also be expressed in terms of stress ratio. The stress ratio is given by Equation 2.6.

$$R = \frac{S_{min}}{S_{max}} = \frac{K_{min}}{K_{max}}$$
<div align="right">*Equation 2.6*</div>

According to Schijve [1], the crack growth rate is a function of K_{max} and K_{min} (or equivalently ΔK and R). This function represents the crack growth resistance of a material based on ΔK and R conditions and can be used to predict the crack growth in different specimens or structures of the same material. This concept is called the similarity principle or similitude approach and is defined by Schijve as quoted below [1]. However, some researchers doubt the validity of this approach as is discussed in Section 2.2.

> *"Similar cyclic conditions (ΔK and R) applied to fatigue cracks in different specimens or structures of the same material should have similar consequences, i.e. similar crack extensions per cycle, thus the same da/dN [1]."*

2.1.2.3 Fatigue Parameters and Fatigue Life Representation

There are multiple options to describe a load cycle as illustrated in Figure 2.4. Next to that there are multiple options to represent the fatigue life of a material or structure. One widely used fatigue life-representation is the Wöhler-curve introduced by Wöhler, illustrated in Figure 2.5 and based on the stress amplitude S_a and the mean stress S_m.
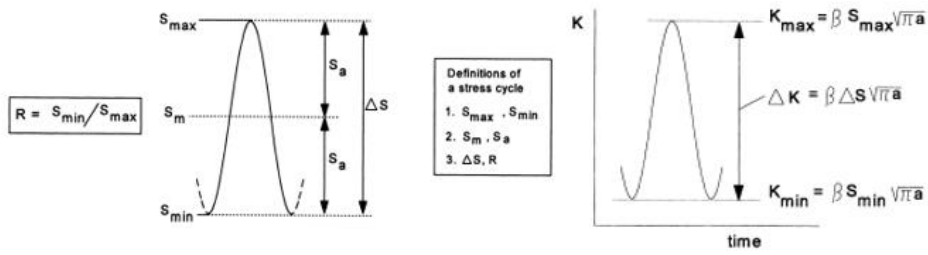
Figure 2.4: Parameters for Fatigue Load Cycle Description [1]

The figure shows the fatigue life of a structure in load cycles N corresponding to a certain applied stress amplitude S_a. The upper asymptote indicates S_u, the ultimate stress the structure can take before it fails. If S_a is equal to S_u, the structure will fail in a single cycle. If S_a is equal or lower than indicated by the lower asymptote, cracks may initiate but will not propagate: An infinite fatigue life is obtained.
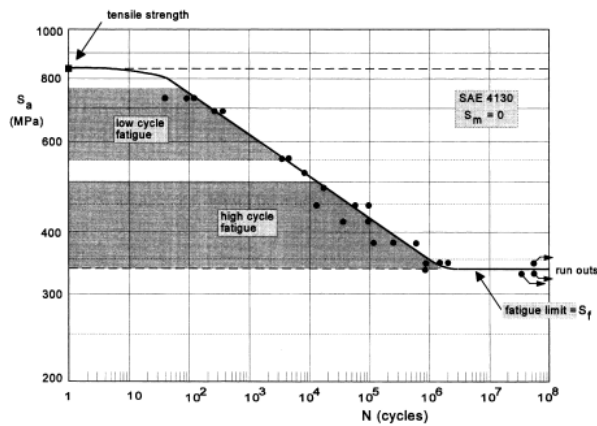
Figure 2.5: Wöhlers S-N Curve for Fatigue Life Prediction [1]

In Figure 2.5 S_m is zero, meaning the applied stress ratio is -1. If S_m is not equal to zero but positive, the same S_a will result in an applied stress closer to S_u than before. This has a consequence on the fatigue life (in this case it shortens the fatigue life of the structure) and thus the *S-N* curve shown in Figure 2.5 will change too. Gerber and Goodman have investigated this mean stress effect and came up with a mean stress effect correction. According to Schijve [1], Gerber's correction factor -shown in Figure 2.12- approximates reality best.

2.1.2.4 Fatigue Crack Growth and the Stress Ratio Effect

For different stress amplitudes, the crack length a after each amount of applied load cycles N can be measured and plotted as an *N-a*-plot. If the derivative thereof is taken, the crack growth rate *da/dN* (mm/cycle) as a function of a can be obtained. This is illustrated in Figure 2.6 for two different applied stress amplitudes.
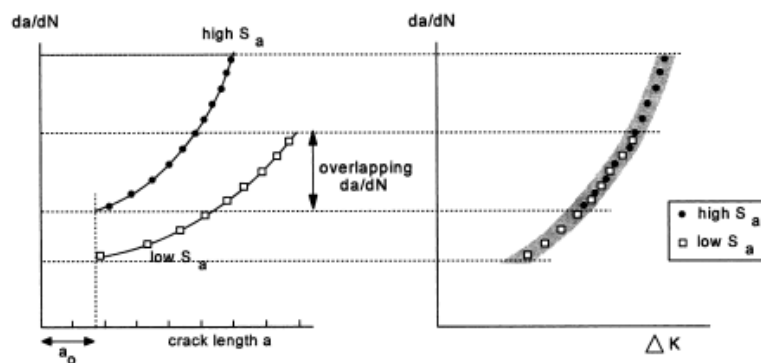
Figure 2.6: Crack Growth Rate as Function of a and SIF [1]

The illustration shows a partial overlap where the crack growth rate is equal, although at different crack lengths. To correlate this phenomenon, Paris introduced the similarity principle discussed in Section 2.1.2.2 [3]. After all, if the applied stress varies between S_{min} and S_{max}, the corresponding SIF

varies between K_{min} and K_{max} and also the stress ratio can be expressed in terms of K_{min} and K_{max}. And thus the resistance of a material should be a function of ΔK and R.

If the crack growth rate for a fixed stress ratio is plotted as a function of ΔK, as done in the left figure of Figure 2.7, the FCG data correlates very well. But Figure 2.7 shows the crack growth rate as a function of the SIF-range ΔK for two different stress ratios: It can be seen that expressing the crack growth rate in terms of ΔK shows good correlation for a single stress ratio, but it shifts for another stress ratio. This is called the stress ratio effect or R-effect, as is further discussed in Section 2.1.2.6.
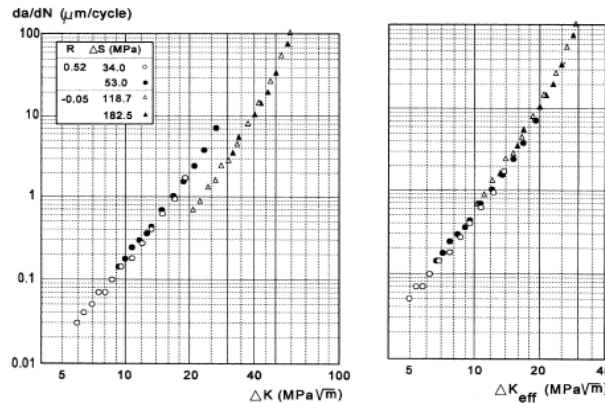
Figure 2.7: Crack Growth Rate as Function of SIF and Effective SIF [1]

2.1.2.5 Regions of Fatigue Crack Growth

Extensive testing has shown that three crack growth regions exist as illustrated in Figure 2.8: The threshold region, the Paris ΔK-region and the stable tearing crack growth region [1]. The left asymptote is at ΔK_{th} whereas the right asymptote is at K_c. The first asymptote shows the threshold ΔK for which the crack will stop propagating (note this is a threshold for macrocracks, not for earlier discussed microcracks) while the second asymptote shows the critical K-value for which the specimen will experience complete failure.

For fatigue the most important region is the Paris region. As can be seen from Figure 2.7 and Figure 2.8, the crack growth rate as function of the SIF range ΔK is approximately linear on a double-log plot. According to Paris [3], this crack growth rate da/dN can be calculated by the following equation:

Figure 2.8: FCG Regions [1]

$$\frac{da}{dN} = C\Delta K^m \hspace{5cm} \textit{Equation 2.7}$$

In this equation, C and m are material constants and K is the SIF as was derived by Irwin [4]. It needs to be taken into account that the Paris-relation does not include region I and III as shown in Figure 2.8 and neither does it include the R-effect. Therefore in literature multiple alternatives have been proposed such as the ones given in Equation 2.8 by Forman [7] and Equation 2.9 by Priddle [8] which do include both the asymptotes as well as the stress ratio influence.
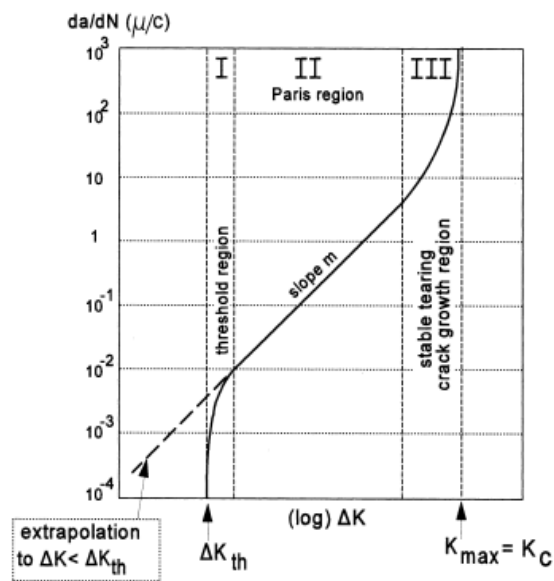
$$\frac{da}{dN} = \frac{C \Delta K^n}{(1-R)(K_c - K_{max})}$$

Equation 2.8

$$\frac{da}{dN} = C \left[\frac{\Delta K - \Delta K_{th}}{K_c - K_{max}}\right]^n$$

Equation 2.9

Equations 2.10-2.12 show other equations proposed to predict FCG [9-11], each based on different parameters, although from literature it seems that Paris' equation is most widely used for the prediction of FCG.

$$\frac{da}{dN} = \frac{CS^2 a}{S_y - S}$$

Equation 2.10

$$\frac{da}{dN} = \frac{S^3 a}{C}$$

Equation 2.11

$$\frac{da}{dN} = CS^2 a$$

Equation 2.12

One needs to be aware that all proposed FCG prediction equations given by Equations 2.7-2.12 are empirically derived. Therefore these equations do not deal with the underlying physics, as is further discussed in Section 2.3.3

2.1.2.6   Plasticity Induced Crack Closure

When a specimen including a crack is loaded in tension, the crack will open. Intuitively one may think that the crack is closed again once the applied load is reduced to zero. However, Elber discovered that the crack is closed already before a zero tensile load is applied [6,23].

When a specimen is loaded between S_{min} and S_{max}, plastic deformation occurs at the crack tip. The largest plastic zone is created if S_{max} is applied, resulting in a permanent elongation in loading direction. During unloading this plastic zone is loaded in compression resulting in a reversed plastic zone. This procedure occurs every load cycle and thus the crack propagates through a plastic zone of previous cycles as illustrated in Figure 2.9. This causes permanent elongation of the material in loading direction and causes the crack to close already before a zero tensile force is applied. This phenomenon is called plasticity induced crack closure. Figure 2.10 shows test results of Elber leading to this theory.
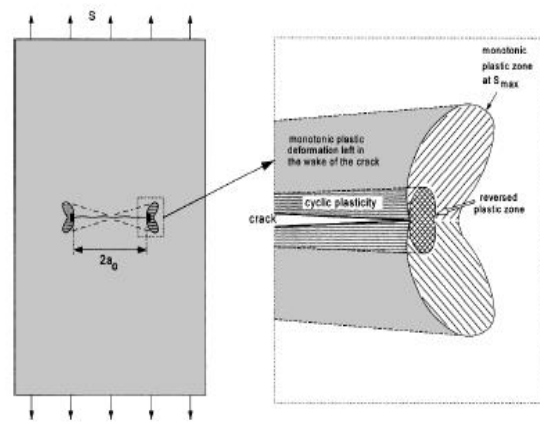
Figure 2.9: Illustration of Plastic Wake [1]
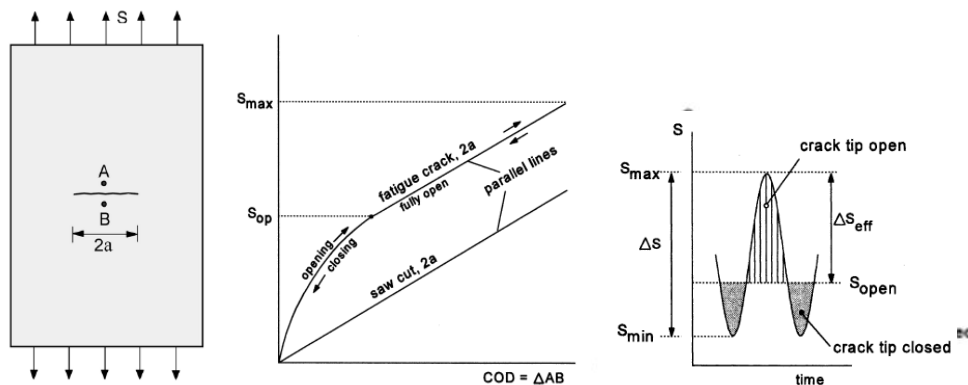
Figure 2.10: COD Test Results of Elber [1]

The Crack Opening Displacement (COD) is non-linear until the opening stress S_{op} is reached. This is because the closure of the crack effectively changes the configuration of the specimen and thus the stiffness. After the non-linear curve the graph becomes linear, as this is where the material starts to behave elastically. As such the COD for a saw cut crack is completely linear.

According to Elber and Schijve a crack can only propagate if a stress singularity at the crack tip occurs [1,23]. In other words, the crack starts to propagate only if S_{op} is overcome. Experiments showed that S_{op} was independent of crack length for constant amplitude load spectra, and thus an effective stress range and effective SIF range were introduced provided by Equations 2.13 and 2.14 respectively [1,6].

$$\Delta S_{eff} = S_{max} - S_{op} \qquad\qquad \textit{Equation 2.13}$$

$$\Delta K_{eff} = K_{max} - K_{op} \qquad\qquad \textit{Equation 2.14}$$

Elber derived an empirical relation for the opening stress S_{op}, later adapted by Schijve to Equation 2.15 [1].

$$\frac{S_{op}}{S_{max}} = 0.45 + 0.22R + 0.21R^2 + 0.12R^3 \qquad\qquad \textit{Equation 2.15}$$

If Paris' equations are used with the effective SIF range, the *R*-effect as mentioned in Section 2.1.2.4 disappears. This is shown in Figure 2.7: Using the ΔK_{eff} instead of ΔK indeed shows good correlation. As such, the similarity principle discussed in Section 2.1.2.2 also changes. Whereas earlier FCG was considered to be a function of ΔK and *R*, it can now be said that FCG is a function of ΔK_{eff} only. Plasticity induced crack closure therewith seems to be the missing key to a full understanding of FCG.

Nowadays this theory of plasticity induced crack closure is disputed as discussed in Section 2.2. In this literature review, the transition point between non-linear and linear load-COD behaviour observed in Figure 2.10 is called the opening stress due to crack closure. This is how many important researchers have interpreted the trend of Figure 2.10. However, it may be a false claim as it seems that other mechanisms can also cause this non-linear load-COD behaviour. The reader therefore needs to realise that whenever this literature refers to 'opening stress' and 'crack closure', also other underlying mechanism might be responsible for this 'opening stress' and 'crack closure'. After the literature review of Chapter 2, it is therefore decided to indicate this transition point between non-linear and linear load-COD behaviour no longer as an opening stress, but as a transition stress S_{tr}. As such it is aimed for to avoid any premature conclusions.

2.1.3 Fatigue from a Strain Energy Release Perspective

So far FCG has been approached from a stress intensity perspective. Another way to approach FCG is from a strain energy release (SER) perspective [1]. If a specimen is loaded, work is done which is stored as potential energy *U*:

$$U = \frac{1}{2}P\delta = \frac{1}{2} \cdot SWt \cdot \frac{S}{E}H = \frac{1}{2}\frac{S^2}{E}HWt \qquad\qquad \textit{Equation 2.16}$$

S is the remote stress, W, t and H are the width, thickness and height of the specimen and E is the elastic modulus. $\frac{1}{2}\frac{S^2}{E}$ is called the strain energy density. If a plate has a crack, the stiffness reduces and as such the stored energy reduces too. Therefore there will be a relaxation of strain energy ΔU if the specimen does not change in length. This is illustrated in Figure 2.11. An increase in released strain energy therefore relates to an increase in crack length and as such the Strain Energy Release Rate (SERR) is often referred to as the crack driving force, although it seems to be more a consequence than a cause.
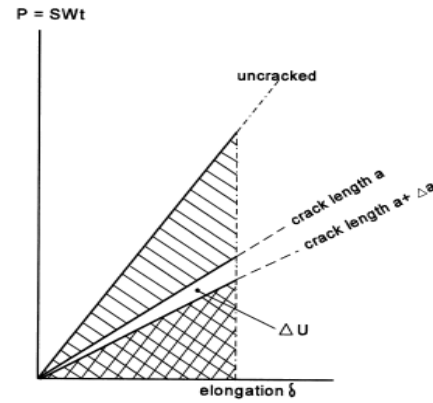
Figure 2.11: SER due to Crack Growth [1]

The strain energy loss due to crack growth can, implicitly derived by Irwin [4], also be expressed in terms of K as shown in Equation 2.17:

$$\Delta U = \frac{K^2}{E^*}\Delta a \qquad\qquad \textit{Equation 2.17}$$

E^* is E for plane stress and $E/(1-v^2)$ for plane strain. The SERR G then becomes as shown in Equation 2.18.

$$G = \frac{dU}{da} = \frac{K^2}{E^*} \qquad\qquad \textit{Equation 2.18}$$

The relation between G and K has been derived by many researchers by combining work of Paris and Irwin, but has actually never been explicitly derived by Paris and Irwin themselves. Nevertheless the relation is widely used and relates FCG prediction based on SER and FCG prediction based on SIF. With this relation, the perception is that fatigue is totally understood. As is discussed in Section 2.2 this may be disputed.

2.2 Criticism on the Conventional Fatigue Approach

Section 2.1 has elaborated on the theories behind fatigue as nowadays widely accepted and used for prediction of FCG. Fatigue is a stress intensity dominated phenomenon that seems to be fully understood: FCG is predicted by a SIF and the resulting R-effect is accounted for by including the effect of plasticity induced crack closure. However, lately these theories have been subject of discussion [12-34]. The discussion mainly concentrates on the validity of the plasticity induced crack closure concept, as discussed in Section 2.2.1. Proposed alternatives for FCG description and prediction are discussed in Section 2.2.2.

2.2.1 Criticism and Concerns on (Plasticity Induced) Crack Closure

As discussed in Section 2.1.2.6, plasticity induced crack closure is thought to be the missing keystone to a full understanding of fatigue crack propagation. However, the mechanism of plasticity induced crack closure has been critically reviewed in recent years. This section discusses the criticism showing that plasticity induced crack closure is anything but an undisputable theory.

2.2.1.1 Early Concerns

Concerns about the validity of plasticity induced crack closure do not only date from recent years, but also earlier work caused confusion. Herzberg for instance experimented with artificial crack closure using shims [25]. By artificially closing the crack an increased stress is needed to open the crack and thus also K_{op} as defined by Elber increases. According to the crack closure theory and the corresponding effective SIF range as discussed in Section 2.1.2.6, one may expect similar FCG behaviour for artificially

and non-artificially closed cracks. For Herzberg it was therefore very confusing that quantitatively the FCG behaviour was far off.

Additional confusion arose from work by Garrett and Knott [26]. They removed the plastic wake by heat-treating the specimen. By continuing the fatigue tests after heat-treating it was, based on the theory in Section 2.1.2.6, expected that the FCG rate would initially increase until a new plastic wake would be created. However, the experiments showed that the heat-treatments had no effect on the FCG rate. More recent work of for instance Vasudevan and Lang also doubts the validity of crack closure [12-21]. Their concerns are for instance based on the hypothesis that non-linear behaviour in load-COD diagrams is not necessarily caused by plasticity induced crack closure, but for instance by the presence of asperities [17,50]. Next to that it seems simply unrealistic that theoretically crack closure occurs above any arbitrarily chosen minimum applied load.

2.2.1.2 ΔK_{eff} because of Residual Stresses instead of Crack Closure

In earlier research, Schijve discovered that an overload after constant amplitude loading could delay the crack growth [27,28]. This was attributed to residual compressive stresses introduced by the overload. These compressive stresses first need to be overcome before the crack will further propagate, as such causing growth retardation. A phenomenon called the memory effect.

As Marci and Lang discuss [12], Schijve could have introduced a ΔK_{eff} based on his memory effect-theory: This ΔK_{eff} should then be the effective SIF range from the point where the residual compressive stresses due to an overload are overcome (similar to S_{op} in crack closure theory) until S_{max}. But from a historical perspective, S_{op} and ΔK_{eff} were indisputably related to plasticity induced crack closure. Therefore Schijve did not explain his observations in terms of S_{op} and ΔK_{eff}, but explained it as a memory effect. It shows that ΔK_{eff} is not necessarily a consequence of plasticity induced crack closure, but for instance residual compressive stresses may cause the same effect. In other words, ΔK_{eff} could have been defined based on multiple underlying mechanisms.

Lang was the first researcher who did not assume that S_{op} was caused by plasticity induced crack closure, but defined a SIF for which the crack starts to propagate: K_{PR} [12,13]. Experiments on the influence of overloads on FCG, showed that the history of the loading has no influence on K_{PR}. Instead, K_{PR} is only dependent on the overload ratio UR and the maximum SIF K_{max}. This new parameter K_{PR} is the SIF for which the (residual) compressive stresses switch to tensile stresses, resulting in a different explanation for ΔK_{eff} than plasticity induced crack closure.

2.2.1.3 Stress Ratio Effect or Mean Stress Effect

More recent support disputing the plasticity induced crack closure theory has arisen by comparing the corrections for stress ratio and mean stress. Equation 2.15 was introduced by Schijve in order to calculate S_{op} corresponding to a certain applied stress ratio. This S_{op} can be used to determine ΔS_{eff} and ΔK_{eff} which in turn shows good correlation for different stress ratios as was discussed in Section 2.1.2.6.

Alderliesten decided to rewrite Elber's crack closure correction and Equation 2.15 in terms of S_m and S_a [24]. The results thereof are plotted in Figure 2.12 together with the mean stress correction of Gerber. Calling the striking correlation between both corrections remarkable would be an understatement, especially as one correction accounts for closure in the wake of a macrocrack while the other corrects for a range where macrocracks are non-significant. Therefrom Alderliesten concludes that it is very likely that both corrections account for some similar mechanism.
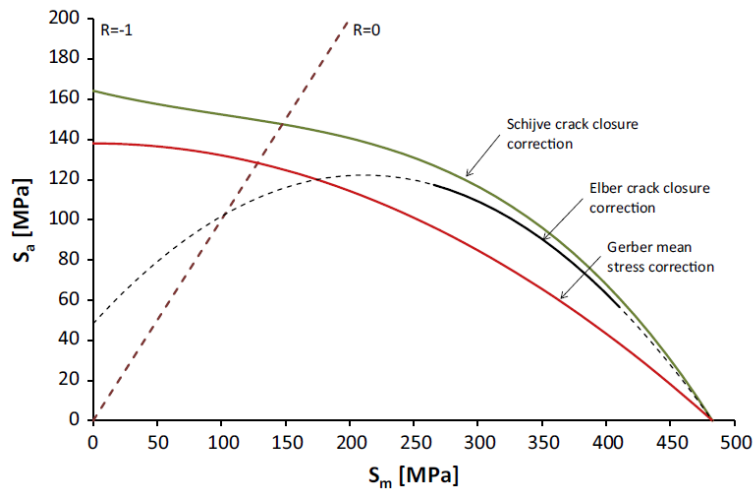
Figure 2.12: Crack Closure Correction and Mean Stress Correction [24]

2.2.1.4 Absence of Stress Ratio Effect in Vacuum

But the biggest problem of the theory that R-effect is a consequence of plasticity induced crack closure lies within experimental results of Kirby and Beevers and Petit and Rangathan on FCG in vacuum [29,49]. The R-effect is especially obvious in the threshold regime, ΔK_{th} [1]. Figure 2.13 shows ΔK_{th} for a large range of stress ratios in both air and vacuum environment.

In vacuum it may be expected that plasticity plays an important role in the closure of the crack, as such causing an R-effect. However, the performed experiments show an absence of R-effect in vacuum. The absence of R-effect implies that the crack does not close due to plasticity in the wake of the crack and as such invalidates Elber's theory of plasticity induced crack closure. However, despite their observations no further attention was paid to the outcome of these tests as the empirical equations provided in Section 2.1.2.5 still showed sufficient correlation with the test results obtained in vacuum environment.
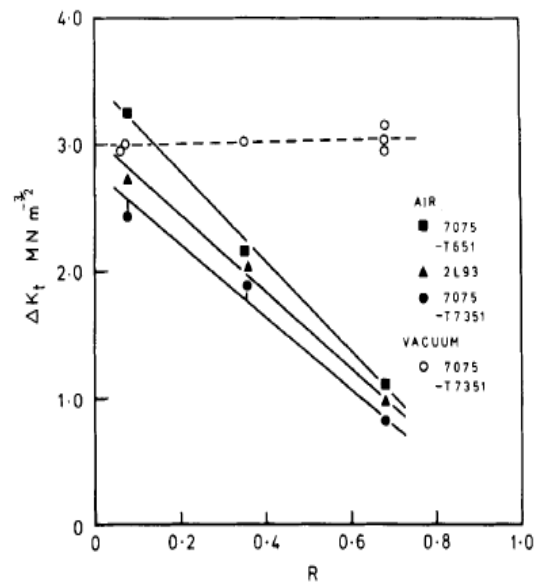
Figure 2.13: Threshold SIF in Air and Vacuum [29]

2.2.1.5 Cyclic Energy Instead of Crack Closure

As briefly discussed in Section 2.1.3, fatigue can also be approached from an energy release point of view instead of a stress intensity point of view. A final major observation leading to concerns about the validity of plasticity induced crack closure comes from work of Alderliesten [30]. Basically Alderliesten aims to show how S_{op} is an artificial stress by approaching the crack closure correction as a cyclic energy problem.

The energy involved in a complete load cycle, called the cyclic energy and illustrated by the blue area in Figure 2.14, can be calculated using Equation 2.19.
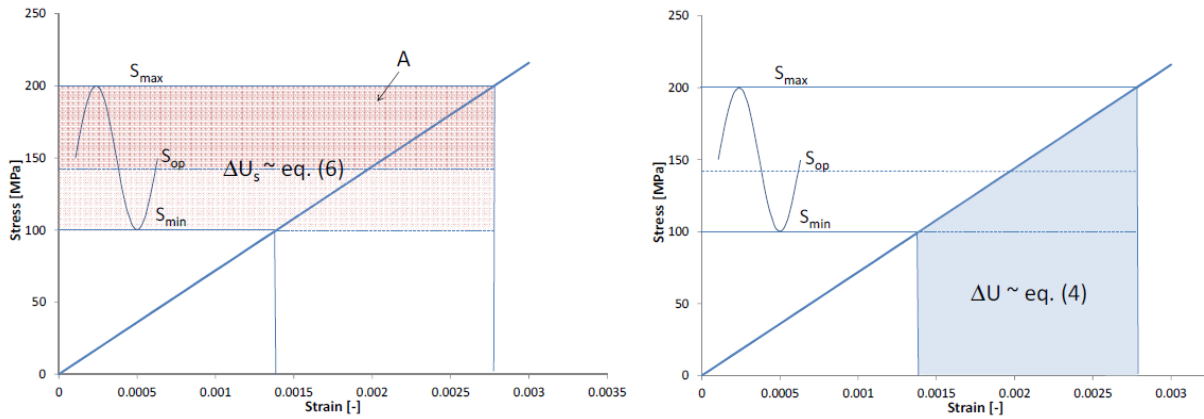
Figure 2.14: Illustration Showing how S_{op} Corrects for Cyclic Energy {36}

$$\Delta U = \frac{1}{2}S_{max}\varepsilon_{max} - \frac{1}{2}S_{min}\varepsilon_{min} \qquad\qquad Equation\ 2.19$$

If also the artificial total energy by means of Equation 2.20 is considered, one can create a correction as in Equation 2.21 but based on energy instead of stress.

$$U_s = (S_{max} - S_{min})\varepsilon_{max} \qquad\qquad Equation\ 2.20$$

$$Y = \frac{\Delta Keff}{\Delta K} = \frac{\Delta U}{U_s} \qquad\qquad Equation\ 2.21$$

The ratio *Y* is the percentage of effective SIF range. In other words, this is the percentage of the total SIF range for which the crack tip is fully open. If this ratio *Y* is expressed in terms of applied cyclic work as percentage of the (artificial) total work, the result as shown in Figure 2.15 is obtained. There is again a striking correlation with the various crack closure corrections.
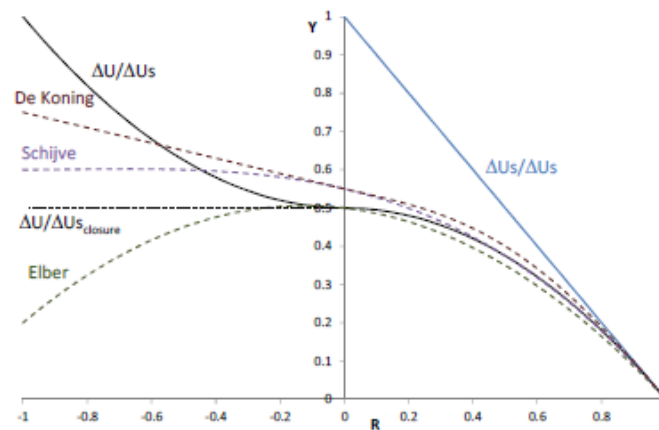
Figure 2.15: Crack Closure Corrections and Cyclic Energy 'Correction' [30]

It is important to notice that the energy of Equation 2.20 is a non-existing, artificial energy (indicated by the sum of the red areas in Figure 2.14) but it is the considered energy if *ΔK* is taken for similitude. From the striking correlation with crack closure corrections, Alderliesten claims that S_{op} as such is a non-existing, artificial opening stress only needed to correct the total artificial work to an amount of work equal to the cyclic applied work. As such crack closure and opening stress correlates for an *R*-effect, while it is actually a cyclic energy problem. Based on this, Alderliesten claims that *ΔK* might be an improper similitude parameter for FCG prediction.

2.2.1.6 Criticism on Relation Between ΔK and SERR

As discussed in Section 2.1.3, *ΔK* can also be related to SERR. However, Equation 2.15 (repeated here as Equation 2.22) was derived for fixed grip conditions subject to quasi-static loading conditions.

$$U = \frac{1}{2}P\delta = \frac{1}{2} \cdot SWt \cdot \frac{S}{E}H = \frac{1}{2}\frac{S^2}{E}HWt \qquad \qquad Equation\ 2.22$$

This means that a fixed displacement and an assumed instant increase in crack length *da*, results in a release of strain energy as shown in Figure 2.11. But *ΔK* is used for a fatigue problem instead of a quasi-static problem. Nonetheless these two expressions are combined by means of Equation 2.23, although obtained for different loading conditions.

$$G = \frac{dU}{da} = \frac{K^2}{E^*} \qquad \qquad Equation\ 2.23$$

The relation between *ΔK* and SERR is therefore criticised by Alderliesten [24,31]. In reality the crack extends non-linearly as illustrated in Figure 2.16.
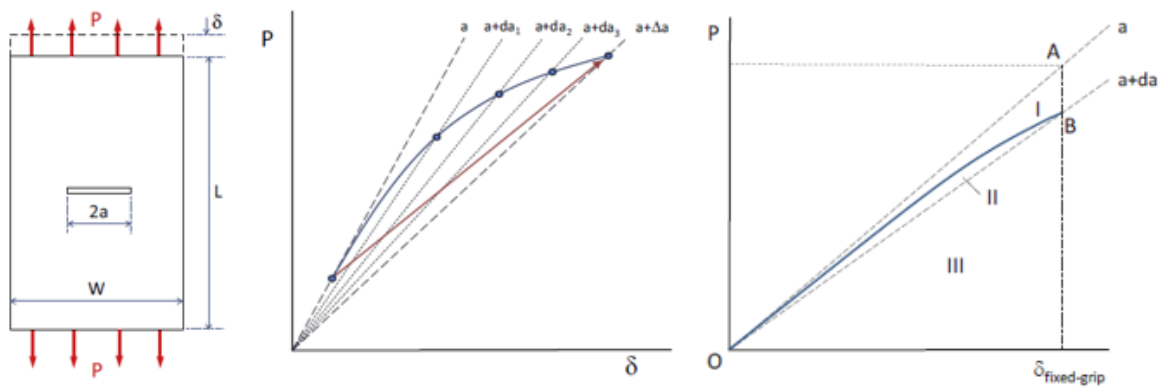
Figure 2.16: Actual Crack Growth and Crack Growth by LEFM [24,31]

The figure clearly shows why Equation 2.22 is incorrect: It calculates the SER as if it is the sum of area I and II and the total applied work as if it is area I + II + III, but in fact area I is strain energy that has never been released nor applied. The effective SER should therefore be only area II and the effective applied work should be only area II and III. So, instead of relating crack growth with the SERR at a single or two fixed points, it seems more reasonable to consider the released energy during an entire fatigue load cycle.

2.2.2 Alternative Fatigue Approach

The theories discussed in Section 2.1 are widely accepted and used in engineering and seem to be well understood. However, the criticism discussed in Section 2.2.1 show that the theories of Section 2.1 are not necessarily correct. Therefore alternative FCG prediction models have been proposed: One model is stress intensity dominated and the other energy release dominated. This section discusses both alternatives in the case of constant amplitude load spectrum.

2.2.2.1 Stress Dominated

The conventional fatigue theories discussed in Section 2.1 treat fatigue most importantly as a stress intensity dominated phenomenon. According to these theories, fatigue can be predicted using the equations of Section 2.1.2.5 by means of a single similitude parameter *ΔK_{eff}*. An apparent *R*-effect is accounted for by the extrinsic mechanism plasticity induced crack closure. An alternative is to aim for an FCG prediction method based on intrinsic mechanisms such as dislocations instead of an extrinsic

mechanism. This alternative FCG prediction model was introduced by Vasudevan and Lang and is named the Uniform Approach [17-21].

Vasudevan determined the ΔK_{th} and K_{max} needed for crack propagation in steel and aluminium for a wide range of stress ratios as illustrated in Figure 2.18. The experiments show that for an increasing stress ratio, ΔK_{th} decreases and at some point stays constant, whereas K_{max} starts constant and at some point starts to increase. The switch point is in both cases at exactly the same stress ratio. The corresponding ΔK_{th} and K_{max} are denoted as ΔK_{th} * and K_{max}*. To ensure FCG, it is required that ΔK_{th} and K_{max} exceed ΔK_{th} * and K_{max}* simultaneously.
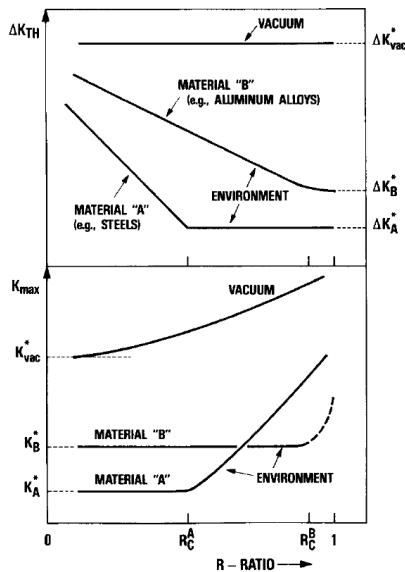
Figure 2.18: ΔK_{th} and K_{max} dependence on R [17]
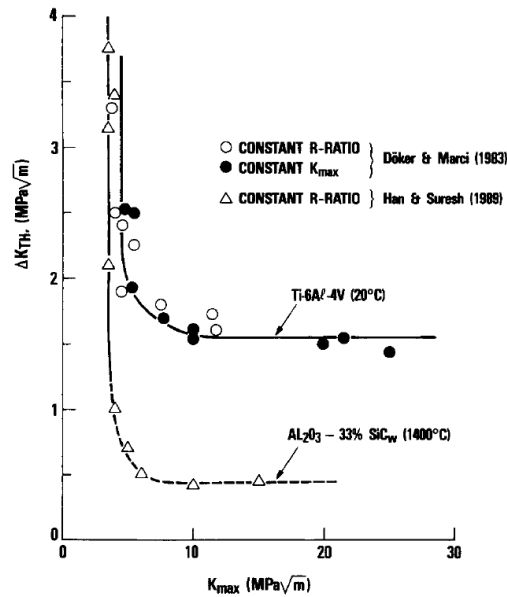
Figure 2.17: Threshold Data from Experiments by Doker et al Analysed by Vasudevan [17]

Therewith FCG is no longer dependent on a single parameter ΔK_{eff}, but on the two parameters ΔK_{th} and K_{max}. To proof the dependency of FCG on these two parameters, Vasudevan analysed a large amount of data [17-21]. One of these analyses is based on data gathered by Doker et al [17]. A set of three different experiments was set-up of which two are considered in this literature review: The first experiment determined ΔK_{th} by decreasing the load amplitude with a constant stress ratio, while the second experiment determined ΔK_{th} by decreasing the load amplitude with a fixed K_{max}. The results were plotted in a ΔK_{th}-K_{max} graph as shown in Figure 2.17, and clearly show that FCG is indeed dependent on the two parameters K_{max}* and ΔK_{th}* (represented by the two asymptotes), which need to be met simultaneously to ensure FCG.

More evidence was gathered by analyzing steel, aluminium alloys and ceramic composites data [18]. For different stress ratios, the FCG rate as a function of K_{max} and as a function of ΔK_{th} was obtained. The obtained data was plotted in a ΔK_{th}-K_{max} format for two different FCG rates: One for the near threshold FCG $da/dN = 10^{-6}$ mm/cycle and one for a FCG rate of $da/dN = 10^{-5}$ mm/cycle. Figure 2.19 shows this ΔK_{th}-K_{max} plot for the steel data set. The results confirm the dependency of FCG on K_{max} and ΔK_{th}. Figure 2.19 provides information for which values of $K_{max}*$ and $\Delta K_{th}*$ the fatigue crack will propagate with a certain rate da/dN. The data from aluminium alloys and ceramic composites showed a similar trend and also in the compressive range (negative stress ratios) FCG turned out to be dependent on two parameters [19].
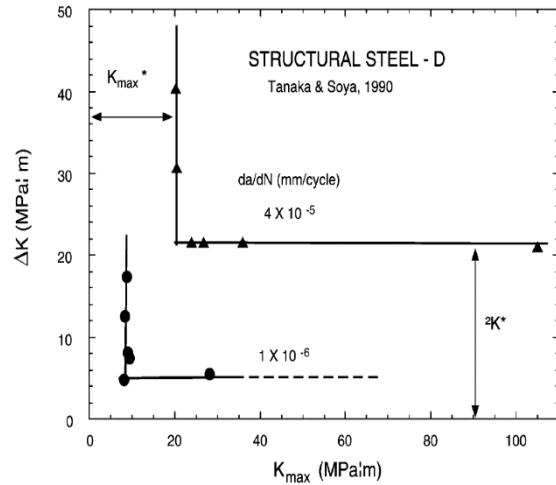
Figure 2.19: K_{max}-ΔK_{th} for Two Different da/dN-Rates in Steel [18]

2.2.2.2   Energy Dominated

Next to the alternative stress dominated fatigue prediction method discussed in the previous section, one could also argue that fatigue should be approached conform the laws of thermodynamics, forgetting about using ΔK as similitude parameter. This philosophy is thoroughly discussed by Alderliesten and Pascoe [24,30,31,33,34] and finds its origin in earlier work of Griffith [5]. As such, Alderliesten proposed to base FCG on an alternative energy balance as given by Equation 2.24.

$$U_0 + U_\uparrow \rightarrow U_0^* + U_\downarrow + U_a + U_{pl} \qquad \qquad \textit{Equation 2.24}$$

In this equation, U_0 is the monotonically applied work at minimum load, $U_\uparrow$ is the work applied by the test machine during loading, $U_\downarrow$ the work applied by the specimen on the test machine during unloading, U_a the energy dissipated because of crack growth and U_{pl} the energy dissipated due to plasticity at the crack tip. U_0^* is the monotonically applied work at the end of the load cycle which is always smaller than U_0. The red area in Figure 2.20 indicates the dissipated energy due to crack growth in case of a displacement controlled experiment.
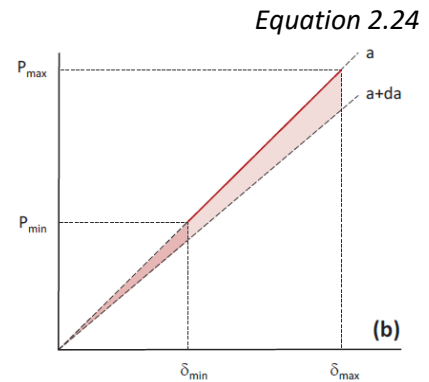
Figure 2.20: SER due to Crack Growth [31]

The strain energy released during a fatigue cycle N is related to the crack growth da in that cycle, using the chain rule this can be mathematically expressed as in Equation 2.25.

$$\frac{dU}{dN} = \frac{dU}{da}\frac{da}{dN} \qquad \qquad \textit{Equation 2.25}$$

In this equation, dU/da is the effective SERR G_{eff}. This is thus the actual SERR for a crack increment da and not the ΔG_{eff} as calculated for quasi-static cases at S_{max}–S_{min}. It needs to be taken into account that dU/dN in Equation 2.25 does not only include strain energy released by crack growth, but also by other energy dissipation mechanisms such as plasticity. Equations 2.24 and 2.25 are no longer based on an empirical relation like the equations in Section 2.1.2.5 or the uniform approach discussed in the previous section are. Instead of that they deal with the underlying physics of the fatigue problem as it relates the crack growth da/dN with the effective SERR G_{eff} and the actual SER during a complete load cycle.
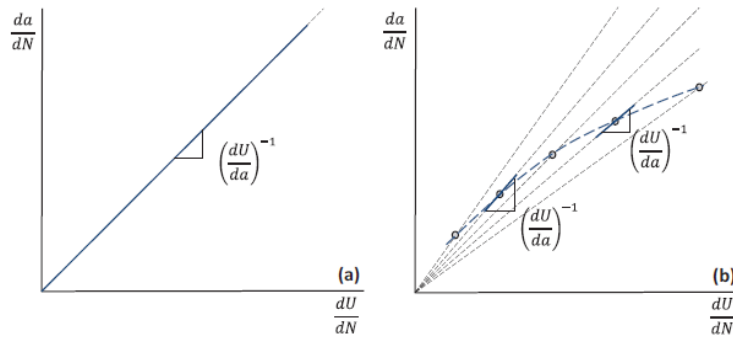
Figure 2.21: da/dN-dU/dN Curve Representation [31]

The SER during a complete load cycle as described by Equation 2.25 can be plotted as illustrated in Figure 2.21. The slope of this graph is the magnitude of G_{eff}; The smaller the slope, the higher the SERR. A linear curve as shown in Figure 2.21 thereby implies that the energy dissipated due to crack extension is equal for each crack extension unit, what in reality can only be the case if the fracture surface for high and low crack growth rates is identical. However, in reality this is often not the case as for higher crack growth rates the surface becomes rougher, thereby creating a larger effective crack area and thus increasing the dissipated energy per extended crack unit. This is illustrated in the right figure of Figure 2.21. The blue dotted line in that figure describes the SERR for a single tested specimen. Since the crack surface -and thus the effective crack length- will increase over the da/dN range, non-linear behaviour is observed. The various linear curves in Figure 2.21 are basically a measure for the roughness of the crack. Also energy dissipation through plasticity causes this non-linear effect.

Representing fatigue in terms of dU/dN-da/dN curves means that the shape of the curve always relates to an intrinsic mechanism and not to stress ratio for instance. Nevertheless the stress ratio may have an influence on these intrinsic mechanisms, as it affects the applied work $U_{\uparrow}$, the energy dissipation dU and the crack increment da [24].

Although experimental results from Pascoe on disbond growth of composite laminates correlate very well, there is still a slight influence of the stress ratio. This was also observed by Alderliesten, who noticed the same effect in the results of a Master thesis study by Pasman on the FCG in metallic round bars containing shoulder fillets [51]. Calling this an R-effect is correct but maybe unlucky, as the behaviour observed in figures such as Figure 2.22 are related to intrinsic energy dissipating mechanisms while R-effect historically tends to be related to the extrinsic mechanism crack closure. The R-effect in Figure 2.22 might for instance be a result of a changing surface roughness or changing plastic zone for a different stress ratio.
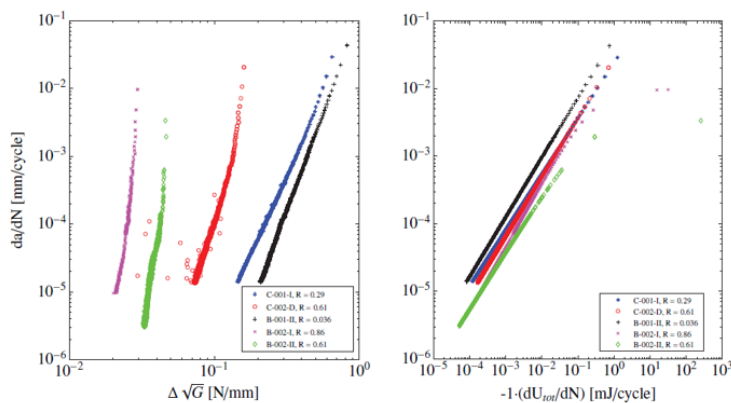
Figure 2.22: da/dN vs $\Delta\sqrt{G}$ (using SERR) and da/dN vs dU_{tot}/dN [34]

For prediction of fatigue using the total dissipated energy per cycle, Equation 2.26 could be the basis.

$$U_0 + U_\uparrow \rightarrow U_0^* + U_\downarrow + \frac{dU}{dN}$$

This equation relates the SER during a single load cycle with the applied work. In Equation 2.26 the applied load or work can therefore be seen as the cause of the consequence crack growth. Thus, if the underlying physics of fatigue can be properly described based on the SER during a fatigue load cycle, one could say that the crack growth becomes a function of U_0 and $U_\uparrow$ as shown in Equation 2.27.

$$\frac{da}{dN} = f(U_0 + U_\uparrow)$$

However, before such a prediction model can be developed, the focus should first be on a full physical understanding of the relation between the SER during a load cycle and the corresponding crack growth per load cycle, as given in equation form in Equation 2.25.

2.3 Historical Development of Conventional FCG Theories

The conventional fatigue theories discussed in Section 2.1 seemed to be properly understood. However, Section 2.2 has shown that many questions are still present regarding the validity of the theories. Alternative FCG description and prediction models have been proposed. This section discusses and critically reviews important historical research leading to conventional LEFM. As such it is aimed for to determine the problems with the theories discussed in Section 2.1.

2.3.1 Rupture of Solids due to Quasi-Static Loads

Griffith was one of the pioneers of fracture mechanics, describing crack growth based on the principle of conservation of energy [5]. If a brittle material is assumed, and hence Hooke's law is valid, then the strain energy per unit volume is given by Equation 2.28.

$$U^* = \frac{1}{V} \int f\, dx = \int \frac{f}{A} \frac{dx}{L} = \int S d\varepsilon = \frac{S\varepsilon^2}{2} = \frac{S^2}{2E}$$

Then fixing the boundaries and introducing a crack causes a reduction of stresses near the crack surfaces thereby releasing strain energy. Figure 2.23 illustrates the reduction of stresses at the crack surfaces.

To calculate the SER Griffith made use of Inglis' solution [35], meaning that under plane stress conditions the side αβ of the two triangles indicated in Figure 2.23 is equal to πα. The SER is then the area of these two triangles multiplied with the strain energy per unit volume given in Equation 2.28. The result is shown in Equation 2.29. Note the minus sign in this equation, which results from the definition that strain energy is *released*.

Figure 2.23: Idealization of Unloaded Region near Crack Flanks [36]

$$E_{rls} = -\frac{S^2}{2E} \pi a^2$$

But energy is not only released, it is also required to break the cohesion of the molecules to form a crack front. This energy is called surface energy absorbed by the material and given by Equation 2.30.

$$E_{req} = 2Ya$$
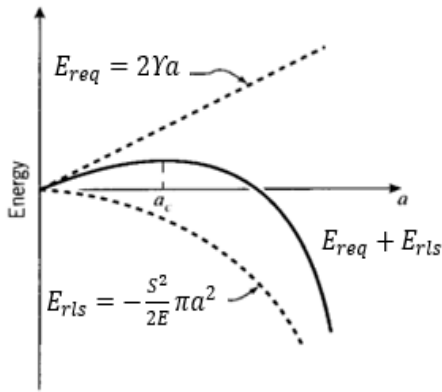
Figure 2.24: Energy Consumed, Energy
Required and Total Energy as Function of
Crack Length [36]

In this equation Y is the surface energy in J/mm^2 [5,44]. The resulting free energy due to the introduction of a crack in the specimen can be calculated by $E_{rls} + E_{req}$. Both the energy released and the energy required are plotted in Figure 2.24 as function of crack length a.

The free energy reaches a maximum at a certain critical crack length a_c. In order to cause crack growth, until this critical crack length energy needs to be added to the system by increasing the stress. After this critical crack length, the release of energy due to the length of the crack controls the energy absorbed by breaking the atomic bonds for additional crack surface and crack propagation becomes self-sustaining (rupture of the material occurs). The critical crack length can be obtained by equating the derivative of the freed energy of the system, $E_{rls} + E_{req}$, to zero as shown in Equation 2.31.

$$\frac{\partial(E_{rls} + E_{req})}{\partial a} = 2Y - \frac{S_f{}^2}{E}\pi a = 0 \qquad \qquad \textit{Equation 2.31}$$

The fracture stress then becomes as follows:

$$S_f{}^2 = \sqrt{\frac{2YE}{\pi a}} \qquad \qquad \textit{Equation 2.32}$$

2.3.1.1   Irwin's Modification and the Stability Criterion

Griffith's theory is limited to brittle materials such as hard glass, rock and ice. However, this changed during research of Irwin and Kies and Orowan [37-41]. First Irwin reformulated Equation 2.31 to a stability criterion. Irwin denoted the second term of the right hand side of Equation 2.31 as the SERR G and the first term as the crack resistance R [41]. As such, Irwin could define a stability criterion for fracture being:

$$G > G_c = R = 2Y \qquad \qquad \textit{Equation 2.33}$$

Although Equation 2.33 is still only valid for brittle materials, by adding an extra term Y_p for the crack resistance in Equation 2.33 suddenly other energy dissipating mechanisms like plasticity are also included [37,39,40]. It is important to notice that Irwin and Kies, and also Orowan, set up this stability criterion not changing the supply side of energy release as determined by Griffith. This energy release was derived for quasi-static fixed grip conditions, as it was derived assuming an instantaneous crack extension, and as such it cannot be said regardless to be valid for fatigue too.

$$S_f{}^2 = \sqrt{\frac{G_c E}{\pi a}} \qquad \qquad \textit{Equation 2.34}$$

2.3.2 The Relation Between G and K

Apart from the previous stability criterion, Irwin approximated the stresses around the crack tip of what he calls a "somewhat brittle" material [4,45]. This means that large plastic deformations may occur, but are always small compared to the crack length as was also mentioned in Section 2.1.2.1. Irwin derived the stresses at the crack tip based on a theory earlier developed by Westergaard [42]. This led to the following set of equations, of which the general form was already provided in Section 2.1.2.1 as Equation 2.2.

$$S_{xx} = \frac{\sqrt{EG}}{\sqrt{2\pi r}} cos\left(\frac{\theta}{2}\right)\left(1 - sin\left(\frac{\theta}{2}\right) sin\left(\frac{3\theta}{2}\right)\right)$$

Equation 2.35

$$S_{yy} = \frac{\sqrt{EG}}{\sqrt{2\pi r}} cos\left(\frac{\theta}{2}\right)\left(1 + sin\left(\frac{\theta}{2}\right) sin\left(\frac{3\theta}{2}\right)\right)$$

Equation 2.36

$$\tau_{xy} = \frac{\sqrt{EG}}{\sqrt{2\pi r}} cos\left(\frac{\theta}{2}\right) sin\left(\frac{\theta}{2}\right) cos\left(\frac{3\theta}{2}\right)$$

Equation 2.37

Irwin's stress equations are only valid near the crack tip, until a distance of around 10% of the total crack length as can be seen by comparing Westergaards exact solution and Irwin's approximation for *y = 0* in Figure 2.25. However, the conditions in this area are according to Irwin of only importance for FCG [4]. The advantage of using Irwin's stress expressions instead of Westergaards solution is at first the clear dependency on *Θ* around the crack tip. Later Paris also used it to define the SIF *K*, as is discussed in more detail in the following section. It can now be easily seen where the relation between SERR *G* and SIF *K* as briefly discussed in Section 2.1.3 comes from (see Equation 2.38 and 2.39).
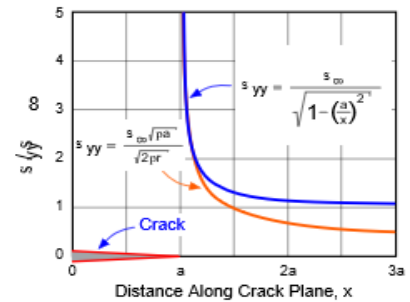
Figure 2.25: Stress Along y = 0 for Westergaards Exact Solution and Irwin's Approximation [52].

$$K = \sqrt{EG} = \sqrt{E\frac{S^2}{E}\pi a} = S\sqrt{\pi a}$$

Equation 2.38

Or:

$$G = \frac{K^2}{E}$$

Equation 2.39

This relation between *G* and *K* has never been explicitly mentioned by neither Paris and Irwin, and it unfortunately is a very important moment in the development of the conventional fatigue theories discussed in Section 2.1.

'Unfortunately', because it shows where *K* is originally derived from and why it is improper to use for FCG description: As has been mentioned multiple times throughout this literature review, *G* is derived for *quasi-static* loading conditions. In the stress equations of Irwin *G* is therefore still only valid for *quasi-static* loading conditions. Nevertheless Paris defined a parameter *K*, the SIF, based on *G* and used this for *fatigue* loading conditions. However, there is no reason to assume that a parameter derived from quasi-static loading conditions is still valid for fatigue loading conditions. In later work it is often insinuated that the SERR *G* can be derived from the SIF *K*, but originally in fact *K* was derived from *G*.

2.3.3 The Adoption of K for Fatigue Crack Growth

Irwin set up a stability criterion for the condition for which crack growth occurs and described the stress field around a crack tip. As explained in the previous section this was all derived for quasi-static loading conditions. But Paris concluded that Irwin's stress equations are valid for any point in time and that this state of stress at the crack tip is determining the crack growth. As such, Paris concluded that Irwin's equations may not only be used for quasi-static problems but also for fatigue problems. With that in mind Paris defined the SIF K [3,25,52].

Initially Paris established a stress ratio parameter, S_{min}/S_{max}, and concluded that a load cycle can be completely described if K_{max} and this stress ratio are known -and thus fatigue should be dependent on these parameters [3]. For a zero stress ratio and a range of K_{max} the crack growth rate indeed correlated on a single curve as shown in Figure 2.26. According to Paris this verified his theory that fatigue is dependent on the maximum SIF and the stress ratio, but in later work Paris acknowledged that this conclusion may have been drawn too early [22].
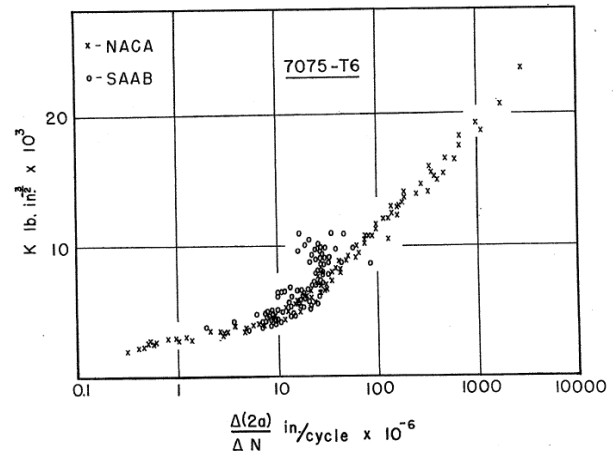
Figure 2.26: Maximum Stress Intensity Factor as Function of Crack Growth Rate [2]

Paris showed that for a limited amount of data not only his own theory could be verified, but also other FCG equations discussed in Section 2.1.2.5. This is shown in Figure 2.27 with a double-log scale, where each equation from Section 2.1.2.5 basically represents a slope. Each of these slopes corresponds with the (limited) amount of data used to verify the corresponding equation in Section 2.1.2.5.
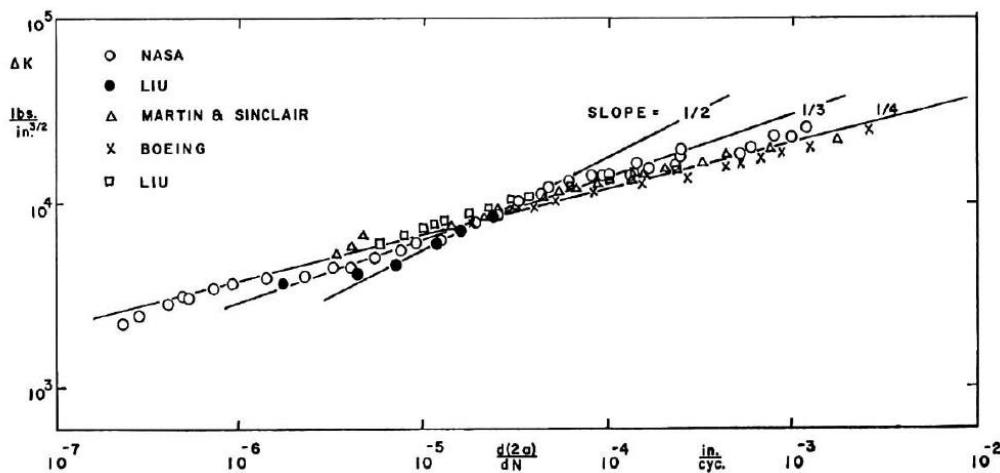
Figure 2.27: Fatigue Crack Growth Data on a Log-Log Plot [22]

If the slope is taken from the total amount of data, so from a large set of data, Paris observed that the line in Figure 2.27 will shift and change slope for different materials. For each material Equation 2.40 is therefore adapted by adapting C and m. These parameters are thus material constants.

$$\log(\frac{da}{dN}) = \log(C) + m\log(\Delta K) \qquad \textit{Equation 2.40}$$

Or:

$$\frac{da}{dN} = C\Delta K^m \qquad\qquad\qquad\qquad \text{Equation 2.41}$$

Equation 2.41

Equation 2.41, nowadays still used to predict FCG, is thus completely empirical. Nevertheless Equation 2.41 is suggested by Paris as the correct one for FCG prediction, although his reasoning does not rely on any physical explanation [22]:

"For that reason the authors suggest that laws which correlate a wide range of test data from many specimens are perhaps the "correct" laws. The results at least indicate that hasty conclusions have been drawn in many earlier works which should be re-examined before any given crack-propagation law is accepted as valid [22]."

Thus, the reasoning of Paris to call Equation 2.41 the correct equation to predict FCG, is apparently solely based on the fact that it correlates with a wide range of test data from many specimens. A physical reasoning for that lacks, as also seems to be realised by Paris himself in a later article [32]:

"Over the years this has led to stating that perhaps this should be explained with some reasoned physical model before anyone claims a correct model or more detailed effects … so it is submitted that physical modelling of fatigue crack growth remains uniquely unsuccessful for all of these 40 years [32]."

So from the previous section it has become clear that using the SIF K as similitude parameter for fatigue problems is incorrect, as it originates from a stability criterion under quasi-static load conditions instead of fatigue load conditions. On top of that, this incorrect similitude parameter is used in a prediction model that is empirically derived without covering the underlying physics. It can therefore be concluded that FCG nowadays is still not well-understood, like even the founder of the theory himself admits. Nonetheless it is interesting to see that Paris' equation has been adopted by many other researchers as the main way to predict FCG. The reason thereof is likely the simplicity of fatigue life prediction using Paris' relation and its practical usability for engineering purposes.

2.3.4 Explanation of the R-effect: (Plasticity Induced) Crack Closure

As was discussed in Section 2.1.2.4, if ΔK is used as similitude parameter a clear R-effect arises. From the previous section it can be concluded that the conventional FCG prediction methods may be practically useful due to their empirical character, but from a scientific point of view they are incorrect. Nonetheless ΔK is widely accepted for FCG prediction, and thus an explanation of the R-effect was needed. This explanation came by means of plasticity induced crack closure discovered by Elber, resulting in adaption from ΔK to ΔK_{eff} [6,23,43,44]. The first sign of the existence of crack closure came from the result shown in Figure 2.28 [6].
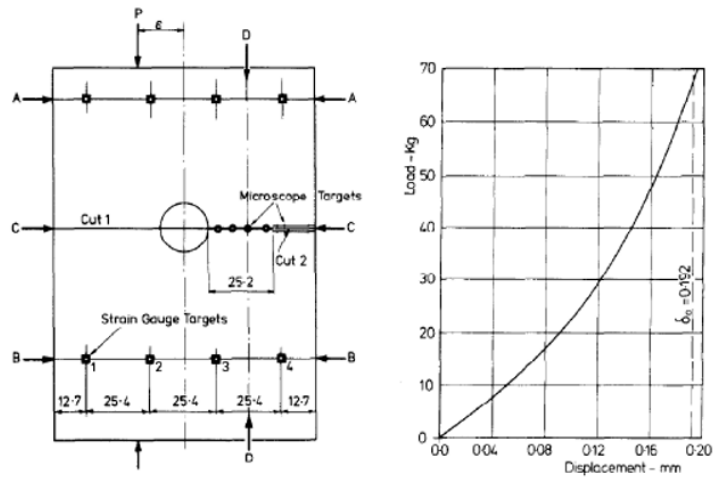
Figure 2.28: Test Specimen and Corresponding Load-Displacement Graph [6]

The left figure of Figure 2.28 illustrates a specimen used by Elber, including multiple strain gauges, that was elastically loaded. The corresponding load-displacement plot is shown at the right side of Figure 2.28. The non-linearity of this curve implies that the stiffness of the specimen is changing, which could according to Elber only happen due to a change in geometry [6]. In other words, the non-linearity of the graph implies crack closure.

As such, Elber further researched this phenomenon and hypothesized that crack closure occurs due to plasticity in the wake of the fatigue crack tip [23,43]. For a saw cut, a crack is open if subject to tensile stresses and closed if subject to compressive stresses. However, for the case of a fatigue crack every load cycle a plastic zone and reversed plastic zone is created while the crack propagates. Therefore there is a plastic wake present behind the crack tip, creating residual compressive stresses. The residual strain introduced by the residual stresses in this plastic wake can result in a decrease of δ_0 in crack opening as illustrated on the left side of Figure 2.29.
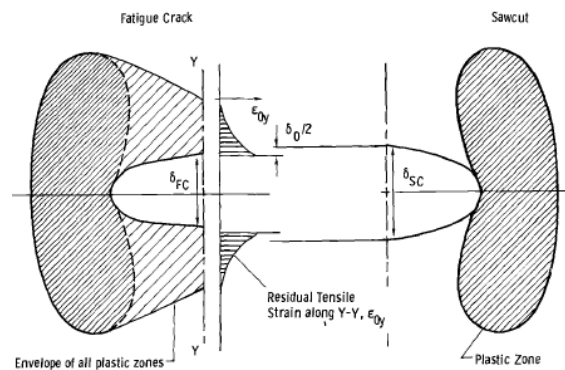
Figure 2.29: Influence of Plastic Wake on Crack Opening Displacement [23]

A specimen with a saw cut does not have such a plastic wake and thus also no residual strain, as illustrated on the right side of Figure 2.29. According to Elber [23,43,44] the crack opening decreases at the same rate during unloading because of the surrounding elastic material, meaning that the crack of a fatigue crack will close before a saw cut crack. In other words, in fatigue crack closure can occur at positive tensile stresses.

In order to test this hypothesis Elber used 5 mm thick aluminium sheets. For each experiment the gauges to determine strain were located on one of the following two locations on the surface of the

specimen: One straddling the crack at 2 mm from the crack tip and one ahead of the crack tip determining the effect of the crack growing through the gauge as illustrated in Figure 2.30 [23]. Elber's tests have been performed under plane stress conditions.
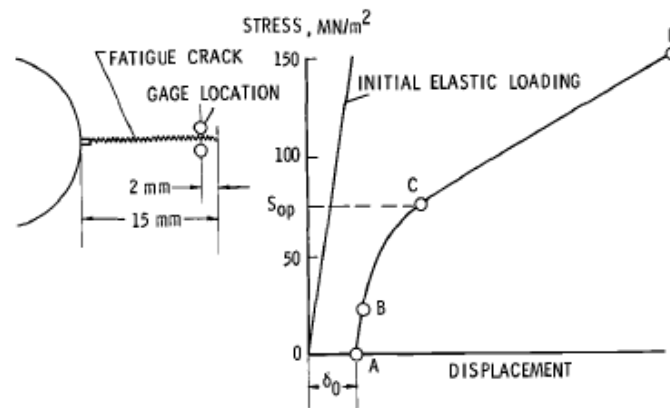
Figure 2.30: Strain Gauge Placement and Load-Displacement Response of Elber's Tests [23]

The result of the displacement measured by the gauge 2 mm behind the crack tip is shown on the right hand side of Figure 2.30, together with the elastic response of an uncracked specimen. It can be seen that between A and B, the stiffness of both plots is equal. According to Elber, this implies that the crack is closed between A and B. Between C and D again a linear relationship is shown, this is equal to the stiffness of a saw cut crack and indicates the crack is open. In between, between B and C, the stiffness is not constant as such indicating that the geometry of the specimen is changing by means of an opening crack [23].

Figure 2.31: Infuence of R-ratio on Effective Stress Intensity Range [23]

Elber argued that the observed crack closure changes the stress field around the crack tip [23], and that FCG only takes place if the crack is fully open. In other words, the minimum applied stress for crack propagation needs to be higher than S_{op} indicated by point C in Figure 2.30. As a consequence the SIF range of influence on FCG was redefined as the effective SIF ΔK_{eff} by multiplying ΔK by a correction factor Y given by Equation 2.21 and repeated below as Equation 2.42

$$Y = \frac{\Delta Keff}{dK} = \frac{\Delta U}{U_s}$$
<div align="right">*Equation 2.42*</div>

Elber determined Y by considering a variety of loading conditions: The influence of ΔK, crack length, and stress ratio were examined, but from the results in Figure 2.31 it can be seen that only the stress ratio has a significant effect on the required correction factor. An empirical equation was fit through the data leading to Equation 2.43 [23]

$$Y = 0.5 + 0.4R$$
<div align="right">*Equation 2.43*</div>

Therewith another empirical relation is required to account for an observed phenomenon (the *R*-effect) if ΔK is used as similitude parameter, which is not very encouraging for the credibility of the

conventional fatigue approach. In fact an empirically determined FCG prediction equation is now corrected by another empirically determined equation.
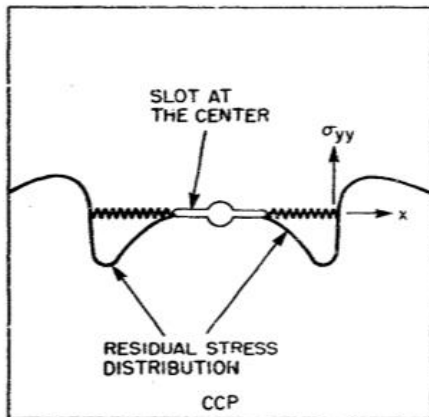
Figure 2.32: Residual Stress Distribution Along Crack Front [44]

Moreover the stress distribution along the crack illustrated in Figure 2.32 is only valid for thin specimens subject to plane stress conditions, exactly Elbers test conditions [23,44]. Taking into account that Elber's tests are executed subject to plane stress conditions means that the plastic zone and plastic wake for the specimen tested by Elber are significantly larger compared to a specimen subject to plane strain conditions. It may therefore be the case that crack closure inside the specimen (having plane strain conditions) is different compared to crack closure near the surface. Multiple researchers indeed noticed a difference in crack closure subject to plane strain and plane stress conditions [43-47].

Apart from that, considering Elber's measurement locations indicated in Figure 2.30, it can be seen that the strain gauge locations are very close to the crack. One could therefore say that maybe not the phenomenon crack closure was measured by Elber, but the residual compressive stresses due to plasticity. In that case the non-linearity in the load-COD diagrams would not be caused by crack closure, but by the fact that first compressive stresses need to be overcome. Therefore multiple mechanisms can be responsible for the non-linear load-COD behaviour, as is already discussed in Section 2.2.1.2.

Furthermore the location of the strain gauges by Elber does not imply any information on crack closure further down the crack tip e.g. does not cover the global crack closure. Over the years many researchers have tried to show crack closure by means of a broad variety of test methods such as strain gauges, ultrasonics, potential drop techniques, rod gauge techniques and optical methods for both plane strain and plane stress conditions and to determine crack closure both on the surface and inside the tested specimen and to monitor both local and global crack closure [43-48]. There has never been an unambiguous result from all test methods performed and the opening SIF K_{op} differs for each method. Besides that, different researchers do not agree what the exact definition is for the crack opening or crack closing stress and which of these stresses is required to obtain the correct ΔK_{eff} [43,44,48].

Elber's deficient way of testing plasticity induced crack closure, the widespread controversy between multiple researchers and a lack of a clear-cut explanation for a variety of observed phenomena can only lead to one conclusion: Plasticity induced crack closure is still a not well-understood and confusing phenomenon. Or one could also say: The *R*-effect is not a consequence of crack closure, but an artefact of choosing *ΔK* as similitude parameter.

2.4 Synthesis

Section 2.1 has elaborated on fatigue theories based on stress intensity, nowadays widely accepted and used within the engineering world. However, this literature review has brought forward that these theories do not deal with the underlying physics and as such are very disputable from a scientific point of view.

The stress parameter *ΔK* has been deeply settled as the similitude parameter to predict FCG, but as discussed in Section 2.3.2 it finds its origin in a SER based stability criterion for the case of quasi-static loading conditions. On top of that, this similitude parameter is used in an equation that is empirically

obtained and thus lacks any physical explanation. Using ΔK introduced an R-effect, explained by the much disputed phenomenon plasticity induced crack closure, but Section 2.2.1.5 showed that the R-effect might also be a cyclic energy phenomenon instead of cyclic stress. Furthermore Section 2.3.4 showed that the correction to account for R-effect is also empirically derived. In short, one may consider R-effect to be the artefact of choosing ΔK as similitude parameter. The alternative stress based fatigue description proposed in Section 2.2.2.1 already indicated that R-effect disappears if fatigue is considered to be dependent on two parameters instead of one: ΔK_{th} and K_{max}. However, this alternative theory basically boils down to representing fatigue data in a different way as it still deals with the SIF K, and as such still does not cover the underlying physics.

As even the pioneers of these theories of fatigue acknowledge that the current theories lack a physical explanation, as discussed in Section 2.3.3, the aim of this thesis is to get a better understanding of fatigue. As discussed in Section 2.2.1.4, test results in vacuum seem to be contradictive with the expectations based on conventional LEFM theories. However, these tests have only been performed in the threshold regime and no further attention was paid. By performing experimental research in both air and vacuum environment, it is aimed for to obtain better insight in using ΔK for similitude and the mechanism crack closure. Furthermore fatigue is approached conform the SER alternative discussed in Section 2.2.2.2, as this seems to be the only alternative method that deals with the underlying physics of fatigue. Once the physics behind fatigue is fully understood, one can start to think about a prediction model based on this new theory.

3 Research Hypotheses, Plan and Theories

From the literature review it has become clear that further investigation is required for a proper understanding of the physics behind fatigue. Fatigue has been treated as a stress dominated phenomenon by means of the similitude parameter ΔK and the resulting R-effect has been explained by means of plasticity induced crack closure. However, the results discussed in Section 2.2.1.4 are a strong sign that the theories are not valid in vacuum while this is the most inert environment a fatigue test can be performed in. Therefore it is thought that a better understanding of fatigue can be obtained through experimental tests in both air and vacuum environment. This chapter covers the research hypotheses for this thesis in Section 3.1 and discusses the theories behind in Section 3.2.

3.1 Research Hypotheses

For a proper understanding of fatigue, on one hand it is necessary to critically review and re-examine historical experimental results and theories based on SIF, and on the other hand fatigue needs to be re-examined starting from the absolute beginning: The laws of thermodynamics by means of SER. Therefore experiments are performed from two different points of view: The SIF point of view and the SER point of view. By executing the experiments in both air and vacuum environment it is expected that conclusions can be drawn on the following hypotheses:

ΔK is an incorrect similitude parameter for FCG

The literature research already provided multiple strong indications why this hypothesis is valid, but it has never been explicitly investigated in a single experimental research. By applying the conventional theories of fatigue for a wide range of test conditions in terms of R and K_{max}, one may expect similar trends in air and vacuum environment. If not, one can say that ΔK is an improper parameter for similitude as there should be no significant difference if fatigue is a stress governed phenomenon.

Fatigue is strain energy release dominated

In line with the previous hypothesis, if fatigue is considered to be energy dominated, again no difference should be observed between air and vacuum when the total dissipated energy during a complete fatigue load cycle is considered. If there is a difference, it should be possible to trace this back by means of the energy dissipation mechanisms such as crack surface roughness and plasticity.

The R-effect is not caused by plasticity induced crack closure

In addition to the previous two hypotheses it is hypothesized that R-effect is not caused by plasticity induced crack closure. The previous hypothesis implies that it must be possible to explain the 'R-effect' from an energy perspective. Furthermore comparing experimental (plasticity induced) crack closure measurements in both air and vacuum in relation to FCG results based on ΔK, may explain if the R-effect is caused by crack closure and whether it is plasticity induced or not.

3.2 Research Plan and Theory

Experimental tests are executed in both a vacuum and air environment, and they are analysed from both a SIF and SER perspective. As such it can be researched what theories and conclusions of Chapter 2 are in line with each other and which ones are contradicting. This should lead to conclusions regarding the hypotheses listed in the previous section. In Section 3.2.1 the plan and theories behind SIF approached fatigue is discussed and Section 3.2.2 discusses fatigue from a SER approach.

3.2.1 Stress Intensity Approach

For the stress intensity approach, basically the experimental results as discussed in Section 2.1.2.4 of Chapter 2 are reproduced. Conform this theory FCG can be described as $f(\Delta K, R)$. ΔK is the SIF range and is the similitude parameter for FCG. That means FCG occurs at a similar growth rate da/dN for a similar ΔK if R is fixed. ΔK can be calculated using Equation 3.1.

$$\Delta K = \beta \Delta S \sqrt{\pi a}$$ <div style="text-align:right">*Equation 3.1*</div>

In this equation, ΔS is the difference between maximum and minimum applied uniaxial stress and a is the normalized crack length. For this thesis it is assumed that crack propagation only occurs in opening Mode I. Therefore no opening mode subscripts or any other subscripts indicating e.g. the toughness SIF are used. β is a dimensionless geometry correction factor which according to Fedderson and the American Society for Testing and Materials (ASTM) E647 can be calculated using Equation 3.2 for a centre cracked tension (CCT) specimen [53].

$$\beta = \sqrt{sec\left(\frac{\pi a}{W}\right)}$$ <div style="text-align:right">*Equation 3.2*</div>

In this equation W is the width of the specimen and a is the normalized length of the crack.

As such, when at every ΔN cycles the crack length a is measured, the crack growth rate at each cycle can be derived by taking the derivative of the N-a curve. Also for each crack length a the corresponding ΔK can be calculated using Equation 3.1 and Equation 3.2, meaning a ΔK-da/dN curve can be constructed. Conform the conventional theories of fatigue as discussed in Section 2.1, the following outcomes may be expected:

- For a fixed R, the FCG rate shows good correlation in both air and vacuum environment if the similitude parameter is ΔK.
- For a varying R, an R-effect should appear in both air and vacuum environment if ΔK is the similitude parameter.
- Conform the theory of plasticity induced crack closure, the load-COD diagrams should contain a non-linear behaviour in both air and vacuum environment.
- The transition point, called S_{op} in conventional fatigue theories, should reduce ΔK to ΔK_{eff} as $\Delta S_{eff} = S_{max} - S_{op}$, or $\Delta K_{eff} = K_{max} - K_{op}$. If ΔK_{eff} is used for similitude, the R-effect mentioned in the second bullet point should disappear.

If the experimental results in both test environments are conform the above listed points, the SIF approach cannot be falsified meaning that ΔK might be the correct similitude parameter for FCG description and prediction -although the plasticity induced crack closure mechanism in this case remains confusing for some of the conditions covered in the literature review.

However, the first and last hypothesis listed in Section 3.1 imply that the experimental results are not expected to be conform the above bullet points. Section 2.2.1.4 in the literature review showed no R-effect for the threshold SIF in vacuum, and equal results are expected over the entire SIF-range.

According to Elbers theory of plasticity induced crack closure, non-linear load-COD behaviour should be obtained in both air and vacuum environment. If this is the case, while in vacuum no R-effect is observed if ΔK is taken for similitude, it confirms the hypothesis that ΔK is an improper similitude parameter for fatigue.

On the other hand, if the R-effect in vacuum collapses but vacuum does not show non-linear load-COD behaviour, it does not falsify ΔK as the proper similitude parameter for FCG. But in that case it does falsify that possible crack closure is plasticity induced, as there is no reason to expect a different plastic behaviour of the material in vacuum compared to air.

3.2.2 Strain Energy Release Approach

Apart from approaching fatigue from stress intensity perspective, one can approach fatigue also from a SER perspective. As discussed in Section 2.3.2, SERR G is related to the SIF K as follows:

$$G = \frac{K^2}{E}$$
<div align="right">*Equation 3.3*</div>

However, as was discussed in Sections 2.3.1 and 2.3.2, in fact K is derived from G while G was derived for quasi-static conditions. In other words, G is derived with the assumption that the crack increments due to an instantaneous load, while it is unknown if this is also valid for fatigue loading. Instead of that, it was proposed by Alderliesten and Pascoe to consider the total energy dissipated after a complete load cycle as discussed in Section 2.2.2.2.

Conform this theory, the total loss in energy after a complete load cycle needs to be considered as mathematically shown in Equation 3.4.

$$U_{in} = U_{out} + \frac{dU}{dN}$$
<div align="right">*Equation 3.4*</div>

In this equation, U_{in} is the amount of energy supplied by the test machine on the specimen, U_{out} the amount of energy supplied by the specimen on the test machine and dU/dN is the amount of energy dissipated due to crack extension and plasticity.

As it is complicated to measure U_{out}, it is proposed to only measure U_{in}. This requires the assumption that the applied energy U_{in} at load cycle $N+\Delta N$ is equal to the energy U_{out} at load cycle N, mathematically given by Equation 3.5.

$$U_{out,N} = U_{in,N+\Delta N}$$
<div align="right">*Equation 3.5*</div>

Substituting this in Equation 3.4 results in Equation 3.6.

$$U_{in,N} = U_{in,N+\Delta N} + \frac{dU}{dN}$$
<div align="right">*Equation 3.6*</div>

As such dU/dN can be simply obtained by taking the derivative of U_{in} at every time interval ΔN.

In the case of linear elasticity, the energy release can therefore be calculated by subtracting the work done at cycle N from the work done at cycle $N+\Delta N$ as given by Equation 3.7.

$$U_{rel} = 0.5P(d_{N+\Delta N} - d_N)$$
<div align="right">*Equation 3.7*</div>

U_{rel} is the energy released by crack extension and plasticity, P is the applied load and d is the displacement of the specimen at load cycle $N+\Delta N$ and N respectively.

The total work at a certain load cycle N can be calculated using Equation 3.8 and the cyclic work at this load cycle can be calculated using Equation 3.9.

$$U_{tot} = 0.5 P_{max} d_{max} \qquad\qquad\qquad \textit{Equation 3.8}$$

$$U_{cyc} = U_{tot} - 0.5 P_{min} d_{min} \qquad\qquad\qquad \textit{Equation 3.9}$$

Figure 3.1 illustrates the applied work for two different stress ratios. For the same stiffness of the panel, a higher stress ratio means that less cyclic work is done. This can be seen by comparing $U_{cyc,1}$ and $U_{cyc,2}$. From the hypothesis that FCG is SER dominated, less cyclic work implies smaller crack growth, as illustrated in Figure 3.1 by means of da_1 and da_2. The corresponding SER, illustrated in the Figure 3.1d and Figure 3.1e, is in this case therefore smaller for a higher stress ratio. From this theory, it is expected that the fatigue life of experiments subject to a higher stress ratio is longer.
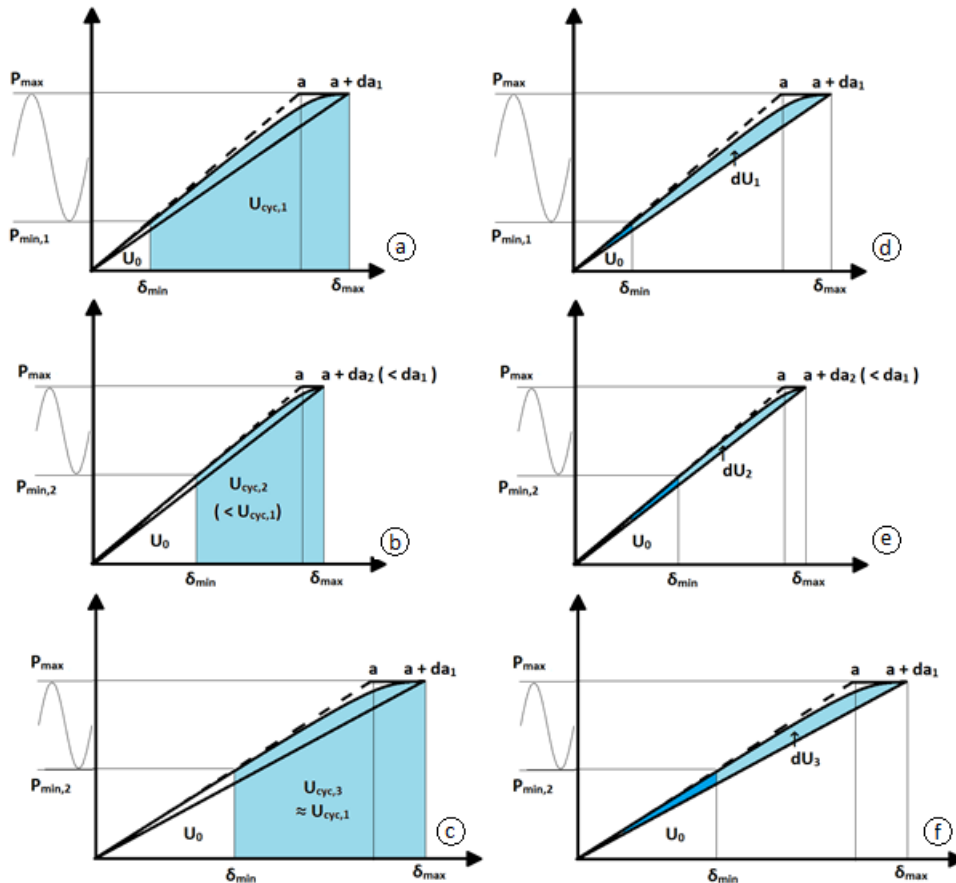
Figure 3.1: Figures abc: Illustration of Applied Cyclic Work for Two Stress Ratios with Corresponding Crack Growth. Figures def: Total and Cyclic Strain Energy Release Corresponding to Crack Growth of Figures abc – No Plasticity Included.

At some point, the stiffness of the panel subject to the higher stress ratio will be such that the applied cyclic work $U_{cyc,3}$ is approximately equal to $U_{cyc,1}$ as illustrated in Figure 3.1c. In this case, the crack increment da is equal to the crack increment in Figure 3.1a. However, the decreased stiffness means that more energy is dissipated as indicated by dU_3 in Figure 3.1f. Therefore, for a similar crack increment da the SER changes with a changing stress ratio. In dU/dN-da/dN plots as such an 'R-effect' may appear.

If it is assumed that the stress ratio has no influence on crack surface roughness and plastic zone, Alderliesten's SER theory implies that the same amount of work applied creates a similar crack length da. in general good correlation should be obtained in dU/dN-da/dN plots. If 'R-effects' arise they should be largely explainable by means of surface roughness and plasticity. If S_{max} is varied, this should also appear as an 'S_{max}-effect': More energy per cycle is dissipated for higher S_{max} for instance through plasticity. Obviously this theory should still be valid in vacuum. Therefore similar trends are expected

in the experimental results of both air and vacuum environment assuming the second hypothesis discussed in Section 3.1 is correct.

Of course there might be discrepancy between *dU/dN-da/dN* plots in vacuum and air, because of a difference in energy dissipation mechanisms such as surface roughness and plasticity. It is therefore important to monitor both mechanisms, in order to research if any discrepancy in energy dissipation between air and vacuum environment can be traced back by means of one of these mechanisms.

3.2.2.1 Crack Closure Correction

From the theory discussed in Section 2.2.1.5, it is very likely that the crack close correction by Elber in fact is a cyclic energy correction. The first hypothesis of Section 3.1 implies that *R*-effect is an artefact of choosing *ΔK* for similitude. Alderliesten disputed crack closure because, according to crack closure theory, crack closure should still occur at very high applied stresses. That seems very unrealistic. Therefore it was hypothesised that S_{op} is only an artificial stress to correct for something that is actually a cyclic energy problem as already discussed in Section 2.2.1.5. It provides an explanation why in *dU/dN-da/dN* plots the *R*-effect would largely disappear: If the crack closure correction really is a cyclic energy problem, this 'correction' is already included if fatigue is approached from an energy perspective.

Despite the striking correlation between Alderliesten's *Y*-ratio and the *Y*-ratio based on SIF, as was illustrated in Figure 2.15, there is some discrepancy between both corrections at lower stress ratios. Regardless whether the non-linear load-COD behaviour is caused by plasticity induced crack closure or something else, it can also be approached from an energy perspective. This is illustrated in Figure 3.2.
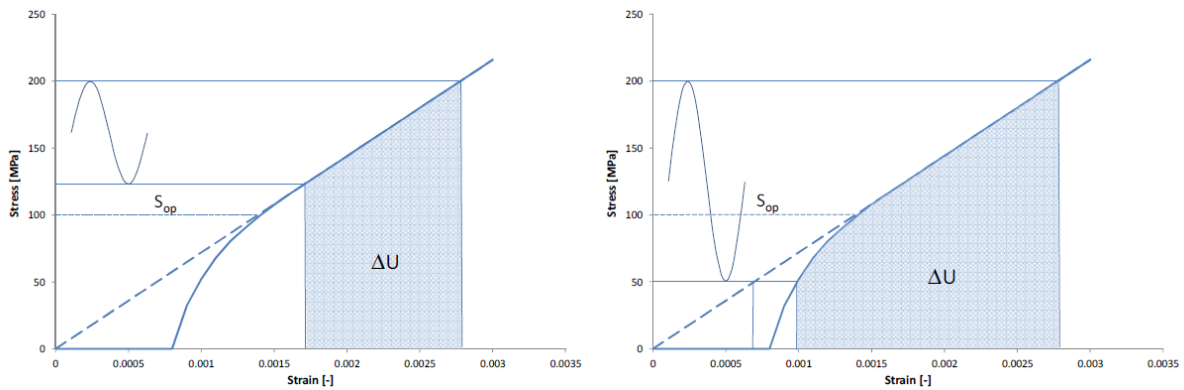
Figure 3.2: Cyclic Applied Work for Two Stress Ratios [30]

The non-linearity causes a decrease of applied cyclic energy for lower stress ratios in comparison with the applied cyclic energy if the load-COD graph would be linear. Also the artificial total applied energy decreases as the maximum displacement ε_{max} in Equation 2.20 (repeated here as Equation 3.10) decreases.

$$U_s = (S_{max} - S_{min})\varepsilon_{max}$$ <div style="text-align:right">*Equation 3.10*</div>

Experiments are designed to calculate this *Y*-ratio for multiple stress ratios at multiple crack lengths, such that it can be investigated if the discrepancy in Figure 2.15 can be accounted for.

4 Experiment Design

In Chapter 3 it was discussed what data is required in order to draw conclusions on the hypotheses of Section 3.1. This is shortly recapped in Section 4.1. Furthermore this chapter covers the design of the experiments. The specimen design is covered in Section 4.2, followed by the used test equipment covered in Section 4.3. Based on this, an initial crack is required as discussed in Section 4.4. The load spectrum and data acquisition program, test matrix and test procedure of the experiment design are covered in Sections 4.5, 4.6 and 4.7 respectively.

4.1 Required Data

This section shortly recaps what data is required to draw conclusions on the hypotheses for this research project as discussed in Section 3.1. On one hand this consists of describing the FCG process by means of stress intensity and on the other hand this consists of approaching fatigue by means of SER. This is done in both air and vacuum environment. Furthermore the crack closure mechanism is monitored in both environments.

For describing the FCG process based on stress intensity, the following data is required:

- Applied S_{max} and S_{min}
- The crack length a at cycle N
- The load-COD diagram for multiple crack lengths a
- The plastic zone size

And for describing the FCG process based on SER, the following data is required:

- Applied S_{max} and S_{min}
- The crack length a at cycle N
- The displacement at S_{max} and the displacement at S_{min} at cycle N
- The load-COD diagram for multiple crack lengths a
- The plastic zone size
- Crack surface roughness

4.2 Specimen Design

The main criteria for the specimen design is that the specimens fit in the Material Test System (MTS) from the Delft Aerospace Structures and Materials Laboratory (DASML). Furthermore it is aimed for to reproduce the specimens used by Elber as much as possible, as Elber's experimental results are a keystone in conventional SIF based FCG theories.

The used MTS bench is a 200 kN bench, and clamps of 160 mm width are used. Therefore the specimen width is also designed at 160 mm. The thickness of the specimen is 5 mm, equal to the thickness of the test specimens of Elber. As such, the tests take place under the same plane stress conditions as Elber's tests. The length of the specimen is designed rather arbitrarily at a length of 350 mm. A schematic of the specimen with corresponding dimensions is given by Figure 4.1.

The chosen material is Aluminium 2024-T3, as this is a frequently used aerospace material and commonly used for experimental tests. Furthermore this material clearly shows striations, which may provide information about the crack surface roughness. Most important is that the same material is used by Elber. The material properties for Aluminium 2024-T3 are provided in Table 4.1. The specimens are produced out of the same material batch, in order to eliminate possible manufacturing defects.
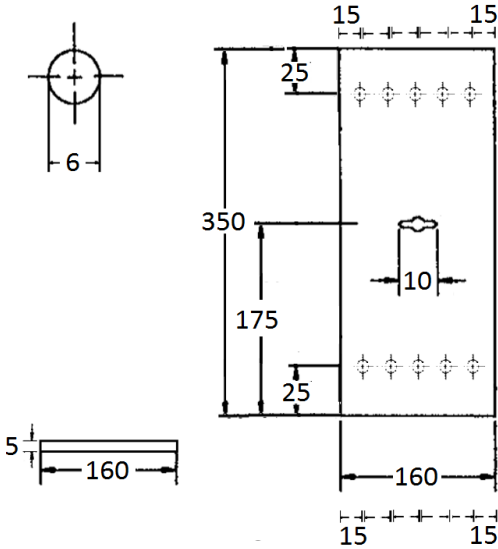
Figure 4.1: Specimen Design

Symbol	Value	Unit
C	2.44E-08	-
m	2.601	-
p	0.5	-
q	1	-
E	73.08	*GPa*
v	0.33	-
K_c	31.87	*MPa√(m)*

Table 4.1: Aluminium 2024-T3 Properties [54]

4.3 Test Equipment

Obviously to obtain the required data discussed in Section 4.1, test equipment is needed. The used fatigue machine is already mentioned in the previous section, and is the 200 kN MTS fatigue bench available in DASML. For the experiments in vacuum environment, a vacuum chamber is installed in the fatigue bench. The tests in vacuum are executed at a pressure *p* of approximately $1\cdot10^{-8}$ bar, because this is the same vacuum environment as the vacuum environment during tests by Kirby and Beevers discussed in the literature review. In the following the test equipment used to obtain the required data listed in Section 4.1 is discussed.

4.3.1.1 Applied Stress

The MTS software contains a procedure application where the test procedure and frequency of data acquisition can be controlled. This is further explained in Section 4.5. The applied loads are controlled by the MTS software and data on the applied loads is collected by the MTS software through calibrated sensors embedded in the MTS fatigue bench.

4.3.1.2 Crack Length

To monitor the crack length *a*, cameras are used. The camera takes a photo every *ΔN* cycles of the specimen. As such it can be traced back at what time in the FCG process the photo is taken. If a strip of graph paper is added below the initial crack, the length of the crack can then simply be determined by the naked eye as shown by Figure 4.2.
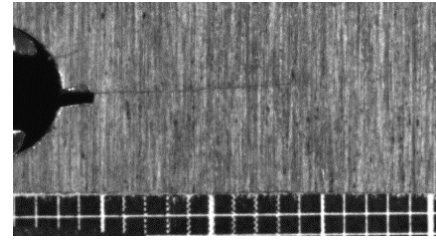
Figure 4.2: Crack Length Measurement

4.3.1.3 Displacement

The minimum and maximum displacement of the specimen at the corresponding minimum and maximum applied load is monitored by the MTS machine. However, the displacement detectors of the MTS include the displacement of the clamps and the vacuum chamber. As it is unknown what the effect thereof is, the displacement is also measured using an extensometer and video image correlation (VIC). The correlation between these measurement techniques is further covered in Section 6.5.1.

4.3.1.4 Load-COD Graphs

For the load-COD graphs, the crack opening in the centre of the specimen is measured. A COD-meter as illustrated in Figure 4.3 is used. The legs of the COD-meter are plugged through a notch in the specimen, the end of the legs hooked behind the other side of the specimen. While the crack opens, the legs of the COD-meter are opening equally therewith affecting the strain measured by the strain gauges. Early tests showed that the legs of the COD-meter available in DASML were too long for the tested specimens, because of a lack of sensitivity of the strain gauges. As such the COD was measured in the noise of the COD-meter, requiring the legs to be shortened. The legs were shortened through trial and error until the correct sensitivity was obtained to measure crack closure.

As for the tests in vacuum environment it is impossible to use a COD-meter for load-COD measurements, the load-COD is also measured using VIC. A speckle pattern of approximately 3x3 pixels is created at the specimen surface. Two High-Definition (HD) cameras are monitoring the movement of the speckles with respect to the speckle pattern before the test is started. It is aimed for to correlate the load-COD results measured by the COD-meter with the results measured by VIC-analysis. As such, the VIC-analysis can collect load-COD data for the vacuum experiments and no COD-meter is needed.
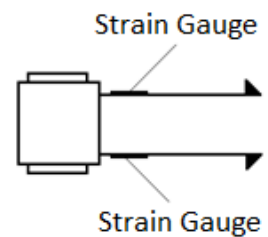
Figure 4.3: COD-meter

4.3.1.5 Plastic Zone and Crack Surface Roughness

Lastly the plastic zone and the crack surface roughness need to be monitored. The plastic zone is monitored using VIC data from COD-measurements. To monitor the crack surface roughness, the tested specimens are researched with the Scanning Electron Microscope (SEM) and the Laser Next Generation Olympus Laser Scanning (LEXT OLS) confocal scanning microscope.

4.4 Initial Crack

The specimen design was covered in Section 4.2. However, there is obviously an initial crack needed to initiate the FCG process. A hole is drilled in the centre of each specimen, needed to plug in the COD-meter as was explained in the previous section. As calibration of the COD-meter showed non-linearity except for the range from 6 to 9 mm, it was chosen to drill a hole of 6 mm diameter as such assuring that the COD is measured over the linear range of the COD-meter.

The pre-cracking is done by creating a sawcut. The length of the sawcut had to be at least 1 mm conform the ASTM E647 standard [53], but it was chosen to create an initial crack of approximately 2 mm to reduce FCG initiation time. It needs to be noticed that the sawcut needs to be created at a very

slow sawing pace. As such no plasticity is created, such that it cannot affect the FCG initiation process. The dimensions of the initial crack are also included in the specimen design sketch provided in Figure 4.1.

4.5 Load Spectrum and Data Acquisition Program

The MTS fatigue machine contains a procedure application. In this application the load spectrum and data acquisition procedure can be programmed. The load spectrum for this thesis is rather simple. As was mentioned multiple times throughout this report, only constant amplitude loading is considered as the main priority of this research is to investigate the physics behind fatigue. The test program is illustrated by means of a block diagram in Figure 4.4.
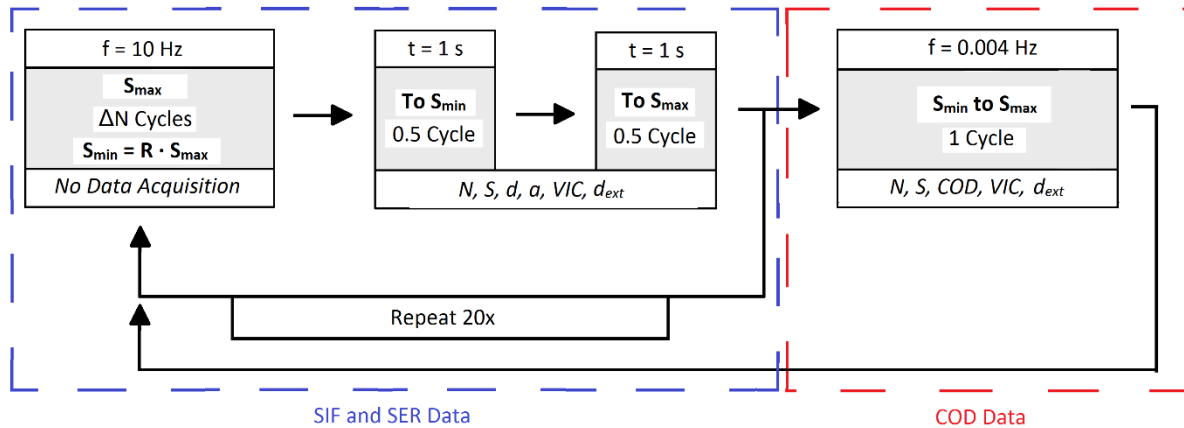
Figure 4.4: Data Acquisition Program

The applied minimum and maximum load is calculated with Equation 4.1 such that the load introduces the desired stress in the specimen.

$$P = SA$$

<div align="right">*Equation 4.1*</div>

The load is sinusoidal shaped and controlled by the MTS procedure application. Tests are performed for a variety of S_{max} and stress ratios R, as shown in Section 4.6.

A block of ΔN cycles is applied without data acquisition in order to keep the amount of data within control. ΔN changes for each test, but is always chosen such that at least 200 data points are obtained for SER calculations. As it was unknown how fast the crack would grow, and thus how large ΔN needed to be, the first few tests ΔN was conservatively based on AFGROW calculations and after the first few tests changed by trial and error. The load frequency is 10 Hz, because for a higher frequency there is a risk that the fatigue machine will start to vibrate in the eigenfrequency of the laboratory floor.

At every block of ΔN load cycles the machine program is interrupted and for one second the minimum load is applied, followed by one second of maximum applied load. In both cases the following data is gathered: The current load cycle N, the minimum and maximum applied stress S, the minimum and maximum displacement d measured by the MTS, a photo to measure crack length a, a photo for VIC-analysis and minimum and maximum displacement d_{ext} measured by the extensometer. This procedure is repeated twenty times.

After each repetition of twenty blocks, for one cycle the applied load is slowly increased from S_{min} to S_{max} at a frequency of 0.004 Hz. During this part of the procedure the following data is gathered: The number N of the current cycle, the stress S, the COD, a photo for VIC-analysis and the displacement measured by the extensometer. For the last block all data except the VIC-data is monitored with an

interval of 0.25 s. The VIC-software was not capable to process the signals by the MTS quick enough. According to ASTM E647 [53] for COD measurements at least 50 data points are needed for reliable results, hence the frequency was adapted to 0.004 Hz such that enough VIC data points are obtained. The entire process provided in Figure 4.4 is repeated until complete failure of the specimen.

4.6 Test Matrix

The experimental tests are performed for multiple specimens for a varying range of S_{max} and R. A test matrix is provided in Table 4.2.

Specimen ID	Environment	S_{max} [MPa]	R [-]	T [°C]	Humidity [%]	ΔN [cycles]	p [bar]
AR002S75	Air	75	0.02	22	55	500	≈ 1
AR005S75	Air	75	0.05	24	51	500	≈ 1
AR01S75	Air	75	0.1	21	57	500	≈ 1
AR03S75	Air	75	0.3	22	50	1000	≈ 1
AR05S75	Air	75	0.5	23	49	1500	≈ 1
AR005S100	Air	100	0.05	23	47	250	≈ 1
AR03S100	Air	100	0.3	25	43	500	≈ 1
VR002S75	Vacuum	75	0.02	22	49	500	≈ $1.2 \cdot 10^{-8}$
VR005S75	Vacuum	75	0.05	24	52	2000	≈ $1.1 \cdot 10^{-8}$
VR01S75	Vacuum	75	0.1	22	57	2000	≈ $1.9 \cdot 10^{-8}$
VR03S75	Vacuum	75	0.3	23	58	2000	≈ $1.3 \cdot 10^{-8}$
VR05S75	Vacuum	75	0.5	24	43	5000	≈ $1.1 \cdot 10^{-8}$
VR005S100	Vacuum	100	0.05	24	47	1200	≈ $1.4 \cdot 10^{-8}$
VR03S100	Vacuum	100	0.3	22	52	3000	≈ $1.6 \cdot 10^{-8}$

Table 4.2: Test Matrix

The temperature and humidity level were obviously not known beforehand, but they have been added to the test matrix table for a quick and clear overview of the test conditions for each specimen. *ΔN* is the cyclic interval where no data has been gathered, as was discussed in Section 4.5 and *p* shows the approximate pressure conditions for the experiments. As was discussed in Section 4.3, for vacuum it was aimed to experiment with a pressure of approximately $1 \cdot 10^{-8}$ bar, based on similar test conditions by vacuum tests of Kirby and Beevers [29].

4.7 Test Procedure

So far this chapter has discussed the specimen design, the test equipment used to gather the required data, the applied load spectrum and data acquisition program and also the test matrix has been provided. Combining all this information results in a sensitive step-by-step test procedure to ensure all required data can be correctly obtained:

- First the clamps are mounted at the ends of the specimen. It is important to include a piece of paper between the clamps and the specimen, to avoid a stress concentration potentially initiating a fatigue crack in the clamp.
- Before the specimen is placed In the fatigue machine, the load detector of the machine is zeroed. As such it can be easily determined if the specimen is already subject to a stress once the specimen is placed in the fatigue machine.
- Once the specimen is placed in the MTS bench, also the displacement sensor of the MTS is zeroed.

- To ensure the correct loads are applied by the test machine, the specimen control parameters need to be determined. This is done by auto-tuning the fatigue machine, it will then automatically determine the required control parameters.
- The COD-meter and extensometer are placed and connected with the MTS sensors. Both measurement tools are zeroed.
- The VIC- and crack length measuring cameras are installed and lamps are added to increase the photo quality.
- The VIC cameras are calibrated using VIC-3D software.
- For the experiments in vacuum environment, then first the compressors for the vacuum chamber are turned on to obtain the desired vacuum level of approximately $1 \cdot 10^{-8}$ bar.
- The load spectrum and data acquisition program is set: The required ΔN, P_{max} and P_{min} are filled in. Important is that for vacuum tests an extra 1.045 kN needs to be added to the required applied load, because the vacuum chamber is applying this as a compressive force on the specimen once the chamber is at vacuum.
- The test is started by starting the program from the previous bullet point discussed in Section 4.5. This program is repeated until complete failure of the specimen.

- After the test, the specimens are cut such that the crack surfaces can be investigated under the SEM and LEXT OLS microscope.

5 Pre-study based on AFGROW and FEA

In advance of the experiments conducted, it was decided to perform a rather simple numerical analysis using FCG prediction software AFGROW and Finite Element Analysis (FEA) software ABAQUS on crack growth rate as function of dissipated strain energy. The goal of this analysis is to determine if any correlation can be observed for the crack growth rate for different load conditions, and whether or not they are in line with the expectations conform the theory in Section 3.2. In Chapter 6 it can then be analysed if results from experimental tests are conform the theory and/or FEA. Furthermore the FEA simulations might be a useful indication of the required route for the development of a new FCG prediction model based on SER. The numerical analysis does not include surface roughness effects, environmental effects and neither does it model the plastic wake. Section 5.1 covers the AFGROW simulation, Section 5.2 the ABAQUS Finite Element (FE) model and Section 5.3 the combined results.

5.1 AFGROW Simulation

For the prediction of FCG, AFGROW is commonly used software. The used model is a hole with a double through-crack as illustrated in Figure 5.1, the corresponding dimensions are given in Table 5.1.
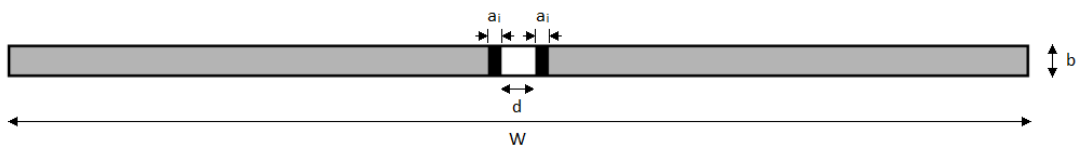
Figure 5.1: Illustration of AFGROW Model

Symbol	Value	Unit
W	160	*mm*
b	5	*mm*
d	6	*mm*
a$_i$	2	*mm*

Table 5.1: Dimensions of AFGROW Model

As this Master thesis is restricted to constant amplitude loading, the applied load spectrum is a constant amplitude load spectrum. But different maximum stresses and different stress ratios are applied. The used material is defined as *Aluminium 2024 – T3 Clad; plt & sht; T-L* taken from AFGROW's material database.

The used equation for FCG in AFGROW is NASGRO, this equation is given by Equation 5.1.

$$\frac{da}{dN} = C \left(\frac{1-f}{1-R} \Delta K \right)^m \frac{\left(1 - \frac{\Delta K_{th}}{\Delta K} \right)^p}{\left(1 - \frac{K_{max}}{K_c} \right)^q} \qquad\qquad \textit{Equation 5.1}$$

In this equation C, m, p and q are material constants, ΔK and ΔK_{th} are the effective and threshold SIF ranges respectively, K_{max} and K_c are the maximum and critical SIF and f is K_{op}/K_{max} where K_{op} is the opening SIF. For the used material the material constants and properties are provided in Table 4.1.

5.2 The Finite Element Analysis Simulation

To calculate the energy dissipated during the FCG process predicted by AFGROW, a method based on the energy balance discussed in Section 2.2.2.2 is used. The energy balance is repeated here as Equation 5.2.

$$U_{in} = U_{out} + U_{rel} \qquad \qquad \textit{Equation 5.2}$$

The theory to determine the energy dissipation using FEA is shortly covered in Section 5.2.1, and then the ABAQUS FEA results are covered in Section 5.2.2.

5.2.1 Energy Balance Method for FE Simulation

In Section 3.2.2 it is assumed that the applied energy U_{in} at load cycle $N+\Delta N$ is equal to the energy U_{out} at load cycle N. Or conform the same assumption: The applied work U_{in} at crack length $a + da$ is equal to the work U_{out} at crack length a as given by Equation 5.3.

$$U_{out,a} = U_{in,(a+da)} \qquad \qquad \textit{Equation 5.3}$$

To obtain an expression describing how the strain energy input U_{in} changes for a specimen with an increasing crack length a compared to a specimen without a crack, the parameter F is introduced by means of Equation 5.4.

$$F(a) = \frac{U_{in,a}}{U_{in,a=0}} \qquad \qquad \textit{Equation 5.4}$$

As such, Equation 5.3 and 5.4 can be combined to rewrite the energy balance given by Equation 5.2 as Equation 5.5.

$$U_{rel} = U_{in,a=0}[F(a) + F(a + da)] \qquad \qquad \textit{Equation 5.5}$$

By taking the derivative with respect to a an expression is obtained for the average SERR given by Equation 5.6.

$$\frac{dU_{rel}}{da} = U_{in,a=0}\frac{dF(a)}{da} \qquad \qquad \textit{Equation 5.6}$$

As was discussed in Section 2.4 the focus of this research is on the dissipated strain energy per cycle in order to understand the physics behind fatigue. The SERR of Equation 5.6 is therefore rewritten to Equation 5.7 using the chain rule. In this equation da/dN is the FCG rate as simulated with AFGROW in Section 5.1.

$$\frac{dU_{rel}}{dN} = \frac{dU_{rel}}{da}\frac{da}{dN} \qquad \qquad \textit{Equation 5.7}$$

5.2.2 The ABAQUS Finite Element Model

So in order to obtain the dissipated energy per cycle, an expression for F is needed by calculating the energy input for a varying crack length. This expression for F is obtained by creating a FE model in ABAQUS. The complete specimen is modelled as a 2D planar shell with a thickness of 5 mm, with material properties equal to the material properties used in the AFGROW analysis provided in Table 4.1.

For meshing, standard quad dominated elements are used and considering the simplicity of the model it is safe to assume that linear reduced integration provides enough accuracy. The top and bottom of the model are partitioned conform the size of the clamps, such that boundary conditions can be applied as realistically as possible. The bottom partition is completely clamped and the top partition is restricted to displacement in U2 (vertical) direction. A reference point is introduced and linked with the top partitioning, such that a load can be applied at the reference point resulting in the desired stress in the actual specimen.

As the energy input needs to be obtained for increasing crack length *a*, the FEA is performed for multiple crack lengths. These cracks are modelled as a seam, meaning the model does not include surface roughness effects. Furthermore the model does not include plastically dissipated energy from previous load cycles. However, the aim of this pre-study is not to accurately simulate the experiments, but more a way to evaluate to observed trends and to determine if the results are globally conform the theory from Chapter 3.
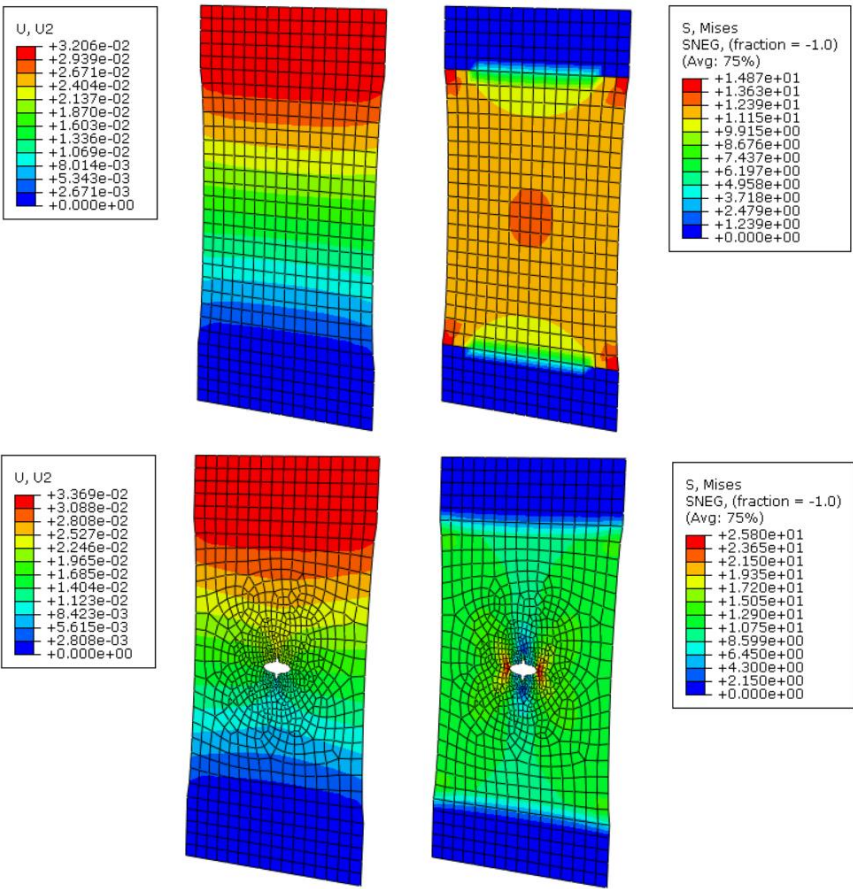
Figure 5.2: FE Results of Displacement and Von Mises Stress for Uncracked Plate (Top) and Plate with 12 mm Crack (Bottom), Scale Factor 100x

Figure 5.2 shows the ABAQUS FE model displaying the displacement and the Von Mises stress for the uncracked specimen and a specimen containing a 12 mm crack. The elastic zone can be clearly seen for the 12 mm crack, but for this numerical pre-study the displacements are most important. The maximum displacement for the (average) top and bottom nodes at the partitioning (representing the end of the top and bottom clamp respectively) are monitored in order to calculate the energy input by means of Equation 5.8.

$$U_{in,a} = 0.5P_{max}(d_{top} - d_{bottom})$$ *Equation 5.8*

This was calculated for multiple crack lengths, the results are shown by means of the black dots in Figure 5.3.
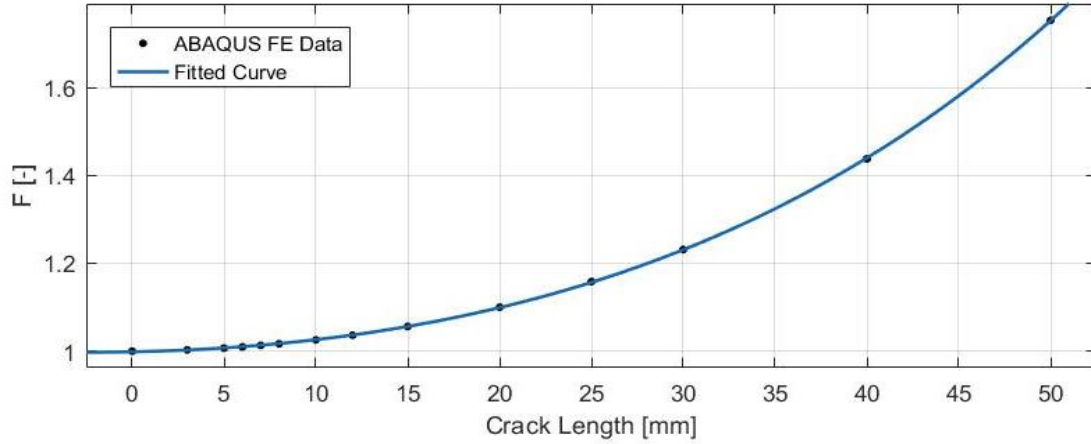
<p align="center">*Figure 5.3: Crack Length vs F determined by FEA*</p>

The figure also shows the fitted two-term exponential function. This function is given by Equation 5.9 and the coefficients are provided in Table 5.2.

$$F(a) = p_1 e^{p_2 a} + p_3 e^{p_4 a}$$ *Equation 5.9*

Coefficient	Value	95% Confidence Bounds
p_1	0.7268	$0.6995 - 0.7542$
p_2	-0.0107	$-0.0122 - 0.00917$
p_3	0.2718	$0.2433 - 0.3002$
p_4	0.03171	$0.03033 - 0.03308$
Equation	R^2	RMSE
Equation 5.9	1.000	0.001085

<p align="center">*Table 5.2: Coefficients for Fitted Curve Equation 5.9*</p>

However, to calculate the SERR and eventually *dU/dN*, the derivative of this equation with respect to *a* is needed. This is given by Equation 5.10.

$$\frac{F(a)}{da} = p_1 p_2 e^{p_2 a} + p_3 p_4 e^{p_4 a}$$ *Equation 5.10*

5.3 Results

Using AFGROW, FCG data for multiple load conditions is simulated. Using ABAQUS, the parameter *F* is obtained needed to calculate the SERR. The SERR is calculated using Equation 5.11 and 5.12 for total and cyclic SERR respectively.

$$\frac{dU_{tot}}{da} = \frac{S_{max}^2}{2E} HWt \frac{dF(a)}{da}$$ *Equation 5.11*

$$\frac{dU_{cyc}}{da} = \frac{S_{max}^2}{2E}(1 - R^2)HWt \frac{dF(a)}{da}$$ *Equation 5.12*

In these equations S_{max} is the maximum applied stress in MPa. *E* is Youngs Modulus of the material in MPa, and *R* is the stress ratio. *H, W* and *t* are respectively the height, width and thickness of the specimens in mm. The unit of the SERR as such becomes J/mm, indicating how much strain energy is required to create a crack length *a* in mm. To obtain *dU/dN* this SERR is then multiplied by *da/dN* with

simulation results from AFGROW, such that the unit becomes J/cycle (the amount of strain energy dissipated per load cycle). The results for the total and cyclic SER per cycle for a range of stress ratios and two different S_{max} are displayed in Figure 5.4.
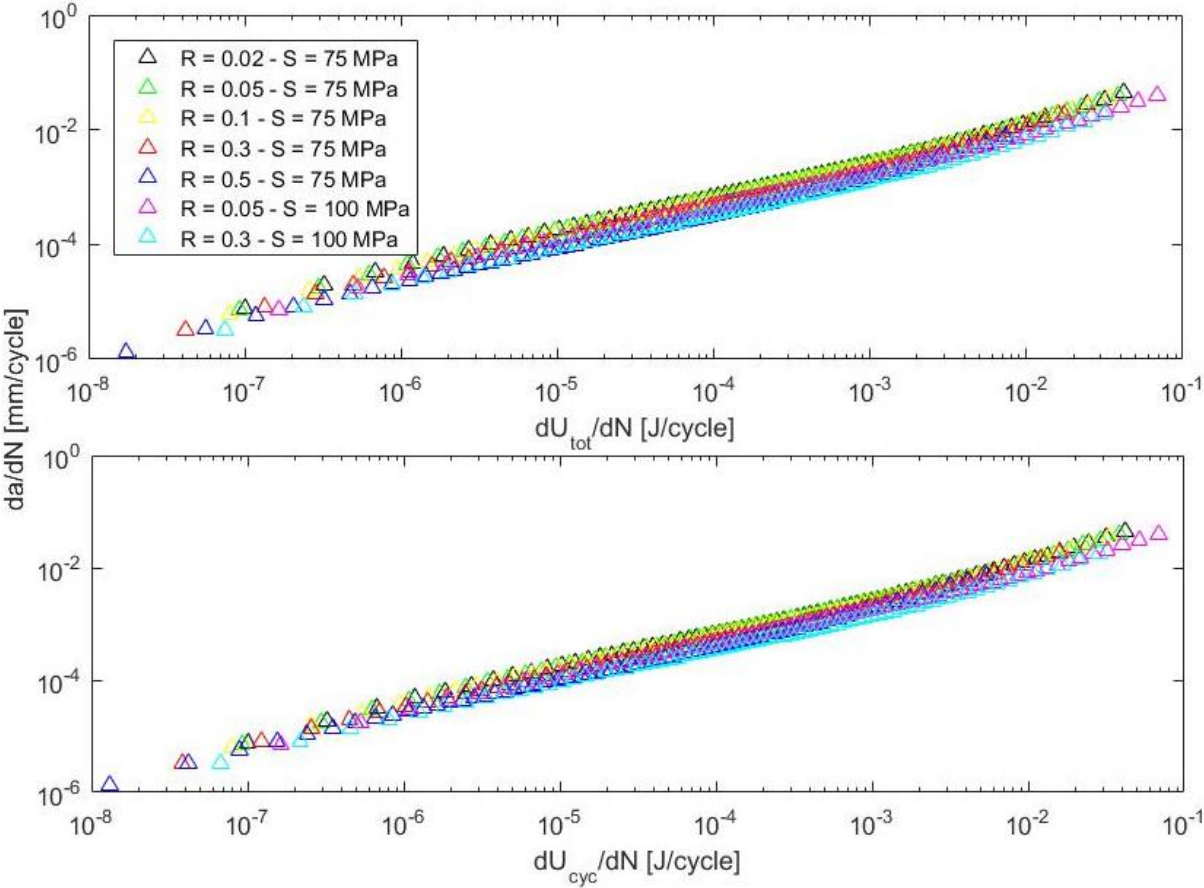
Figure 5.4: Results of Numerical Analysis of SER versus Crack Growth Rate

The results of the numerical study show good correlation, and the outcome is conform expectations as discussed in Section 3.2.2. Figure 5.4 clearly shows that for a fixed S_{max} the SER correlates very well with the FCG rate. But still there is a slight 'R-effect' visible. Furthermore the results show better correlation if the cyclic dissipated energy is considered instead of the total dissipated energy. Also an 'S_{max}-effect' is present, also conform the theory discussed in Section 3.2.2.

The results of the numerical analysis again indicate that fatigue should be approached from a SER perspective. However, with the numerical analysis in mind, experimental tests should confirm these findings. Furthermore the experiments include energy dissipation mechanisms such as crack surface roughness and plastically dissipated energy, which are energy dissipation mechanisms not included in this numerical analysis. Furthermore more detailed research is required to determine how these kind of analyses can be used in the development of a proper FCG prediction method based on SER.

6 Results

This chapter presents the results of the experiments. The experiment results are divided into four main measurement categories: The crack growth measurements, energy measurements, COD measurements and plastic zone and crack surface roughness measurements. For the presentation of the measurement data, a fixed method is used as is discussed in Section 6.1. Then the fatigue life results are briefly covered in Section 6.2. Section 6.3 provides the crack growth rate determination followed by FCG descriptions based on SIF in Section 6.4. Then obtained data for energy considerations and the processing thereof are covered in Section 6.5. FCG is described based on SER in Section 6.6, followed by the results related to plasticity induced crack closure in Section 6.7. Furthermore results on treating the crack closure correction from a SER perspective are provided in Section 6.8, followed by the results on plasticity and crack surface roughness in Section 6.9 and Section 6.10 respectively.

6.1 Presentation of Experimental Data

As in this thesis many comparisons are made, a fixed colour and symbol code scheme is applied. As such it is aimed for to obtain an easy and quick overview for comparison purposes. The main comparisons for this research are based on stress ratio, maximum stress and environmental test conditions. The code scheme to indicate to what conditions the experiment has been subject to is provided in Table 6.1.

R [-]	0.02	0.05	0.1	0.3	0.5	0.05	0.3
S_{max} [MPa]	75	75	75	75	75	100	100
Air	*	*	*	*	*	*	*
Vacuum	O	O	O	O	O	O	O

Table 6.1: Colour Scheme used for Presentation of Experimental Data

6.2 The Fatigue Life

First of all some general FCG results are presented. Figure 6.1 shows the number of cycles to failure, N_f, for each tested specimen.
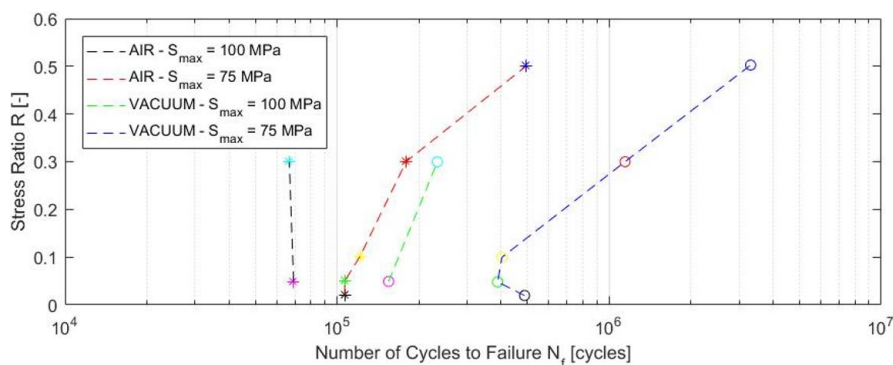
Figure 6.1: Fatigue Life of Tested Specimens

As can be seen from the figure, the number of cycles to failure increases for a higher stress ratio which is conform the expectation discussed in Section 3.2.2. The only outliers are a specimen tested in air with a stress ratio of 0.3 and S_{max} of 75 MPa (fatigue life too short conform expectations) and a specimen tested in vacuum with a stress ratio of 0.02 and S_{max} of 75 MPa (fatigue life too long conform expectations). However, this is a result of the fact that the sawcuts in these specimens were too long and too short respectively, affecting the initiation period.

Furthermore, if the stress ratio is kept constant, it can be noticed that the fatigue life is longer for specimens subject to a lower S_{max}. Also from Figure 6.1 it can be seen that the fatigue life of specimens tested in vacuum environment is considerably larger than specimens tested in air. This is all conform earlier research by for instance Schijve [58], whose results are provided in Figure 6.2.
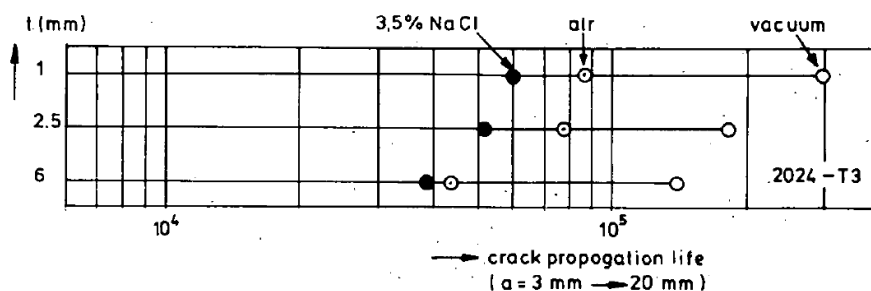
Figure 6.2: Fatigue Life of Tested Specimens by Schijve – Shows Similar Result with Figure 6.1 [58]

The difference in fatigue life between experiments in air and vacuum is mainly due to a significantly longer crack initiation period in vacuum compared to air. It is unknown what causes such a significant difference in crack initiation, but as for this research only FCG is considered no further attention is paid.

6.3 Crack Growth Rate

For both the SIF approach and the SER approach, it is required to determine the FCG rate at every load cycle N during each test. To obtain this crack growth rate, an N-a plot is needed. In Section 4.5 it was discussed how after every ΔN block of load cycles a variety of data is collected. However, this ΔN is chosen such that enough data points are obtained for SER analysis purposes. As crack length data is gathered over the same interval of ΔN blocks, too many data points are gathered to accurately read off the crack length for each block of ΔN load cycles.

As such, it is assumed that 25 data points per experiment are sufficient to determine a realistic curve fit for the entire crack growth. The camera capture software enables to save the images with a file name containing the corresponding total number of applied load cycles. As such the 25 crack length data points can be easily plotted as a function of applied load cycles N.

However, as using graph paper to read off the crack growth length causes some inaccuracy, the incremental polynomial method conform the ASTM E647 standard [53] using MATLAB is applied to reduce the inaccuracy. This method involves fitting a local second-order polynomial to sets of *(2n+1)* successive data points and then recalculate a using the local polynomial fit. As 25 data points are considered for each test, it is decided to perform the method for *n = 2*. The recalculated crack lengths are plotted in Figure 6.3 for specimen AR005S75. The data for all other specimens are obtained by the same procedure and can be found in Appendix A.
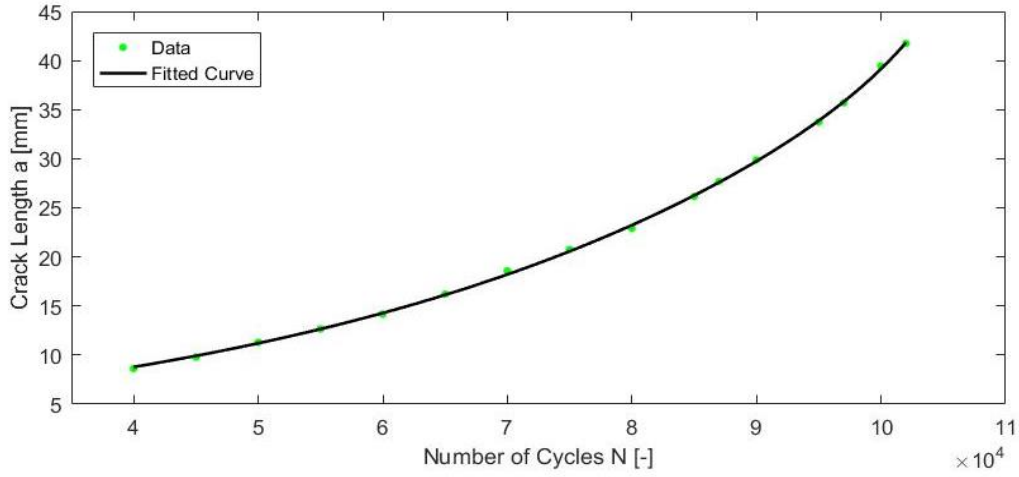
Figure 6.3: N-a Curve for Specimen AR005S75

A two-term exponential curve based on the Least Squares Method (LSM) is fit through the data points using MATLAB. The general equation for this two-term exponential is given by Equation 6.1.

$$a = p_1 e^{p_2 N} + p_3 e^{p_4 N} \qquad\qquad\qquad\qquad\qquad\qquad\qquad \textit{Equation 6.1}$$

In Figure 6.3 the fitted curve is plotted as the black line for specimen AR005S75. The corresponding parameters and quality of the fit are provided in Table 6.2.

Coefficient	Value	95% Confidence Bounds
p_1	3.326	$3.164 - 3.488$
p_2	2.429E-05	$2.362\text{E-}05 - 2.497\text{E-}05$
p_3	2.2E-10	$-3.548\text{E-}09 - 3.987\text{E-}09$
p_4	2.258E-04	$6.011\text{E-}06 - 3.915\text{E-}04$
Equation	R^2	RMSE
Equation 6.1	0.9997	0.205

Table 6.2: Coefficients for Fitted Curve Equation 6.1

The fitted curves for all other specimens are provided in Appendix A. The final step to calculate *da/dN* is taking the derivative of Equation 6.1 given by Equation 6.2.

$$\frac{da}{dN} = p_1 p_2 e^{p_2 N} + p_3 p_4 e^{p_4 N} \qquad\qquad\qquad\qquad\qquad\qquad \textit{Equation 6.2}$$

6.4 FCG from Stress Intensity Perspective

So for every cycle *N*, the crack growth rate at that point can be calculated with Equation 6.2. The crack length at the same load cycle *N* can be calculated using Equation 6.1. This section will present the FCG data if fatigue is considered from a stress intensity perspective. Section 6.4.1 shows the results for FCG in air and Section 6.4.2 shows the results for FCG in vacuum.

The determination of *ΔK* has actually already been covered in Section 3.2.1. With the crack length known, by using Equation 6.1, the SIF *ΔK* corresponding to a certain FCG rate can be calculated using Equation 6.3.

$$\Delta K = \beta \Delta S \sqrt{\pi a} \qquad\qquad\qquad\qquad\qquad\qquad\qquad\qquad \textit{Equation 6.3}$$

ΔS is the applied S_{max} - S_{min} in MPa and *a* is the crack length in mm. β is the geometry correction factor needed because the specimen is a finite plate, and given by Equation 6.4.

$$\beta = \sqrt{sec\left(\frac{\pi a}{W}\right)}$$

In this equation *W* is the width of the specimen in mm and *a* the crack length in mm.

6.4.1 Air Environment

The results for all experiments have been plotted in a single double-log scaled figure for each testing environment in order to compare the *R*- and S_{max}-effect. The test results for the experiments in air environment are provided in Figure 6.4.
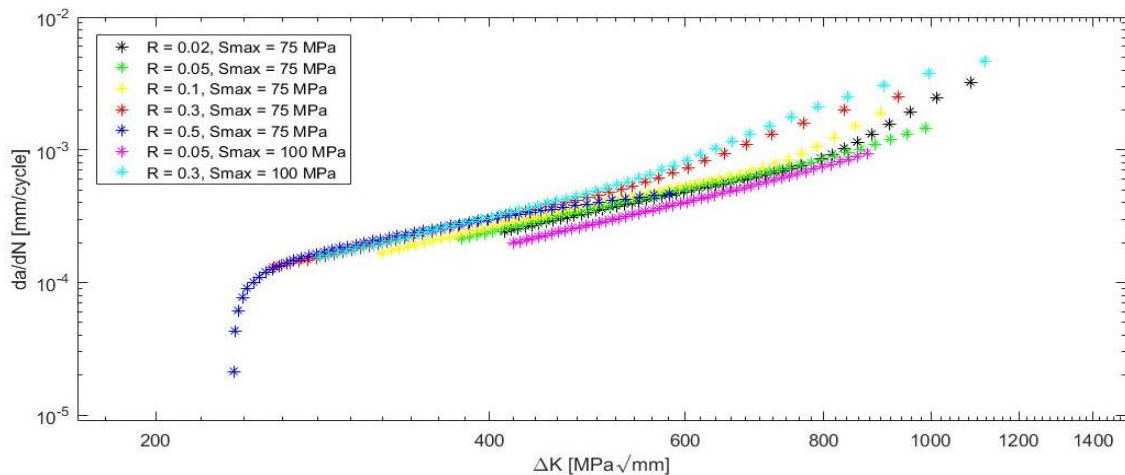
Figure 6.4: FCG Description based on SIF ΔK - Air

For stress ratios of 0.3 and higher, especially the FCG rates until a *ΔK* of approximately 600 MPa√mm need to be considered as for higher *ΔK* the FCG rate starts to approach the stable tearing crack growth region. For stress ratios lower than 0.3 this point is at a SIF of approximately 800 MPa√mm. As can be observed from the figure, in air there is a clear *R*-effect. This is what was expected based on the conventional theories of fatigue as discussed in Section 2.1.

The only slight exception is the FCG rate of the specimen tested with a stress ratio of 0.5. From the threshold $ΔK_{th}$ to a *ΔK* of approximately 400 MPa√mm the FCG rate of this test is still conform expectation, but then the FCG rate starts to drop in comparison with experiments subject to a different stress ratio. The frequency of data acquisition might have been too low for this experiment. In other words, the block of *ΔN* load cycles for which no data was gathered might have been too large meaning that the FCG rate in the last phase of this experiment has not been properly monitored.

On the other hand are the results given in Figure 6.4 obtained over a range where actually data was gathered, meaning no extrapolation has taken place, meaning the results for *R* = 0.5 should still provide a correct representation of the FCG rate. The deviation from the trend observed for other stress ratios of the specimen subject to *R* = 0.5 is therefore unknown and can maybe be best referred to as the unpredictability of nature -or simply an error in measurements. The same counts for the test at an S_{max} of 100 MPa and stress ratio of 0.05: This FCG rate is slightly lower than the experiment with same stress ratio and an S_{max} of 75 MPa. Conform expectations these FCG results should correlate with each other, like the tests executed at a *R* = 0.3 do. The most important conclusion that can be drawn from Figure 6.4 is that an *R*-effect is visible conform expectations based on the literature study.

The conventional theories of fatigue explain this *R*-effect by means of plasticity induced crack closure as discussed in Section 2.1.2.6. The SIF range *ΔK* is therefore corrected to an effective SIF $ΔK_{eff}$. A widely used crack closure correction is the correction by Schijve, given by Equation 6.5 [1].

$$\frac{\Delta K_{eff}}{\Delta K} = 0.55 + 0.33R + 0.12R^2 \qquad\qquad\qquad \textit{Equation 6.5}$$

If this correction is applied over the results of Figure 6.4, Figure 6.5 is obtained. It can be easily observed that the FCG rate indeed correlates very well as a function of ΔK_{eff}, with a slight discrepancy of two experiments for abovementioned reasons.
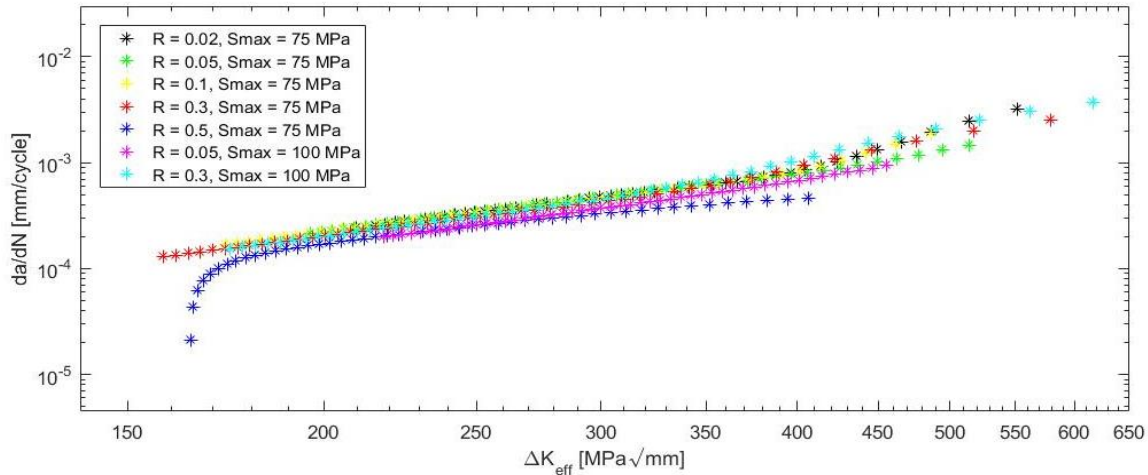
Figure 6.5: FCG Description based on effective SIF ΔK_{eff} - Air

6.4.2 Vacuum Environment

So far, all results from experiments in air environment are conform expectations and as such SIF based FCG theories do not show any cracks. In this section the experimental results for the tests in vacuum are presented.
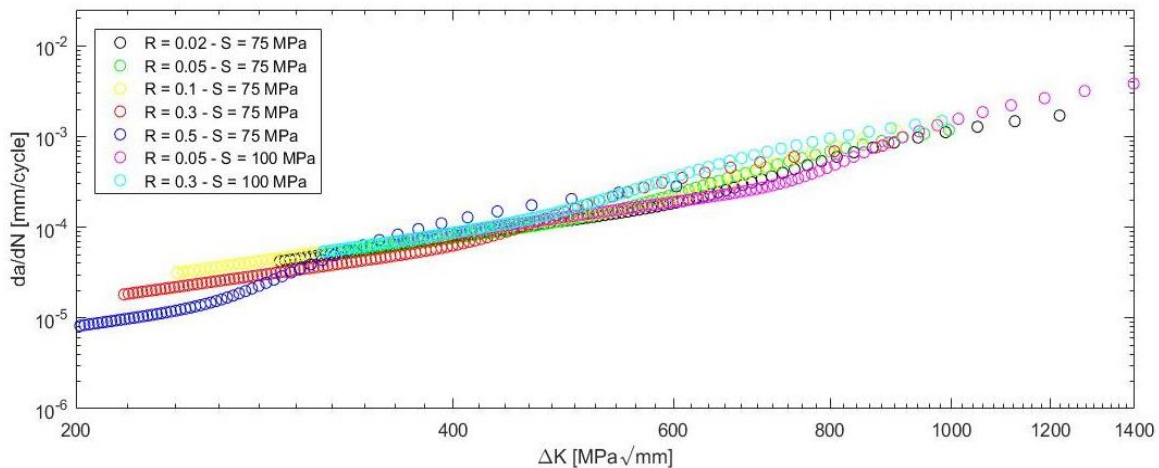
Figure 6.6: FCG Description based on SIF ΔK - Vacuum

Figure 6.6 shows the FCG rate as a function of ΔK in vacuum. It immediately catches the eye that from the clear R-effect in air, as displayed in Figure 6.4, is not much left in vacuum. From a SIF range of approximately 200-600 MPa√mm there is no R-effect at all. And if there is, it is the opposite R-effect as may be expected from the SIF based FCG theory discussed in Section 2.1.2.4.

For the ΔK range of approximately 600-850 MPa√mm the correlation is not as convincing anymore as for lower ΔK, and one could even observe an R-effect over this range. However, if this really is an R-effect conform the SIF based FCG theory, the offset between each FCG curve should be constant like

the case in Figure 6.4 for air. If this offset is not constant, it will be impossible to properly correlate the FCG rate using ΔK_{eff}.

To better illustrate that Figure 6.6 indeed does not show an R-effect equal as in Figure 6.4, it is decided to plot the FCG rate in vacuum also as a function of ΔK_{eff}. Applying the plasticity induced crack closure correction should in this case actually cause an R-effect instead of correlation as in Figure 6.5. The result of applying the crack closure correction of Equation 6.5 over the results of Figure 6.6 is shown in Figure 6.7.
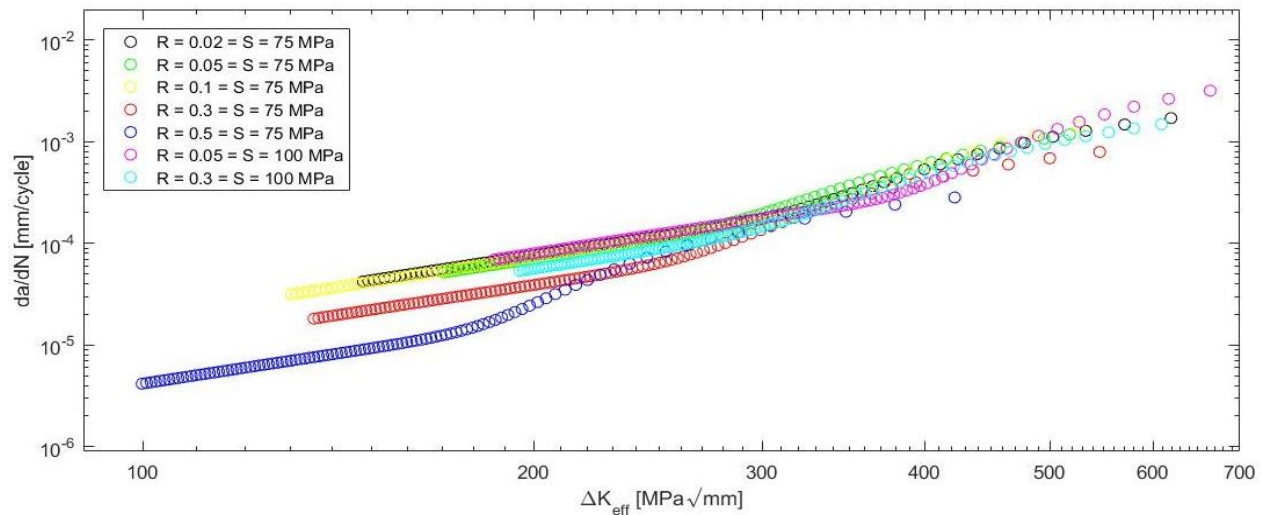
Figure 6.7: FCG Description based on Effective SIF ΔK_{eff} - Vacuum

Especially for lower ΔK_{eff} it can be observed that indeed an R-effect is introduced, confirming the missing R-effect for lower ΔK in Figure 6.6. This observation is conform the experimental results by Kirby and Beevers discussed in Section 2.2.1.4.

For the observed R-effect in Figure 6.6 over the range of approximately 600-850 MPa√mm, the correlation observed in Figure 6.7 indeed improves. But the correlation is by no means as clear as in air environment. Actually the only clear correlation occurs at a ΔK_{eff} of approximately 320 MPa√mm and afterwards again an R-effect is introduced. The R-effect in Figure 6.7, except for a ΔK_{eff} of 320 MPa√mm, confirms that such an R-effect is weak or absent in the FCG rate presentation of Figure 6.6 using ΔK.

To conclude, the overall range of ΔK in vacuum indicates in no way a convincing R-effect conform the conventional SIF based theories of fatigue as is the case in air. Or at least one could say that the results using ΔK as similitude parameter significantly differ in air and vacuum. As such one could say that ΔK, or ΔK_{eff}, are improper similitude parameter for FCG. A possible exception would be that the plasticity induced crack closure concept differs between air and vacuum environment. This is further researched in Section 6.7.

6.5 Energy Data

In Section 6.3 the crack growth rate was determined as a function of the applied load cycle N and in the previous section FCG was approached from a SIF perspective. To approach FCG also from a SER perspective, energy data is required. This section discusses how useful and reliable energy data is retrieved.

6.5.1 Correlation between Multiple Displacement Measurement Tools

The work applied at the specimen is calculated based on displacement measurements. As was mentioned in Section 4.3.1.3, the displacement is monitored by the MTS software. However, the displacement sensors in the clamps are not measuring the displacement of the actual specimen, but include the displacement of the clamps itself and in case of vacuum also the displacement of the vacuum chamber. Therefore the displacements are also measured using an extensometer and VIC analysis. This section covers the correlation between the three measurement tools.

As each measurement tool measures the displacement between two different points on the specimen, it is useless to correlate the absolute displacements. As such the strain is considered instead of the absolute displacement. The displacement measurements on a specimen without any cracks and over a stress range from 0 to 120 MPa are correlated. The results of this correlation analysis are provided in Figure 6.8.
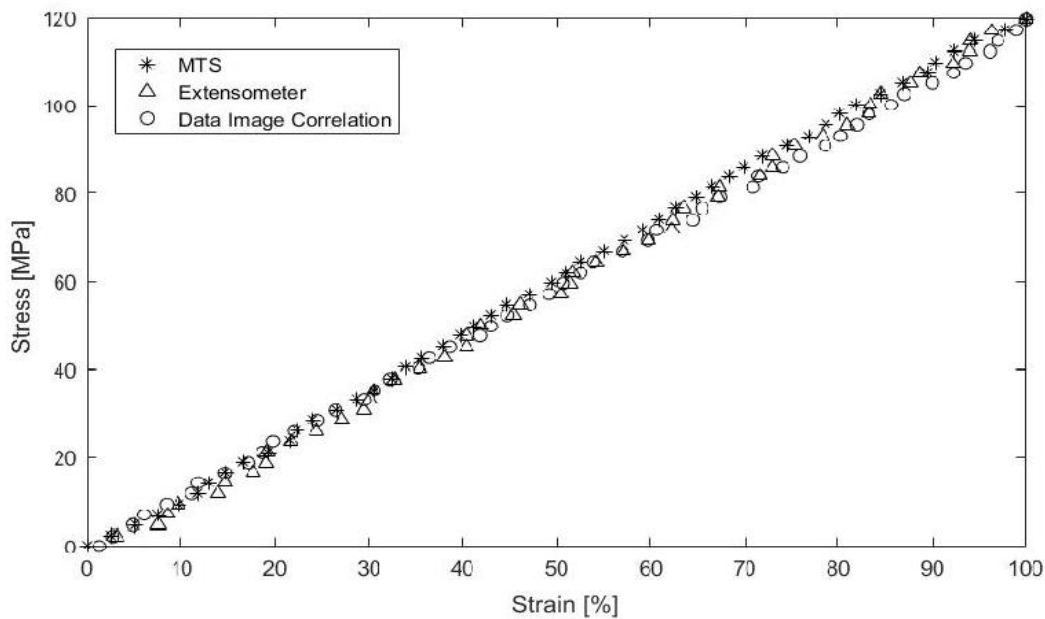
Figure 6.8: Correlation between Used Measurement Tools

It can be clearly observed that the used measurement techniques correlate. It seems therefore obvious to use the MTS data for all experiments as this does not require any external test equipment. However, the measured minimum displacements for the entire test of specimen AR005S75 are provided in Figure 6.9.
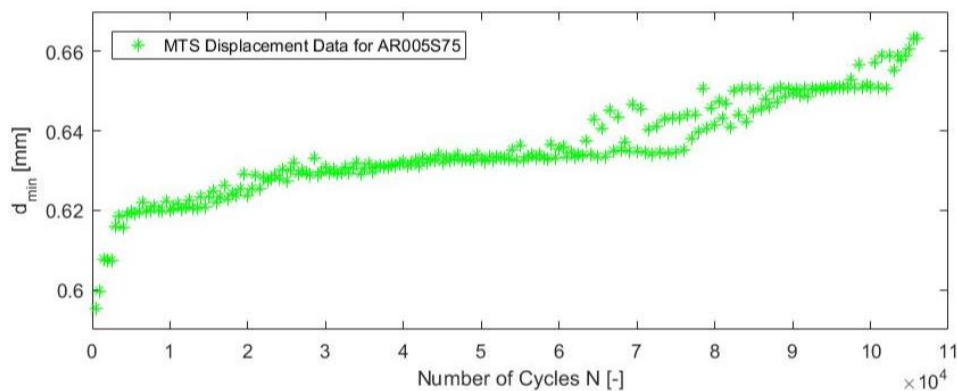
Figure 6.9: Displacements Measured by MTS during Total Test

A decreasing displacement implies that less energy is applied by the test machine. In other words, based on Equation 3.4 this implies energy is created by the specimen which can obviously not be true. The noise in Figure 6.9 may be caused due to multiple reasons. It may for example be caused by a lack of sensitivity of the displacement sensors for the actual displacement. It might also be, keeping in mind the MTS displacement sensors are not just measuring the displacement of the specimens, that external factors such as heavy cabling, the stiffness of the clamps or for instance a moving bolt cause these results. The exact cause is unknown, but the results are considered too unreliable for analysis.

Therefore VIC-data is used for SER analysis, as this measurement method is completely independent of MTS software and also measures the displacement of the actual specimen. To determine the accuracy of VIC for displacement measurements, two photos of the same specimen are taken without applying a force on the specimen. One photo is then analysed with the other photo as a reference. The displacements calculated by the VIC-3D software are then a measurement for the accuracy or sensitivity of VIC-analysis.

In air environment the accuracy corresponding to the total displacement of the specimen at minimum and maximum applied load is very small, but with the vacuum chamber installed the accuracy of VIC decreases. This is likely caused by the window of the vacuum chamber where the pictures need to be taken through. The sensitivity is still good enough for the displacements of the total specimen as this involves relatively large absolute displacements, but it might have an influence on the determination of the plastic zone as is discussed in Section 6.9.

6.5.2 Determination of Total and Cyclic Applied Work

As discussed in Section 4.5, for every block of ΔN load cycles the minimum and maximum displacement corresponding to minimum and maximum applied load are measured. To calculate the energy supplied by the fatigue bench at the specimen, linear load-displacement is assumed. This is obviously not completely true as discussed in Section 2.2.1.6, but it means that it is assumed that over a range of ΔN load cycles this deviation between calculated and actual SER is negligible.

With this assumption the total and cyclic applied work can be calculated using the theory discussed in Section 3.2.2. However, to calculate the total applied work also the displacement at a load of zero Newton needs to be determined. As a linear extrapolation between d_{min} and d_{max} does not necessarily go through the origin, as illustrated in Figure 6.10, d_0 needs to be calculated using Equation 6.6.

$$d_0 = d_{min,m} - \left(\frac{d_{max,m} - d_{min,m}}{P_{max,m} - P_{min,m}} \right) P_{min,m} \qquad \textit{Equation 6.6}$$

Furthermore the data acquisition program of the MTS fatigue bench captures the applied load with a certain sampling speed. The measured $P_{max,m}$ and $P_{min,m}$ with corresponding measured displacements $d_{max,m}$ and $d_{min,m}$ may therefore be captured after the actual maximum and minimum load $P_{max,a}$ and $P_{min,a}$ are applied with corresponding $d_{max,a}$ and $d_{min,a}$. This is illustrated in Figure 6.10. To take this into account, the slope between the measured data points is calculated and extrapolated using Equations 6.7 and 6.8 such that the actual displacements and the actual applied loads are calculated.
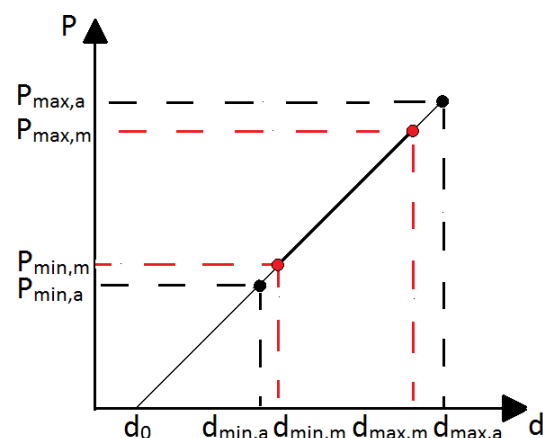
Figure 6.10: Determination of Actual Loads and Displacements and d_0 based on Linear Load-Displacement Assumption

$$d_{min,a} = d_0 + \left(\frac{d_{max,m} - d_{min,m}}{P_{max,m} - P_{min,m}}\right) P_{min,a} \hspace{2cm} \textit{Equation 6.7}$$

$$d_{max,a} = d_0 + \left(\frac{d_{max,m} - d_{min,m}}{P_{max,m} - P_{min,m}}\right) P_{max,a} \hspace{2cm} \textit{Equation 6.8}$$

Having $d_{min,a}$, $d_{max,a}$ and d_0, the total and cyclic energy can be calculated using Equations 3.8 and 3.9 as previously discussed in Section 3.2.2.

As already discussed in Section 6.5.1, the absolute displacement for the different measurement tools is different as the displacements are measured at different points on the specimen. If VIC is used for analysis, it is therefore important to determine the displacement between two equal distant points on each tested specimen. Only then proper comparisons can be made between each specimen, as otherwise the calculated absolute displacements differ resulting in a different SER. The results for U_{tot} and U_{cyc} for specimen AR05S75 are provided in Figure 6.11 and the results of all other specimens can be found in Appendix B.
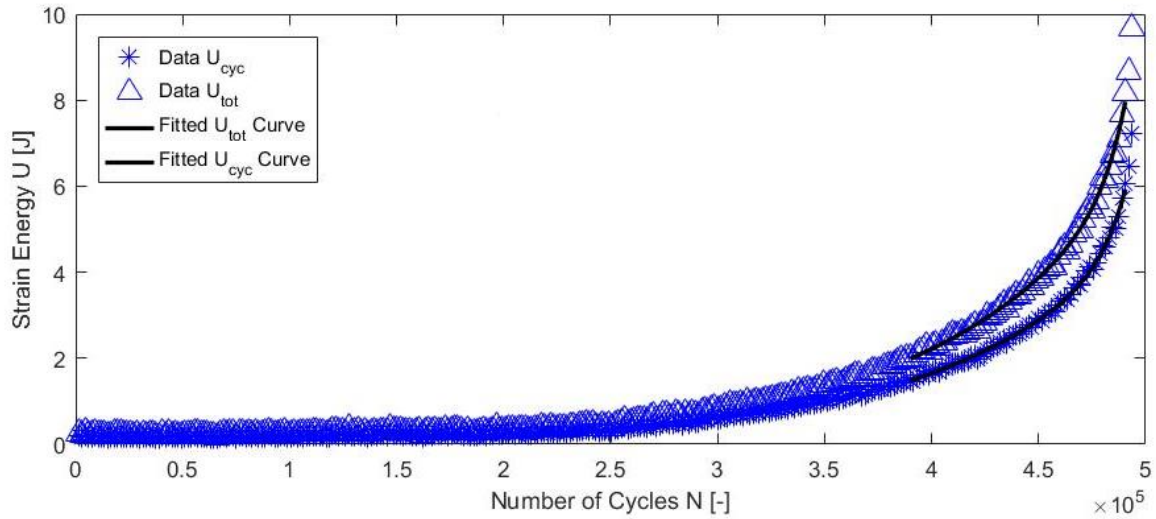
Figure 6.11: Total and Cyclic Applied Work with Fitted Curves for Specimen AR05S75

A curve can be fit through the data for the complete range of *N-U*. However, for the SER analysis it is only required to determine SER over the interval that FCG occurs. For a better fit, a curve is therefore only fitted through the part of *N-U* where FCG occurs. Also for a better fit, the number of applied load cycles *N* is shifted using Equation 6.9.

$$N_{shifted} = N_{actual} - \min(N_{actual}) \hspace{2cm} \textit{Equation 6.9}$$

$N_{shifted}$ is the new number of applied load cycles used for the fit, N_{actual} is the actual number of applied load cycles and *min(N_{actual})* is the smallest number of actual applied load cycles over the range where the curve is fit.

A two-term exponential curve based on LSM is fit through the data using MATLAB. The general equations for these two-term exponentials are given by Equation 6.10 and 6.11.

$$U_{tot} = p_1 e^{p_2 N} + p_3 e^{p_4 N} \hspace{2cm} \textit{Equation 6.10}$$

$$U_{cyc} = p_1 e^{p_2 N} + p_3 e^{p_4 N} \hspace{2cm} \textit{Equation 6.11}$$

In Figure 6.11 the fitted curves are plotted as the black lines for specimen AR05S75. The number of applied load cycles is translated back to the actual number of applied load cycles using Equation 6.12.

$$N_{actual} = N_{shifted} + \min(N_{actual})$$ *Equation 6.12*

The corresponding parameters and quality of the fits are provided in Table 6.3 and Table 6.4 respectively. The fitted curves for all other specimens are provided in Appendix B.

Coefficient	Value	95% Confidence Bounds
p₁	1.985	1.942 – 2.028
p₂	1.096E-05	1.04E-05 – 1.151E-05
p₃	1.388E-04	-1.311E-04 – 4.087E-04
p₄	9.524E-05	7.654E-05 – 1.139E-04
Equation	R^2	RMSE
Equation 6.10	0.97	0.08522

<p align="center">*Table 6.3: Coefficients for Fitted Curve Equation 6.10*</p>

Coefficient	Value	95% Confidence Bounds
p₁	1.48	1.448 – 1.512
p₂	1.095E-05	1.039E-05 – 1.151E-05
p₃	1.107E-04	-1.032E-04 – 3.246E-04
p₄	9.452E—05	7.595E-05 – 1.131E-04
Equation	R^2	RMSE
Equation 6.11	0.9971	0.06299

<p align="center">*Table 6.4: Coefficients for Fitted Curve Equation 6.11*</p>

The final step to calculate dU_{tot}/dN and dU_{cyc}/dN is taking the derivative of Equation 6.10 and 6.11, given by Equation 6.13 and 6.14 respectively.

$$\frac{dU_{tot}}{dN} = p_1 p_2 e^{p_2 N} + p_3 p_4 e^{p_4 N}$$ *Equation 6.13*

$$\frac{dU_{cyc}}{dN} = p_1 p_2 e^{p_2 N} + p_3 p_4 e^{p_4 N}$$ *Equation 6.14*

6.6 FCG Description based on Strain Energy Release

In Section 6.4 FCG is described based on the SIF *ΔK*. By comparing the results in air and vacuum environment it is shown that the theory of *ΔK* as similitude parameter does not hold. In Section 3.2.2 it was hypothesized what the expected outcome is if FCG is based on SER. The numerical analysis in Chapter 5 emphasised the likelihood of this hypothesis. This section covers the experimental results of describing FCG based on SER. In Section 6.3 it was discussed how the crack growth rate *da/dN* is obtained and in Section 6.5.2 it was discussed how the SER *dU_{tot}/dN* and *dU_{cyc}/dN* are obtained. In Section 6.6.1 these results are shown for FCG in air and Section 6.6.2 shows the results of FCG in vacuum.

6.6.1 Air Environment

The results for the SER versus crack growth rate for air are provided in Figure 6.12. From the figure it is immediately clear that in general the results correlate very well for a fixed maximum stress. This is conform the theory discussed in Section 3.2.2. For each maximum stress, 75 and 100 MPa respectively, there is still a slight *R*-effect observed. The lower the *R*-ratio, the less energy per cycle is dissipated for a certain crack growth rate. This is also conform the theory of Section 3.2.2.
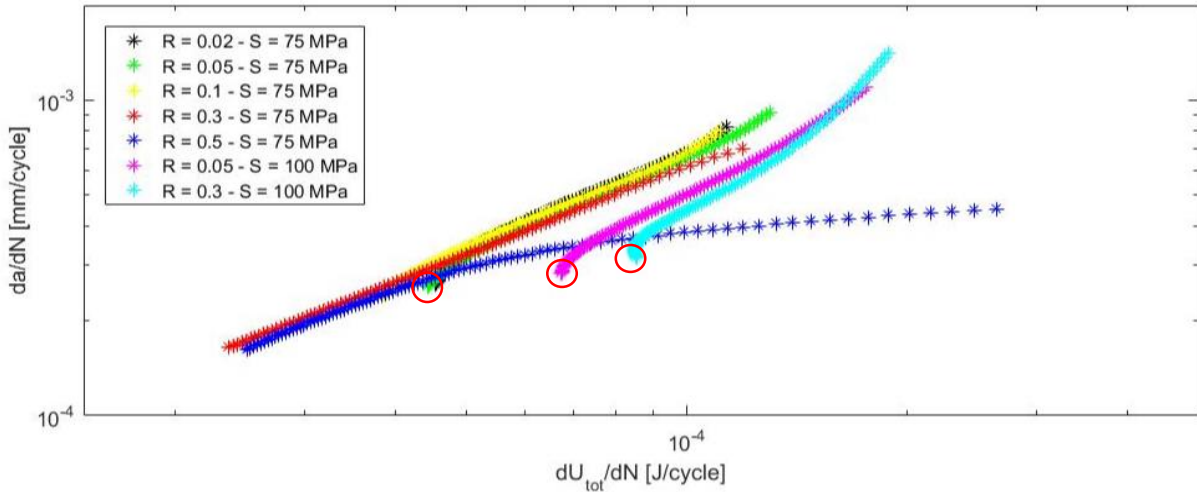
Figure 6.12: Total SER versus Crack Growth Rate in Air

Remarkable from Figure 6.12 is the rather big difference in total dissipated energy per cycle between the specimens tested at S_{max} of 75 MPa and specimens tested at S_{max} of 100 MPa, especially for lower crack growth rates. Clearly this difference is larger compared to the results obtained through numerical analysis in Chapter 5, which may be attributed to the energy dissipation mechanisms crack surface roughness and plasticity as both mechanisms are not included in the numerical analysis. This is further investigated in Section 6.9 and 6.10.

Furthermore some of the results show a hooked shape for lower crack growth rates, encircled in red. This is because the fitted curve for *N-U* data, discussed in Section 6.5, starts to deviate from the measured raw data at low N_{shift}. As a result the derivative for low N_{shift} is too large, not representing the actual SER anymore. This causes the hook-shaped curve.

Lastly, the result of *R* = 0.5 at S_{max} is 75 MPa completely deviates from all other results. At the lower crack growth rates the result still correlates very well with the other specimens, but at some point starts to deviate significantly. This might have to do with the fact that at *R* = 0.5 the crack is already very long for higher FCG rate, meaning that almost quasi-static failure occurs. However, this specimen also showed unclear behaviour for SIF based FCG description. The exact reason is thus unknown.
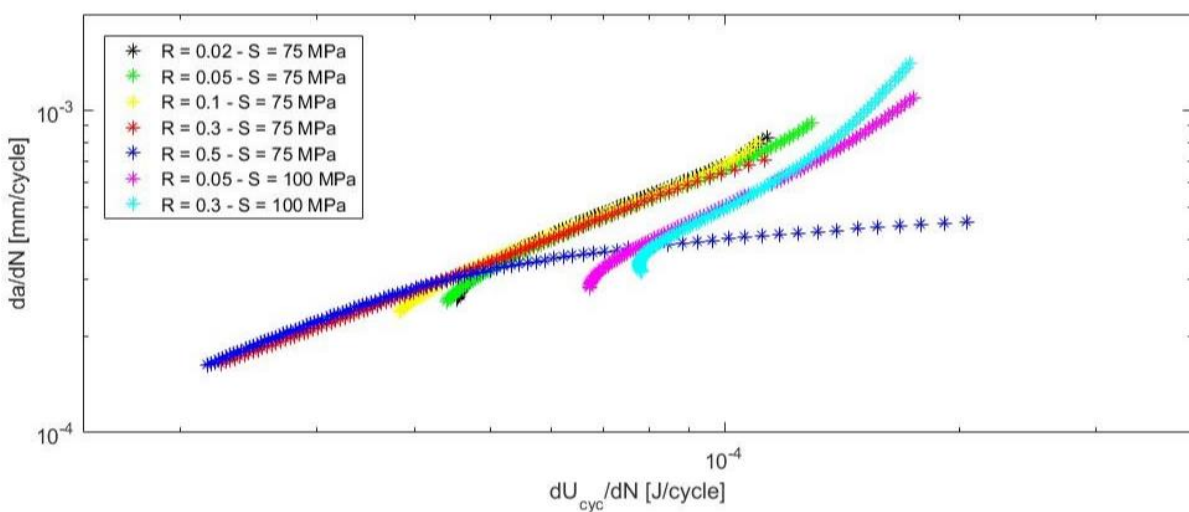
Figure 6.13: Cyclic SER versus Crack Growth Rate in Air

If the cyclic strain energy dissipation is considered instead of the total dissipated energy, the SER as a function of FCG rate becomes as shown in Figure 6.13. The general result, including the hook-shaped ends and the unclear deviation of the test at R = 0.5, is equal as in Figure 6.12. However, a significant difference is that the R-effect has become less clear. This is also conform the theory discussed in Section 3.2.2.

6.6.2 Vacuum Environment

In this section the experimental results from tests in vacuum are considered. The results of the total SER as a function of the crack growth rate are provided in Figure 6.14. It immediately protrudes that, in contrary to FCG experiments based on SIF, the trends observed in air can still be observed in vacuum.
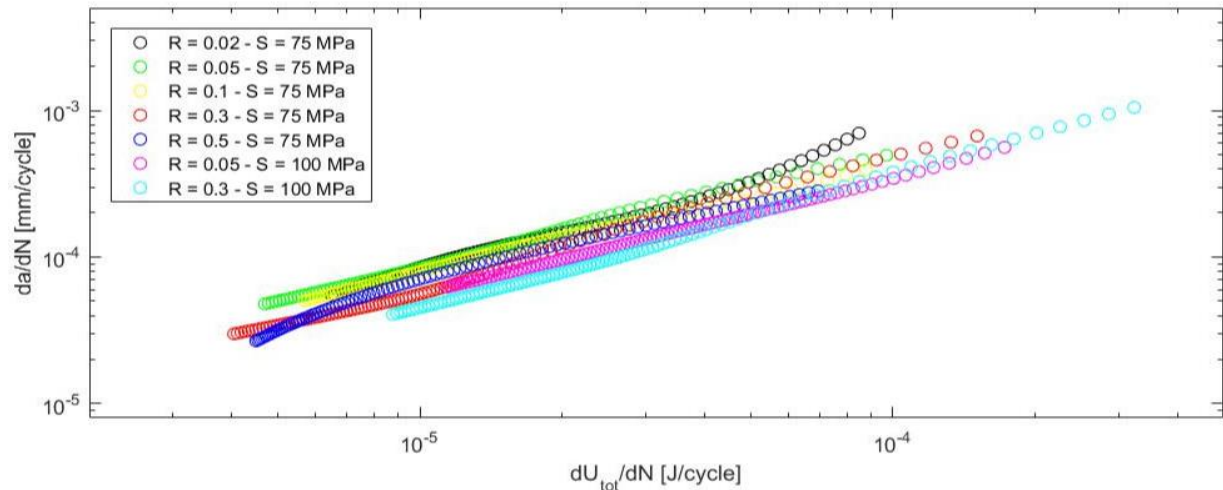
Figure 6.14: Total SER versus Crack Growth Rate in Vacuum

Again there is a general good correlation between the results, especially if attention is paid on a fixed S_{max}. Also, equal as in Section 6.6.1 and conform expectations discussed in Section 3.2.2, there is a slight R-effect visible. The energy dissipation between the two different S_{max} does not differ as much as it does in air. According to the theory of Section 3.2.2 it must be able to explain this difference by a difference in energy dissipations mechanisms such as surface roughness and plasticity. This is further researched in Section 6.9 and 6.10. However, one could say vacuum is the most inert environment one could test in, meaning that vacuum tests should be most conform the theory of Section 3.2.2 and the numerical analysis of Chapter 5, as it does not include any energy dissipation mechanisms potentially introduced by an air environment.

In general the experiments in vacuum are indeed very conform the theory discussed in Section 3.2.2 and show almost identical behaviour as numerically predicted in Chapter 5. The test results from Figure 6.14 therefore provide clear evidence that the second hypothesis of Section 3.1 is still correct.

In Figure 6.15 the results are shown if the cyclic dissipated energy is considered instead of the total dissipated energy. Again, like the experimental results in air environment, the results in Figure 6.15 show a similar trend as the results in Figure 6.14. With again an important difference: The results correlate better and the R-effect has decreased. This confirms the theory discussed in Section 3.2.2.
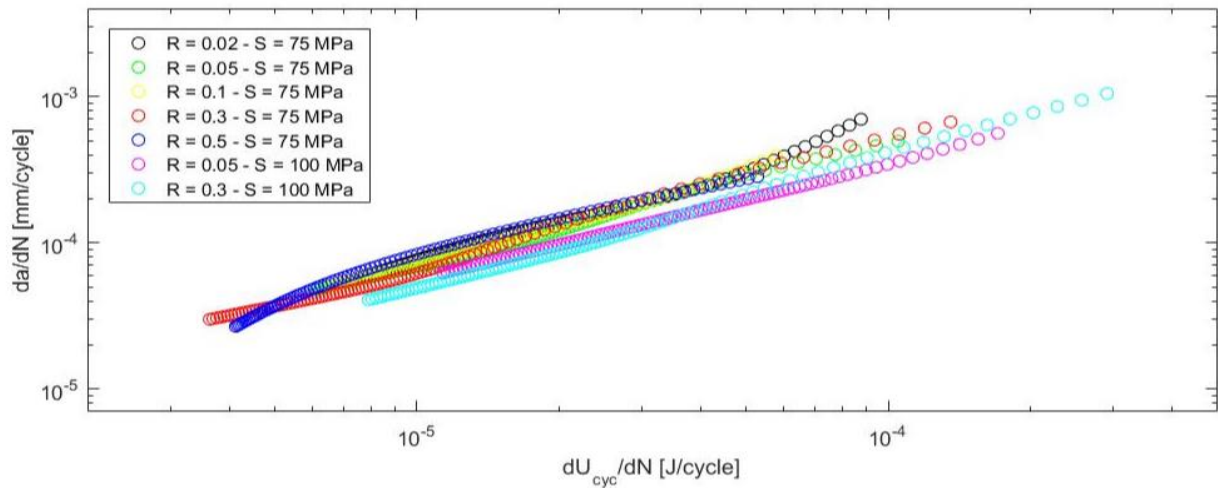
Figure 6.15: Cyclic SER versus Crack Growth Rate in Vacuum

6.7 (Plasticity Induced) Crack Closure

As discussed in Chapter 2, the R-effect introduced when using ΔK as similitude parameter can be accounted for if plasticity induced crack closure is considered. The stress corresponding to this crack closure is denoted as S_{op}. ΔK_{eff} is then given by $S_{max}–S_{op}$. If ΔK_{eff} is considered instead of ΔK, good correlation is obtained. As such plasticity induced crack closure is a key concept in the understanding of conventional FCG theory as discussed in Section 2.1.2.6. The test results covered in Section 6.4.1 confirmed this theory for air environment. However, Section 6.4.2 showed that the theory does not hold anymore in vacuum environment. The only reason to not falsify ΔK as similitude parameter based on the results of Section 6.4, is if the difference between air and vacuum is explainable by a difference in crack closure results.

This section covers the findings of crack closure. Or actually, 'crack closure' is a rather misleading term as it presumes that plasticity induced crack closure actually exists. But the criticism discussed in Chapter 2 showed that other mechanisms can also be responsible for the non-linear load-COD behaviour. For objectivity it is therefore preferred to mention the 'crack closure'-phenomenon as non-linear load-COD behaviour. And the stress corresponding to the transition point of non-linear to linear load-COD behaviour (previously denoted as S_{op} in conventional fatigue theories) is from now on denoted as S_{tr}.

In air environment, the COD is measured by two independent tools: The COD-meter and VIC-analysis. However, in vacuum it is impossible to measure the COD by means of the COD-meter due to the plastic cabling. Therefore the two measurement tools are correlated in air, such that in vacuum only VIC-analysis is sufficient. The correlation between the different measurement tools is discussed in Section 6.7.2.

6.7.1 Air Environment

This section covers the load-COD behaviour in air. As mentioned in the introduction of this section, the load-COD graph is measured by two independent measurement techniques. As discussed in Section 4.3.1.4, the sensitivity of the COD-meter was initially not sufficient to accurately perform COD measurements, as such requiring the legs of the COD-meter to be shortened. However, the shortening of the legs obviously has its limitations. The legs were shortened as much as possible in order to create the best possible sensitivity with the available COD-meters in DASML. The shortening unfortunately

resulted in non-linear calibration of the COD-meter except over a displacement range of 6 to 9 mm. Therefore a hole of 6 mm was drilled in the specimens.

The sensitivity of the COD-meter becomes worse for shorter crack lengths as the measured displacement intervals in this case are smaller compared to longer crack lengths. For shorter crack lengths therefore more noise may be expected in the results. The same counts for too small load intervals between measurement points. However, the sensitivity of the COD-meter could not be further improved and as such the results obtained should provide a sufficient idea of COD.

One may wonder why instead of a COD-meter no results of VIC-analysis are used. According to ASTM E647 [53] at least 50 data points are required to reliably draw conclusions on crack closure. Due to technical problems with the cabling and VIC-software, unfortunately about a third of the required amount of data points was obtained for the experiments in air. This problem was solved for the experiments in vacuum. Despite the limited amount of VIC-data for air, it is still aimed for to correlate between COD-meter and VIC measurements as is discussed in Section 6.7.2.

The load-COD result using the conventional COD-meter for specimen AR002S75 at a crack length of 25.8 mm is provided in Figure 6.16. For all other specimens the load-COD data can be found in Appendix C. Conform ASTM E647 standard [53], a linear curve from no more than $0.9S_{max}$ through approximately 25% of the cyclic applied stress range is fit. This fitted equation is also plotted in Figure 6.16. As can be easily observed, there is indeed non-linear behaviour visible. The transition point is where the data starts to deviate from the linear fit. However, this point is rather arbitrarily as to a certain extend it is based on personal interpretation [58]. The transition stress S_{tr} corresponding to the transition point is in Figure 6.16 approximately 20 MPa.
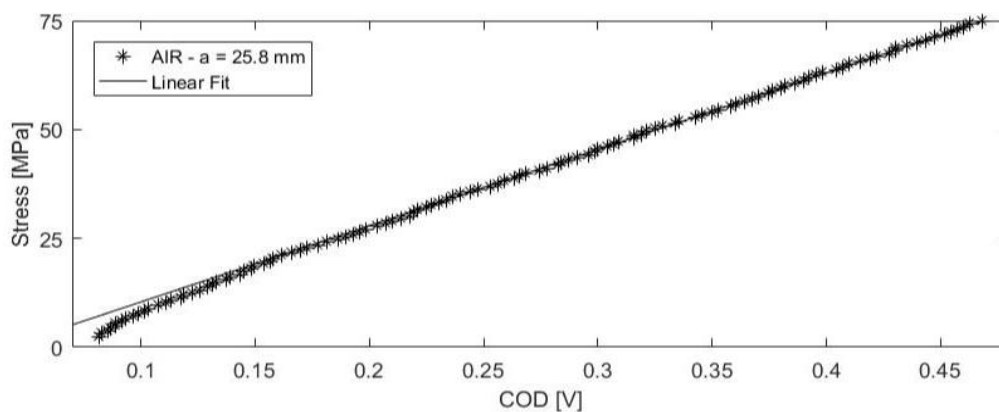
Figure 6.16: Stress-COD Curve for AR002S75 - a = 25.8 mm and S_{max} = 75 MPa

6.7.1.1 Crack Length Effect on Transition Point

According to the theory of plasticity induced crack closure, there should be no non-linearity observed if the load-COD curve of a sawcut is considered. For specimen AR002S75 the result of the load-COD measurement for a sawcut is given by Figure 6.17.
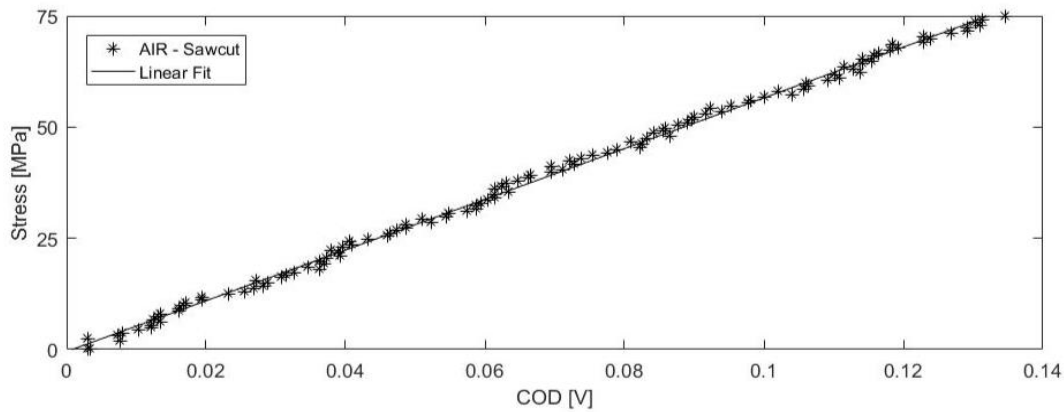
Figure 6.17: Stress-COD Curve for AR002S75 – Sawcut and S$_{mac}$ = 75 MPa

Although the noise in the results starts to be more significant compared to the larger crack of Figure 6.16, there is rather obvious no non-linear behaviour observed. The same results were obtained for all other experiments as shown in Appendix C.

Once the crack develops, the transition point should according to plasticity induced crack closure theory not change as it is independent of crack length. In Figure 6.18 the load-COD result for a shorter crack length of specimen AR002S75 is provided.
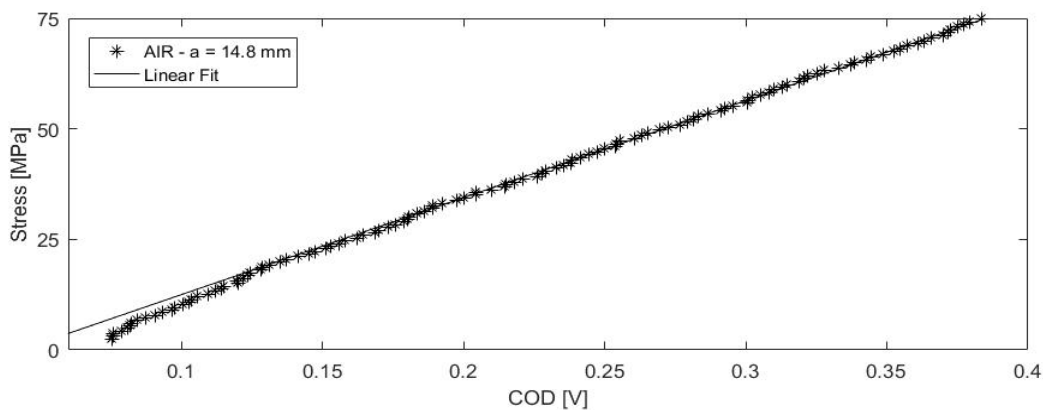
Figure 6.18: Stress-COD Curve for AR002S75 - a = 14.8 mm and S$_{max}$ = 75 MPa

Although the noise again plays a more significant role compared to the results in Figure 6.16, one can clearly observe the non-linear behaviour of the graph again, and the transition point from non-linear to linear is again approximately 20 MPa. For all other tested specimens with an applied S$_{max}$ of 75 MPa where non-linear load-COD behaviour is observed, the transition point stress is also approximately 20 MPa as can be seen in Appendix C. This confirms the independency of the transition point on crack length.

6.7.1.2   Stress Ratio Effect on Transition Point

Figure 6.16, 6.19, 6.20, 6.21 and 6.22 show the load-COD results for the complete range of tested stress ratios in air, for a fixed maximum stress of 75 MPa. According to plasticity induced crack closure theory, the transition point should increase for increasing stress ratio.
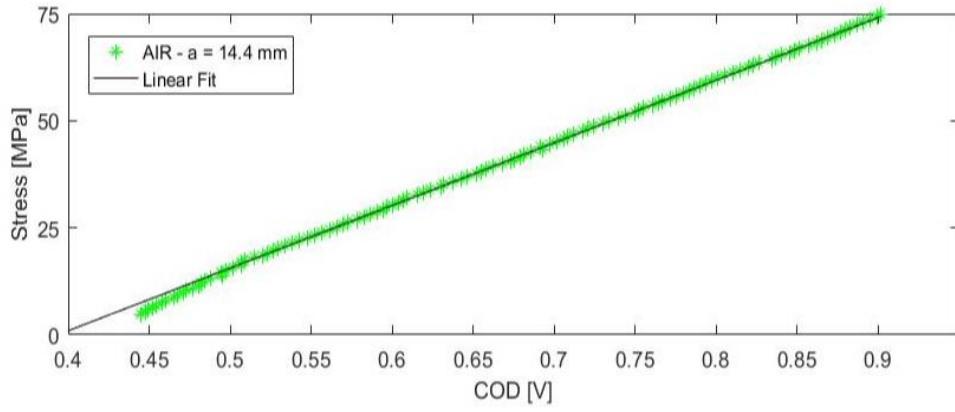
Figure 6.19: Stress-COD Curve for AR005S75 - a = 14.4 mm and S_{max} = 75 MPa
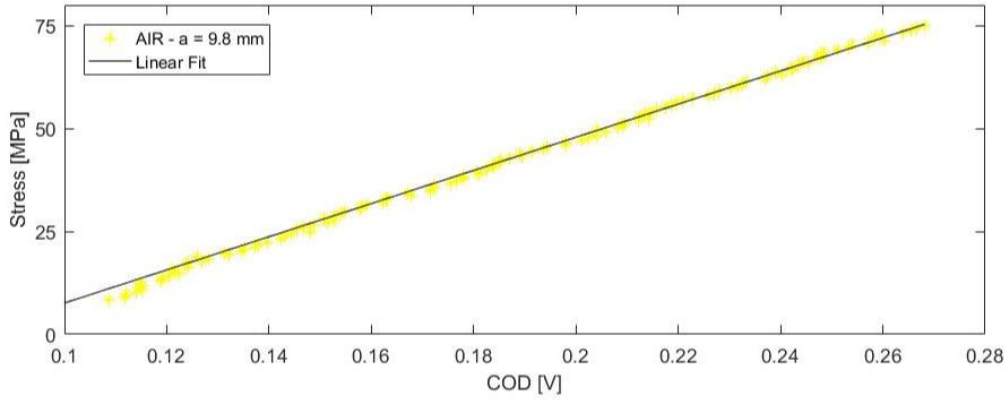
Figure 6.20: Stress-COD Curve for AR01S75 - a = 9.8 mm and S_{max} = 75 MPa
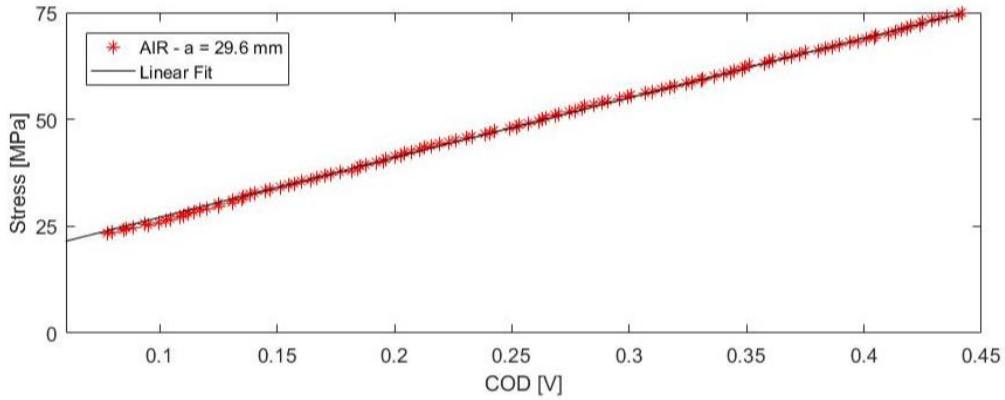
Figure 6.21: Stress-COD Curve for AR03S75 - a = 29.6 mm and S_{max} = 75 MPa
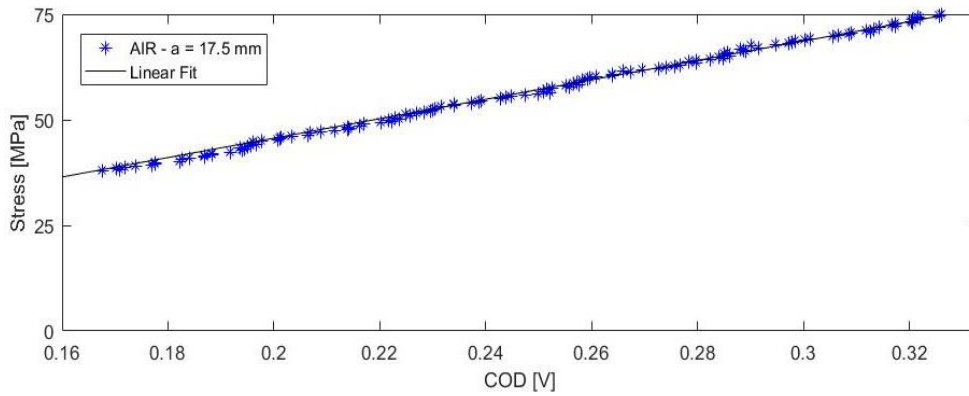
Figure 6.22: Stress-COD Curve for AR05S75 - a = 17.5 mm and S_{max} = 75 MPa1

However, the results from the figures show that the non-linearity becomes less obvious for increasing stress ratio. For the stress ratio of 0.3 and 0.5 the deviation from the linear fit is so small that it might be doubted if a transition point is present at all. For stress ratios lower than 0.1 there is however clear non-linear behaviour. But in contradiction with the expectations based on the theory of Section 2.1.2.6, the transition point is not increasing for increasing stress ratio.

In fact, the transition point is always around an applied stress of 20 MPa. If this transition point is indeed independent of stress ratio, it is immediately evident why the non-linearity as observed in Figure 6.16, 6.19 and 6.20 is absent in Figure 6.21 and 6.22: The minimum stress for a stress ratio of 0.3 and 0.5 is above 20 MPa. If the non-linearity is indeed caused by crack closure, this seems logical: It makes no sense to hypothesize that a crack would still be closed even for arbitrarily high S_{min}. In contradiction to crack closure theory provided in Section 2.1.2.6, the results in this section imply that the transition point is independent of the stress ratio.

As mentioned before, the amount of data obtained for VIC-analysis is too limited for a proper analysis according to ASTM E647 standard. However, the limited amount of VIC-data showed a similar behaviour as measured by the COD-meter as can be seen in Appendix C. As two independent measurement tools show the same behaviour. It is thought that the results provide a proper idea of the load-COD behaviour of the various specimens.

6.7.1.3   Maximum Stress Effect on Transition Point
In Figure 6.23 and 6.24 the load-COD results are given for the experiments of a stress ratio of 0.05 and 0.3, but with a maximum applied stress of 100 MPa instead of 75 MPa.
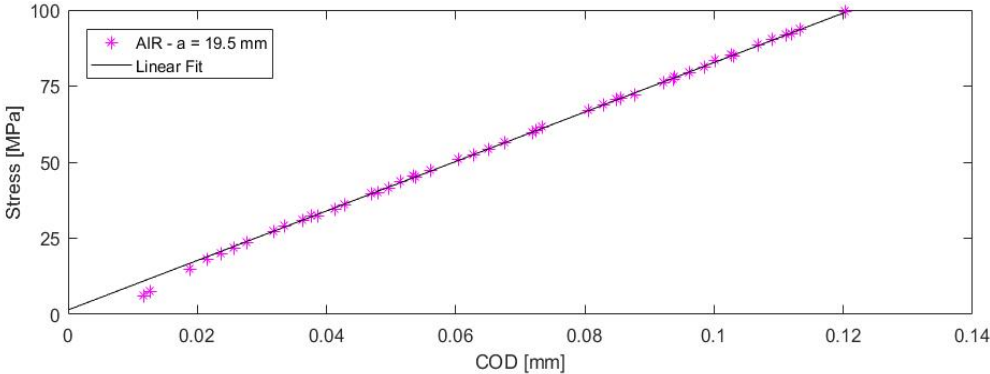
Figure 6.23: Stress-COD Curve for AR005S100 - a = 19.5 mm and S_{max} = 100 MPa
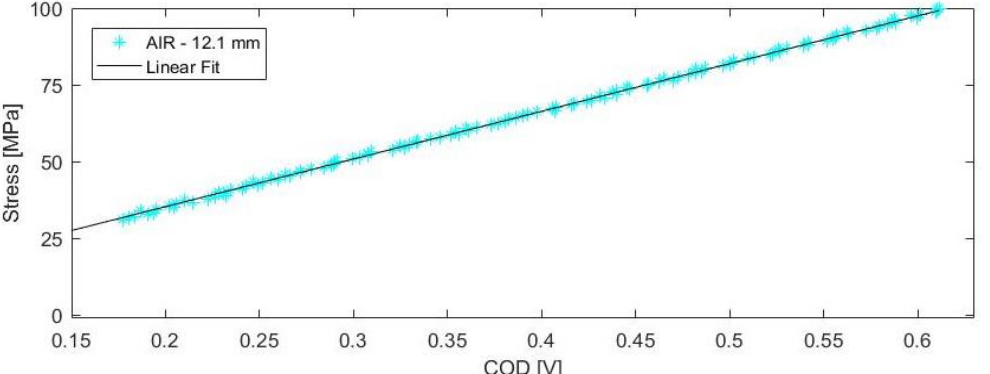
Figure 6.24: Stress-COD Curve for AR03S100 - a = 12.1 mm and S_{max} = 100 MPa

The larger load interval implies that the relative noise level of the COD-meter reduces, resulting in clearer results. The results indeed have a lower noise level as compared to the results provided in Section 6.7.1.2.

It can be seen from Figure 6.23 and 6.24 that the transition point is indeed only observed for R = 0.05 and that the load-COD result for R = 0.3 does not show any non-linearity. Furthermore also for S_{max} of 100 MPa the transition point is independent of the crack length as can be observed from the figures in Appendix C. The observed transition point for Figure 6.23 is close to 25 MPa.

With these results it can be concluded that the maximum applied stress does have a slight but no big influence on the transition point and the non-linearity of the load-COD curve. This is again contradicting with Elber's theory discussed in Section 2.1.2.6. The load-COD results in air show that, for a fixed maximum stress, the presence of a transition point is completely dependent on the applied minimum stress.

6.7.2 Correlation COD-Meter and VIC-analysis

As mentioned the COD is also measured by VIC-analysis. According to the ASTM E647 standard, at least 50 data points are required to obtain reliable results. But as discussed in the introduction of this section, there is not enough VIC-data gathered for reliable VIC-analysis of load-COD behaviour in air. However, the limited amount of VIC-data in air is still used to verify if the same trend is observed as observed using the COD-meter.

The load-COD graph for the same specimen and crack length as in Figure 6.16 is shown in Figure 6.25 using VIC instead of the COD-meter.
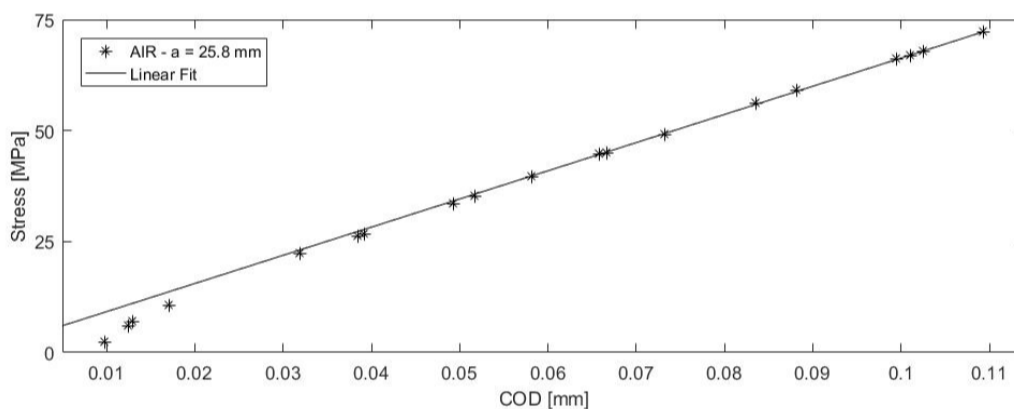
Figure 6.25: Stress-COD Curve measured by VIC for AR002S75 - a = 25.8 mm and S$_{max}$ = 75 MPa

The figure strongly indicates that the same trend is followed using the COD-meter, and also the transition point seems to be around 20 MPa. As other experiments also showed similar trends for both COD-meter and VIC-analysis as can be seen in Appendix C, it is assumed that the VIC-analysis and COD-meter are equally reliable measurement tools for determination of the transition point.

6.7.3 Vacuum Environment

Figure 6.26 shows the load-COD curve for specimen VR002S75. Appendix C contains the load-COD results for all other tested specimens. The specimen from Figure 6.26 was subject to the same conditions, apart from being executed in vacuum instead of air, as specimen AR002S75 whose load-COD curve is shown in Figure 6.16. It can be clearly observed that the result in Figure 6.26 is almost identical to the result of Figure 6.16: There is clear non-linear behaviour and the transition point is again approximately 20 MPa.
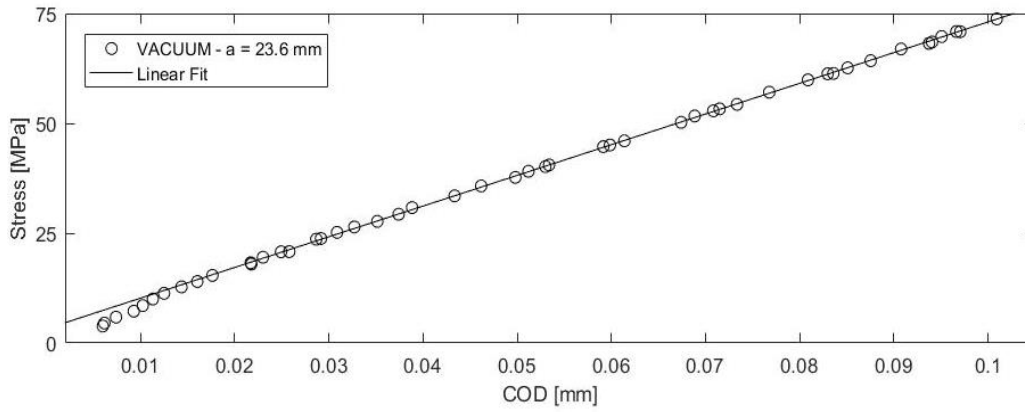
Figure 6.26: Stress-COD Curve for VR002S75 - a = 23.6 mm and S$_{max}$ = 75 MPa

This non-linear behaviour in vacuum is expected based on the theory of plasticity induced crack closure, and earlier tests of Schijve in air and vacuum showed the same result [58]. However, this research was done for a single stress ratio (*R* of 0.1) and did not consider the validity of *ΔK* as similitude parameter.

6.7.3.1 Crack Length Effect on Transition Point

Equal to the results in air, the transition point in vacuum should according to crack closure theory also be independent of the crack length. Figure 6.27 shows the load-COD result for specimen VR002S75 at a sawcut. Figure 6.28 presents the load-COD for the same specimen, but at a shorter crack length compared to Figure 6.26.
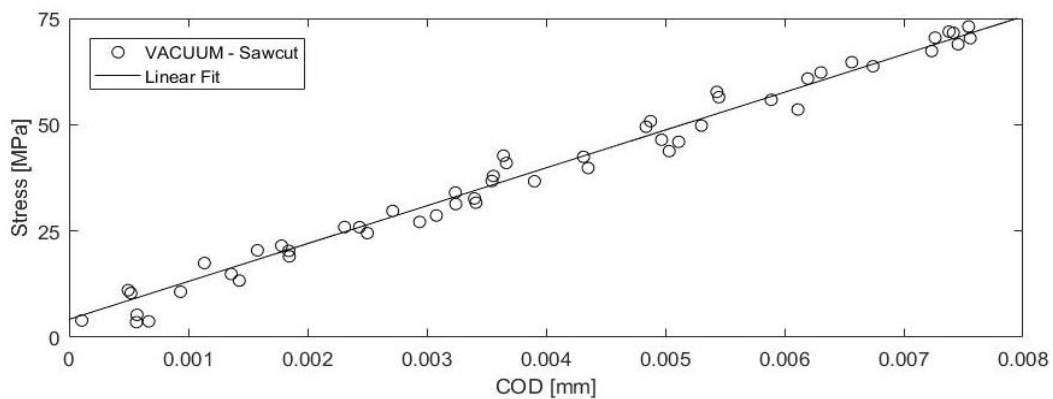
Figure 6.27: Stress-COD Curve for VR002S75 - Sawcut and S$_{max}$ = 75 MPa
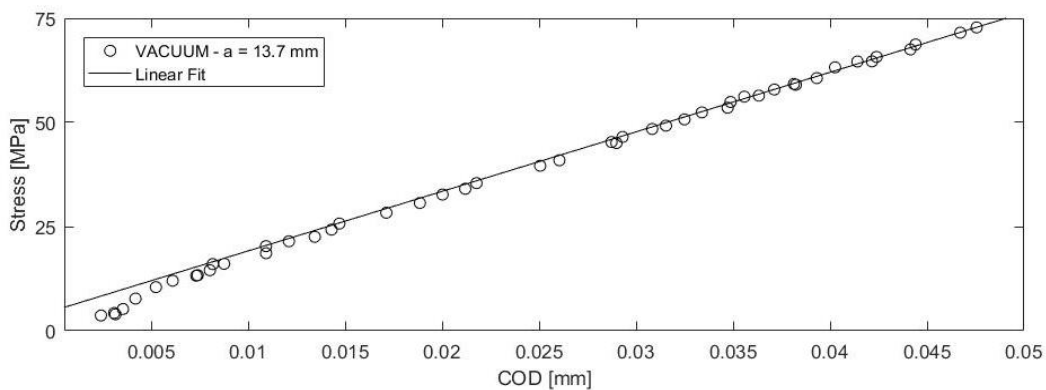
Figure 6.28: Stress-COD Curve for VR002S75 - a = 13.7 mm and S$_{max}$ = 75 MPa

The measurements using VIC show some noise in Figure 6.27. However, the general trend seems to be linear, as may be expected from plasticity induced crack closure theory. On the contrary, the result of Figure 6.28 shows again a clear non-linear behaviour. The transition point is again approximately at a stress of 20 MPa. For the other tested specimens in vacuum showing non-linear behaviour the transition point is also independent of the crack length. As such the load-COD measurements in vacuum seem to show identical results as the same experiments in air environment.

6.7.3.2   Stress Ratio Effect on Transition Point

To determine if the load-COD results in vacuum are not only identical to the results in air for a stress ratio of 0.02, the effect of the stress ratio on the transition point in vacuum is also analysed. Figure 6.26, 6.29, 6.30, 6.31 and 6.32 show the load-COD results for the complete range of tested stress ratios in vacuum, with a maximum applied stress of 75 MPa.
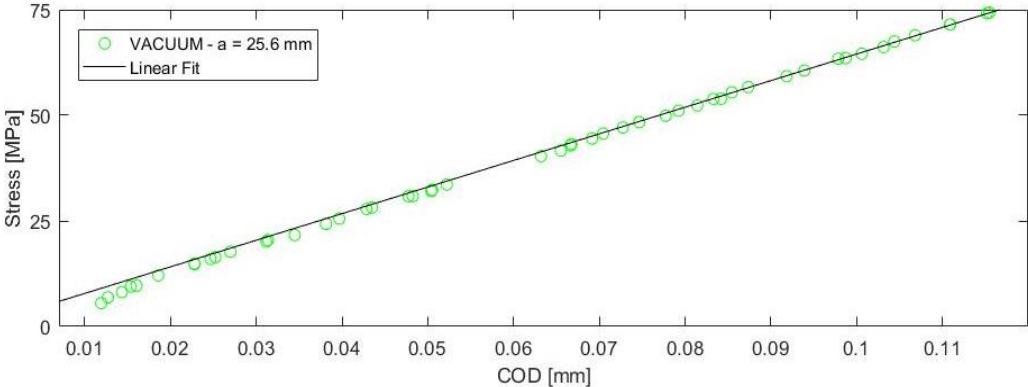
Figure 6.29: Stress-COD Curve for VR005S75 - a = 25.6 mm and S_{max} = 75 MPa
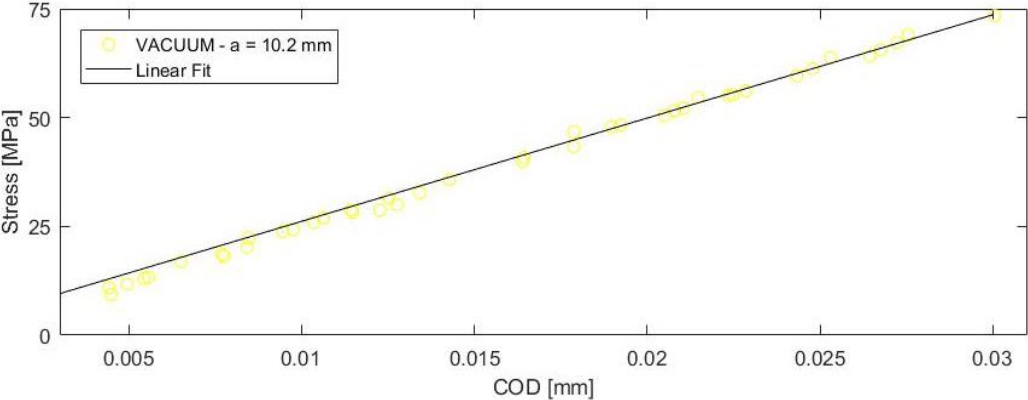
Figure 6.30: Stress-COD Curve for VR01S75 - a = 10.2 mm and S_{max} = 75 MPa
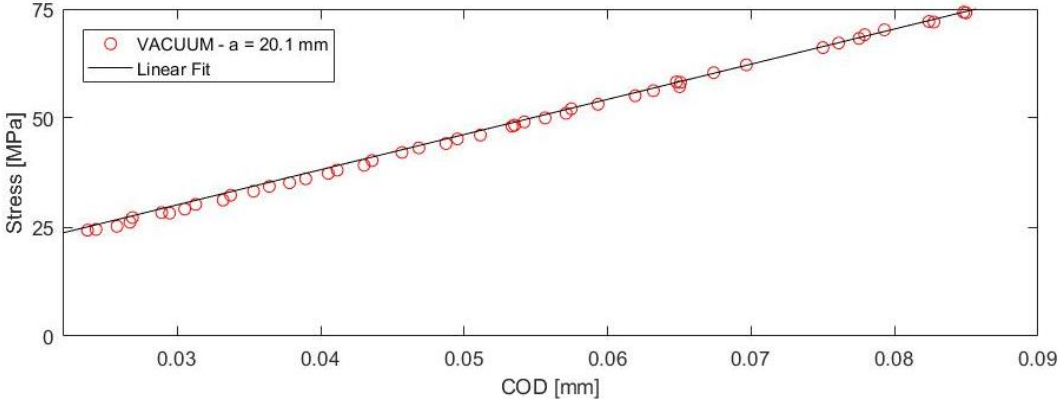
Figure 6.31: Stress-COD Curve for VR03S75 - a = 20.1 mm and S_{max} = 75 MPa
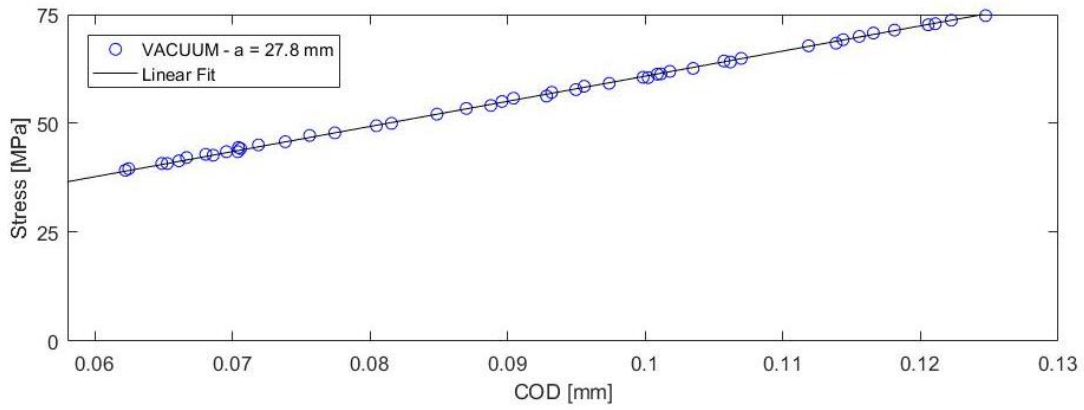
Figure 6.32: Stress-COD Curve for VR05S75 - a = 27.8 mm and S_{max} = 75 MPa

It is immediately evident that there is no difference in load-COD behaviour between air and vacuum. Again stress ratios of 0.3 and higher do not show any non-linear behaviour, while stress ratios of 0.1 and lower do. It is furthermore remarkable that the transition point is also independent of stress ratio, with all transition points again around a stress of 20 MPa.

6.7.3.3   Maximum Stress Effect on Transition Point

For completeness also the effect of a different maximum stress in vacuum environment is considered. Figure 6.33 and 6.34 show the load-COD results for a stress ratio of 0.05 and 0.3 with maximum stress of 100 MPa instead of 75 MPa.
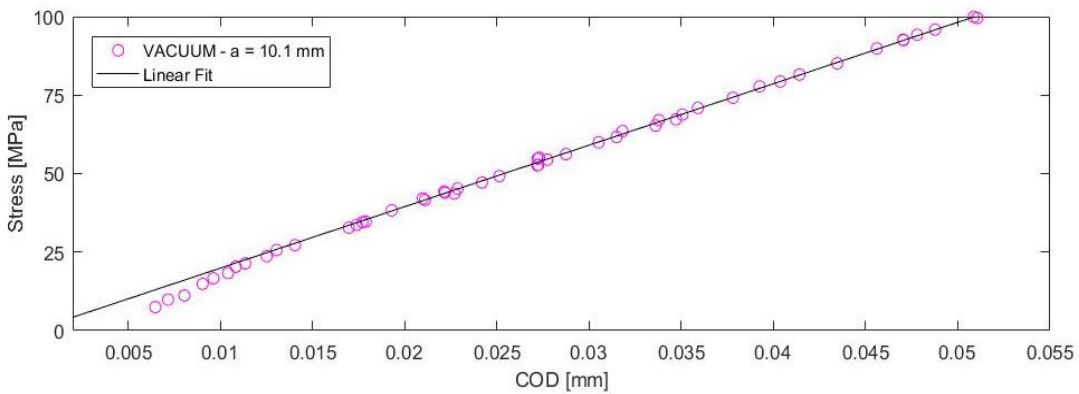
Figure 6.33: Stress-COD Curve for VR005S100 - a = 10.1 mm and S_{max} = 100 MPa
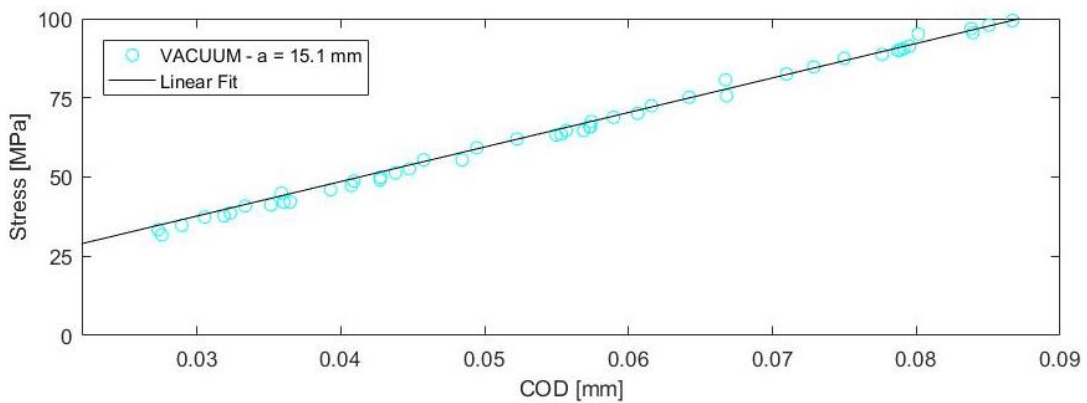
Figure 6.34: Stress-COD Curve for VR03S100 - a = 15.1 mm and S_{max} = 100 MPa

The results thereof are again in line with earlier findings in air environment: Non-linear behaviour is barely to not observed in the experiment with a stress ratio of 0.3, while for a stress ratio lower than 0.1 there is non-linear behaviour with the transition point at approximately 25 MPa. To take away any remaining doubts whether experiments in vacuum and air show identical load-COD behaviour or not, the VIC-results for air and vacuum are for each test condition also combined in a single plot. These plots are provided in Appendix C. The results emphasize that the environment tested in, has no influence on the load-COD behaviour.

6.7.4 Comparison S_{tr} by Schijve and Elber vs Experimental Measurements

For a quick overview, the most important results of Section 6.7 are summarized in Figure 6.35. The figure shows the stresses S_{tr} corresponding to the transition point from non-linear to linear load-COD behaviour for the stress ratios where this point is actually observed. Hence the figure does not include transition points for stress ratios above 0.1.
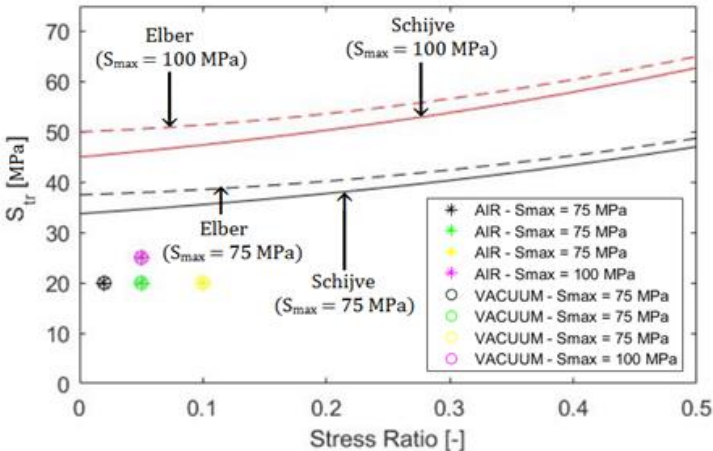
Figure 6.35: Transition Stresses according to Elber and Schijve and Experimentally Determined Transition Points

Furthermore the figure contains the expected transition point stresses based on crack closure corrections by Elber and Schijve proposed in literature. It is immediately evident that the measured transition stresses significantly differ from the theoretical values. Apart from that there is obviously no stress ratio-effect observed, whereas the corrections by Elber and Schijve do contain such an effect.

6.7.5 Intermezzo: Discussion about Crack Closure Observations

The results of Section 6.7.1 and 6.7.3 show that load-COD behaviour is independent of the environment tested in. Some trends observed are conform plasticity induced crack closure theory: A linear load-COD curve for a specimen with only a sawcut, and non-linear load-COD behaviour for longer cracks with a transition point independent of the crack length. Also earlier research by Schijve on crack closure in a specimen subject to a stress ratio of 0.1 in vacuum showed similar behaviour in air and vacuum [58].

However, there are also observations not in line with plasticity induced crack closure: At higher stress ratios (or maybe one should say above a certain S_{min}), there is no non-linear load-COD behaviour observed anymore, while according to for instance Equation 2.15 crack closure should theoretically even occur at very high applied minimum stresses. Furthermore the tests show that the transition point is at approximately the same applied stress, independent of stress ratio and only slightly influenced by S_{max}. This is also in contradiction with plasticity induced crack closure theory. Lastly the transition point is significantly off compared to the expected values as illustrated in Section 6.7.4.

As such one could conclude that the load-COD measurements provided in Section 6.7.1 and 6.7.3 have failed to reproduce results from literature. However, earlier in this report the validity of theory of plasticity induced crack closure as the keystone to explain the *R*-effect in FCG description using *ΔK* as similitude parameter has already been disputed. Opening stress seems to be an artificial stress needed regardless, as otherwise the *R*-effect in FCG description cannot be accounted for.
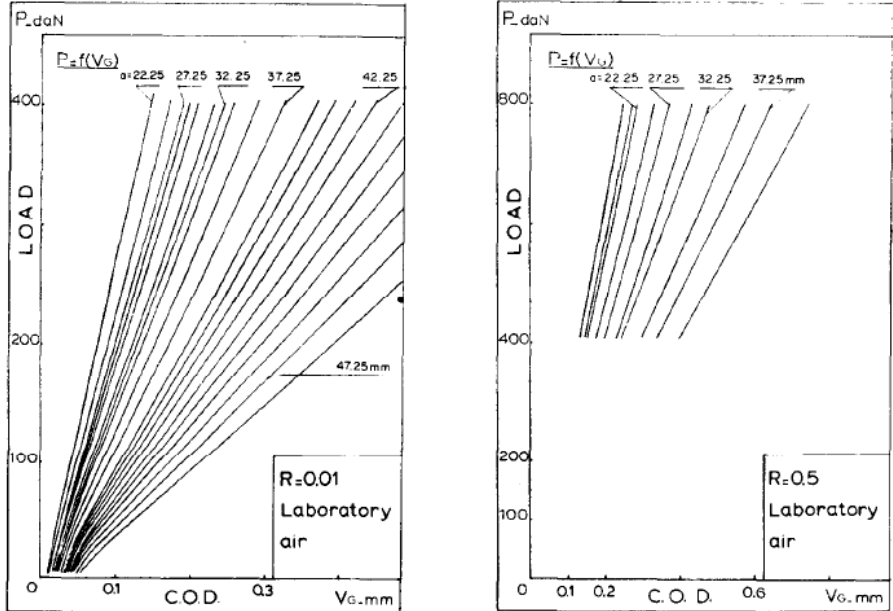
Figure 6.36: Load-COD Measurement Results of Bathias and Clerivet [55]

There seems to be no unambiguous method to measure COD and no scientific reports were found with an accurate description on how the COD was measured. On top of that, in general, reports involving crack closure measurements only mention the opening stress but do not provide load-COD results. A positive exception is work by Bathias and Clerivet [55]. Their research on opening stresses has also been referred to in work of Schijve [56].

Figure 6.36 and 6.37 show the load-COD results of Bathias and Clerivet, also measured by a notch COD-meter like the results discussed in Section 6.7.1 and 6.7.3. It can be seen that the observed trends are equal to the trends observed in Section 6.7.1 and 6.7.3: At a stress ratio of 0.01 there is non-linear behaviour and the transition point is approximately equal independent of crack length. There is a transition point observed for the low stress ratio, but not for the high stress ratio.
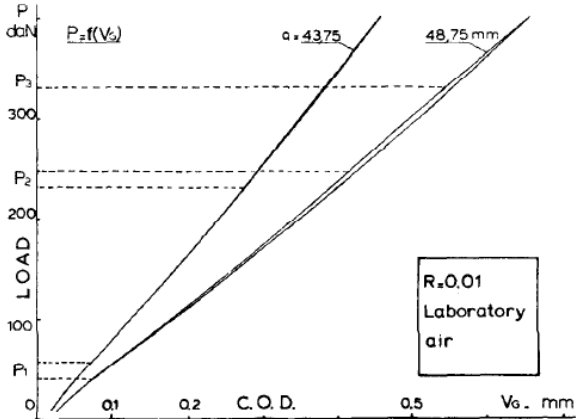
Fig. 8. Crack opening determination with the notch displacement.

Figure 6.37: Opening Stresses Observed by Bathias and Clerivet [55]

However, Bathias and Clerivet claim that an opening stress is observed in Figure 6.36 and Figure 6.37 for loads well above a load of 100 N. Figure 6.37 shows where Bathias and Clerivet notice a transition point from non-linear to linear load-COD behaviour, indicated with P_2. The mentioned opening stresses

are accordingly referred to by Schijve in his work on fatigue crack closure; observations and technical significance [56].

According to Figure 6.36 and 6.37 it therefore seems that the results of Section 6.7.1 and 6.7.3 are correct. However, it seems to be very unlikely that opening stresses can be claimed so accurately as done in Figure 6.37. It is therefore thought that crack opening stress is an artificial stress picked by researchers irrespective of whether it is actually observed or not, as otherwise no clear explanation exists for the observed R-effect if ΔK is used as similitude parameter for FCG description.

6.8 'Crack Closure Correction' approached by Cyclic Energy

From the results discussed in Section 6.7 the main conclusion drawn is that the transition point is not conform the expected opening stress as discussed in Section 2.1.2.6 of the literature review. The opening stress in literature seems to be an artificial stress only required to account for an R-effect introduced when using ΔK as similitude parameter. Section 2.2.1.5 in the literature review already indicated that crack closure effect may in fact be a cyclic energy correction. This section will further cover this hypothesis, as the crack closure correction should also be explainable by means of energy if fatigue should really be approached from a SER perspective as hypothesised in Section 3.1.

Figure 2.14 of Section 2.2.1.5 is for convenience shown here again as Figure 6.38.
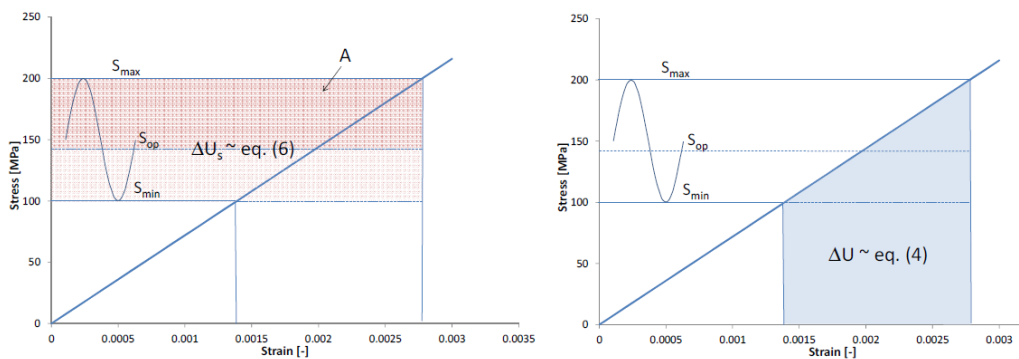
Figure 6.38: Illustration Showing how S_{op} Corrects for Cyclic Energy {36}

As came forward from Section 6.7.5, it may be disputed if the opening stresses conform equations such as Equation 2.15 and 2.40 are actually observed. The reason that the opening stress is needed is clear: An R-effect using ΔK for similitude needs to be corrected to an ΔK_{eff} to obtain good correlation. Equation 6.15 provides this crack closure correction, it is the ratio of the effective SIF range divided by the total SIF range.

$$Y = \frac{\Delta Keff}{dK} = \frac{\Delta U}{U_s}$$

Equation 6.15

If, instead of stresses, this equation is considered in terms of work one could say that the total, artificial applied work can be given by Equation 6.16 and the cyclic, actual applied work by Equation 6.17.

$$U_s = (S_{max} - S_{min})\varepsilon_{max}$$

Equation 6.16

$$\Delta U = \frac{1}{2}S_{max}\varepsilon_{max} - \frac{1}{2}S_{min}\varepsilon_{min}$$

Equation 6.17

Alderliesten expressed this ratio in terms of Equation 6.15, resulting in a correction similar to the crack closure corrections of Schijve en Elber as shown in Figure 6.41. Figure 6.38 illustrates what this implies: The total red area is the artificial total work applied if ΔK is used for similitude. However, in fact the cyclic work involved is less and given by the blue area. The artificial energy thus needs to be corrected

for, by introducing an opening stress. Introducing the artificial opening stress reduces the total applied work as illustrated by the dark red area in Figure 6.38. Now the applied work is equally large as the cyclic applied work (the blue area).

As can be observed in Figure 6.41, there is some discrepancy between Alderliesten's result and the corrections by Elber and Schijve. This can be caused by non-linear behaviour observed in the load-COD results, as illustrated in Figure 6.39.
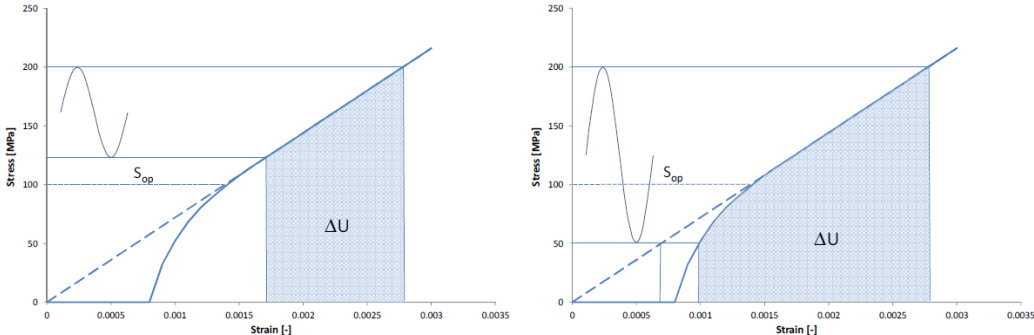
Figure 6.39: Cyclic Applied Work for Two Stress Ratios [30]

The non-linearity causes the applied cyclic work for low stress ratios to be less in comparison with linear behaviour. Also the artificial total energy decreases as ε_{max} decreases. Therefore Alderliesten's curve in Figure 6.41 will shift.

To test this theory, the load-COD needs to be measured over the range from zero applied load to S_{max} as it is important to capture the non-linear behaviour at low applied stresses. This non-linearity is needed to determine ε_{max} for the artificial total work. Unfortunately, during the experiments the COD is only measured from S_{min} to S_{max}.

Therefore it is assumed that only load-COD measurements from the low stress ratios (0.02 and 0.05) sufficiently capture the non-linear behaviour. From the transition point measurements discussed in Section 6.7 it came forward that the transition point is always at approximately the same stress, independent of stress ratio. Therefore no transition point is observed for high stress ratios: For these cases S_{min} is larger than the transition point stress. It is therefore assumed that the complete load-COD curve, from zero stress to S_{max}, does not change for a changing stress ratio. In other words, it is assumed that by increasing S_{min} from zero to S_{max} for a fixed load-COD curve, the *Y*-ratio for the complete stress ratio range is covered.

Figure 6.40 shows the load-COD results for AR002S75, together with a 7th order fitted polynomial given by Equation 6.18.
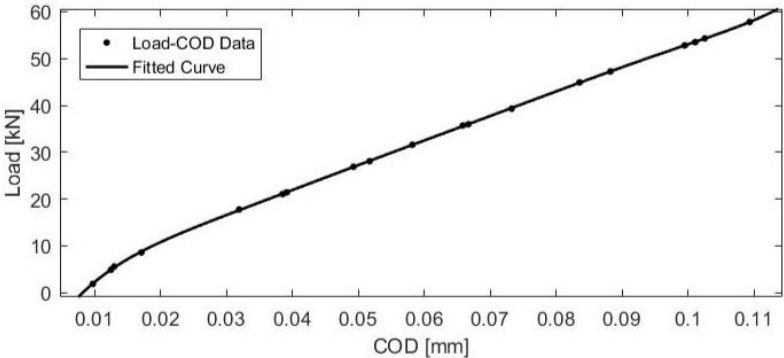
Figure 6.40: Load-COD Data and Fitted Curve for AR002S75, a = 25.8 mm and S_{max} = 75 MPa

$$P = p_1 x_{cod}^7 + p_2 x_{cod}^6 + p_3 x_{cod}^5 + p_4 x_{cod}^4 + p_5 x_{cod}^3 + p_6 x_{cod}^2 + p_7 x_{cod} + p_8 \qquad \textit{Equation 6.18}$$

In this equation, P is the applied load and x_{cod} is the COD. The coefficients of this polynomial and the quality of the fit are provided in Table 6.5.

Coefficient	Value	95% Confidence Bounds
p_1	0.3587	0.009123 – 0.7082
p_2	-0.3664	-0.6127 – -0.1202
p_3	-0.7504	-2.183 – 0.6824
p_4	0.3935	-0.4323 – 1.219
p_5	0.5174	-1.208 – 2.242
p_6	-0.2551	-1.014 – 0.5039
p_7	17.36	16.81 – 17.91
p_8	31.7	31.55 – 31.84
Equation	R^2	RMSE
Equation 6.18	0.9999	0.1309

Table 6.5: Coefficients for Fitted Curve Equation 6.18 - mean 0.05848 and std 0.03312

The load-COD curves with their corresponding polynomial fits for the other experiments are provided in Appendix D. Also the load-COD curves of Figure 6.36 obtained by Bathias and Clerivet are included in the analysis.

The integral of Equation 6.18 is used to calculate the cyclic work. S_{min} is varied from zero to S_{max}, such that the cyclic energy for all stress ratios between 0 and 1 is obtained. The total artificial work applied is calculated using Equation 6.17. The correction Y can then be calculated using Equation 6.15. The results are provided in Figure 6.41, together with the crack closure corrections of Schijve and Elber and the cyclic energy correction by Alderliesten.
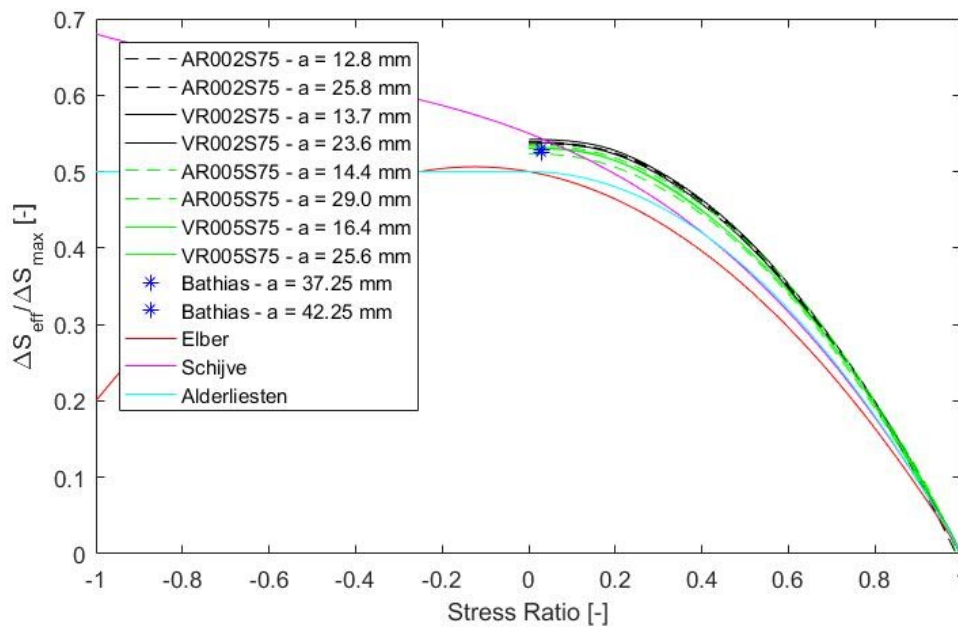
Figure 6.41: Cyclic Energy Correction from Multiple load-COD Results

As can be observed in Figure 6.41, the cyclic energy correction does not fully account for the discrepancy between the solution of Schijve and Alderliesten. The experimental cyclic energy corrections overcompensate this discrepancy. This is because Alderliesten assumes for higher stress ratios that the complete load-COD curve from $S = 0$ to S_{max} is linear. However, this assumption is

thought to be incorrect as in this research it is assumed that the non-linear load-COD behaviour still occurs for higher stress ratios. It is just not captured in the load-COD plot from S_{min} to S_{max}. But despite the discrepancy from Alderliesten's correction, there is still a striking correlation observed in Figure 6.41 between experiments and plasticity induced crack closure corrections proposed in literature.

More interesting is that the experimental cyclic energy corrections in Figure 6.41 show clear correlation independent of test environment, applied stress ratio and crack length. Even the experimental results subtracted from the plots of Bathias and Clerivet, which have been conducted at complete different load conditions and have been obtained for a complete different specimen, show clear correlation with the other cyclic energy corrections.

The discrepancy of the experimental cyclic energy corrections with for instance Schijve's correction is considerably small. Schijve's correction is empirically obtained, whereas the cyclic energy corrections are based on the laws of thermodynamics. From the striking correlation with other crack closure corrections and the independency of environment, load, stress ratio, crack length and specimen dimensions it can be safely said that the crack closure corrections do not correct for crack closure: It is a cyclic energy correction. It also explains why treating FCG from a SER perspective as in Section 6.6 provides such good correlation: The 'crack closure correction', which thus is a cyclic energy phenomenon, is already implicitly included if fatigue is approached from a SER perspective.

6.9 Plasticity

Plasticity in fatigue is an important phenomenon. According to conventional FCG theories, plasticity causes crack closure. Although this research claims S_{op} and ΔK_{eff} are artificial stresses required only because ΔK is used for similitude, the cause for the non-linear behaviour in the results of Section 6.7 may actually be caused by crack closure and plasticity. This section discusses the elastic-plastic zone, to determine if there are any differences between plastic behaviour of the material in vacuum and air environment. Furthermore the results may provide information in relation to the SER results of Section 6.6. The aim of this research is not to accurately quantify the plastic zone and the amount of energy dissipated through plasticity, but to observe important trends which may be related to observed results in Section 6.6 and 6.7. For easy comparison, the plastic zones in this chapter are observed at the same load cycle N as where the load-COD graphs in Section 6.7 are determined.

The elastic-plastic zone is observed using VIC. The determination of the sensitivity of VIC-analysis is already discussed in Section 6.5.1. The sensitivity for air experiments is sufficiently accurate to observe elastic-plastic behaviour of the material, but the window of the vacuum chamber has a negative effect on the sensitivity of the VIC-analysis. This increased noise has no influence on the displacement measurements of Section 6.5, but for the elastic-plastic zone determination the absolute displacements are a lot smaller than in Section 6.5.

The increase in noise due to the window in the vacuum chamber is determined by performing two similar tests, one in the vacuum chamber and one without. It turned out that the window in the vacuum chamber significantly increases the noise level in the elastic-plastic zone determination. Nonetheless both tests showed a similar trend in terms of elastic-plastic zone. It is therefore assumed that, despite an increase in noise level due to the window, the results stills are sufficiently accurate to compare between the elastic-plastic zones of experiments in air and vacuum.

Furthermore the elastic-plastic zone is considered, and thus not specifically the plastic zone that is responsible for energy dissipation. It is assumed that a similar elastic-plastic zone dissipates a similar amount of energy.

6.9.1 Air Environment

This section discusses the plastic zones for the experiments in air environment. Like crack closure experiments, the influence of crack length, stress ratio and maximum stress on the plastic zone is investigated in Section 6.9.1.1, 6.9.1.2 and 6.9.1.3 respectively.

6.9.1.1 Crack Length Effect on Plastic Zone

If the same load conditions apply, the plastic zone r_p should according to Equations 6.19 and 6.20 provided by Schijve increase for increasing crack length [1].

$$r_p = \frac{1}{\pi}\left(\frac{K}{S_{0.2}}\right)^2 \quad \textit{(plane stress)} \qquad\qquad \textit{Equation 6.19}$$

$$r_p = \frac{1}{3\pi}\left(\frac{K}{S_{0.2}}\right)^2 \quad \textit{(plane strain)} \qquad\qquad \textit{Equation 6.20}$$

Figure 6.42 shows the elastic-plastic zones for specimen AR03S75 at a crack length of 10.3 and 20.7 mm. It can be easily observed that the results confirm the theory of Schijve: The elastic-plastic zone increases for increasing crack length. The other tested specimens show similar behaviour as can be seen in Appendix E.
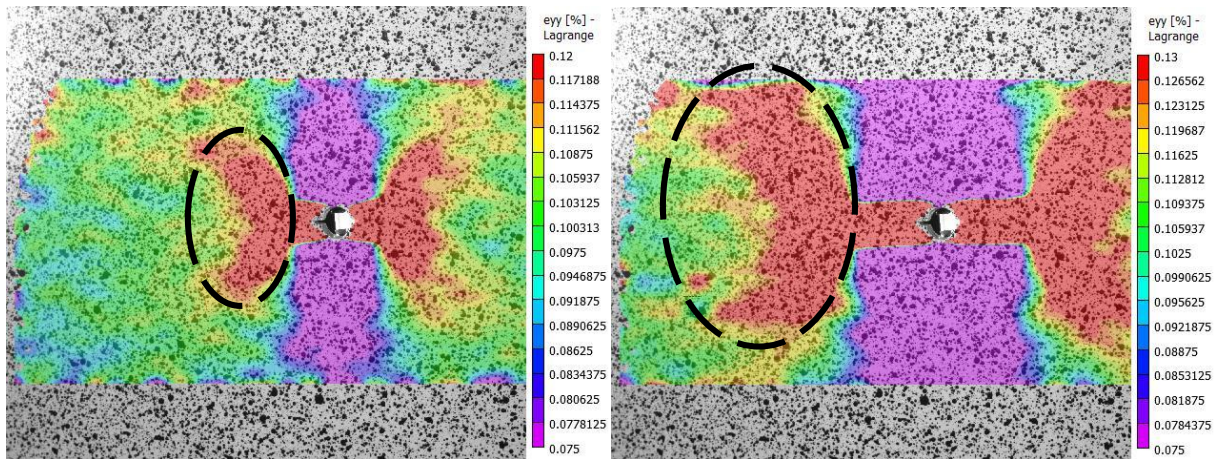
Figure 6.42: Elastic-Plastic Zones for Specimen AR03S75 at a = 10.3 mm (left) and 20.7 mm (right) – Area with Similar Strain Percentage Encircled.

6.9.1.2 Stress Ratio Effect on Plastic Zone

This section covers the *R*-effect on the plastic zone. Figure 6.43 shows the elastic-plastic zone for the stress ratios 0.02, 0.1, 0.3 and 0.5 at a crack length of 25.8, 23.9, 20.7 and 31.0 mm respectively. For proper comparison purposes in terms of *R*-effect, it is important that the crack length at each stress ratio is equal.

However, as data is only obtained every *ΔN* load cycles it cannot be exactly determined beforehand at what crack length the data is obtained. The chosen crack lengths in Figure 6.43 are as close to each other as possible. Furthermore it is aimed for to optically show the elastic-plastic zone as clear as possible, but sometimes this went at the expense of a different strain range legend. As the strain range given in the legend is not always equal, the area with the same strain range is encircled in black.

One can see that the elastic-plastic zone for R of 0.02, 0.1 and 0.3 is of approximate equal size. The elastic-plastic zone for the experiment with a stress ratio of 0.5 is larger, but this is because the crack length of this analysis is considerably larger than the other crack lengths. It therefore seems to be safe to say that the stress ratio does not have an influence on the elastic-plastic zone if S_{max} stays constant.
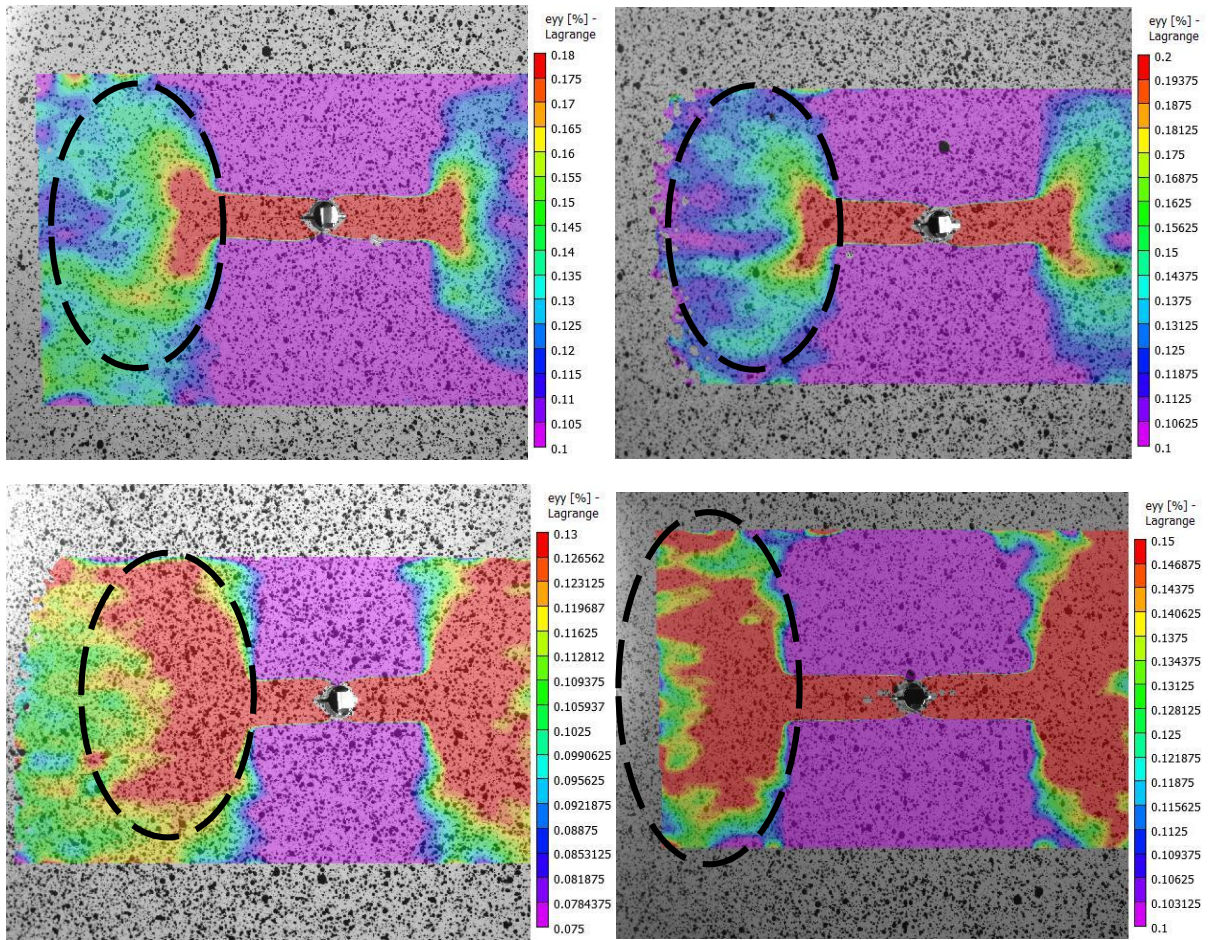
Figure 6.43: Elastic-Plastic Zones for: Top Left; Specimen AR002S75 at a = 25.8 mm, Top Right; Specimen AR01S75 at a = 23.9 mm, Bottom Left; Specimen AR03S75 at a = 20.7 mm, Bottom Right: Specimen AR05S75 at 31.0 mm - Area with Similar Strain Percentage Encircled

6.9.1.3   Maximum Stress Effect

According to Equation 6.19 and 6.20, the plastic zone size is dependent on crack length and S_{max}, but independent on stress ratio. The effect of S_{max} is covered in this section, crack length and stress ratio have already been covered in previous sections.

Figure 6.44 shows the elastic-plastic zone for the specimens with a stress ratio of 0.3 at a maximum stress of 75 MPa (crack length 20.7 mm) and 100 MPa (crack length 23.9 mm).
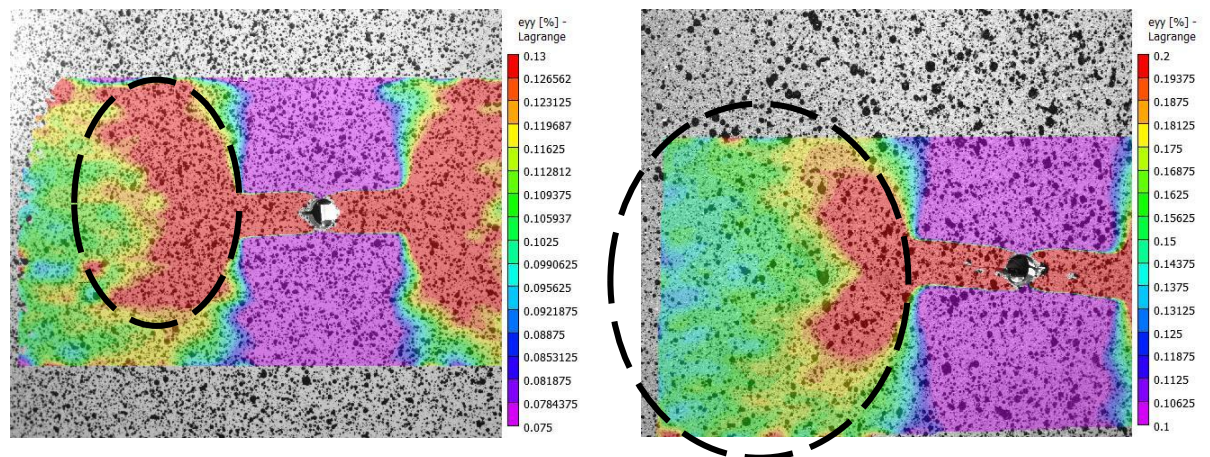
Figure 6.44: Elastic-Plastic Zones for: Left; Specimen AR03S75 at a = 20.7 mm and S_{max} = 75 MPa, Right; Specimen AR03S100 at a = 23.9 mm and S_{max} = 100 MPa - Area with Similar Strain Percentage Encircled

It can be easily seen that the elastic-plastic zone for S_{max} of 100 MPa is significantly larger. It is therefore concluded that the maximum stress indeed significantly influences the elastic-plastic zone. It explains the S_{max}-effect observed in the results of Section 6.6.1.

6.9.2 Vacuum Environment

This section covers the elastic-plastic behaviour for the various test conditions in vacuum. As such, it can be investigated if the same trends are observed in vacuum and air to relate the observations in this section to the observations of Sections 6.4, 6.6 and 6.7.

6.9.2.1 Crack Length Effect on Plastic Zone

Figure 6.45 shows the elastic-plastic zones for specimen VR002S75 at a crack length of 13.7 and 23.6 mm.
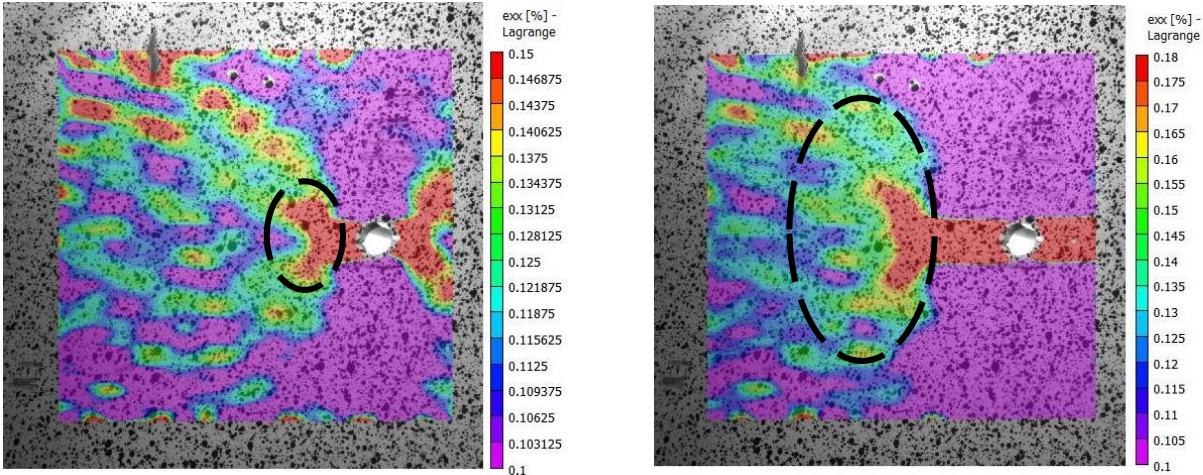
Figure 6.45: Elastic-Plastic Zones for: Left; Specimen VR002S75 at a = 13.7 mm, Right; Specimen VR002S75 at a = 23.6 mm - Area with Similar Strain Percentage Encircled

It can be observed that, in line with the observations in air, the elastic-plastic zone is increasing for increasing crack length. Furthermore the strain range is approximately equal to the strain range observed in the results in air environment. As discussed in the introduction of this section, the window of the vacuum chamber has some influence on the noise level of the VIC-analysis. It can be seen from the figures that indeed some noise is introduced, but as discussed previously it is assumed that the results in general still provide a good view of the elastic-plastic behaviour of the specimen.

6.9.2.2 Stress Ratio Effect on Plastic Zone

Figure 6.46 shows the results of the elastic-plastic zone for specimens tested in vacuum at a stress ratio of 0.02, 0.1, 0.3 and 0.5, with crack lengths of 23.6, 22.1, 20.1 and 27.8 mm respectively. Although noise plays a more significant role, it can still be observed that a similar trend is obtained as for the results in air. Apart from the similar trends in air and vacuum, also the strain range is of equal magnitude for results in air and vacuum. Again the elastic-plastic zone of the specimen tested at $R = 0.5$ is larger compared to other stress ratios, but this can again be attributed to a larger crack length.
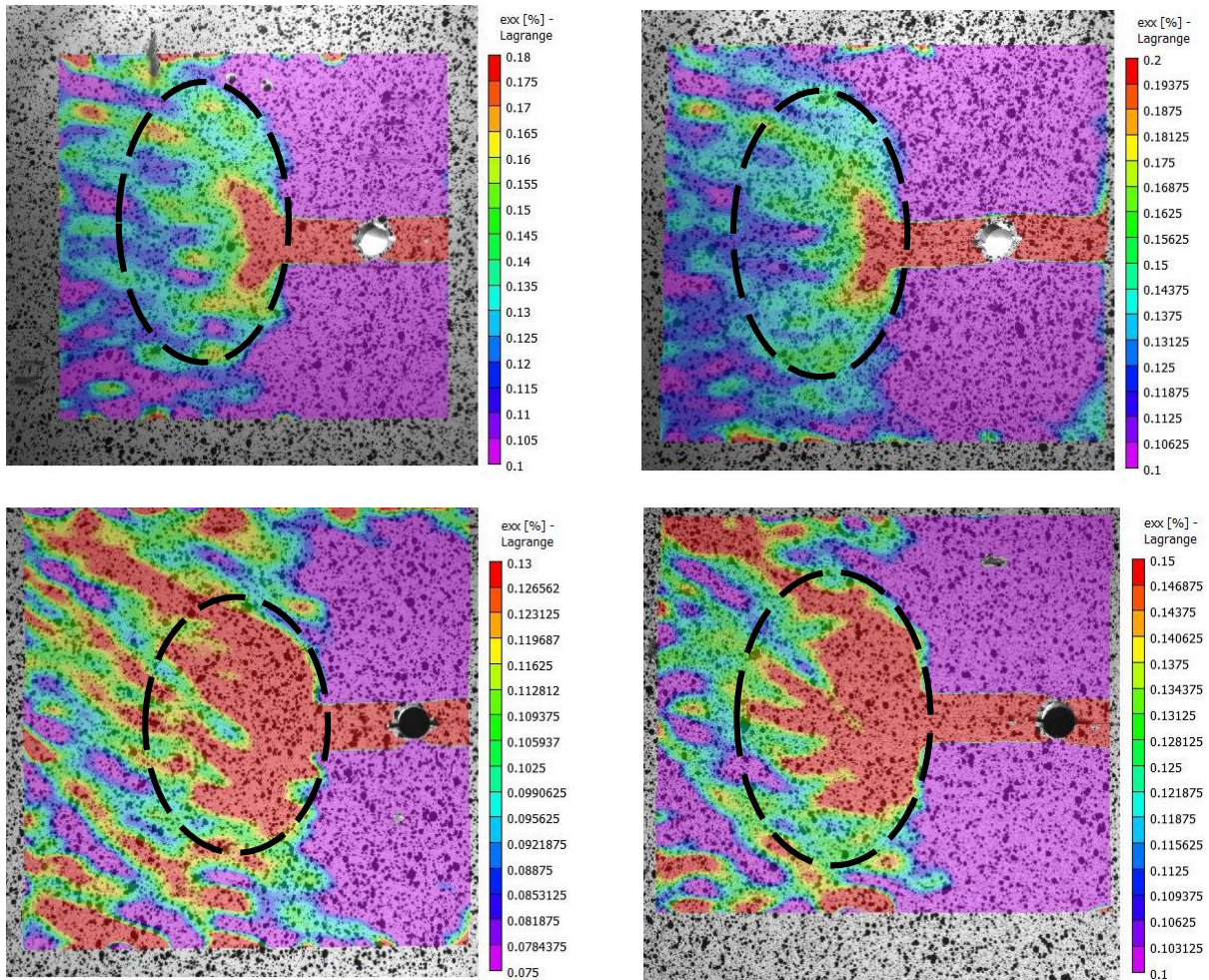
Figure 6.46: Elastic-Plastic Zones for: Top Left; Specimen VR002S75 at a = 23.6 mm, Top Right; Specimen VR01S75 at a = 22.1 mm, Bottom Left; Specimen VR03S75 at a = 20.1 mm, Bottom Right: Specimen VR05S75 at 27.8 mm - Area with Similar Strain Percentage Encircled

6.9.2.3 Maximum Stress Effect on Plastic Zone

Lastly the effect of the maximum stress is investigated. Figure 6.47 shows the results for the elastic-plastic zone of a similar stress ratio of 0.05, but with a different S_{max} of 75 MPa (crack length of 25.6 mm) and 100 MPa (crack length of 21.7 mm).
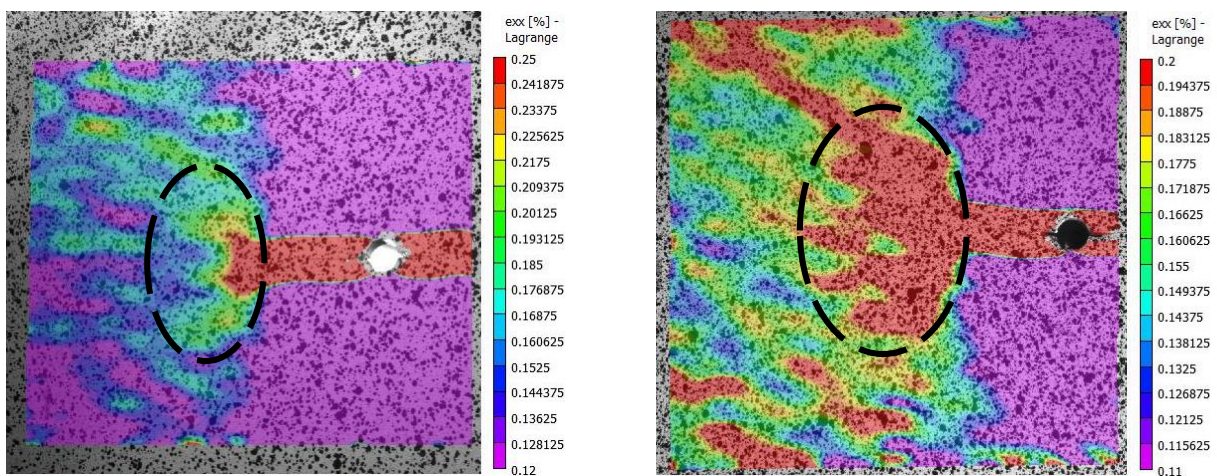
Figure 6.47: Elastic-Plastic Zones for: Left; Specimen VR005S75 at a = 25.6 mm and S_{max} = 75 MPa, Right; Specimen VR005S100 at a = 21.7 mm and S_{max} = 100 MPa - Area with Similar Strain Percentage Encircled

Again the results are conform the results observed in air: A higher S_{max} implies a larger elastic-plastic zone. Moreover the results are also in terms of strain range similar as the results from tests in air environment. It can therefore be concluded there is no difference observed between the elastic-plastic behaviour of experiments tested in air and in vacuum. It explains why the load-COD curves in Section 6.7 show similar behaviour if it is related to plasticity. Moreover there is no R-effect on plasticity, such that the transition point of the results in Section 6.7 is independent of stress ratio. Lastly the 'S_{max}-effect' observed in Section 6.6 can be related to the findings in this section.

6.10 Surface Roughness

Lastly the results on determination of crack surface roughness are presented. A rougher crack means that more energy has dissipated. As such it is aimed for to explain some of the trends observed in the figures of Section 6.6. The surface roughness is monitored by two microscopes: The LEXT OLS and the SEM. The used approach is discussed in Section 6.10.1. The influence of crack length, stress ratio and maximum applied stress are analysed. The results from specimens tested in air environment are covered in Section 6.10.2 and specimens tested in vacuum environment in Section 6.10.3. For a quick (numerical) overview of the combined results of Section 6.10.2 and 6.10.3 is referred to Section 6.10.4. Section 6.10.4 also roughly shows what the influence of the results is on the SER based FCG representation of Section 6.6.

6.10.1   Roughness Measurement

The NEXT OLS microscope is capable to determine surface roughness up to an accuracy of 0.2 μm [59]. The used objective is 10x, meaning that the microscope determined the surface roughness over an area of approximately 1 mm^2. The aim of crack surface roughness measurements is just like plasticity determination not to accurately quantify the effective crack surface, but to provide an idea of the trends in terms of crack surface roughness. And to determine if this is in line with observations from Section 6.6.

At different crack lengths (obviously with an inaccuracy of approximately 0.5 mm), the roughness is monitored. The roughness is monitored as the ratio area over the effective area, denoted as A/A_{eff}. As the roughness is only determined over an area of 1 mm^2, for each crack length three measurements are done. There was negligible deviation between the three measurements, such that it is assumed that the average of the three measurements provides a proper indication of the crack surface roughness corresponding to the crack length measured at. For crack surface roughness at electron level, the shape of striations is studied using the SEM. These photos are taken at a magnification of 5000x.

6.10.2   Air Environment

This section covers the observations from the crack surface roughness in air. The specimen tested at a stress ratio of 0.3 and S_{max} of 100 MPa is not included in this analysis as the crack surface was unfortunately damaged. For the other specimens the trends in terms of crack length effect, stress ratio effect and S_{max} effect are considered.

6.10.2.1 Crack Length (FCG rate) Effect on Crack Surface Roughness
Three-dimensional (3D) views of the crack surface of the first and last data point of specimen AR002S75 (at a crack length of 1 and 30 mm respectively), together with the SEM photos corresponding to the same crack length, are provided in Figure 6.48 and Figure 6.49 respectively. The 2D photos of the surface and the (analysed) photos of the other data points are provided in Appendix F.
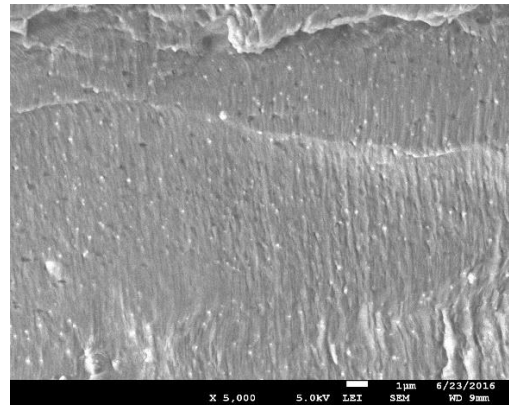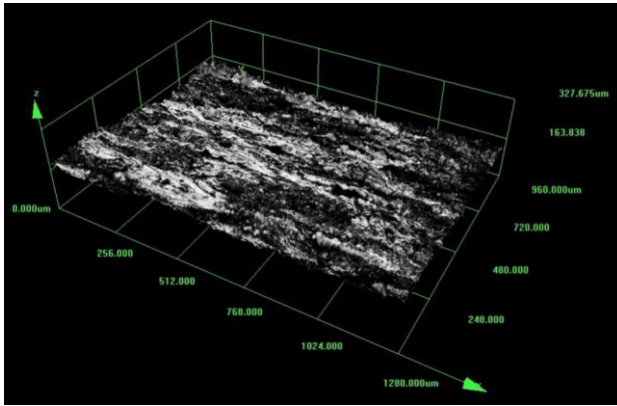
Figure 6.48: Crack Surface Roughness for Specimen AR002S75 at a = 1 mm
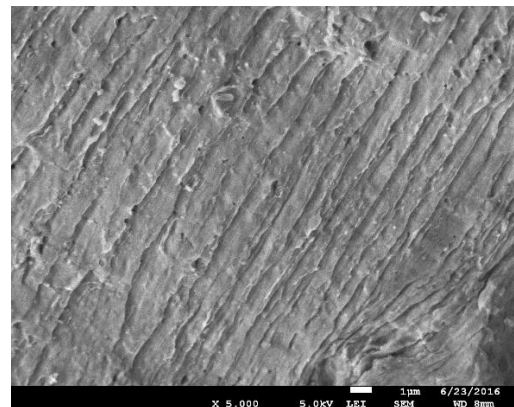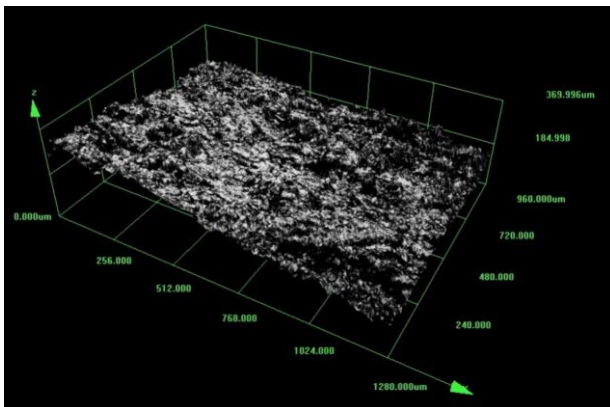
Figure 6.49: Crack Surface Roughness for Specimen AR002S75 at a = 30 mm

It can be observed from Figure 6.48 and 6.49 by the NEXT OLS that the crack surface becomes more dimpled for an increasing crack length. It seems that the crack surface becomes rougher for an increasing crack length (in other words, the crack surface becomes rougher for an increasing FCG rate). This trend is observed for all investigated specimens as can be seen in Appendix F. The SEM photos also indicate a rougher surface for increasing crack length, and also the distance between striations increases. In other words, an increasing crack length (and thus increasing FCG rate), implies that more energy per cycle is dissipated which is conform observations in Section 6.6.

6.10.2.2 Stress Ratio Effect on Crack Surface Roughness
Figure 6.50 and 6.51 show the crack surface roughness for a stress ratio of 0.1 and 0.5 at a crack length of 1 mm respectively. At first glance there is no clear difference between Figure 6.48, 6.50 and 6.51. However, as discussed in Section 6.10.4 there is a slight *R*-effect. From a closer look at especially the SEM photos it seems that there is indeed a slightly rougher surface in case of a higher stress ratio. The same trend is observed at other crack lengths and for different stress ratios. It may therefore be said that stress ratio has a slight but definite effect on the crack surface roughness in air experiments. This clarifies why there is still a slight *R*-effect observed in the results of Section 6.6.
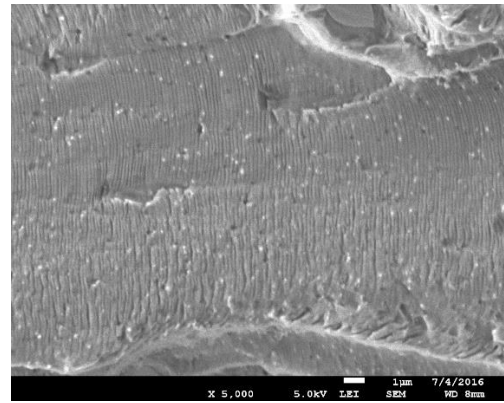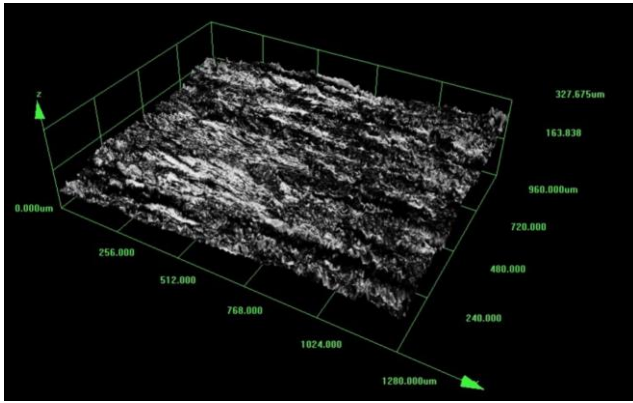
Figure 6.50: Crack Surface Roughness for Specimen AR01S75 at a = 1 mm
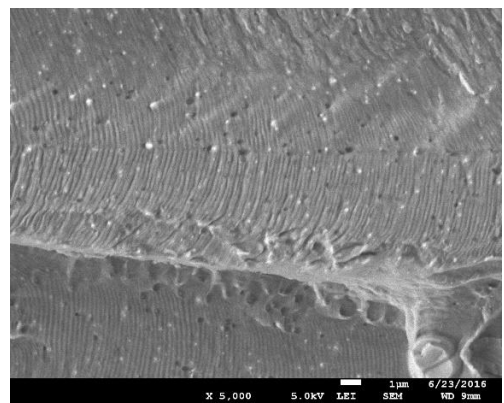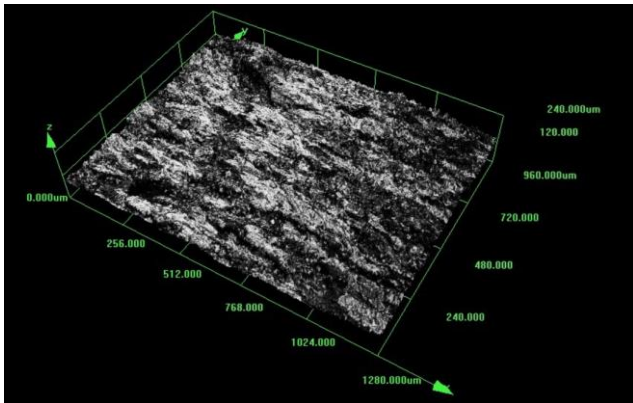
Figure 6.51: Crack Surface Roughness for Specimen AR05S75 at a = 1 mm

6.10.2.3 Maximum Stress Effect on Crack Surface Roughness

Lastly the influence of a different maximum applied stress is analysed. Figure 6.52 and 6.53 show the roughness results for a stress ratio of 0.05 at a crack length of 1 mm, but Figure 6.52 for a maximum applied stress of 75 MPa and Figure 6.53 for a maximum applied stress of 100 MPa.
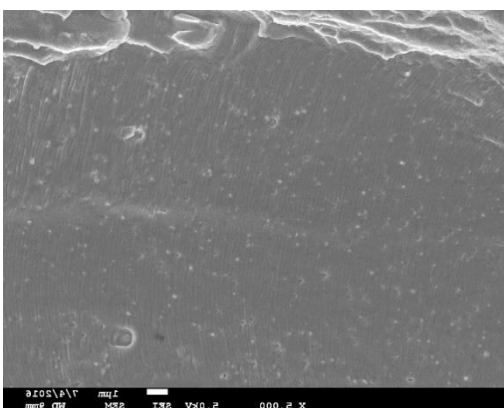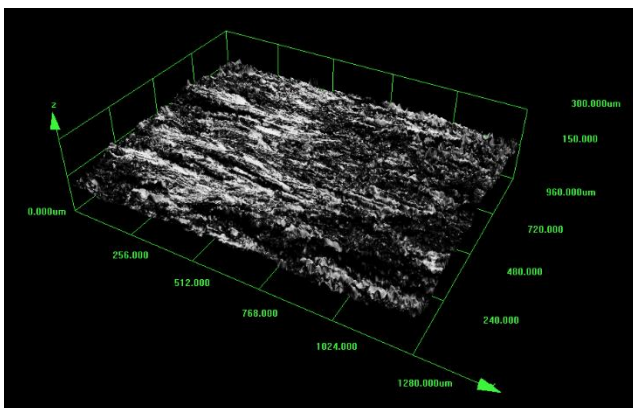
Figure 6.52: Crack Surface Roughness for Specimen AR005S75 at a = 1 mm
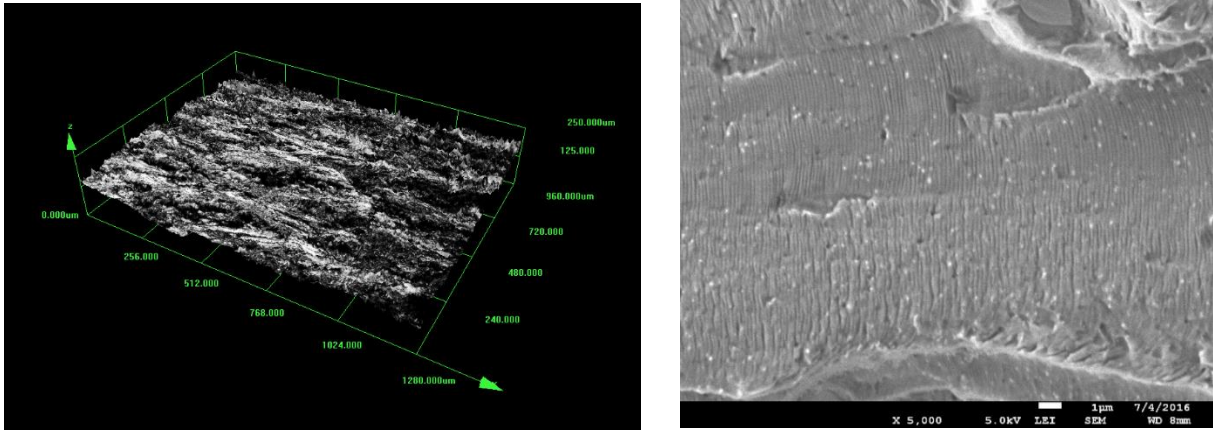
Figure 6.53: Crack Surface Roughness for Specimen AR005S100 at a = 1 mm

The NEXT OLS photos do not show a clear influence of the maximum stress on the crack surface roughness However, as this is difficult to observe with the naked eye, the numerical analysis of the crack surface roughness discussed in Section 6.10.4 provides an outcome. The SEM photos and the FCG data discussed in Section 6.6 indicate that maximum stress indeed does have an influence of the crack surface roughness.

6.10.3   Vacuum Environment

The results of crack surface roughness determination of experiments executed in air, show an increasing roughness for increasing FCG rate, increasing stress ratio and increasing S_{max} and therewith show a trend as may be expected from the results obtained in Section 6.6. This section covers the observed crack surface roughness trends in vacuum.

6.10.3.1 Crack Length (FCG Rate) Effect on Crack Surface Roughness

The 3D views of the crack surface and SEM photos for specimen VR005S75 are provided in Figure 6.54 and Figure 6.55 for a crack length of 1 and 30 mm.
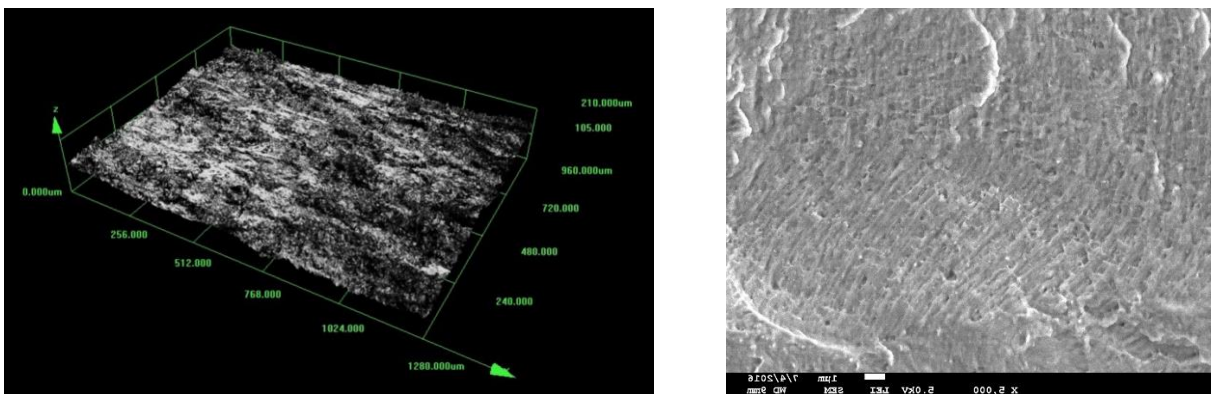
Figure 6.54: Crack Surface Roughness for Specimen VR005S75 at a = 1 mm
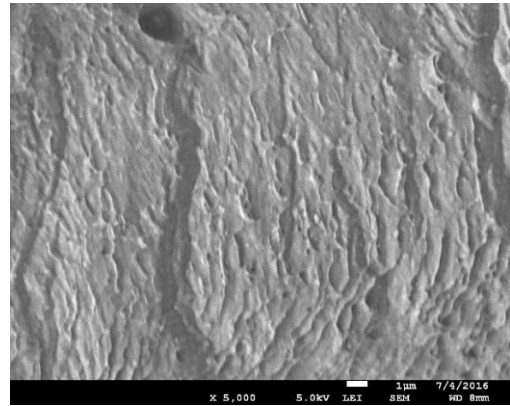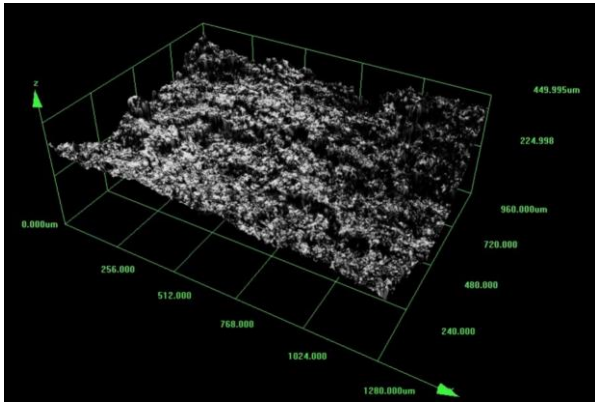
Figure 6.55: Crack Surface Roughness for Specimen VR005S75 at a = 30 mm

Equal as in air environment, it can be observed that the crack surface roughness increases for increasing crack length (or increasing FCG rate). However, in vacuum this increase in roughness is considerably clearer in comparison with air. These findings are conform similar research by Yoshinaka and Nakamura [57].

For the other specimens and data points a similar trend is observed as can be seen in Appendix F. Again the trends are in line with the findings of Section 6.6: For an increasing *da/dN* also the energy dissipated per cycle increases.

6.10.3.2 Stress Ratio Effect on Crack Surface Roughness
Figure 6.56 and 6.57 show the crack surface roughness for specimens tested at a stress ratio of 0.1 and 0.3 both at a crack length of 1 mm.
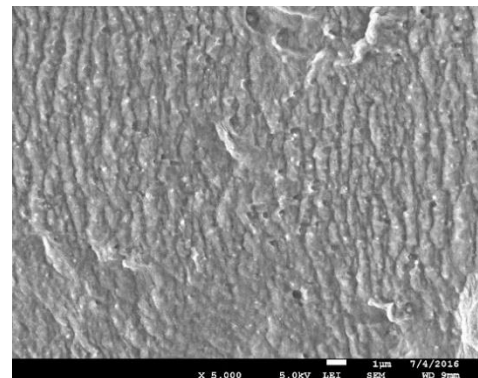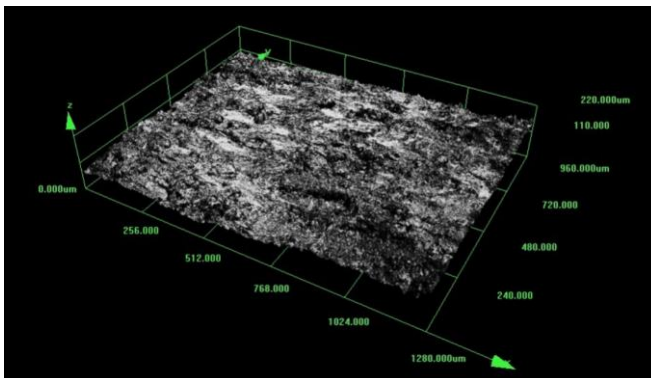
Figure 6.56: Crack Surface Roughness for Specimen VR01S75 at a = 1 mm
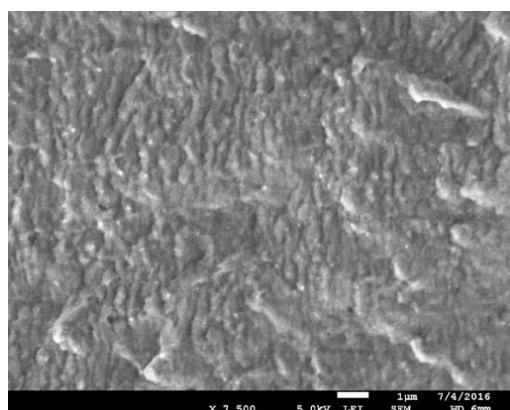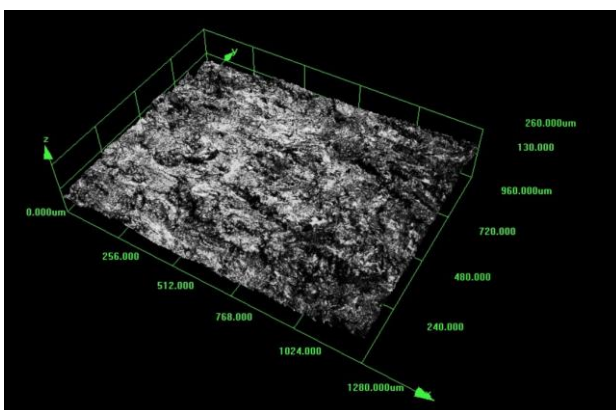
Figure 6.57: Crack Surface Roughness for Specimen VR03S75 at a = 1 mm

Although at first glance there is no clear difference, it still seems that larger *R*-effect causes a slightly rougher crack surface. The effect seems to be clearer in vacuum compared to air. This would be conform observations in Section 6.6, but the numerical results in Section 6.10.4 provide a clearer picture of the stress ratio effect on surface roughness.

6.10.3.3 Maximum Stress Effect on Crack Surface Roughness

Lastly the results of the crack surface roughness for two specimens subject to a different maximum applied stress are given in Figure 6.58 and 6.59, both at a crack length of 1 mm.
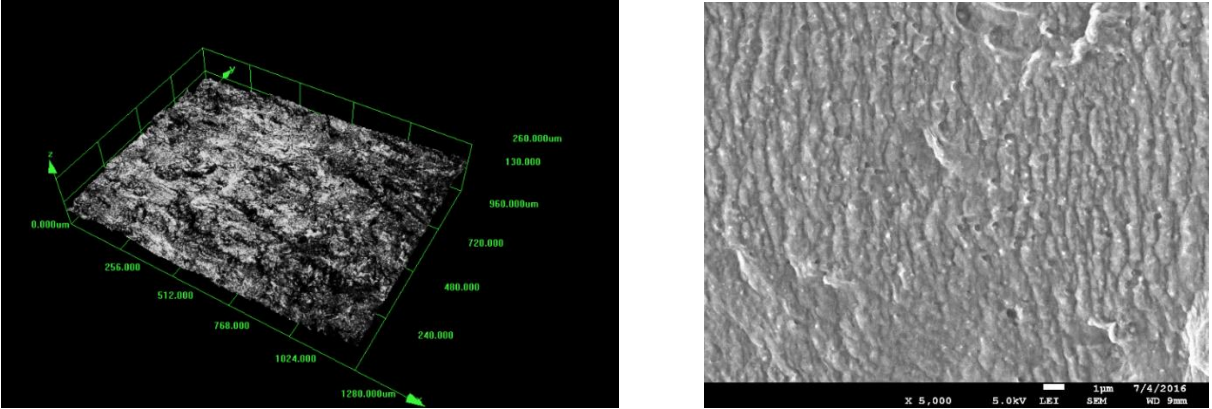
Figure 6.58: Crack Surface Roughness for Specimen VR03S75 - a = 1 mm
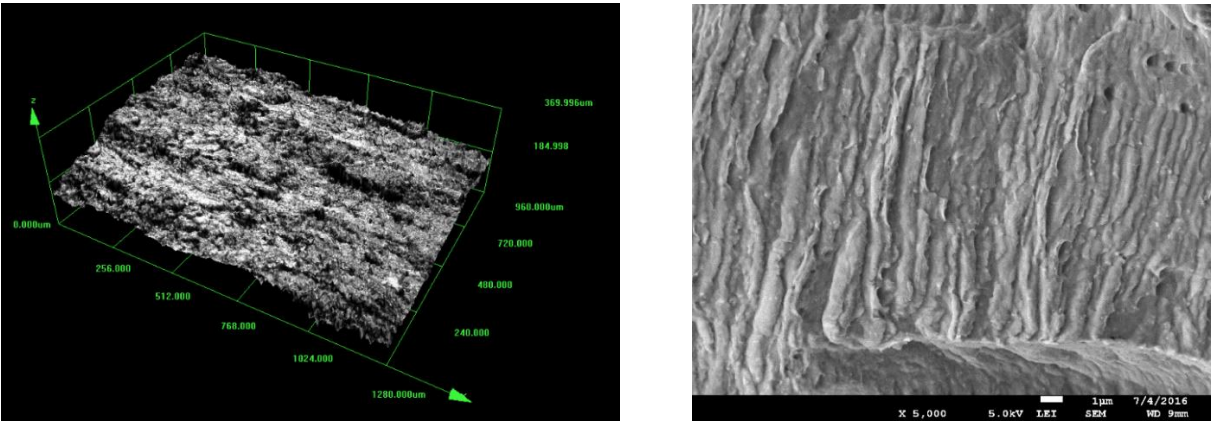
Figure 6.59: Crack Surface Roughness for Specimen VR03S100 - a = 1 mm

Again, similarly as in air environment, there is a clear difference observed in crack surface roughness if a different maximum stress is applied. Also in vacuum environment the crack surface becomes rougher for a higher applied stress. This is conform observations on SER as discussed in Section 6.6.

6.10.4   Numerical Roughness Results and Influence on SER FCG Data

Section 6.10.2 and 6.10.3 presented the crack surface roughness results in terms of a 3D representation and by means of SEM photos. Although this provides a good indication of the surface roughness, this section provides the numerical values obtained with the NEXT OLS microscope in Section 6.10.4.1. Also a rough indication of the effect of the crack surface roughness on the SER data presented in Section 6.6 is provided in Section 6.10.4.2.

6.10.4.1 Crack Surface Roughness: Numerical Summary

Figure 6.60 shows the value A/A_{eff} for both air and vacuum environment at a fixed maximum applied stress of 75 MPa. The lower A/A_{eff}, the rougher the crack surface.
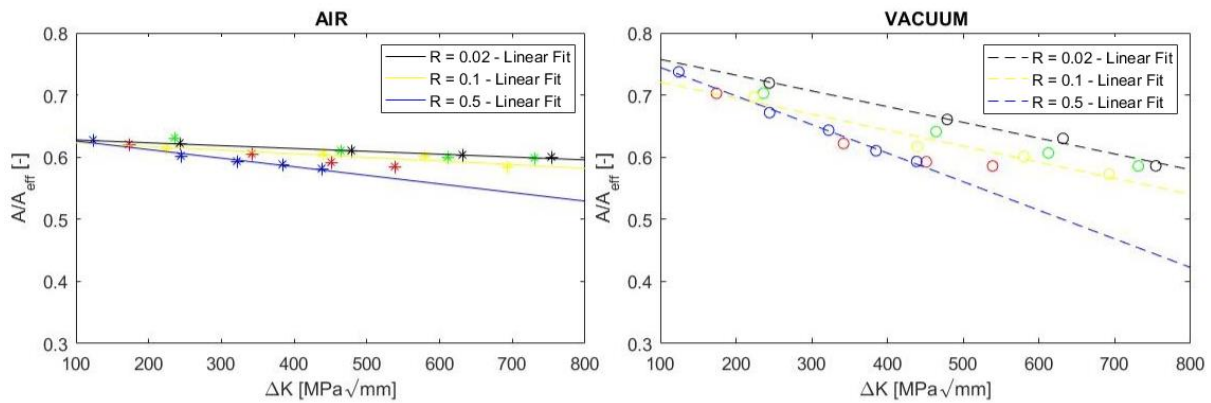
Figure 6.60: Crack Surface Roughness for a fixed S_{max} of 75 MPa. Left: Air Environment. Right: Vacuum Environment.

It can be clearly observed there is a difference in crack surface roughness (development) between air and vacuum. However, there are also some similar trends observed. As the maximum stress is fixed, on can clearly see that the crack surface roughness increases for an increasing crack length. Furthermore one can observe a slight but definite *R*-effect. For the stress ratios of 0.02, 0.1 and 0.5 a linear trend line is fit through the data points in order to better show this *R*-effect. All these observations correlate with the observations in Section 6.6 and the SER.

The difference between air and vacuum is that the crack surface in air is initially rougher than in vacuum. However, the surface roughness increases less for an increasing crack length. Therefore there is a switch point and eventually the crack surface is rougher in vacuum than in air. This is all conform earlier crack surface roughness research by Yoshinaka and Nakamura [57] and also conform SER data provided in Section 6.6.

Lastly the influence of a different maximum stress on the crack surface roughness is provided. This is given by Figure 6.61.
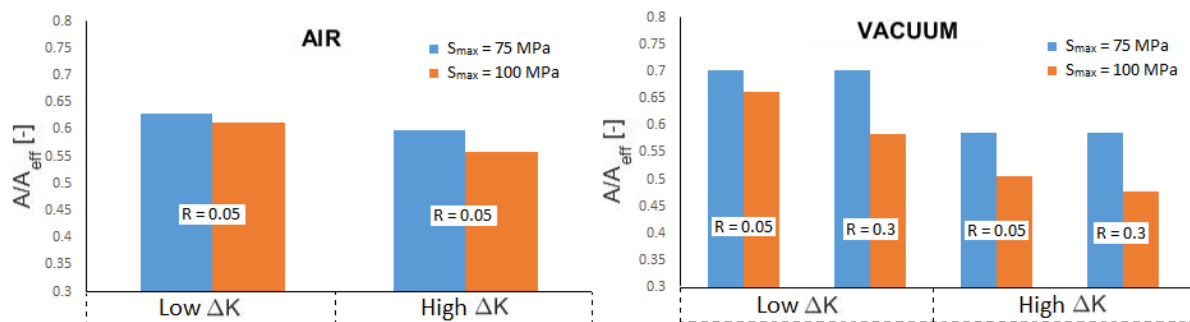
Figure 6.61: Influence of S_{max} on Crack Surface Roughness. Left: Air Environment. Right: Vacuum Environment.

The figure shows that the crack surface roughness is, independent of stress ratio and crack length, rougher for a higher applied maximum stress. The figure also emphasizes earlier observations that the roughness increases for an increasing crack length, there is a slight *R*-effect and there is a switch point where the crack surface roughness in vacuum becomes larger than in air.

6.10.4.2 Effect of Crack Surface Roughness on SER Data

The results of the previous section are used to determine the effect on the SER data provided in Section 6.6. As discussed in the previous section, for each tested specimen there is a linear line fit through the roughness data points as indicated in Figure 6.60. As such a function for the ratio *A/A$_{eff}$* is obtained dependent on *ΔK* (or equivalently the crack length *a*).

The *da/dN* data previously obtained can as such also be easily transformed to the effective crack growth rate *da_eff/dN* by multiplying *da/dN* by the inverse of *A/A_eff*:

$$\frac{da_{eff}}{dN} = \frac{da}{dN}\frac{a_{eff}}{a}$$ *Equation 6.21*

One needs to take into account that the linear trend lines fitted in Figure 6.60 provide only a rough estimation of the crack surface roughness. As such also the $\frac{da_{eff}}{dN}$ calculated using Equation 6.21 is only a rough estimation. For an accurate effective area consideration further research is required. However, it is assumed that the rough estimation provides a proper idea of crack surface roughness influence on SER data.

For comparison purposes, in Figure 6.62 the results of the numerical analysis performed in Chapter 5 are provided again.
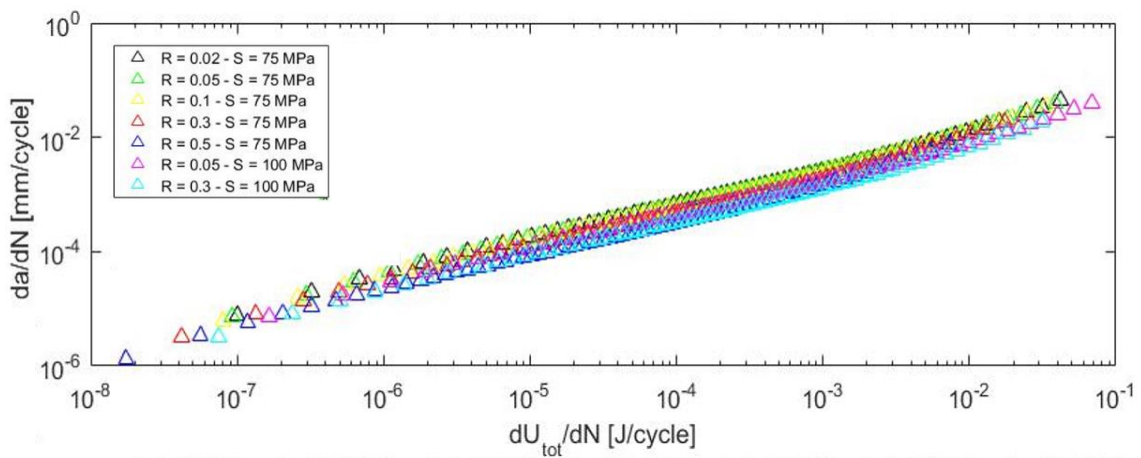
Figure 6.62: Numerical Analysis of Total SER versus FCG Rate

Figure 6.63 shows the SER as a function of FCG rate as given in Section 6.6 for the experiments performed in air environment and Figure 6.64 shows the same results but with the effective crack growth rate *da_eff/dN*.
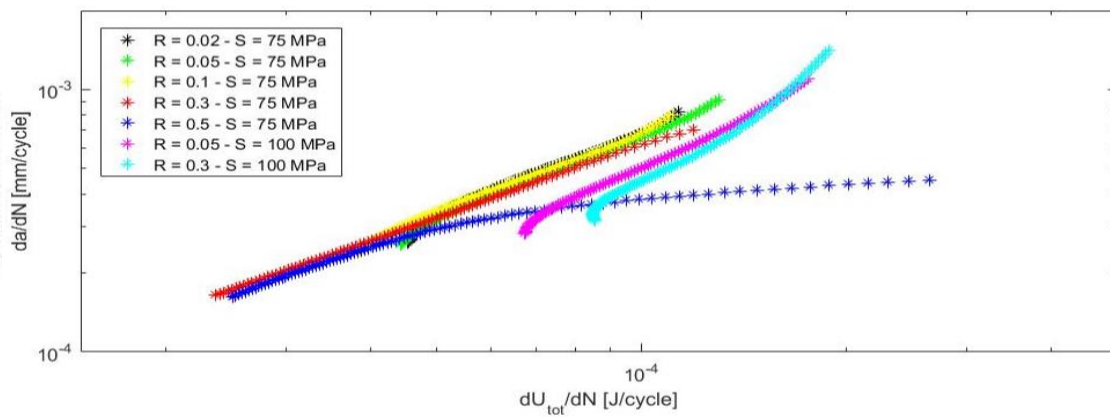
Figure 6.63: Total SER Data versus FCG Rate Data in Air
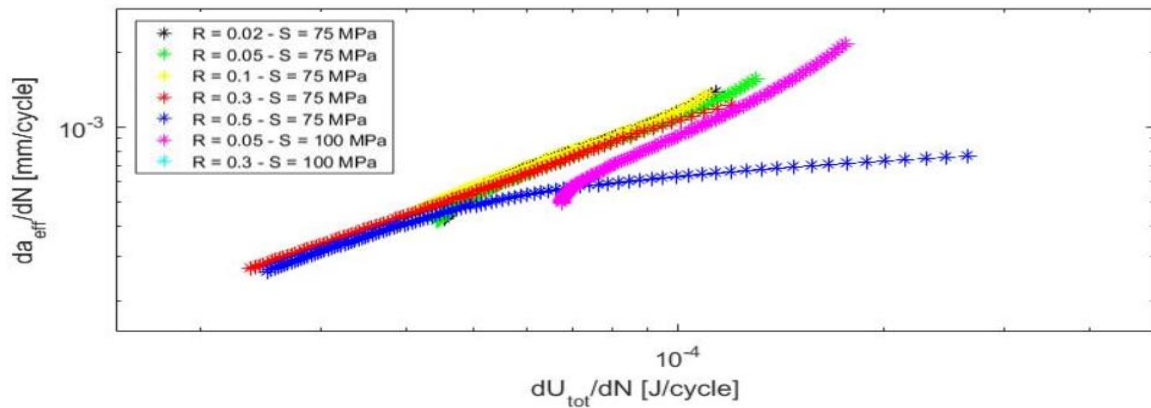
Figure 6.64: Total SER Data versus Effective FCG Rate Data in Air

It can be clearly observed that the experimental results in air environment are conform the numerically predicted trend and conform the theory in Chapter 3. Furthermore it can be observed that the results correlate better if da_{eff}/dN is considered. This is most clearly noticed for the specimen tested at R = 0.05 and a maximum applied stress of 100 MPa, whose results significantly shift towards the other results. At low crack growth rates there is still an obvious S_{max}-effect in terms of SER. As discussed in Section 6.9 this might be a result of a difference in SER due to plasticity. To correlate for this difference, the energy release through plasticity will need to be quantified and also other energy dissipation mechanisms such as corrosion will need to be taken into account. Furthermore a_{eff} needs to be quantified more accurately.

Figure 6.65 and 6.66 show the SER data for respectively da/dN and da_{eff}/dN in vacuum environment.
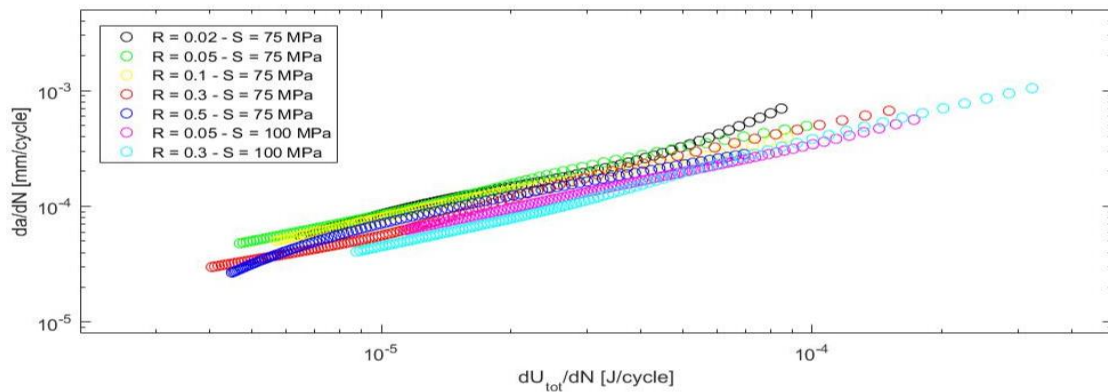
Figure 6.65: Total SER Data versus FCG Rate Data in Vacuum
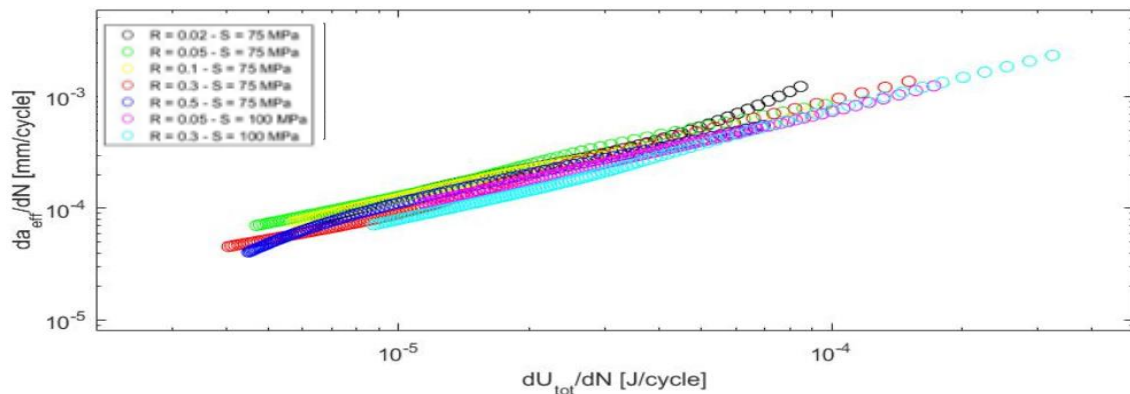
Figure 6.66: Total SER Data versus FCG Rate Data in Vacuum

Figure 6.65 and 6.66 again show a striking correlation with the numerical results of Figure 6.62. Vacuum environment is an inert environment, meaning that energy dissipation mechanisms dependent on external factors, such as corrosion in air environment, are not present in vacuum. It is therefore in line with the expectations that the experimental results in vacuum environment correlate best with the numerical analysis. Furthermore it can be clearly observed that the results correlate significantly better if da_{eff}/dN is considered instead of da/dN. This is also in line with the hypotheses of Chapter 3. If for instance energy dissipated through plasticity can also be quantified, it is expected that even better correlation is obtained. As such the results of this Master thesis show that FCG should be approached from a SER perspective.

7 Discussion

From the literature review in Chapter 2, it came forward that a better understanding of fatigue is required. Based on the literature review three hypotheses were formulated: ΔK is an improper similitude parameter for FCG, FCG should be approached from a SER perspective and the R-effect is not caused by plasticity induced crack closure. This section discusses the results of Chapter 5 and 6 in relation to the hypotheses and theories behind the hypotheses discussed in Chapter 3. Each section discusses one of the hypotheses, and Section 7.4 discusses the overall research approach of this thesis.

7.1 ΔK is an incorrect similitude parameter for FCG

The literature review in Chapter 2 already strongly indicated this hypothesis is correct. By using ΔK as similitude parameter, an R-effect arises. This is accounted for by the theory of plasticity induced crack closure, reducing ΔK to an effective ΔK_{eff}. FCG shows good correlation if ΔK_{eff} is considered. In Section 6.4.1, where FCG is approached from this SIF perspective, these trends are successfully reproduced. Furthermore in Section 2.1.3 it is discussed that an equation relating the SIF K with the SERR G exists, as such insinuating FCG is completely understood.

However, the literature review showed how G historically is derived for quasi-static loading conditions, but later adopted in a SIF definition used for fatigue loading conditions. It cannot be claimed that a parameter derived for quasi-static loading conditions is also applicable to fatigue loading conditions. This SIF K was then rather arbitrarily adopted as a parameter for FCG description, but the famous Paris equation to predict FCG is nothing more than an empirically determined equation as discussed in Section 2.3.3. Also the crack closure corrections to determine ΔK_{eff} are empirically derived equations. As such there does not exist a proper scientific theory of FCG.

Early tests by Kirby and Beevers, discussed in Section 2.2.1.4, showed no R-effect for threshold SIF in vacuum. In Section 6.4.2 the R-effect over the entire SIF range was covered, and in vacuum indeed no (clear) R-effect was observed. Based on the results of Section 6.4 at least it can be concluded that FCG from a SIF perspective shows complete different results in air and vacuum, although there should be no reason for such a difference based on the conventional theories of fatigue.

A collapse of the R-effect in vacuum could maybe be attributed to a difference in (plasticity induced) crack closure measurements. However, Section 6.7 showed that load-COD results in air and vacuum are identical. Since Section 6.9 shows a similar elastic-plastic behaviour for each tested specimen in air and vacuum environment, it may indeed be expected based on the plasticity induced crack closure theory that similar load-COD results are observed. In earlier work of Schijve containing experiments in air and vacuum a similar trend was observed [58]. However, this research was only performed for a single stress ratio and as such not related to the absence of an R-effect.

Furthermore the crack closure correction is actually a cyclic energy problem as is discussed in Section 7.3. By choosing ΔK for similitude actually an incorrect applied work is considered. This needs to be

corrected for by an opening stress, but effectively the incorrect applied work is only corrected for the actual applied cyclic work.

7.2 Fatigue is Strain Energy Release Dominated

As mentioned in Section 7.2 the SERR G cannot be related to K because of different loading conditions, and as such G cannot be used for FCG description. Instead of that, the SER during a complete fatigue load cycle is considered. The theory in Section 3.2.2 discussed that good correlation should be obtained if FCG is approached from a SER perspective, with a possible slight R-effect due to a difference in applied cyclic work for a different stress ratio. However, any R- or S_{max}-effects observed in the SER should be able to be traced back by means of energy dissipation mechanisms such as plasticity and crack surface roughness.

The numerical analysis in Chapter 5 already showed a trend indicating the validity of the hypothesis explained in Chapter 3. Good correlation is obtained, especially for a fixed S_{max}, but the analysis did not include possible energy dissipation mechanisms such as crack surface roughness, a plastic wake and environmental effects.

The results in Section 6.6 clearly show that the observed trends correlate with the expectations from the theory of Section 3.2.2 and the numerical analysis in Chapter 5. The results in both air and vacuum environment are conform an expected trend, in contrary to the SIF based FCG results. It can therefore be said that FCG is indeed SER dominated instead of SIF dominated.

Nevertheless the results in Section 6.6 showed some discrepancy between air and vacuum. The R-effect for a fixed maximum stress is for Instance stronger in vacuum than in air. This discrepancy cannot come from plastic dissipated energy, as the results in Section 6.9 showed similar elastic-plastic behaviour in air and vacuum. However, the crack surface roughness analysis in Section 6.10 showed that the R-effect on crack surface roughness is stronger in vacuum and if the effective crack length is considered the large R-effect in vacuum is largely accounted for.

Furthermore there seems to be a larger SER difference between a varying S_{max} in air than in vacuum, although the axes scales make it optically slightly worse than it effectively is. The fact that more energy per cycle is dissipated for a larger S_{max} is completely conform observations in Section 6.9: A larger S_{max} increases the elastic-plastic zone significantly. However, this increase is similar for experiments in air and vacuum, whereas the SER results of Section 6.6 show a larger S_{max}-effect in air than in vacuum. Also the crack surface roughness discussed in Section 6.10 does not completely account for this discrepancy, although the S_{max}-effect on crack surface roughness is stronger in vacuum than in air.

It is therefore not fully known where this discrepancy, especially for lower FCG rates, comes from. It might be possible that the discrepancy can be traced back by some kind of energy dissipation mechanism introduced by air environment such as corrosion. However, vacuum is the most inert environment one can test in. As such this should provide the best correlation with the theory discussed in Section 3.2.2 and the numerical analysis in Chapter 5. This is obviously the case, meaning that it is safe to say FCG should be approached from a SER perspective.

7.3 The R-effect is not caused by Plasticity Induced Crack Closure

By using ΔK as similitude parameter, an R-effect arises. This was attributed to plasticity induced crack closure. Due to plasticity, a crack can close before a zero tensile load is applied. Therefore a certain opening stress needs to be overcome before the crack will propagate. This reduces the SIF ΔK to an effective SIF ΔK_{eff}. FCG shows good correlation if a crack closure correction is applied, reducing ΔK to ΔK_{eff}.

However, the literature covered in Section 2.2.1 already heavily disputed this theory. Many contradicting results with regards to crack closure have been observed. Furthermore it seems to make no sense to assume that a crack is closed before S_{min} is applied even for arbitrarily high applied S_{min}. Also a different presentation of SIF based fatigue data, covered in Section 2.2.2.1, showed that R-effect disappears if FCG data is presented in a different form. However, this alternative presentation of FCG still does not cover the physics of fatigue as it is still based on the SIF K.

The results of FCG based on SIF in Section 6.4 showed that an apparent R-effect in air disappears in vacuum. According to crack closure theory, this should only be possible if no crack closure is observed in vacuum. However, the results on elastic-plastic zones in vacuum are similar as in air and also the load-COD results are similar. Although this means that plasticity may indeed cause the crack to close before a zero tensile stress, it also means that the R-effect is not caused by crack closure.

The non-linear to linear load-COD transition point occurs at significant lower stresses than crack closure corrections by Elber and Schijve prescribe. The opening stress, or transition point, is conform earlier experiments independent on crack length and stress ratio, and only slightly dependent on maximum stress. For all experiments in Section 6.7 the non-linearity in load-COD results disappear as soon as S_{min} is larger than the stress corresponding to the transition point. It is unknown what causes the non-linear part of the load-COD curve, but it is not necessary related to crack closure. Compressive stresses may for instance cause the non-linear part too. Although one could say that the results of Section 6.7 have failed to reproduce results from conventional FCG theory, the intermezzo of Section 6.7.5 proofed the contrary. Actually similar results have been obtained by other researchers, but disputable opening stresses have been assigned to the obtained load-COD data. It seems that opening stresses are simply depicted conform crack closure corrections as otherwise the R-effect cannot be correlated for.

In line with this observation, the crack closure correction could also be approached from an energy perspective. The results provided in Section 6.8 show that the opening stress is an artificial stress required to correct for cyclic energy. If ΔK is chosen for similitude, actually an incorrect cyclic energy is considered. This is corrected for by an artificial opening stress, such that the actual cyclic energy is obtained. The results in Section 6.8 show if the crack closure correction is considered from an energy perspective, that great correlation is observed with crack closure corrections from for instance Schijve and Elber. These results also explain why the SER based FCG results do not show an R-effect: This cyclic energy is already implicitly included if fatigue is approached from an energy perspective. It shows that R-effect is an artefact of choosing ΔK for similitude. Furthermore it can be safely said that plasticity induced crack closure, whether it exists or not, does not cause the R-effect.

7.4 Overall Research Approach

This section discusses the overall research approach. Obviously no research happens without unforeseen setbacks. For this research for instance the determination of the SER turned out to be more complicated than initially expected. As FCG is generally considered from a SIF perspective instead of SER perspective, there is no standard manual to measure displacements.

The displacements of the specimens used for this research are very small. It was not foreseen that the displacement would be so small, that in fact they were measured within the noise of the displacement sensors of the MTS fatigue bench. However, as the fabrication of the specimens is rather time consuming it was no option to redesign the specimens. Instead of that it was decided to measure the displacements with different measurement tools. However, for future work it would be recommendable to have a standard test manual for SER analysis.

Likewise there is no clear standard for accuracy requirements of a COD-meter. As was mentioned in Section 4.3.1.4 the COD-meter available at DASML at first was not accurate enough to determine COD. After the legs of COD-meter were maximum shortened, the COD-meter turned out to be non-linearly calibrated except for the range of 6-9 mm. Although this is obviously not ideal, and although for very small crack lengths there was more noise than desired, the specimen notch was adapted to this shortcoming of the COD-meter and it was assumed that sufficiently accurate load-COD measurements could be performed. On top of this, there was a technical problem with the cabling and the VIC software, such that for the experiments in air not enough data was collected for reliable load-COD determination based on VIC-analysis. In future work this could obviously be improved. Besides these practical test problems, a variety of other problems occurred ranging from non-working cabling to wrong calibrations and from wrong VIC speckle patterns to emergency stops.

Furthermore it was unfortunately decided to approach the crack closure correction as a cyclic energy phenomenon in a later stage of the research project, meaning that not the complete load-COD curves are determined. Although this could be backed up for results at lower stress ratios, in future work it should be taken into account that for cyclic energy correction determination not just the COD between S_{min} and S_{max} needs to be measured, but the COD from zero stress to S_{max}.

Furthermore the hypotheses and the theory of FCG based on SER are partially based on SER as a consequence of FCG instead of a cause. Although this does not have an influence on the hypothesis that FCG is SER dominated, it may be a problem to develop an FCG prediction model based on SER. Also the numerical analysis performed in Chapter 5 cannot be used as a scientifically correct FCG prediction model, as the AFGROW part of these simulations are based on the invalidated SIF K.

Lastly even stronger conclusions on FCG as a SER dominated phenomenon could be drawn if all energy dissipating mechanisms such as plasticity and crack surface roughness are quantified. In the end, if all these mechanisms can be accurately quantified, a correlation without any discrepancy should be observed for SER based FCG presentation no matter in which environment it was tested. As FCG based on SER is only in its early phase, there is still a lot of research ahead to fully understand the physics behind SER based fatigue in order to develop a FCG prediction model based on SER.

8 Conclusions and Recommendations

This chapter draws conclusions and provides recommendations based on the hypotheses and findings through experimental research performed during this Master thesis. The conclusions drawn from this research are provided in Section 8.1. Recommendations for future work are provided in Section 8.2.

8.1 Conclusions

This section provides the conclusions drawn based on the hypotheses and results provided throughout this Master thesis report. Each of the conclusions is separately listed Below. After these listed (sub-)conclusions, they are combined to serve as the basis for the main conclusions on the hypotheses of Chapter 3.

- The fatigue life is longer if a low S_{max} and/or a high stress ratio is applied. Furthermore the fatigue life is longer in vacuum than in air.

- If ΔK is used for similitude, in air environment there appears an R-effect in experimental FCG data. However, if ΔK is used for similitude in vacuum environment, this R-effect disappears.

- The load-COD behaviour of the experiments is equal in air and vacuum environment.

- Non-linear load-COD behaviour is only observed if the applied S_{min} is below the transition point from non-linear to linear load-COD behaviour (and thus it is only observed for low stress ratios).

- The transition point from non-linear to linear is significantly lower than conventional crack closure corrections prescribe.

- The transition point is independent on R and a, but is dependent on S_{max}.

- If the SER is used for similitude, good correlation is obtained for a fixed S_{max} in both air and vacuum environment. A slight R-effect is present, which is conform SER dominated FCG theory discussed in Chapter 3. Also an apparent S_{max}-effect is conform this theory and better correlation is obtained if cyclic energy dissipation in considered instead of total energy dissipation.

- The crack closure corrections attributed to plasticity induced crack closure are only an artefact of using ΔK for similitude. The crack closure corrections actually correct for applied cyclic energy and therefore the R-effect largely disappears if SER is considered.

- Elastic-plastic behaviour is similar in air and vacuum environment: The elastic-plastic zone (or equivalently the amount of energy dissipated through plasticity) is dependent on S_{max} and a but independent on R.

- Crack surface roughness is different in air and vacuum. Initially the crack surface is rougher in air, but for increasing crack length the roughness becomes larger in vacuum. Also a larger S_{max} causes a rougher surface. Furthermore an R-effect is observed: A larger stress ratio causes a rougher crack surface.

- Rough indications of the effect of crack surface roughness on SER data show that observed trends are due to a difference in crack surface roughness.

According to conventional FCG theories, the experimental results in both air and vacuum environment should show an R-effect. In vacuum this effect disappears, which then should be explainable by a difference in load-COD behaviour. However, both the load-COD behaviour and the elastic-plastic behaviour did not change in vacuum. Furthermore it is shown that the crack closure corrections proposed in literature are actually a cyclic energy correction. The transition point from non-linear to linear is lower than corrections proposed in literature and disappears if the applied S_{min} exceeds S_{tr}. The 'opening stress' proposed in literature therefore is an artificial stress needed to correct for something that is actually a cyclic energy problem. In other words, the R-effect is only an artefact of choosing ΔK for similitude. And thus the first hypothesis of Chapter 3 can be confirmed:

ΔK is an improper similitude parameter for FCG description and prediction

When SER dU/dN is used for similitude, a similar trend is observed in air and vacuum environment. Good correlation is observed for a fixed S_{max}, with a slight R-effect conform the theory of Chapter 3. Furthermore the analysis of SER mechanisms plasticity and crack surface roughness show trends in line with FCG data as a function of dU/dN: More energy is released at higher FCG rates, higher stress ratios and higher S_{max}. If the FCG rate is expressed in terms of effective crack length, differences in SER are largely accounted for. Lastly the conventional crack closure corrections are actually a cyclic energy correction. Therefore also the second hypothesis of Chapter 3 can be confirmed:

Fatigue is a strain energy release dominated phenomenon

As the R-effect is present in air but absent in vacuum and as the R-effect is usually attributed to plasticity induced crack closure, a difference in R-effect should be explainable by a difference in load-COD or elastic-plastic behaviour. However, both the load-COD and the elastic-plastic behaviour does not differ in air and vacuum environment. Although this does not necessarily falsify that crack closure exists and actually is plasticity induced, it does confirm the third hypothesis of Chapter 3:

R-effect is not caused by plasticity induced crack closure

8.2 Recommendations

Although this Master thesis has shed an important light on FCG and crack closure, there is also room for further research. This section lists the recommendations for future work.

- First of all, as fatigue is usually not approached from a SER perspective, a uniform SER determination manual should be created. As such standard test and measurement procedures can be described for proper further research.

- This thesis only measured the SER in order to get a better understanding of the underlying physics of fatigue. Besides a standard test manual, therefore also a prediction model based on SER needs to be determined.

- Furthermore some trends in the SER data are qualitatively explained, but not yet quantitatively. To determine the exact influence of energy dissipation mechanisms on SER data, more accurate crack surface roughness models are needed.

- In line with the previous recommendation, also the energy dissipated through plasticity needs to be accurately quantified. Furthermore other dissipation mechanisms such as corrosion need to be researched and quantified to determine if all differences in SER between air and vacuum can be accounted for.

- Although there are evidently conditions where the load-COD behaviour consists of a non-linear and linear part, it is still unknown what causes the non-linearity. It requires further research to determine if this is caused by for instance crack closure or compressive stresses.

- For completeness, the experiments in this test should also be performed over the complete stress ratio range (including negative stress ratios), displacement instead of load controlled tests, variable amplitude instead of constant amplitude loading and different environmental conditions such as water.

References

[1]   Schijve J., *Fatigue of Structures and Materials*, 2nd edition, Springer Science + Business Media B.V.; 2009.

[2]   Peterson R. E*., Stress Concentration Design Factors,* John Wiley & Sons, 1953*.*

[3]   Paris P.C., Gomez M.P., Anderson W.E., *A Rational Analytic Theory of Fatigue*, Trend in Engineering; 13:9–14; 1961.

[4]   Irwin G.R., *Analysis of Stresses and Strains Near the End of a Crack Traversing a Plate*, Journal of Applied Mechanics 24, Transaction of the American Society of Mechanical Engineers; 79:361–4; 1957.

[5]   Griffith A.A., *The Phenomenon of Rupture and Flow in Solids*, Philosophical Transactions of the Royal Society of London; A221:163-198; 1920.

[6]   Elber W., *Fatigue Crack Closure under Cyclic Tension*, Engineering Fracture Mechanics; 2:37–45; 1970.

[7]   Forman R.G., Kearney V.E., Engle, R.M., *Numerical Analysis of Crack Propagation in Cyclic-Loaded Structures*, Journal of Basic Engineering, Transaction of the American Society for Mechanical Engineers; D89:459–464; 1967.

[8]   Priddle E.K., *High Cycle Fatigue Crack Propagation under Random and Constant Amplitude Loadings*, International Journal of Pressure Vessels & Piping; 4:89; 1976.

[9]   Head A.K., *The Propagation of Fatigue Cracks*, Journal of Applied Mechanics, American Society for Mechanical Engineers; 23:406; 1956.

[10]   Frost N.E., Dugdale D.S., *The Propagation of Fatigue Cracks in Sheet Specimens*, Journal of the Mechanics and Physics of Solids; 6:92–110; 1958.

[11]   Liu H.W., *Fatigue Crack Propagation and Applied Stress Range – An Energy Approach*, Journal of Basic Engineering, Transcription of American Society of Mechanical Engineers; 85:116–20; 1963.

[12]   Lang M., Marci G., *Reflecting on the Mechanical Driving Force of Fatigue Crack Propagation*, Fatigue and Fracture Mechanics: 29th Volume, American Society for Testing and Materials; 474-495; 1998.

[13]   Lang M., *Description of Load Interaction Effects by the ΔK_{eff}-concept*, Advances in Fatigue Crack Closure Measurement and Analysis, American Society for Testing and Materials

Standard, West Conshohocken, USA; 2:207–223; 1999.

[14]   Lang M., Huang X., *The Influence of Compressive Loads on Fatigue Crack Propagation*, Fatigue and Fracture of Engineering Materials and Structures; 2:65–83; 1998.

[15]   Lang M., *A Model for Fatigue Crack Growth, Part I: Phenomenology*. Fatigue and Fracture of Engineering Materials and Structures; 23:587–601; 2000.

[16]   Lang M., *A Model for Fatigue Crack Growth, Part II: Modelling*. Fatigue and Fracture of Engineering Materials and Structures; 23:603–17; 2000.

[17]   Vasudevan A.K., Sadananda K., Louat N., *A Review of Crack Closure, Fatigue Crack Threshold and Related Phenomena Materials*, Science and Engineering; A188:1-22; 1994.

[18]   Sadananda K., Vasudevan A.K., *Crack Tip Driving Forces and Crack Growth Representation under Fatigue*, International Journal of Fatigue; 26:39–47; 2004.

[19]   Vasudevan A.K., Sadananda K., *Application of Unified Fatigue Damage Approach to Compression–Tension Region*, International Journal of Fatigue; 21:S263–S273; 1999.

[20]   Vasudevan A.K., Sadananda K., *Analysis of Fatigue Crack Growth under Compression– Compression Loading*, International Journal of Fatigue; 23:S365–S374; 2001.

[21]   Vasudevan A.K., Sadananda K., Glinka G., *Critical Parameters for Fatigue Damage*, International Journal of Fatigue; 23:S39–S53; 2001.

[22]   Paris P.C., Erdogan F., *A Critical Analysis of Crack Propagation Laws*, Transaction of American Society of Mechanical Engineers; 528–33; 1963.

[23]   Elber W., *The Significance of Fatigue Crack Closure,* Damage Tolerance in Aircraft Structures, American Society for Testing and Materials Standard; 486:230–42; 1971.

[24]   Alderliesten R.C., *How Proper Similitude Can Improve our Understanding of Crack Closure and Plasticity*, International Journal of Fatigue; 82:263–273; 2015.

[25]   Hertzberg R.W., Newton C.H., Jaccard R., *Crack Closure: Correlation and Confusion*, Mechanics of Fatigue Crack Closure, American Society for Testing and Materials Standard, Philadelphia; 139-148; 1988.

[26]   James M.N., Knott J.F., *On the Effect of Crack Closure on the Rate of Fatigue Crack Propagation*, Fatigue of Engineering Materials and Structures; 8:177; 1985.

[27]   Schijve J., Jacobs F.A., *Program-Fatigue Tests on Notched Light Alloy Specimens of 2024 and 7075 Material*, NLR-Report M 2070, National Aerospace Laboratory (NLR), Amsterdam; 1960.

[28]   Schijve, J., *Fatigue Crack Propagation in Light Alloy Sheet Material and Structures*, Advances in Aeronautical Sciences, Pergamon Press; 3:387-408; 1962.

[29]   Kirby B.R., Beevers C.J., *Slow Fatigue Crack Growth and Threshold Behaviour in Air and Vacuum of Commercial Aluminium Alloys*, Fatigue of Engineering Materials and Structures; 1:203; 1979.

[30]   Alderliesten R.C., *The Explanation of Stress Ratio Effect and Crack Opening Corrections for Fatigue Crack Growth in Metallic Materials*, Advanced Materials Research Journal; 891–892:289–94; 2014.

[31]   Alderliesten R.C., *How Proper Similitude Could Have Improved our Understanding about Fatigue Damage Growth*, 28th ICAF Symposium, Helsinki, 3–5 June; 2015.

[32]   Paris P.C., *Fracture Mechanics and Fatigue: A Historical Perspective*, Fatigue and Fracture of Engineering Materials and Structures; 21:535–40; 1998.

[33]   Pascoe J.A., Alderliesten R.C., Benedictus R., *On the Relationship Between Disbond Growth and the Release of Strain Energy*, Engineering of Fracture Mechanic; 133:1–13; 2015.

[34]   Pascoe J.A., Alderliesten R.C., Benedictus R., *Towards Understanding Fatigue Disbond Growth via Cyclic Strain Energy*, 20th European Conference on Fracture (ECF20), Procedia Materials Science; 3:610–5; 2014.

[35]   Inglis C.E., *Stresses in Plates Due to the Presence of Cracks and Sharp Corners*, Transactions of the Institute of Naval Architects; 55:219-241; 1913.

[36]   Roylance D., *Introduction to Fracture Mechanics*, Department of Materials Science and Engineering Massachusetts Institute of Technology Cambridge, MA 02139, June 14, 2001.

[37]   Irwin G.R., *Fracture Dynamics*, Fracturing of Metals, American Society for Metals; Ibid 40A:147-166; 1948.

[38]   Orowan E., *Fundamentals of Brittle Behavior in Metals*, Wiley, Fatigue and Fracture of Metals, New York; 1950.

[39]   Irwin G.R., Kies J.A., *Fracturing and Fracture Dynamics*, Welding Journal Research Supplement; 31:95-100; 1952.

[40]   Irwin G.R., Kies J.A., *Critical Energy Rate Analysis of Fracture Strength*, Welding Journal Research Supplement; 33:193s–198s; 1954.

[41]   Janssen M., Zuidema J., Wanhill R.J.H., *Fracture Mechanics*, 2nd edition, Delft, The Netherlands: VSSD; 2002.

[42]   Westergaard H.M., *Bearing Pressures and Cracks*, Transaction of the American Society of Mechanical Engineers; 61:A49-A53; 1939.

[43]   Marcus H.L., McEvily A.J., *On Crack Closure and Crack Tip Shielding During Fatigue Crack Growth*, Review of Progress in Quantitative Nondestructive Evaluation, Springer United States; 1651-1656; 1999.

[44]   Banerjee S., *A Review of Crack Closure*, Report AWAL-TR-84-4031, Air Force Wright Aeronautical Laboratories, Wright Patterson Air Force Base, Dayton, Ohio; 1984.

[45]   Gomez M.P., Ernst H., Vazquez J., *On the Validity of Elber's Results on Fatigue Crack Closure for 2024-T3 Aluminium*, International Journal of Fracture; 12:178-180; 1976.

[46]   Kemp R.M.J., *Fatigue Crack Closure – A Review*, Royal Aircraft Establishment Technical Report No. 90046, Farnborough, United Kingdom; 1990.

[47]   Minakawa K., McEvily A.J., *On Crack Closure in Near-Threshold Region*, Scripta Metallurgica; 15:633-636; 1981.

[48]   Fleck N.A., Smith R.A., *Crack Closure – Is it just a Surface Phenomenon?*, International Journal of Fatigue; 157-160; 1982.

[49]   Petit J., Ranganathan N., de Fouquet J., *Vacuum Effect on Fatigue Crack Propagation at Low Rate*, Laboratoire de Mécanique et de Physique des Matériaux, Equipe Recherche Asociée au Centre National de la Recherche Scientifique, Ecole Nationale Supérieure de Mécanique et d'Aérotechnique, Poitiers, France; 123; 1975.

[50]   Sadananda K., Ramaswamy D.N.V., *Role of Crack Tip Plasticity in Fatigue Crack Growth*, Philosophical Magazine A; 81:5:1283-1303; 2001.

[51]   Pasman D.J., *Fatigue Crack Growth in Solid Round Metallic Bars with a Shoulder Fillet,* Master of Science Thesis, Delft, Faculty of Aerospace Engineering, 27 March 2015.

[52]   McGinty B., *Stress Intensity Factor,* web: www.fracturemechanics.org/sif.html, October 2014

[53]   ASTM International, *Standard Test Method for Measurement of Fatigue Crack Growth,* Designation E647-15, November 2011.

[54]   Forman R.G., Shivakumar V., Newman J.C., *Fatigue Crack Growth Computer Program Material Database NASA/FLAGRO*, January 1993.

[55]   Clerivet A., Bathias C., *Study of Crack Tip Opening under Cyclic Loading Taking into Account the Environment and R-Ratio,* Engineering Fracture Mechanics; 12:599-611; 1979.

[56]   Schijve J., *Fatigue Crack Closure: Observations and Technical Significance,* Mechanics of Fatigue Crack Closure, American Society for Testing and Materials, Philadelphia; 5-34; 1988.

[57]   Yoshinaka F., Nakamura T., *Effect of Vacuum Environment on Fatigue Fracture Surfaces of High Strength Steel,* Mechanical Engineering Letters, Hokkaido University; 2:15; 25 January 2016.

[58]   Schijve J., Arkema W.J., *Crack Closure and the Environmental Effect on Fatigue Crack Growth,* Report VTH-217, Delft University of Technology, 1976.

[59]   Olympus NEXT OLS4100 Specification Overview, web: *http://www.olympus- ims.com/en/ metrology/ols4100/#!cms[tab]=%2Fmetrology%2Fols4100%2Fspecifications*

Appendices

Appendix A: N-a Curves

APPENDIX A - N-a Curves
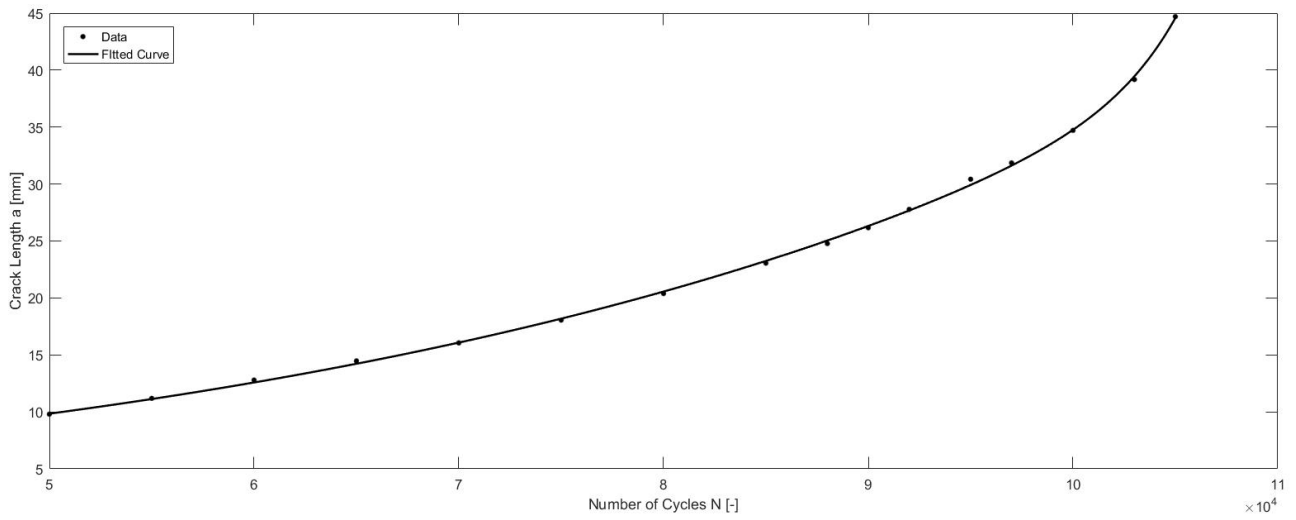
A 1: N-a Curve of Specimen AR002S75
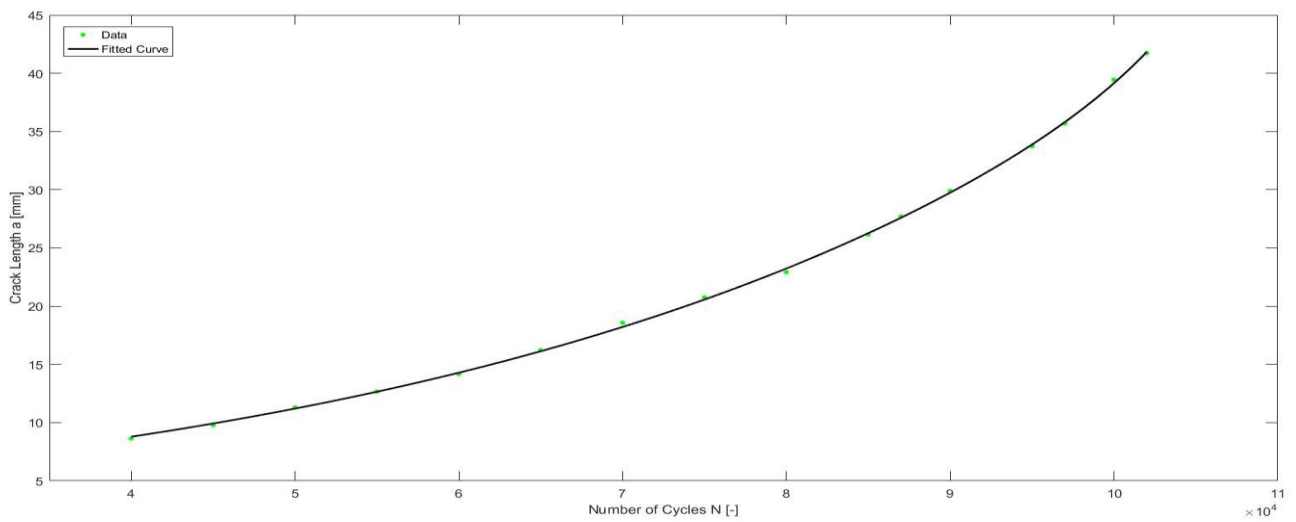
A 2: N-a Curve of Specimen AR005S75
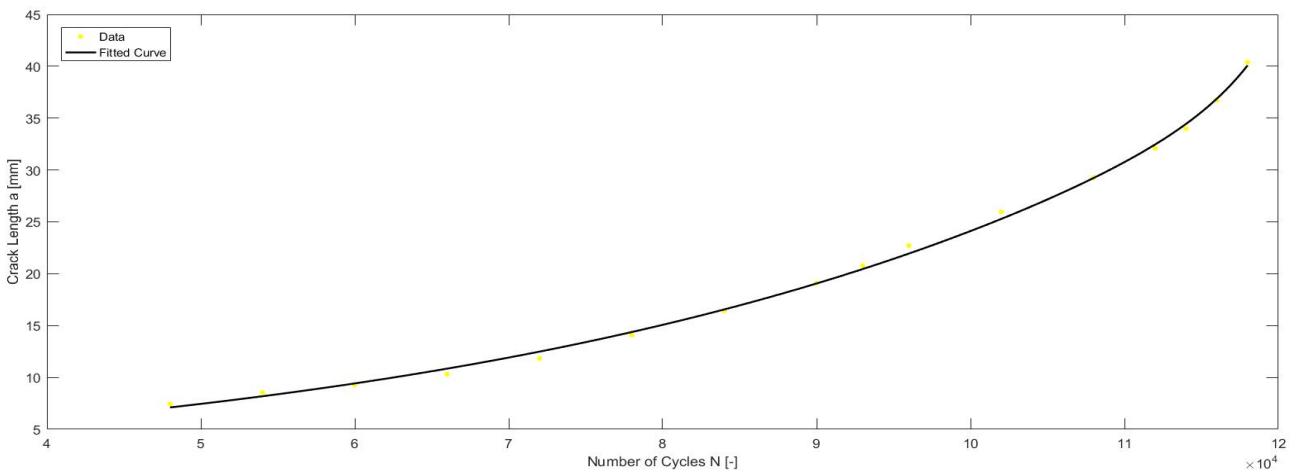
A 3: N-a Curve of Specimen AR01S75

APPENDIX A - N-a Curves
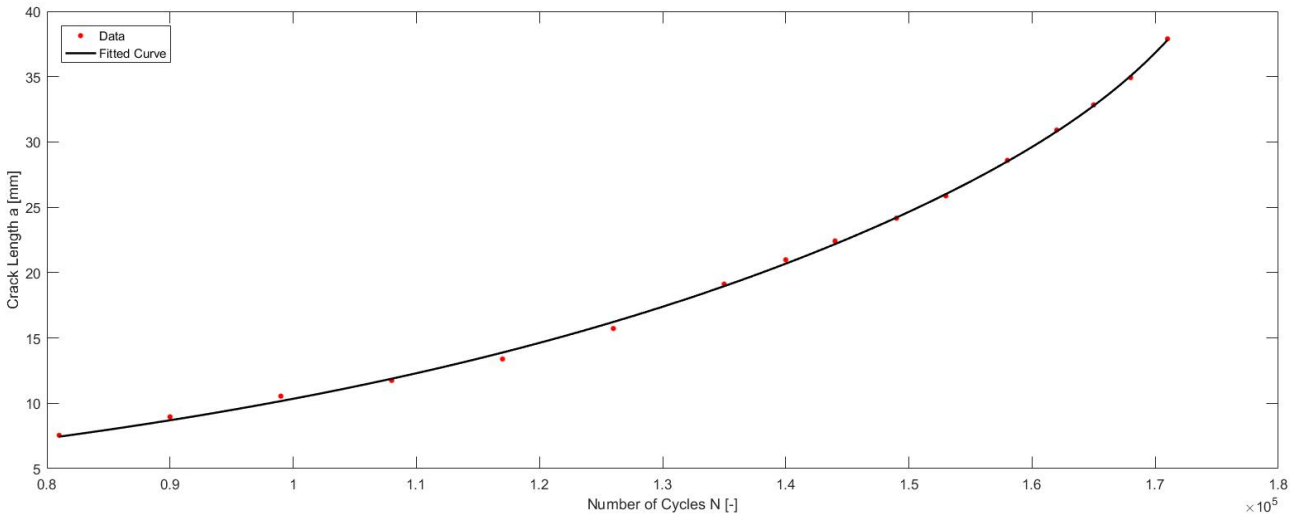
A 4: N-a Curve of Specimen AR03S75
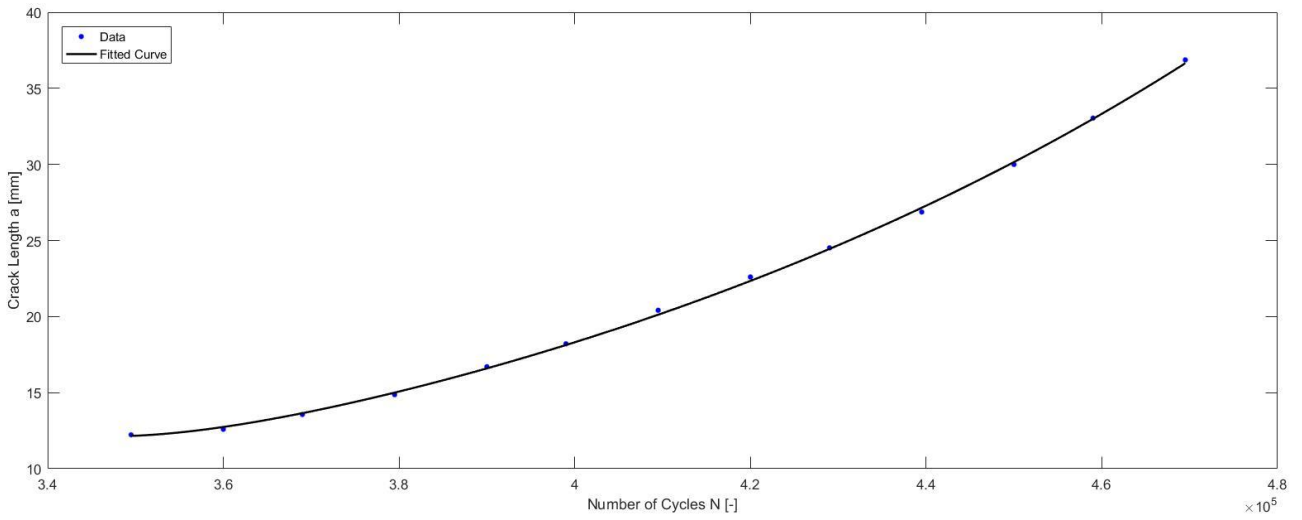
A 5: N-a Curve of Specimen AR05S75
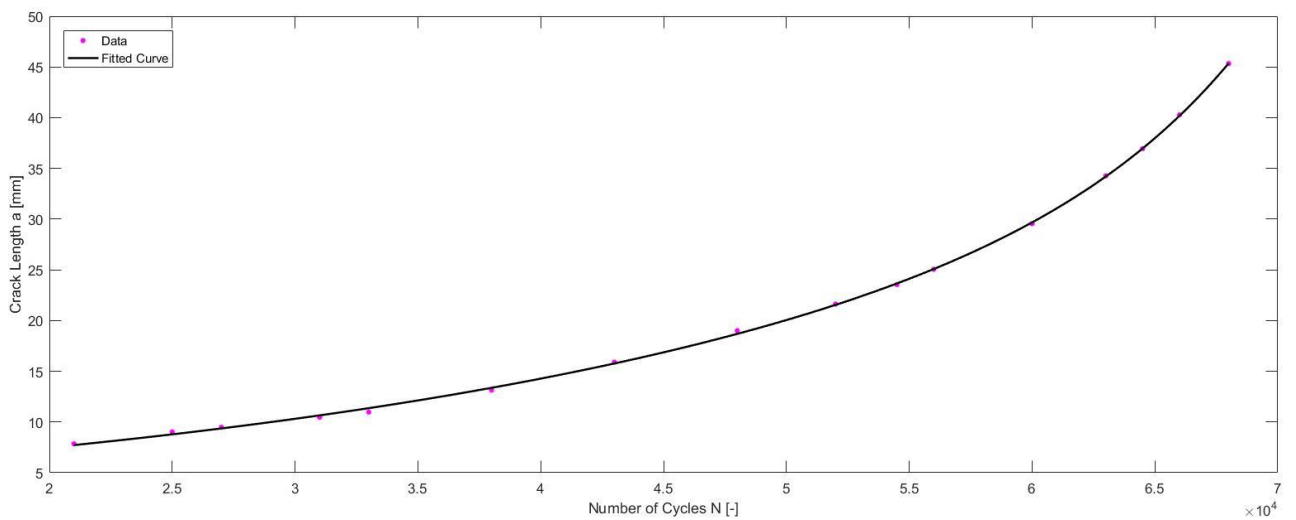
A 6: N-a Curve of Specimen AR005S100

APPENDIX A - N-a Curves
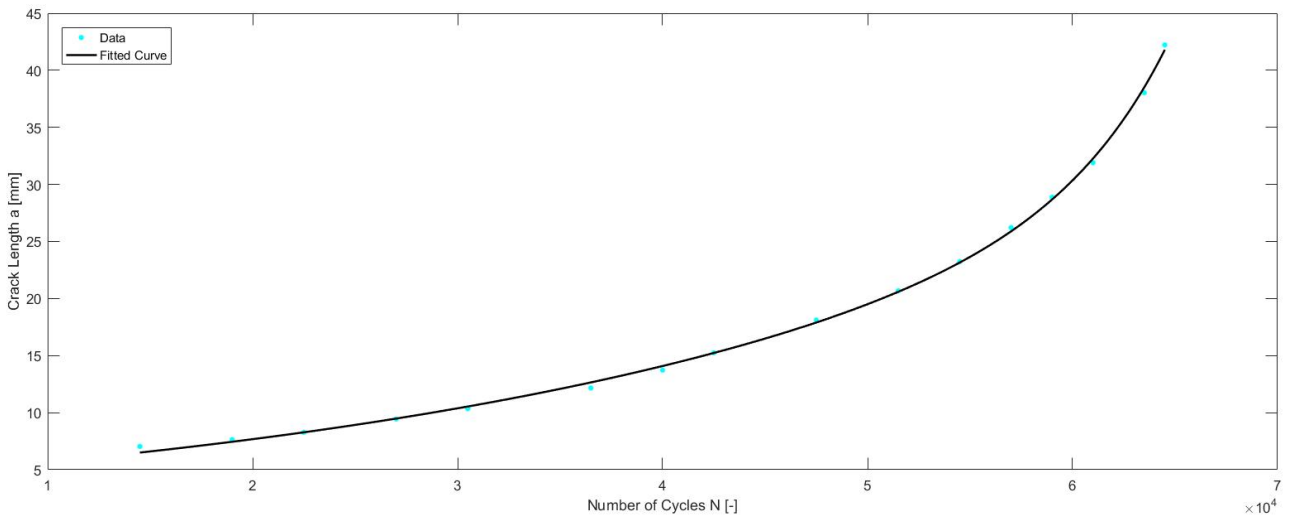
A 7: N-a Curve of Specimen AR03S100
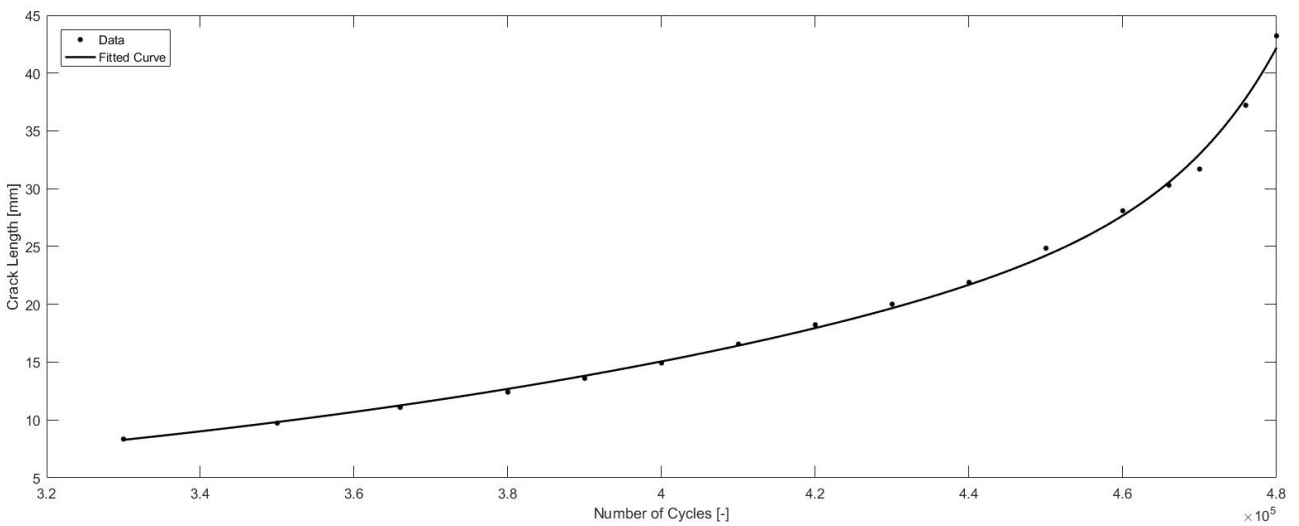
A 8: N-a Curve of Specimen VR002S75
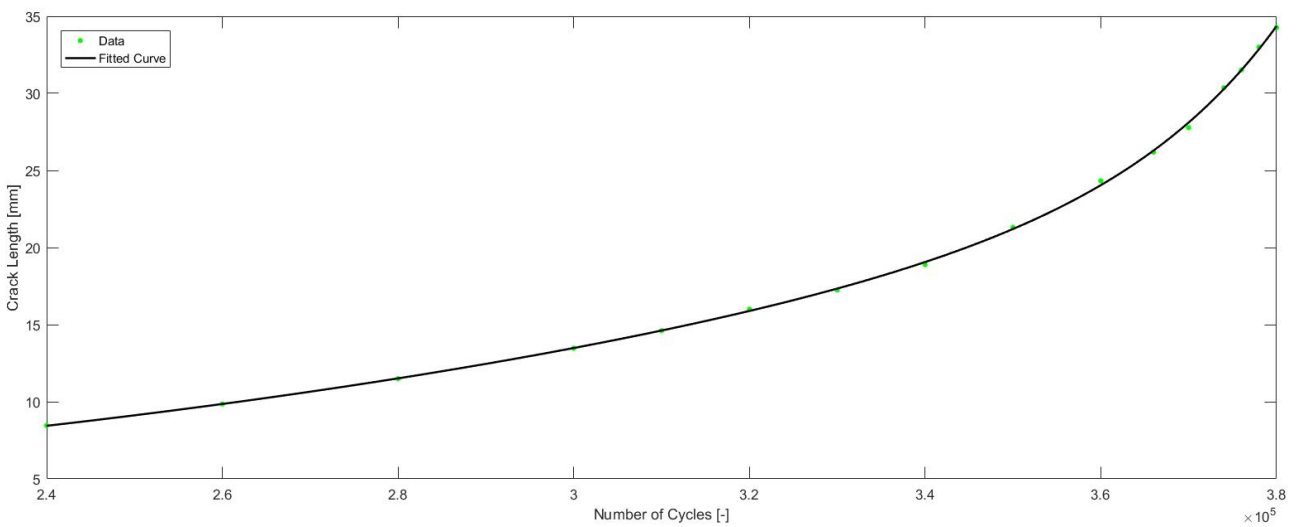
A 9: N-a Curve of Specimen VR005S75
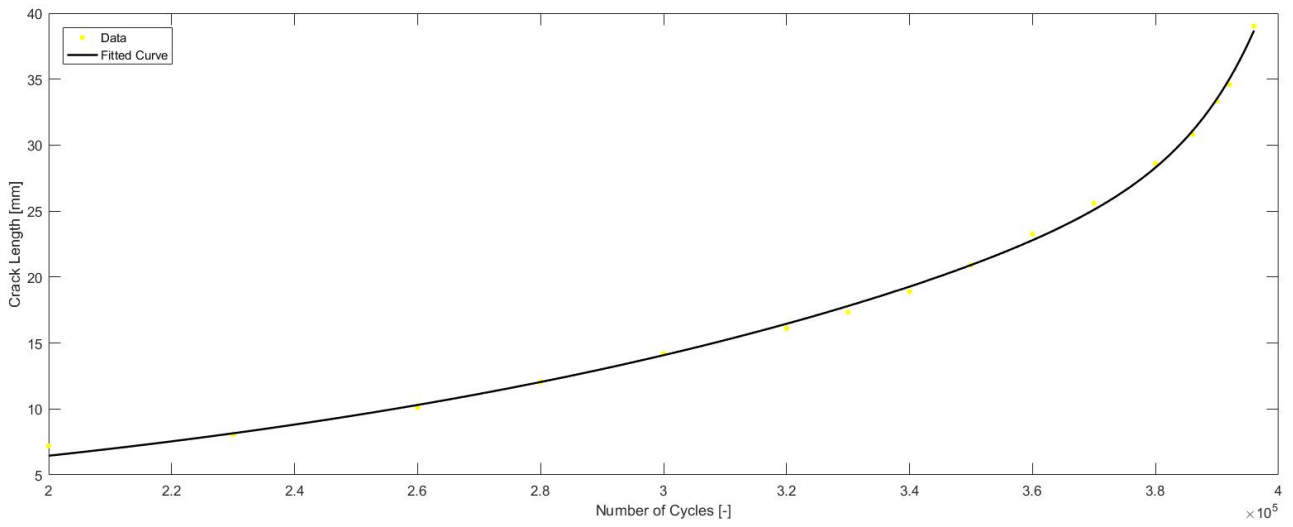
A 10: N-a Curve of Specimen VR01S75
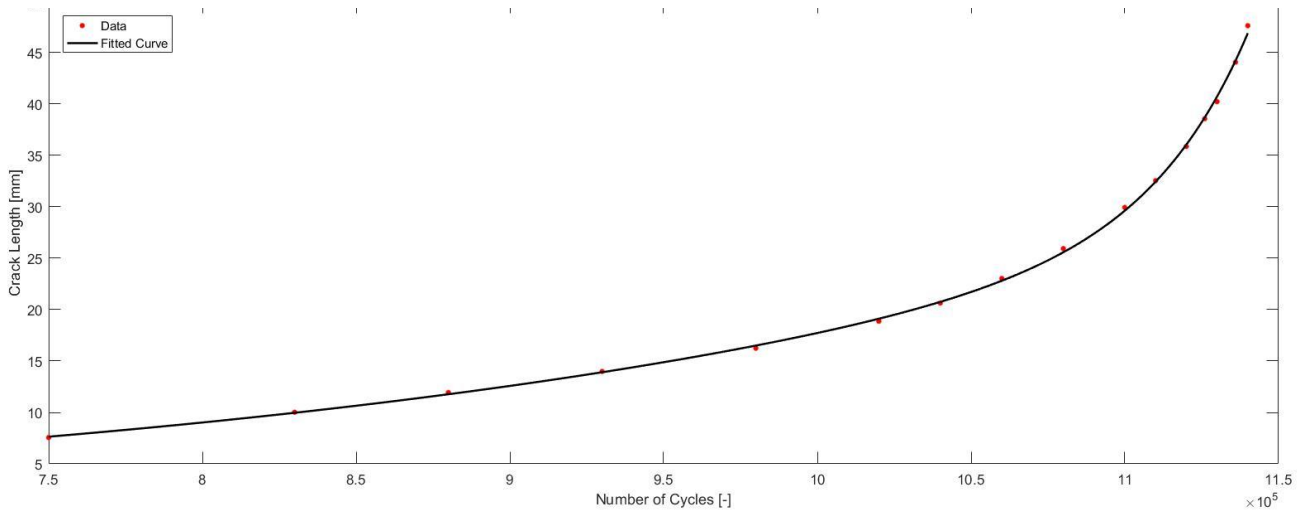
A 11: N-a Curve of Specimen VR03S75
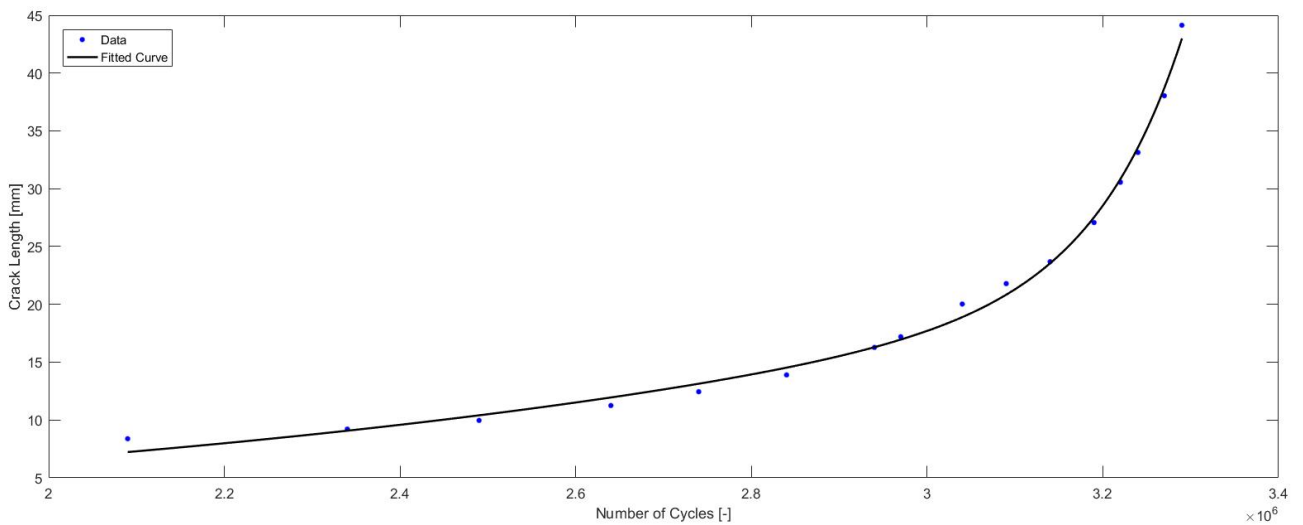
A 12: N-a Curve of Specimen VR05S75

APPENDIX A - N-a Curves
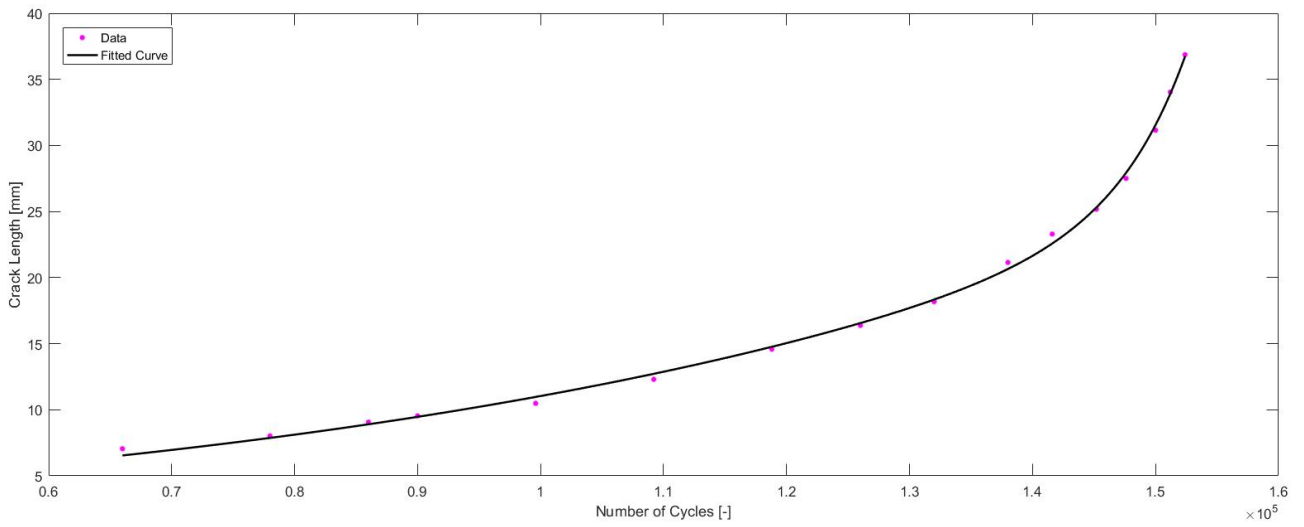
A 13: N-a Curve of Specimen VR005S100
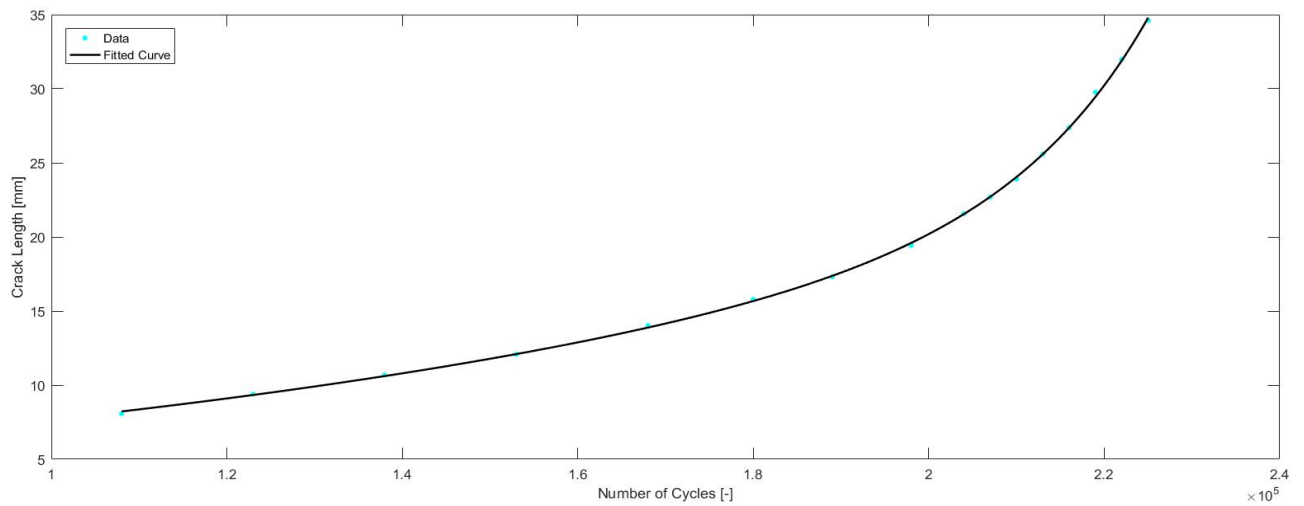
A 14: N-a Curve of Specimen VR03S100

Appendix B – N-U Curves

APPENDIX B – N-U Curves
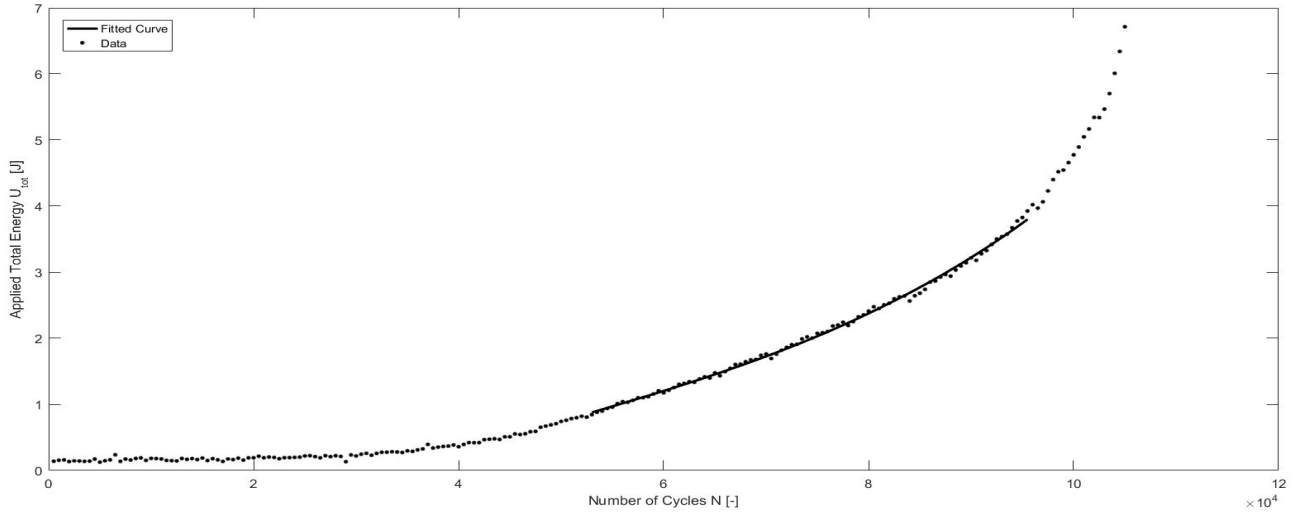
B 1: N-U$_{tot}$ Curve for Specimen AR002S75
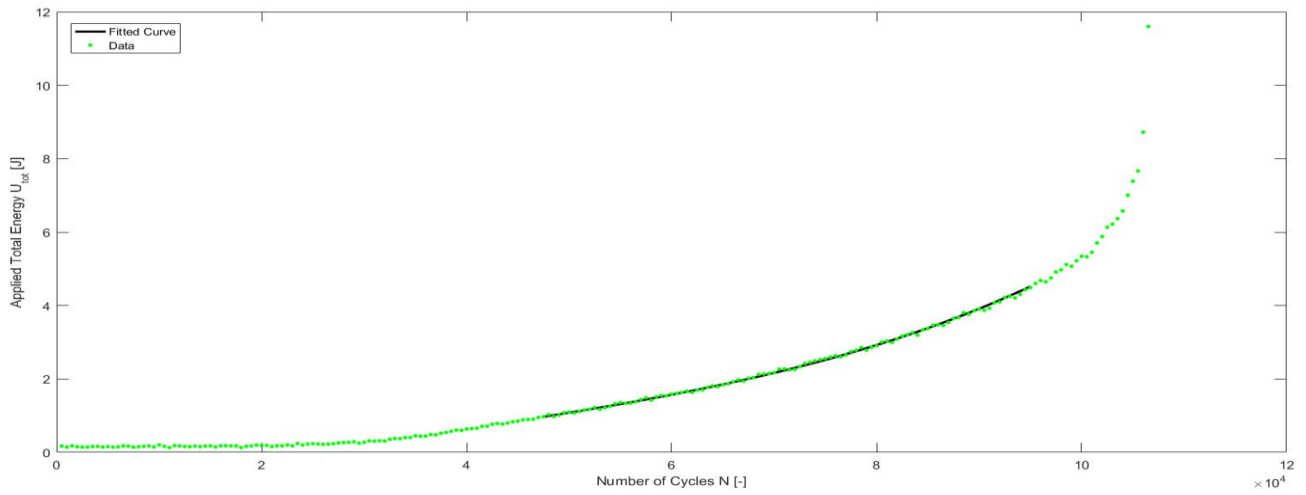
B 2: N-U$_{tot}$ Curve for Specimen AR005S75
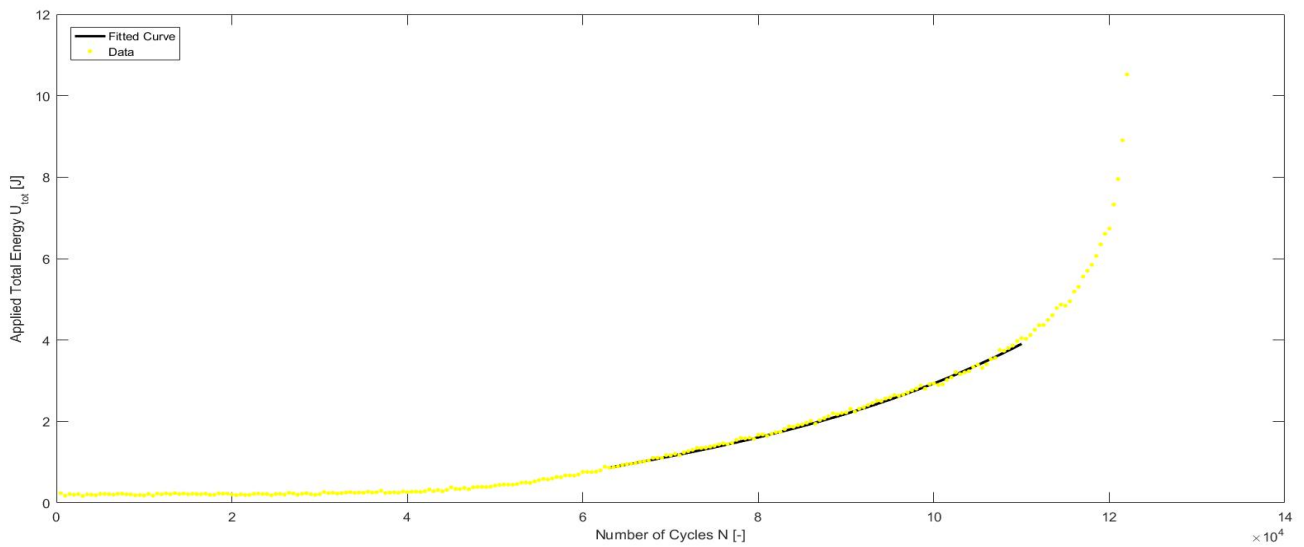
B 3: N-U$_{tot}$ Curve for Specimen AR01S75

APPENDIX B – N-U Curves
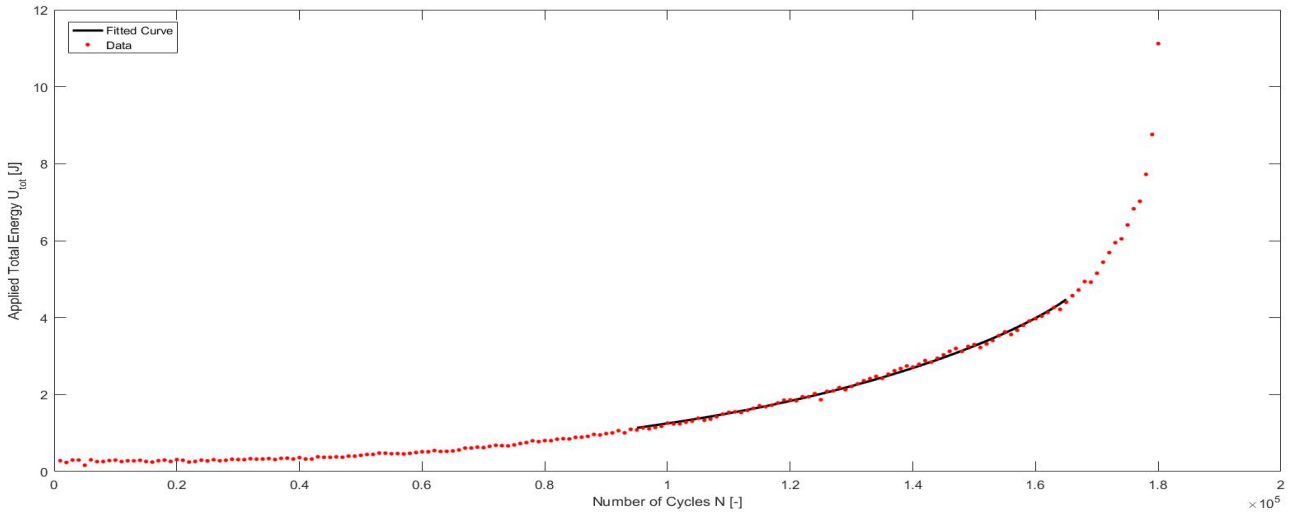
B 4: N-U$_{tot}$ Curve for Specimen AR03S75
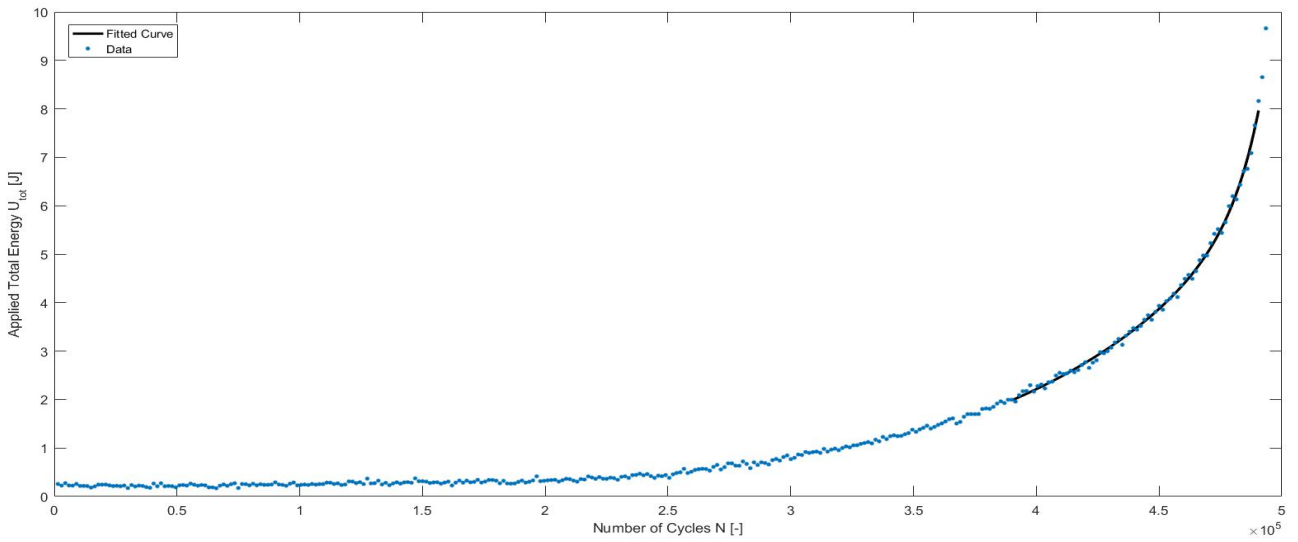
B 5: N-U$_{tot}$ Curve for Specimen AR05S75
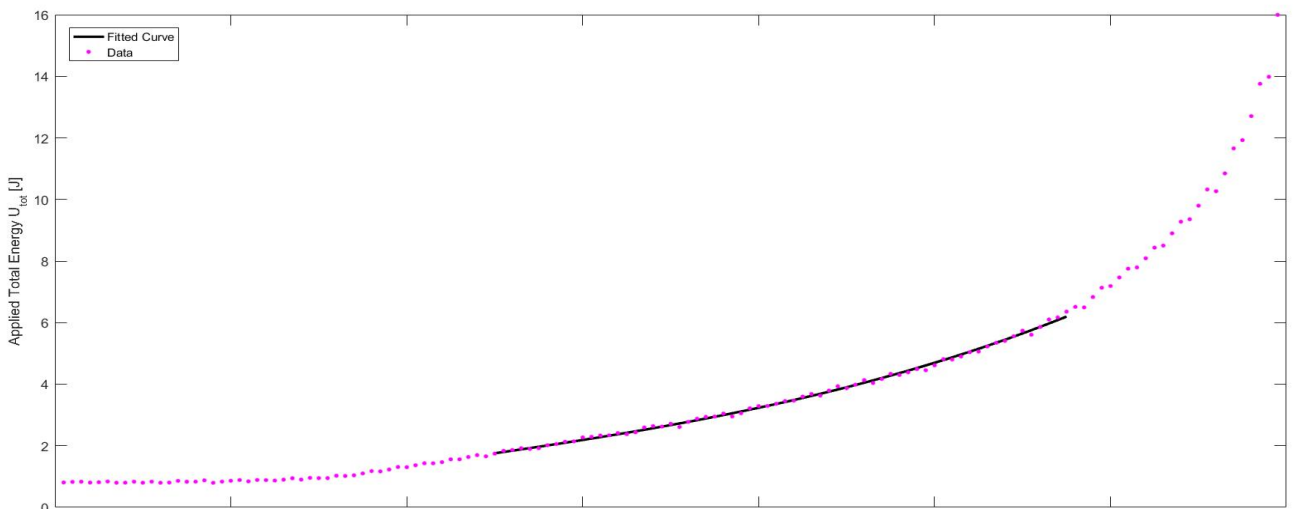
B 6: N-U$_{tot}$ Curve for Specimen AR005S100

APPENDIX B – N-U Curves
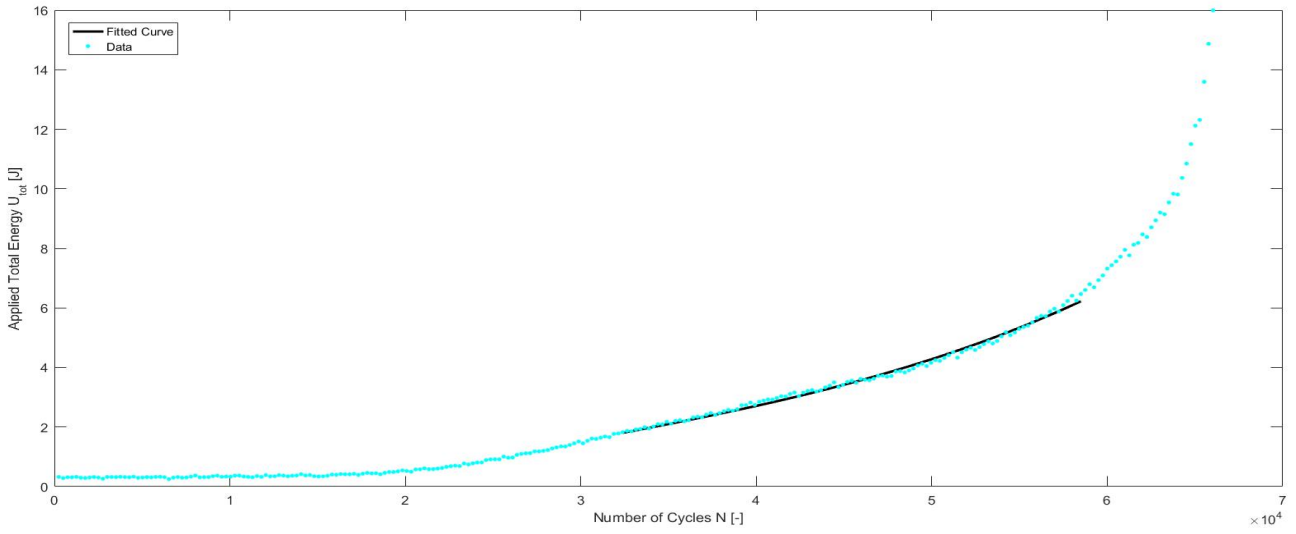
B 7: N-U$_{tot}$ Curve for Specimen AR03S100
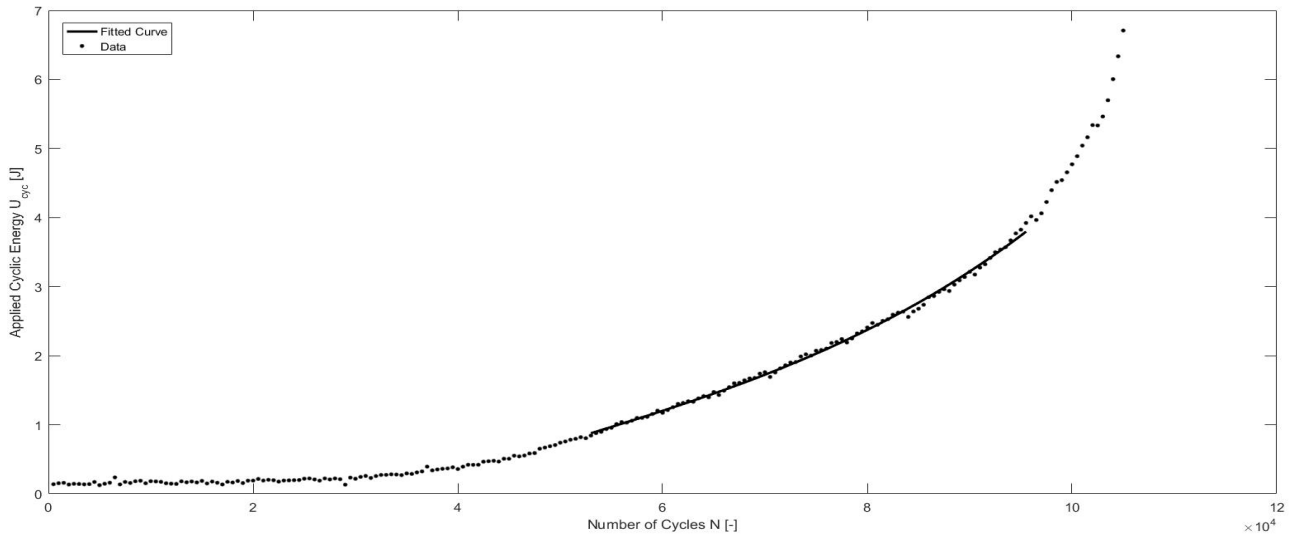
B 8: N-U$_{cyc}$ Curve for Specimen AR002S75
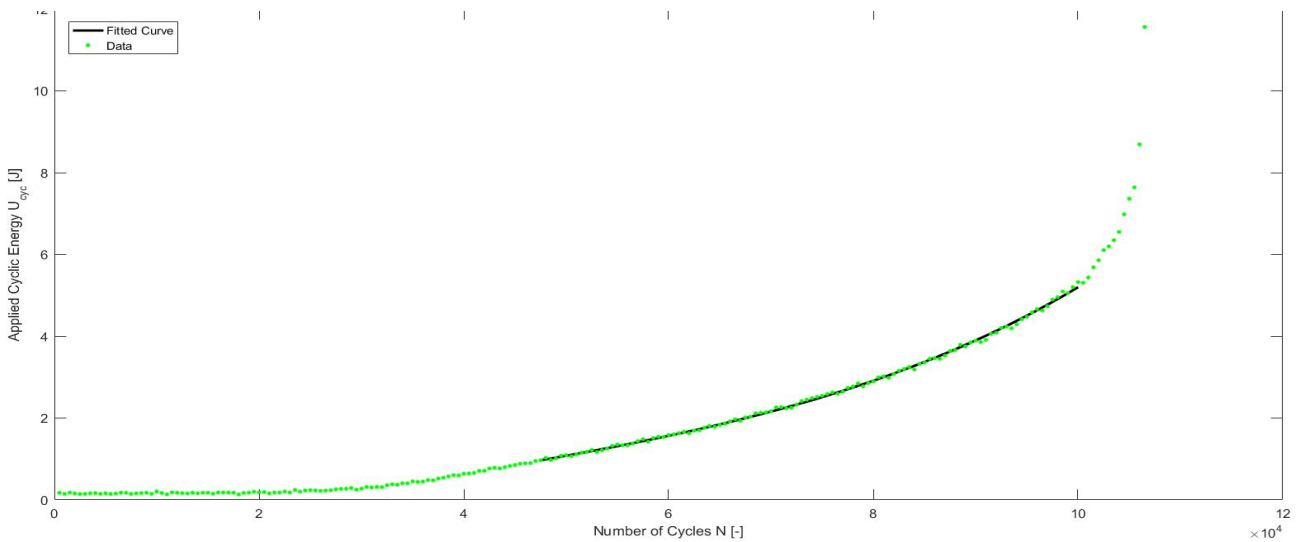
B 9: N-U$_{cyc}$ Curve for Specimen AR005S75

APPENDIX B – N-U Curves
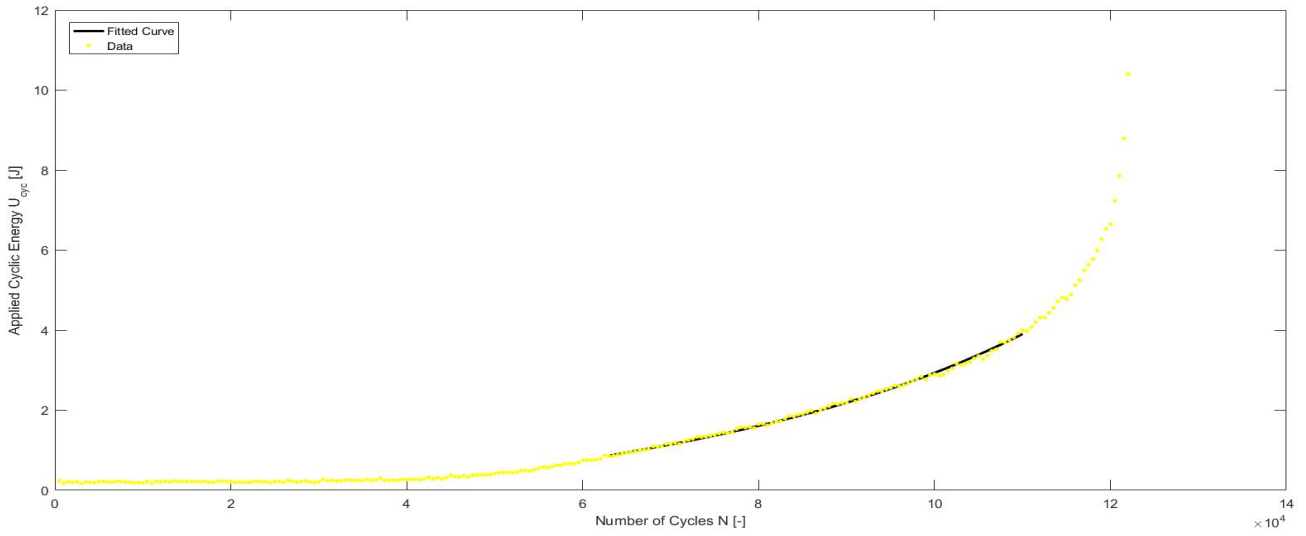
B 10: N-U$_{cyc}$ Curve for Specimen AR01S75
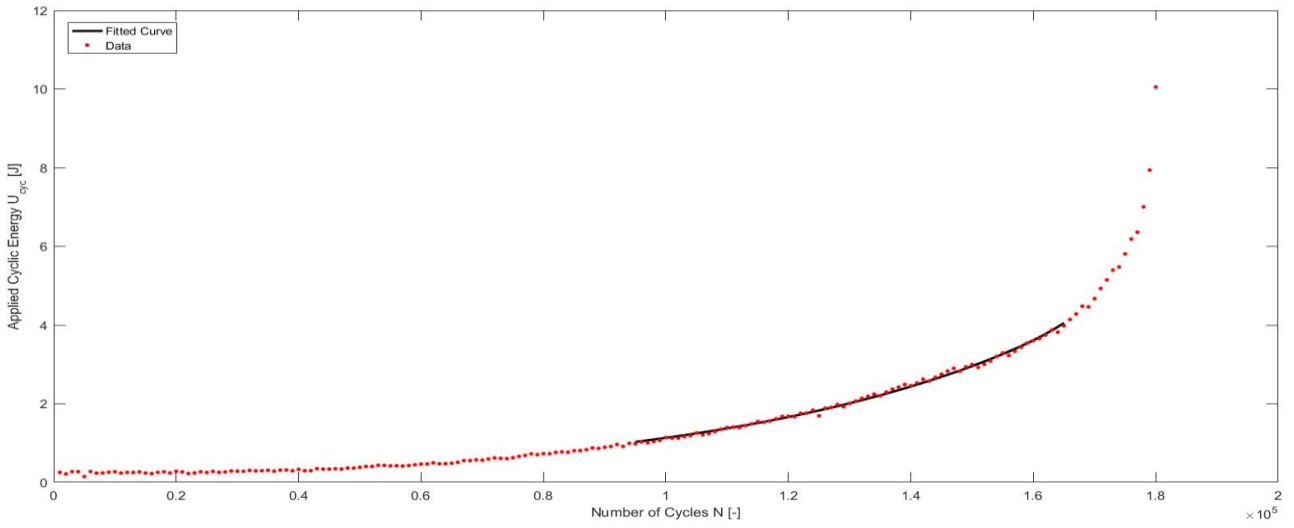
B 11: N-U$_{cyc}$ Curve for Specimen AR03S75

B 12: N-U$_{cyc}$ Curve for Specimen AR05S75

B 13: N-U$_{cyc}$ Curve for Specimen AR005S100

B 14: N-U$_{cyc}$ Curve for Specimen AR03S100

B 15: N-U$_{tot}$ Curve for Specimen VR002S75
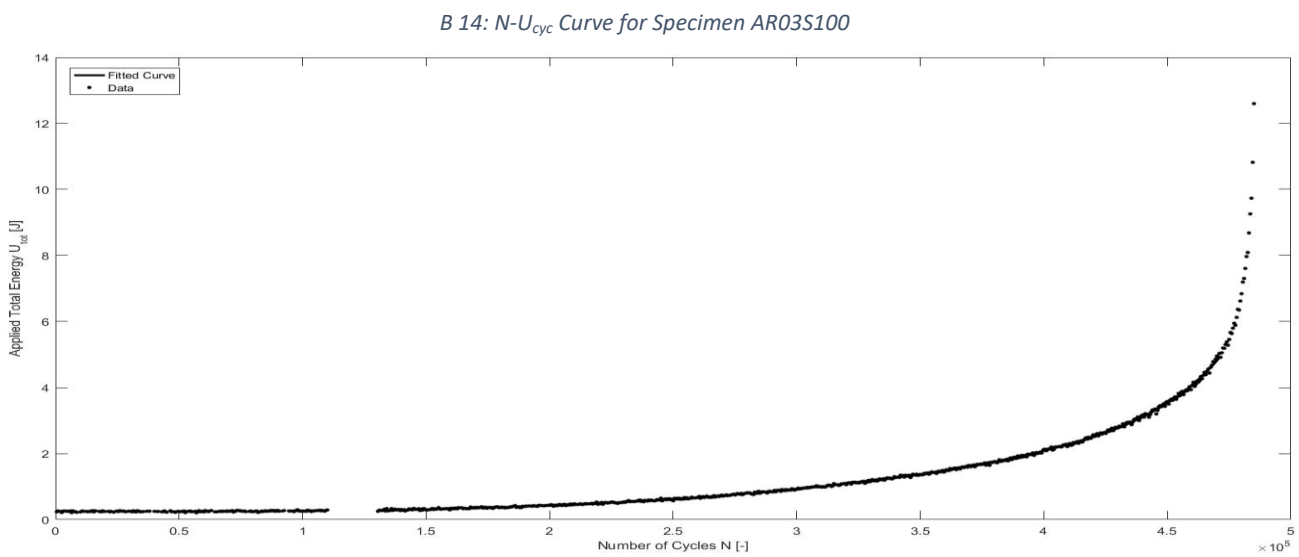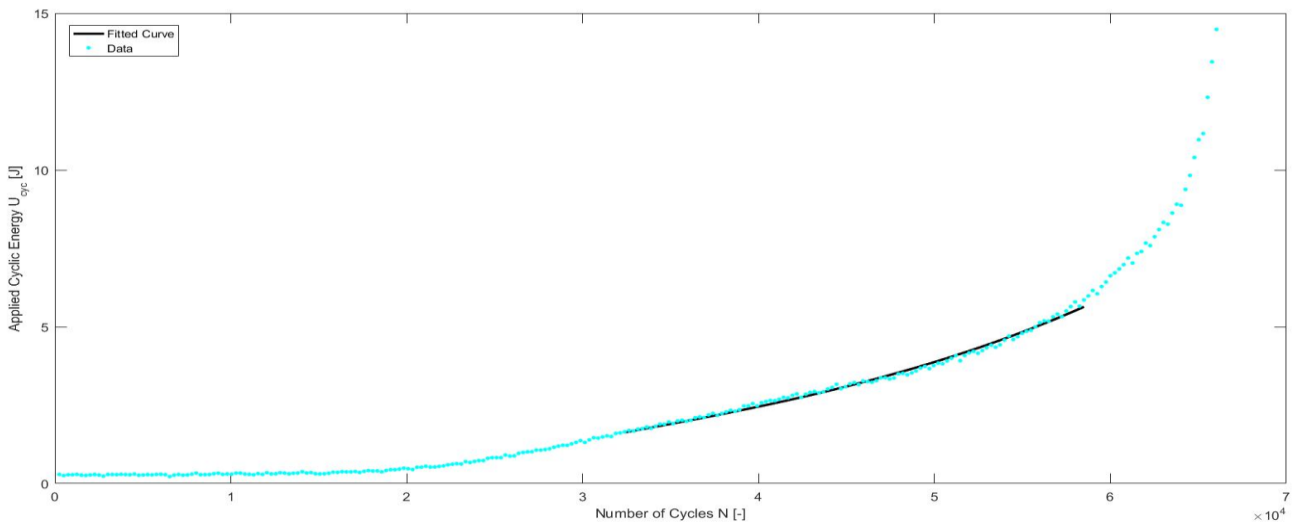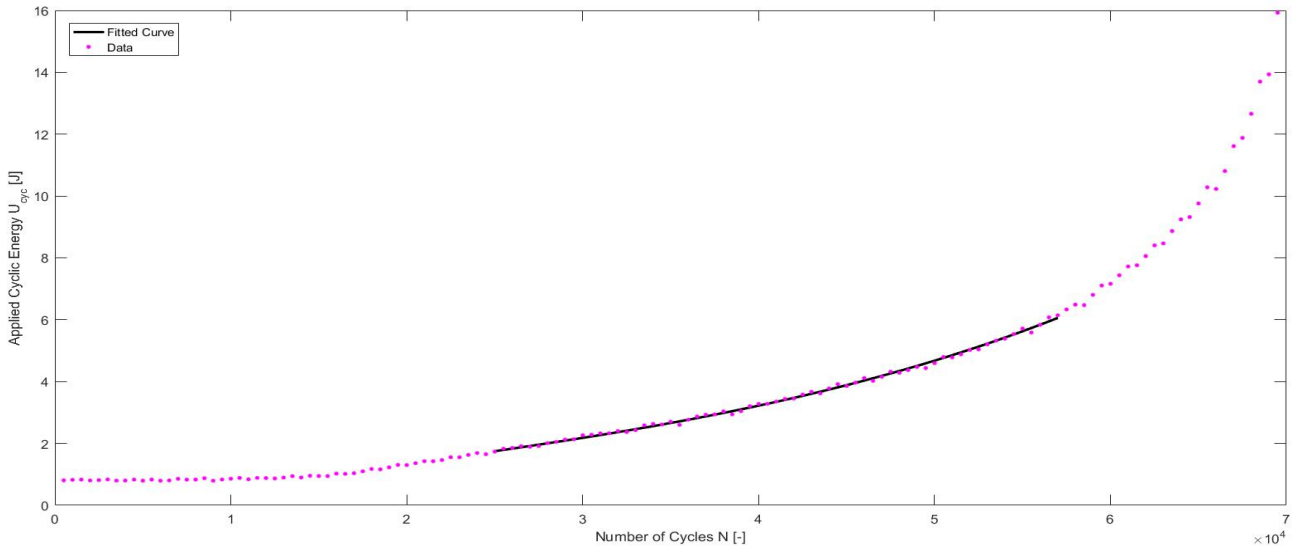
APPENDIX B – N-U Curves

B 16: N-U$_{tot}$ Curve for Specimen VR005S75
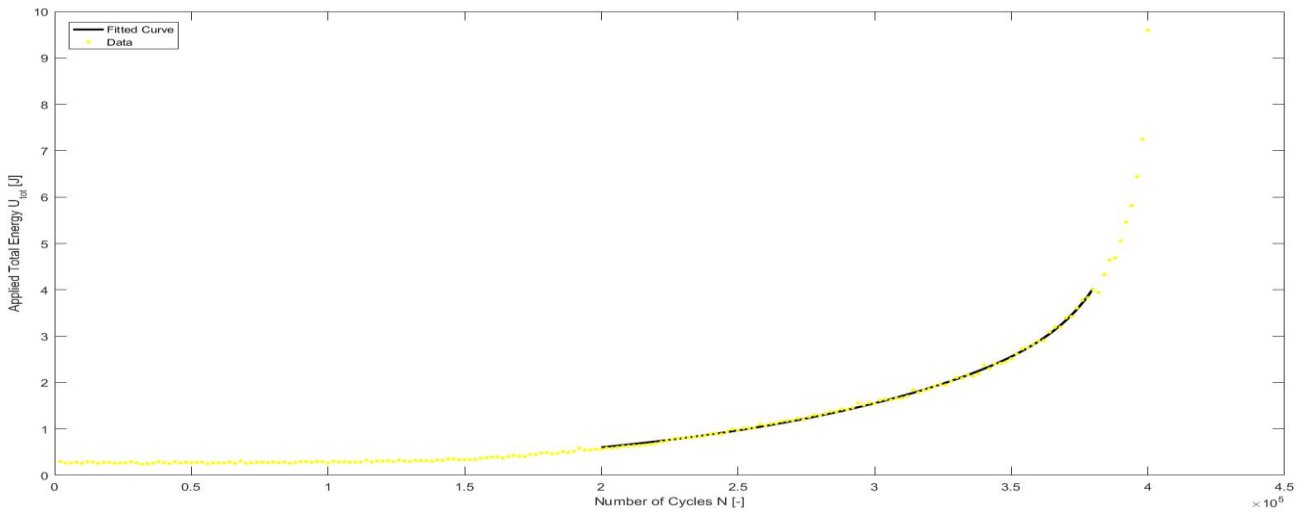
B 17: N-U$_{tot}$ Curve for Specimen VR005S75
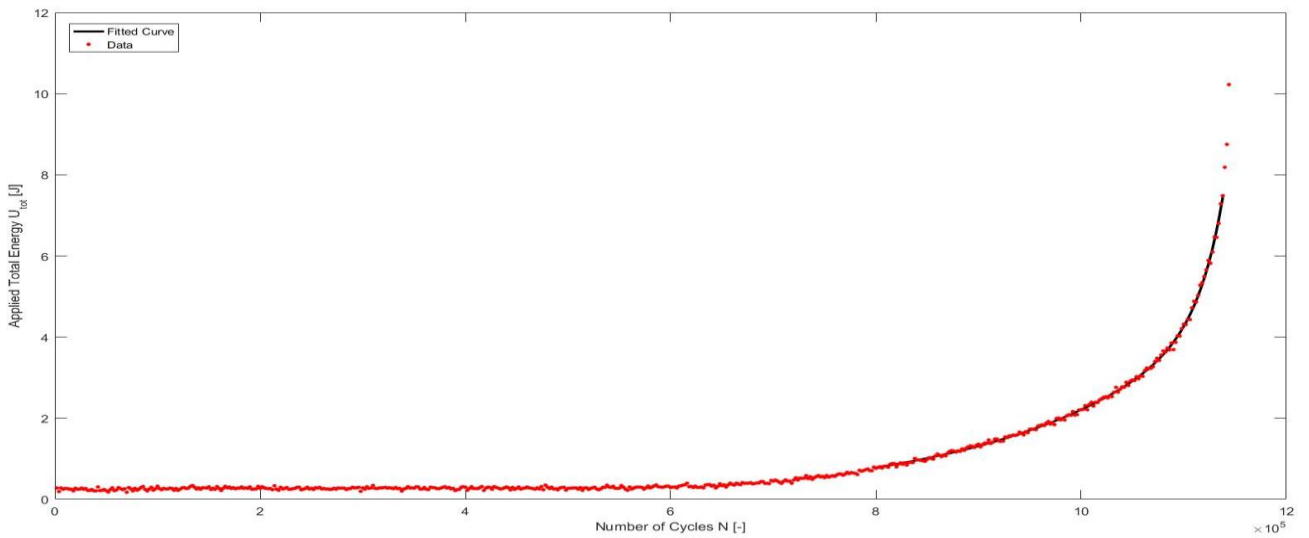
B 18: N-U$_{tot}$ Curve for Specimen VR03S75

APPENDIX B – N-U Curves
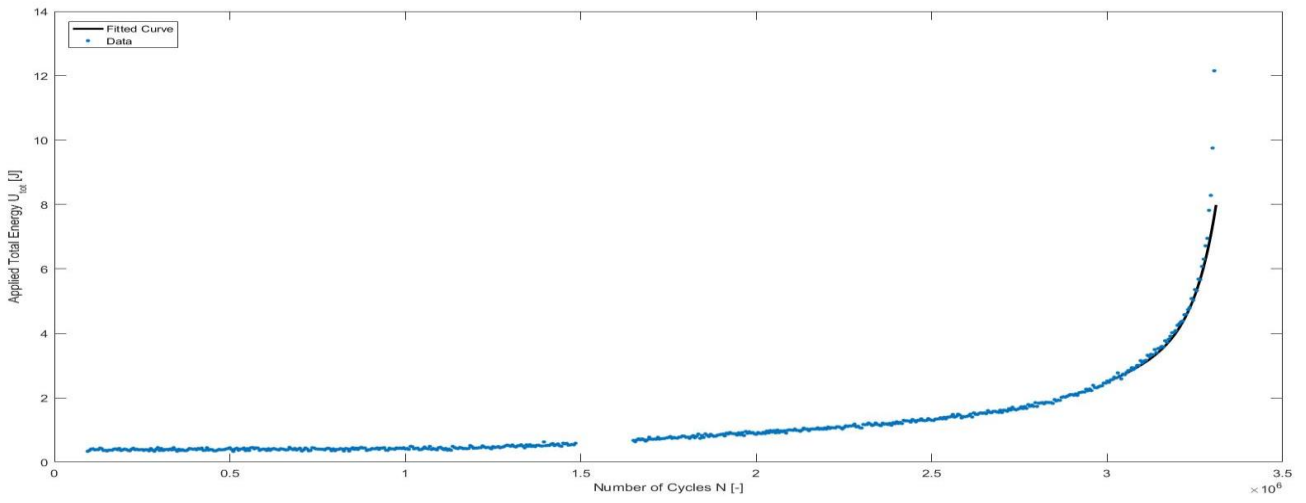
B 19: N-U$_{tot}$ Curve for Specimen VR05S75
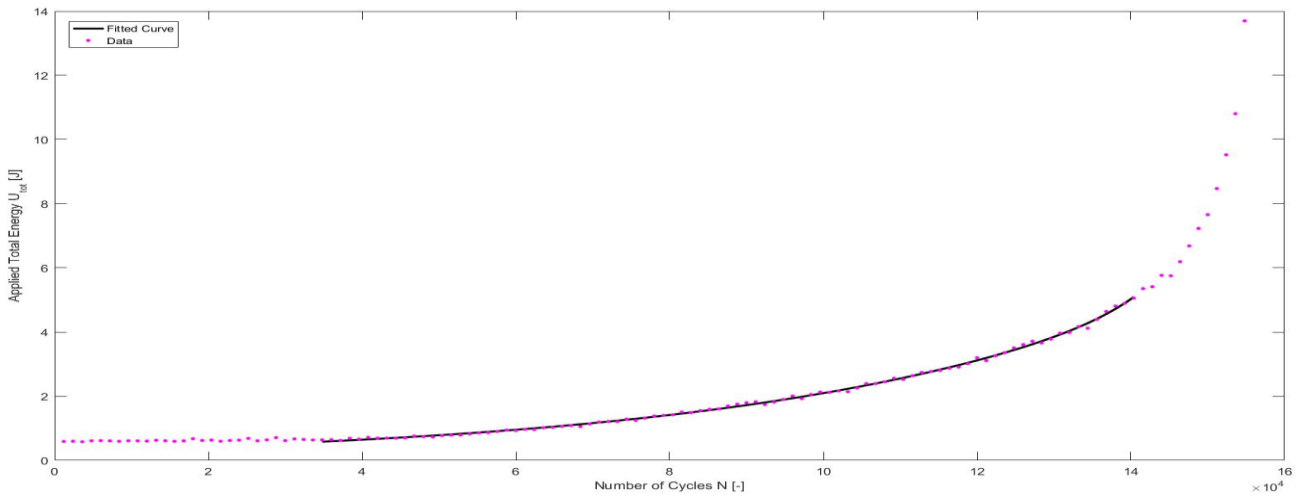
B 20: N-U$_{tot}$ Curve for Specimen VR005S100
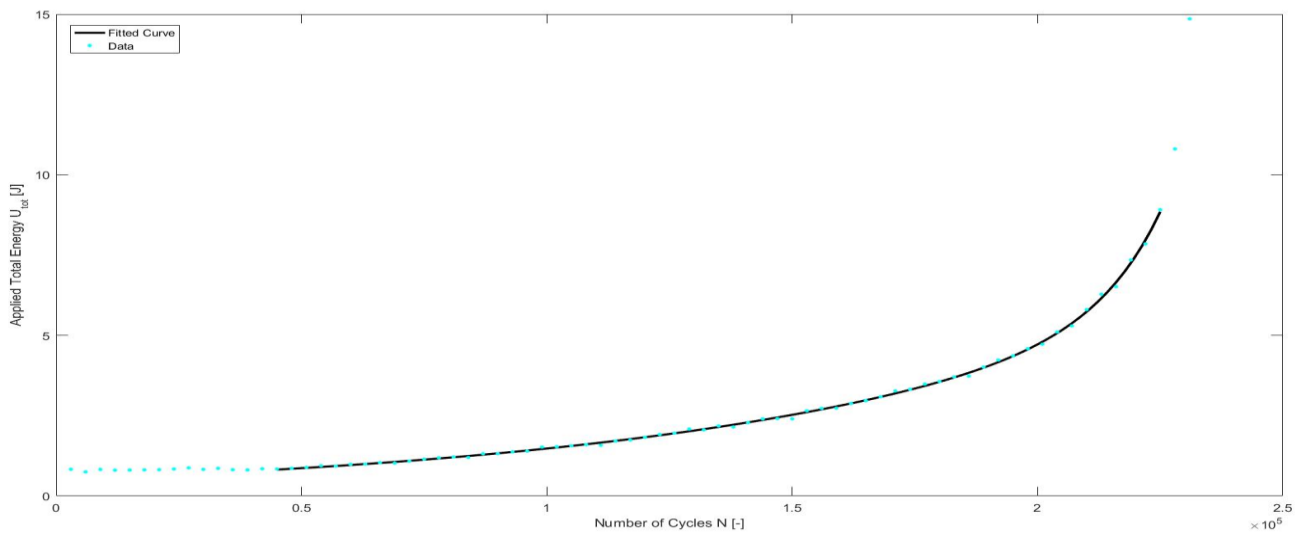
B 21: N-U$_{tot}$ Curve for Specimen VR03S100

APPENDIX B – N-U Curves
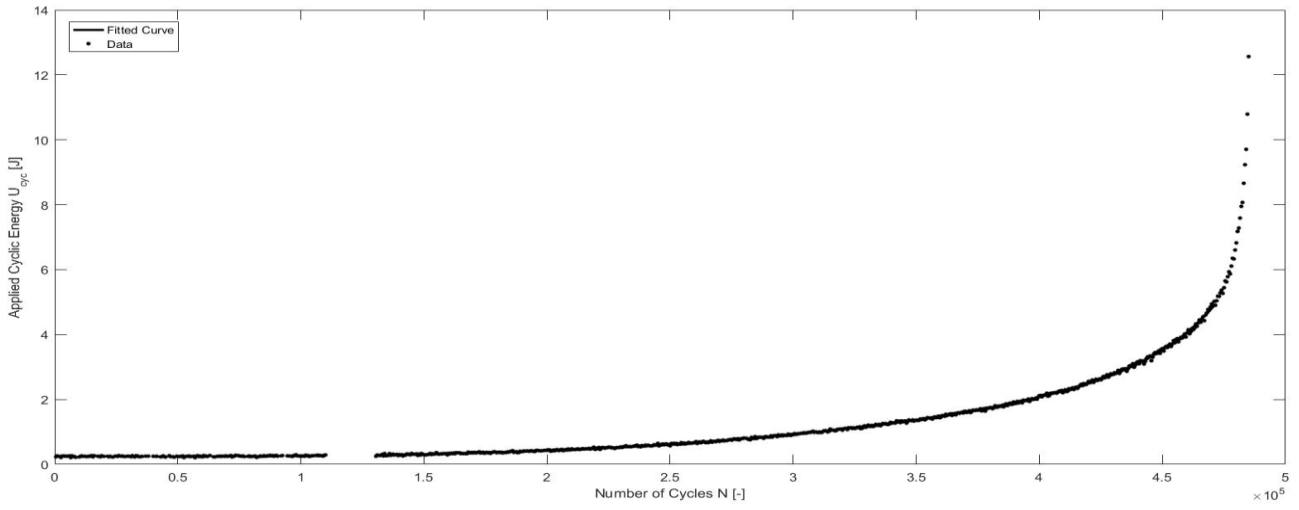
B 22: N-U$_{cyc}$ Curve of Specimen VR002S75
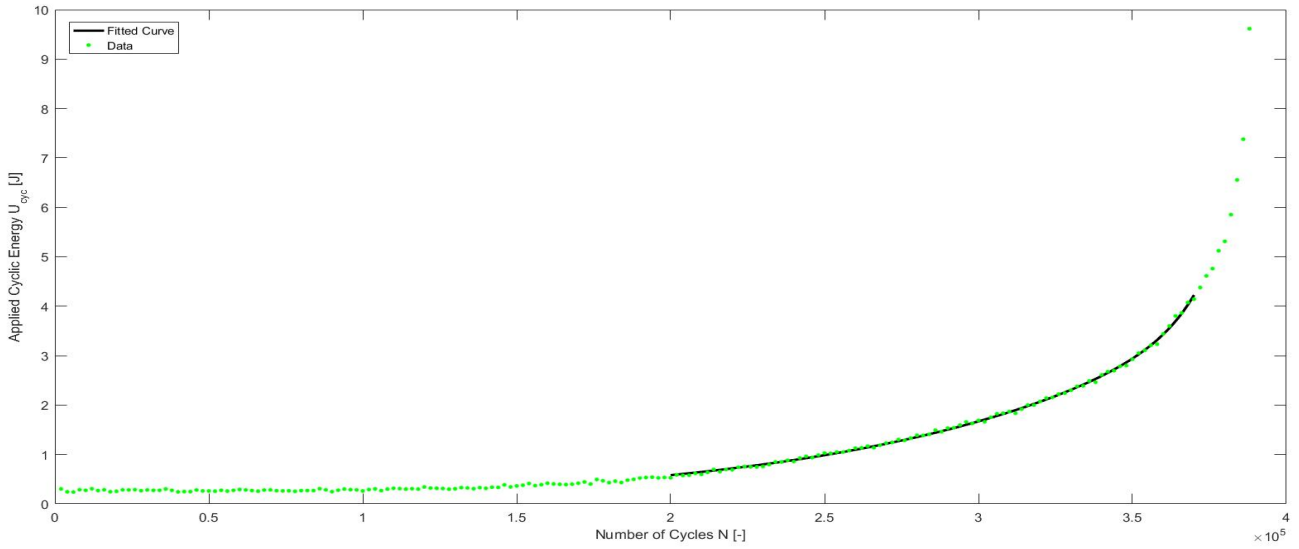
B 23: N-U$_{cyc}$ Curve of Specimen VR005S75
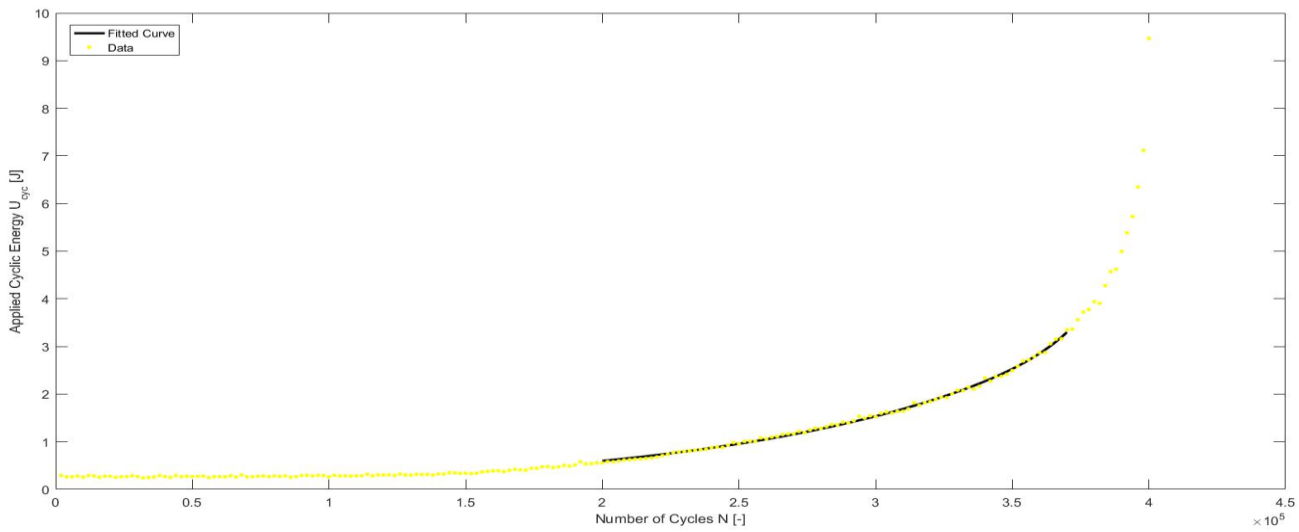
B 24: N-U$_{cyc}$ Curve of Specimen VR01S75

B 25: N-U$_{cyc}$ Curve for Specimen VR03S75
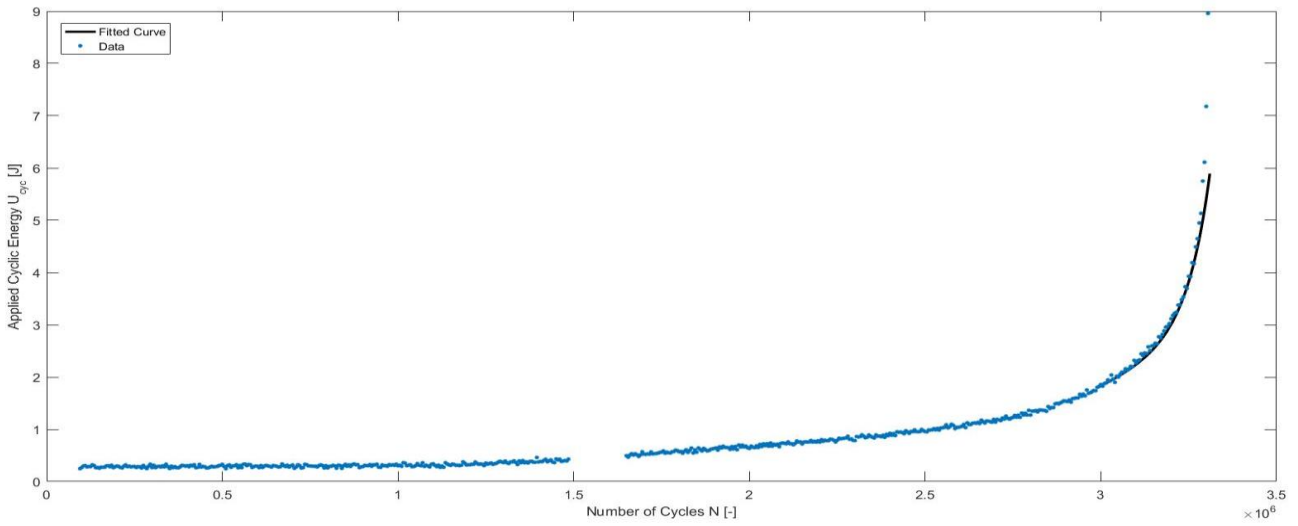
B 26: N-U$_{cyc}$ Curve for Specimen VR05S75
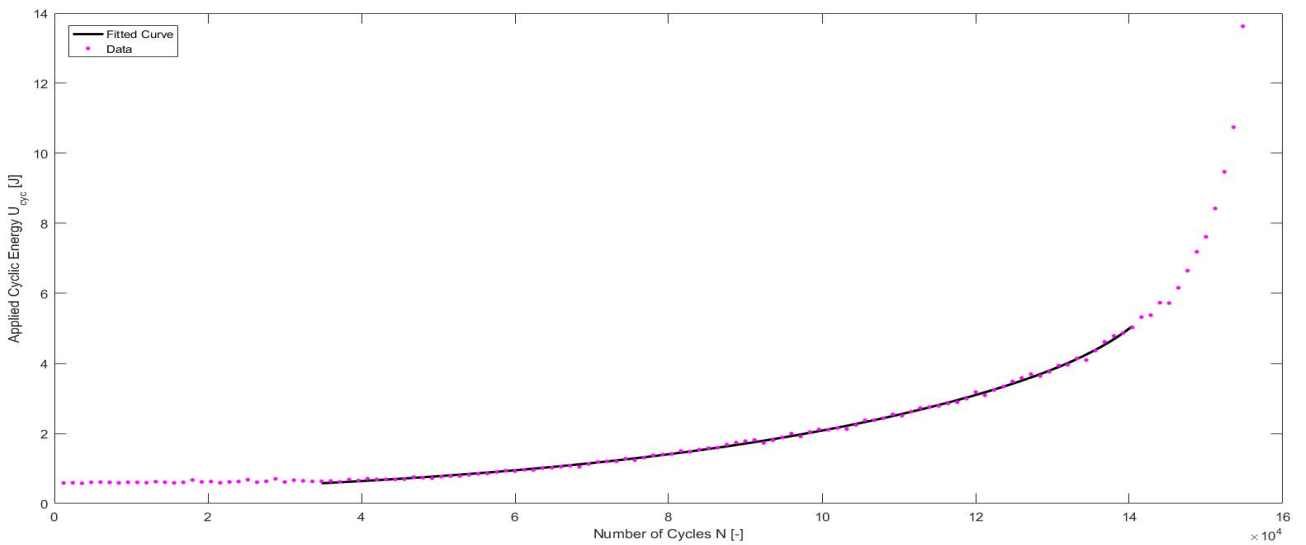
B 27: N-U$_{cyc}$ Curve for Specimen VR005S100

APPENDIX B – N-U Curves
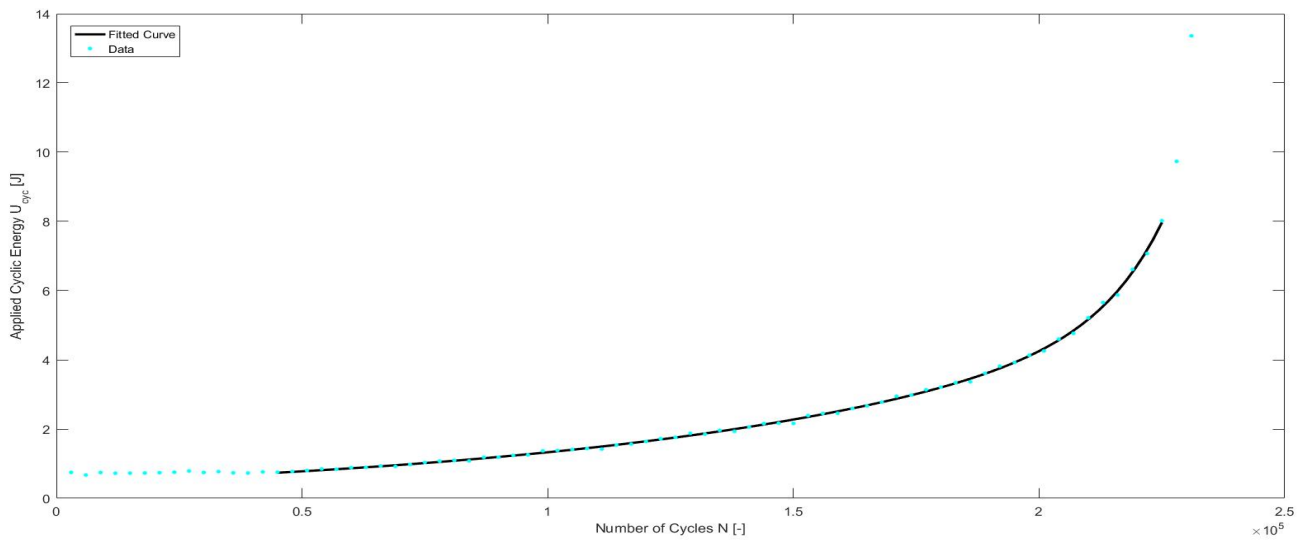
B 28: N-U$_{cyc}$ Curve for Specimen VR03S100

Appendix C – Load-COD Data

APPENDIX C – Load-COD Data
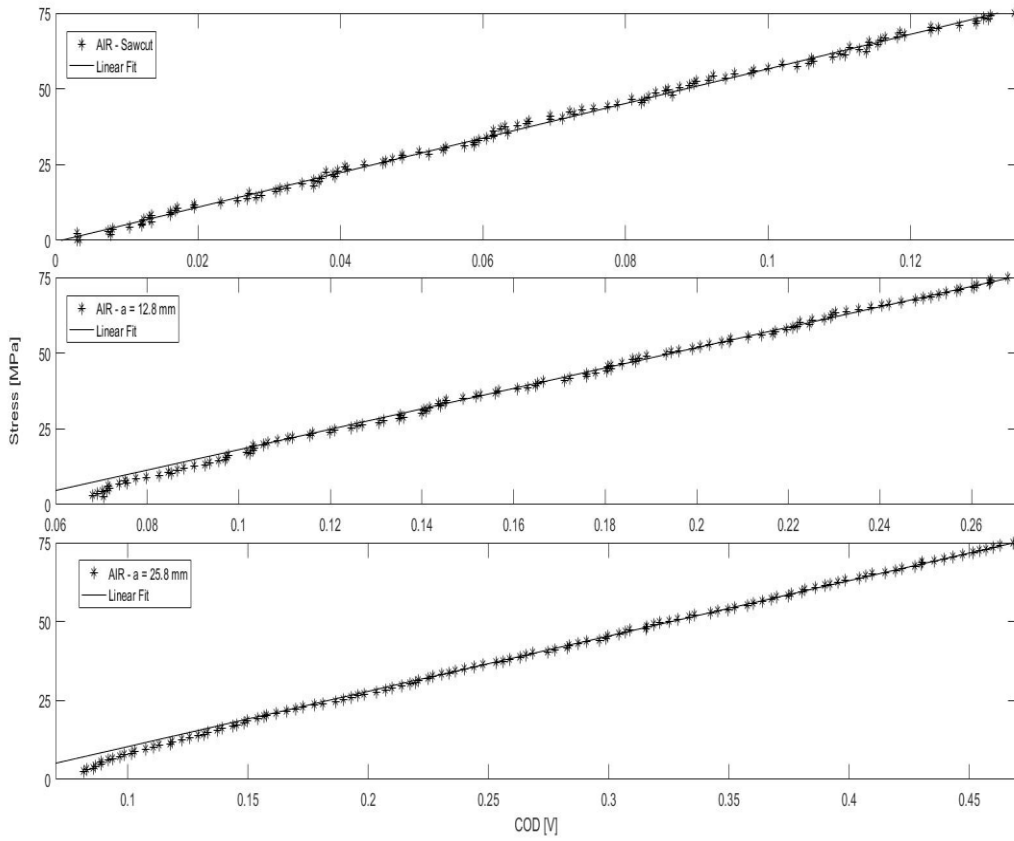
C 1: Load-COD Data of AR002S75 - COD-meter
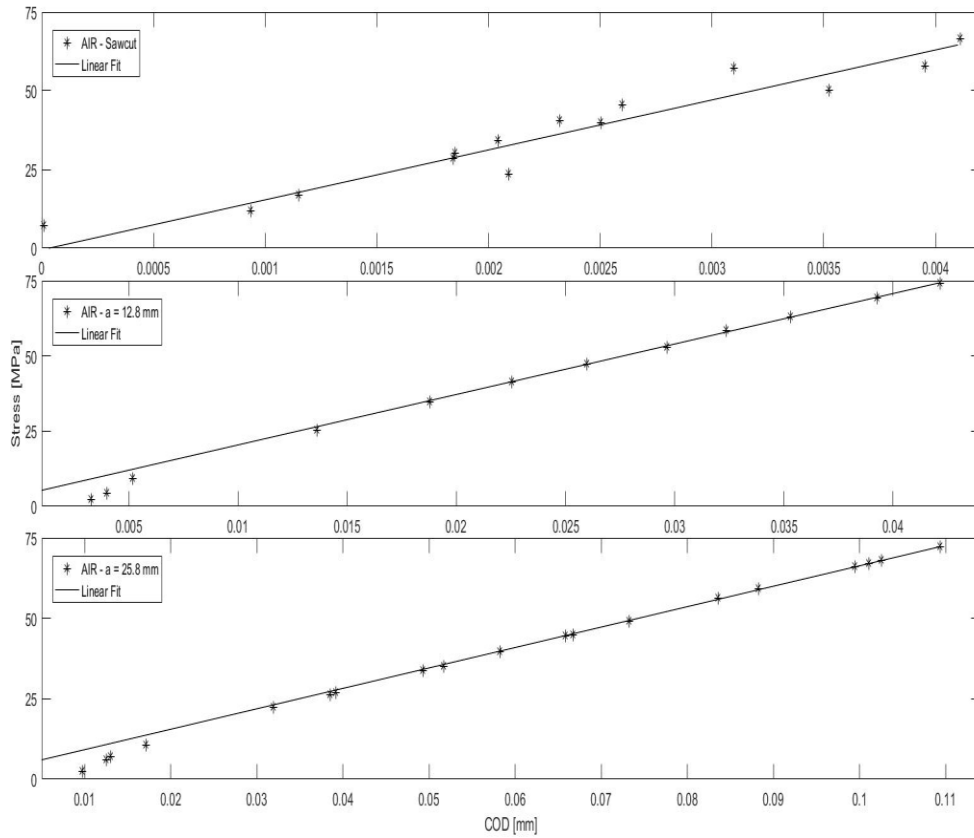
C 2: Load-COD Data of AR002S75 - VIC

APPENDIX C – Load-COD Data
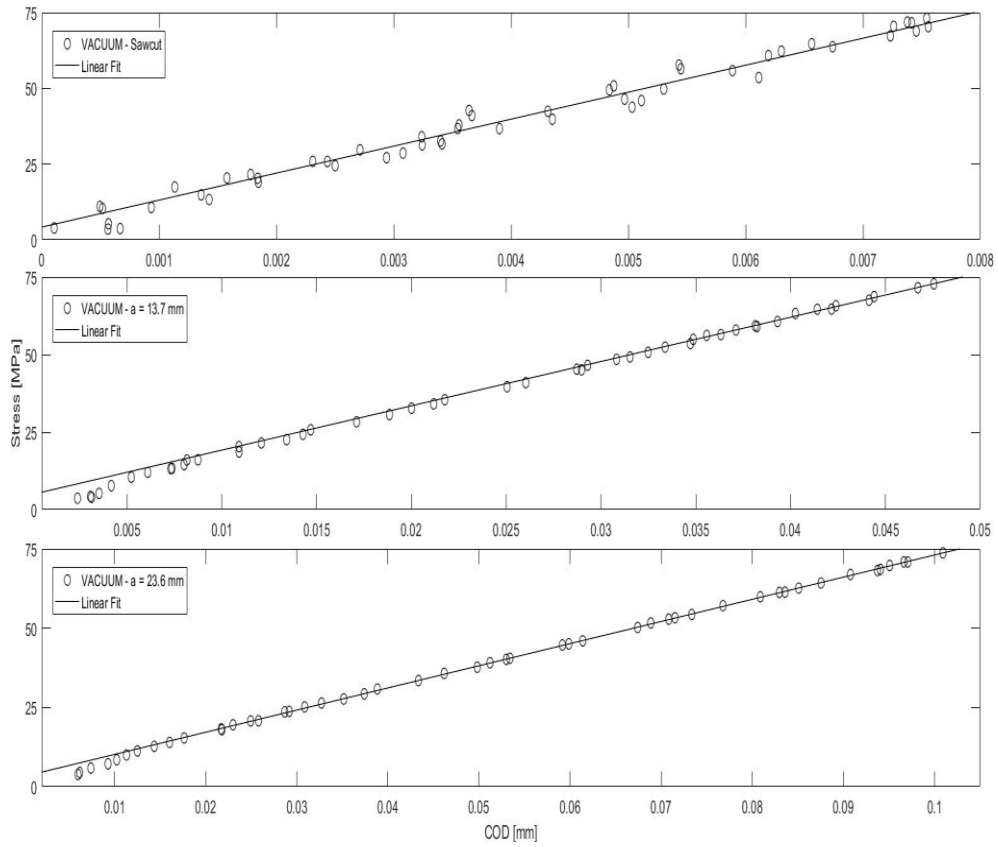
C 3: Load-COD Data of VR002S75 - VIC
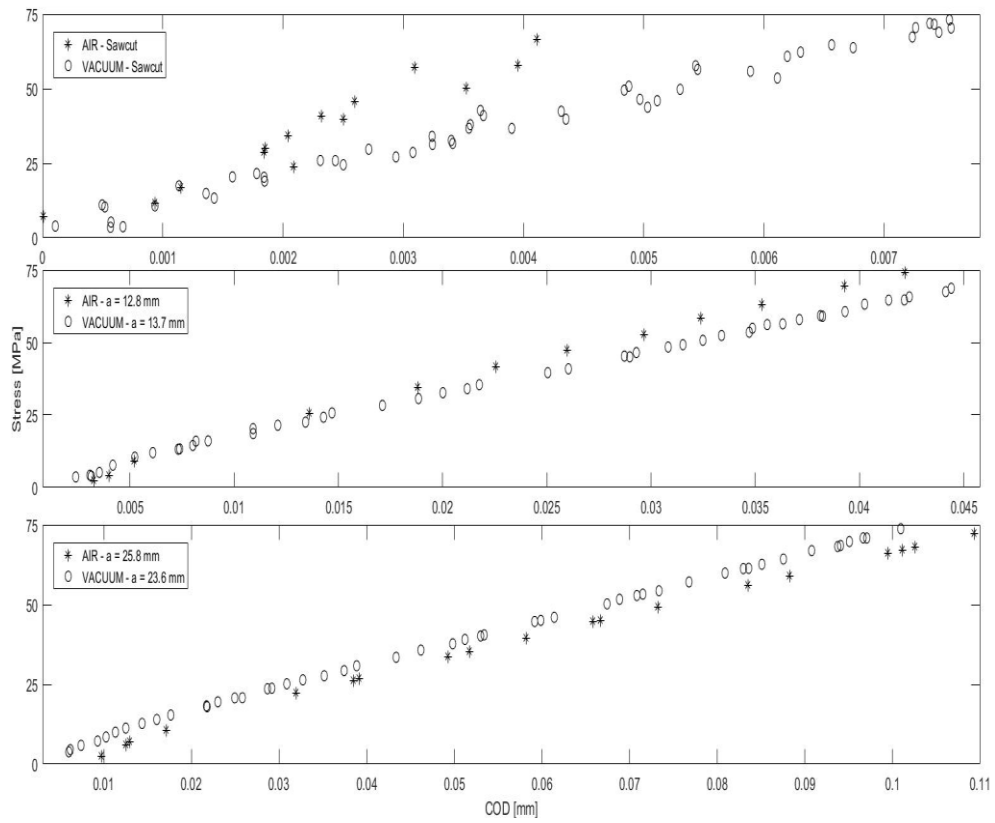
C 4: Load-COD Data of AR002S75 vs VR002S75 - VIC

APPENDIX C – Load-COD Data
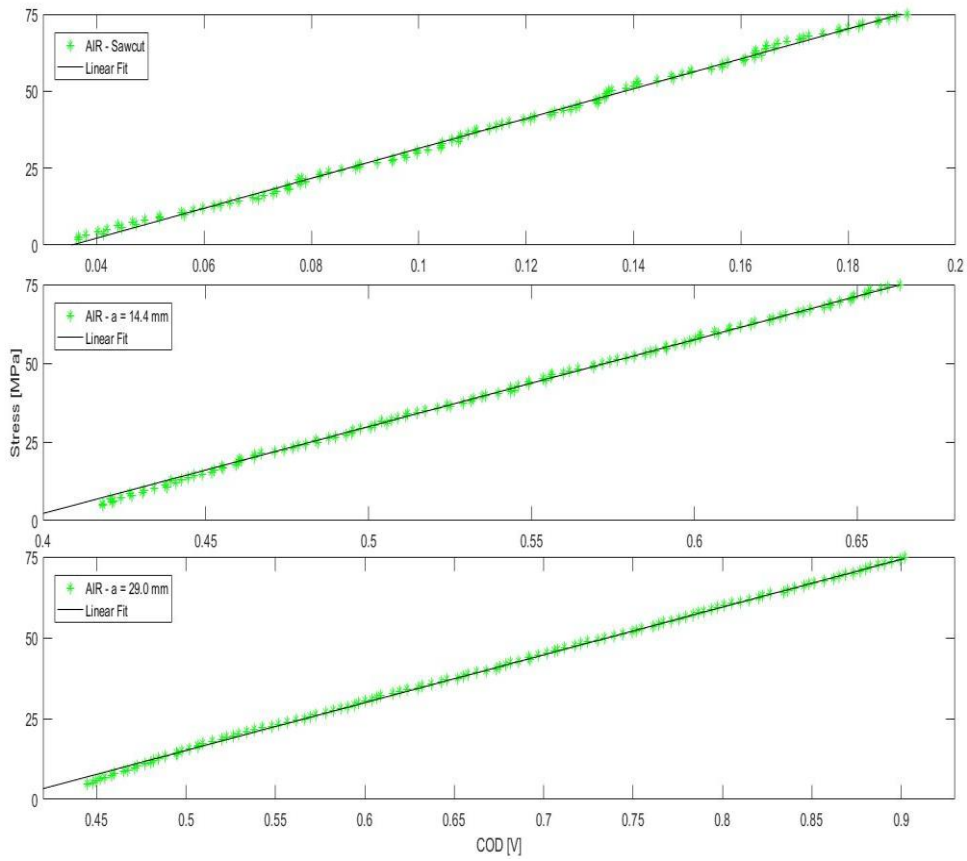
C 5: Load-COD Data of AR005S75 - COD-meter
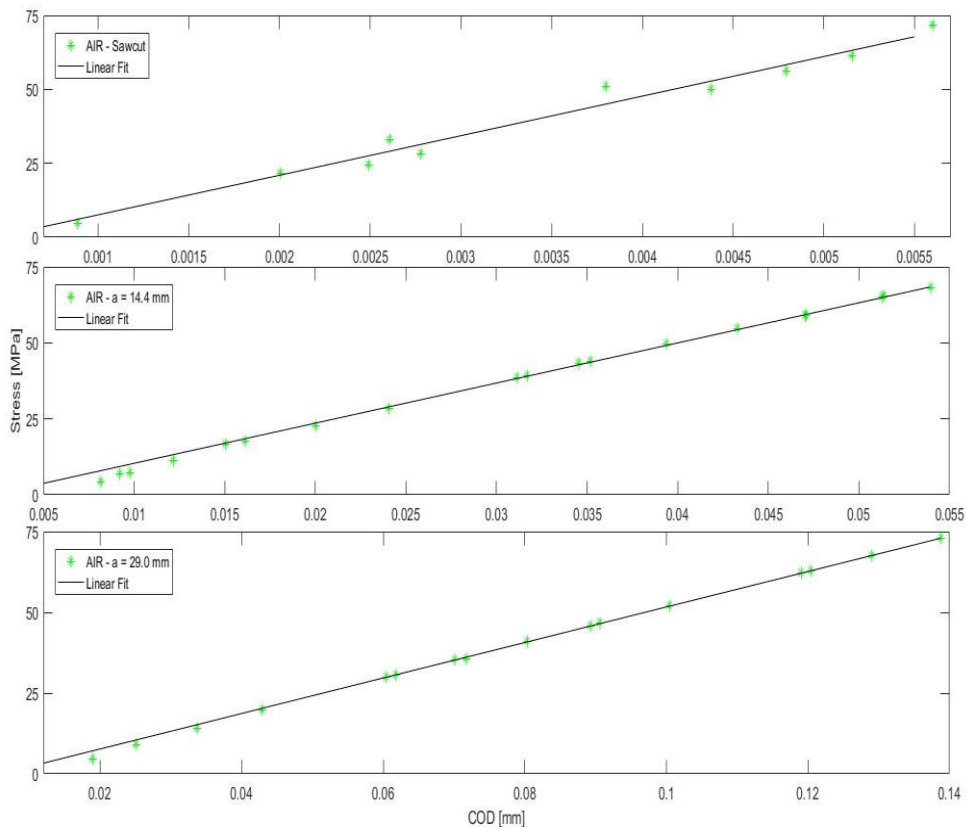
C 6: Load-COD Data of AR005S75 - VIC

APPENDIX C – Load-COD Data
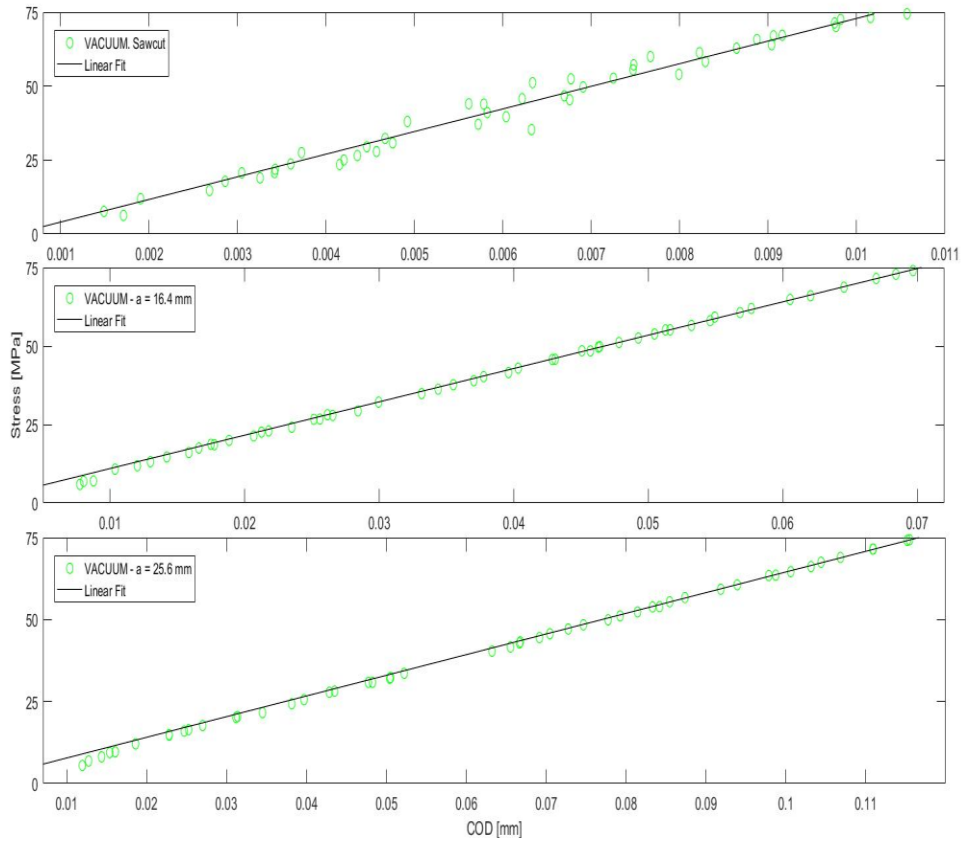
C 7: Load-COD Data of VR005S75 - VIC
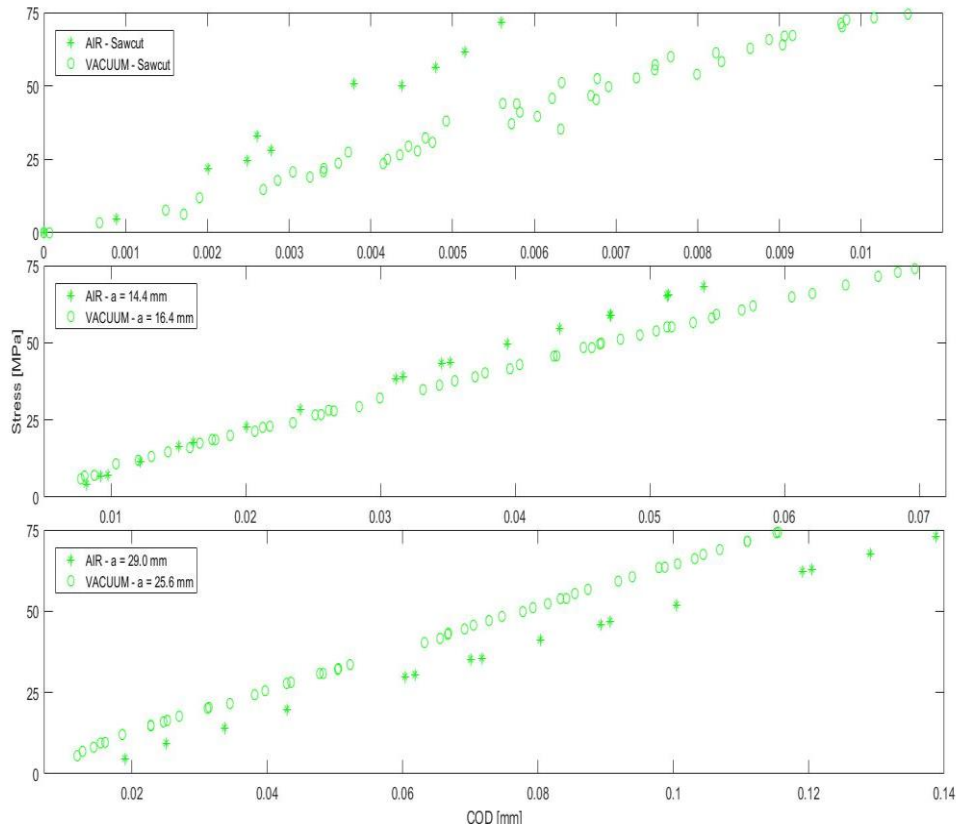
C 8: Load-COD Data of AR005S75 vs VR005S75 - VIC

APPENDIX C – Load-COD Data
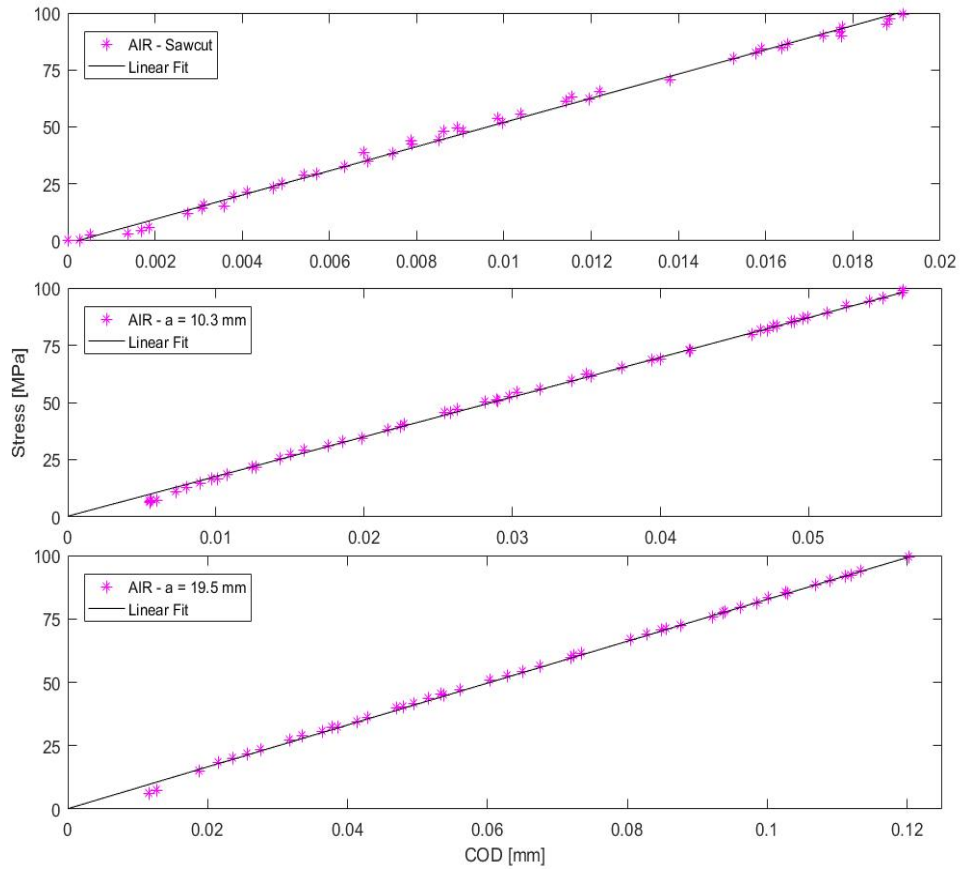
C 9: Load-COD Data of AR005S100 - VIC
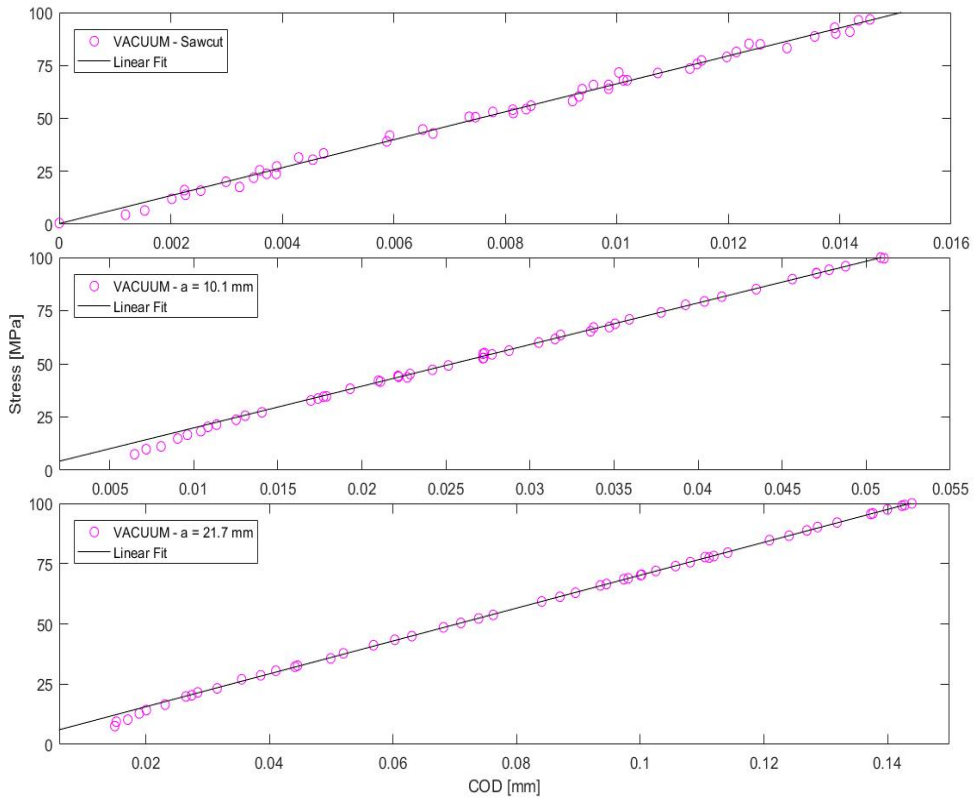
C 10: Load-COD Data of VR005S100 - VIC

APPENDIX C – Load-COD Data
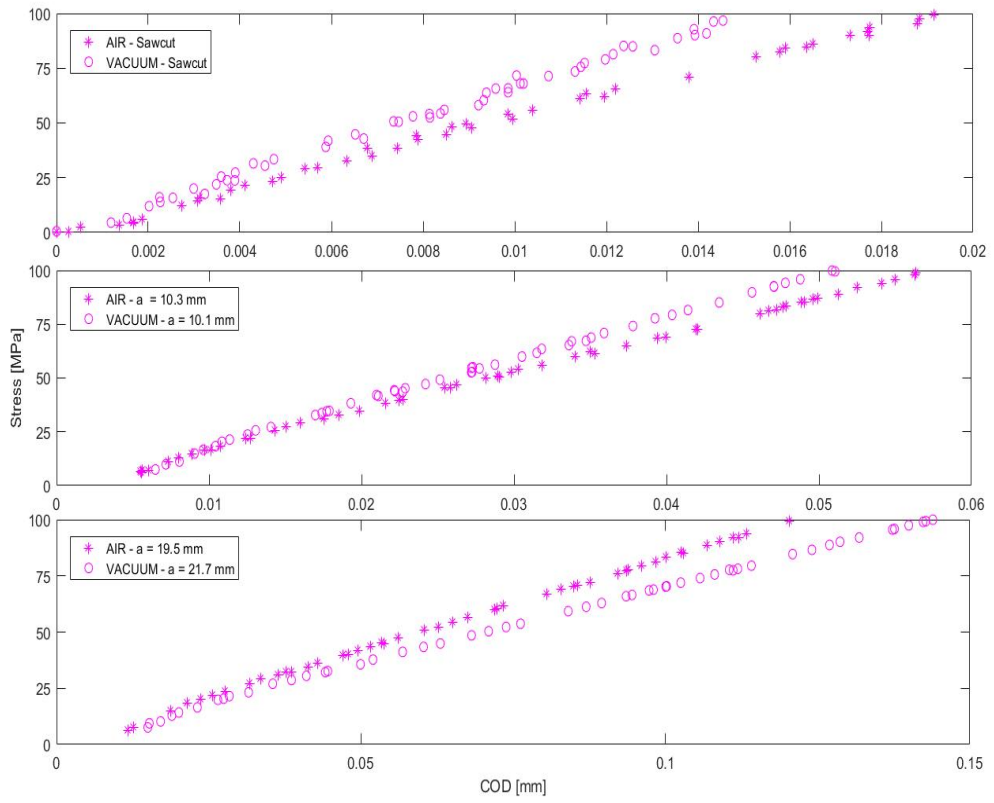
C 11: Load-COD Data of AR005S100 vs VR005S100 - VIC

APPENDIX C – Load-COD Data
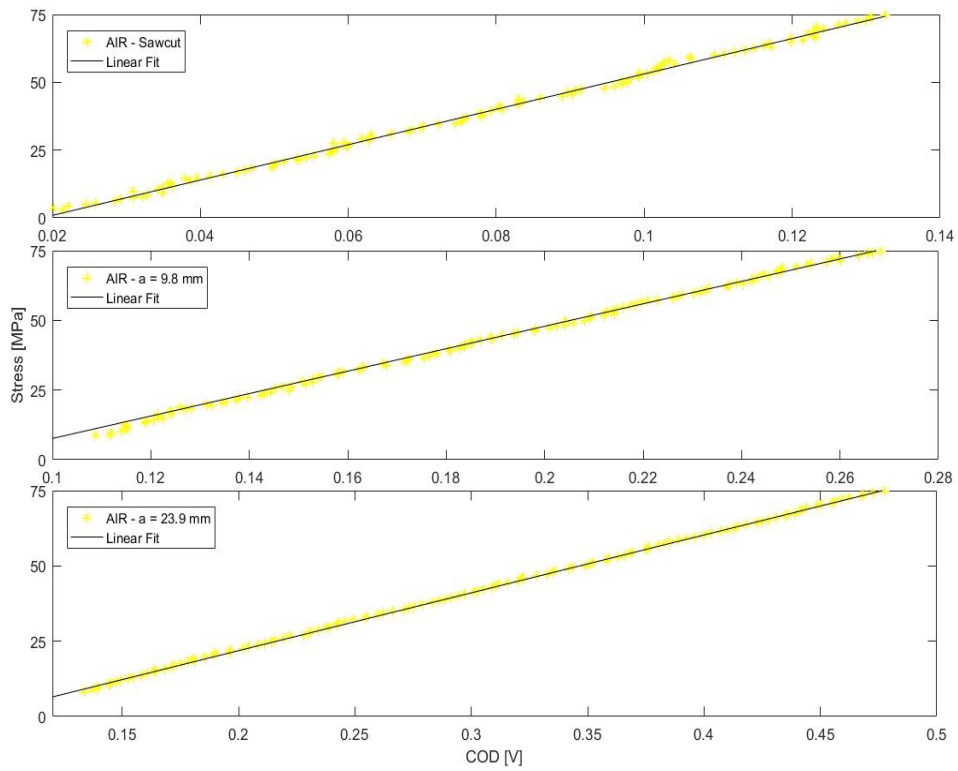
C 12: Load-COD Data of AR01S75 - COD-meter
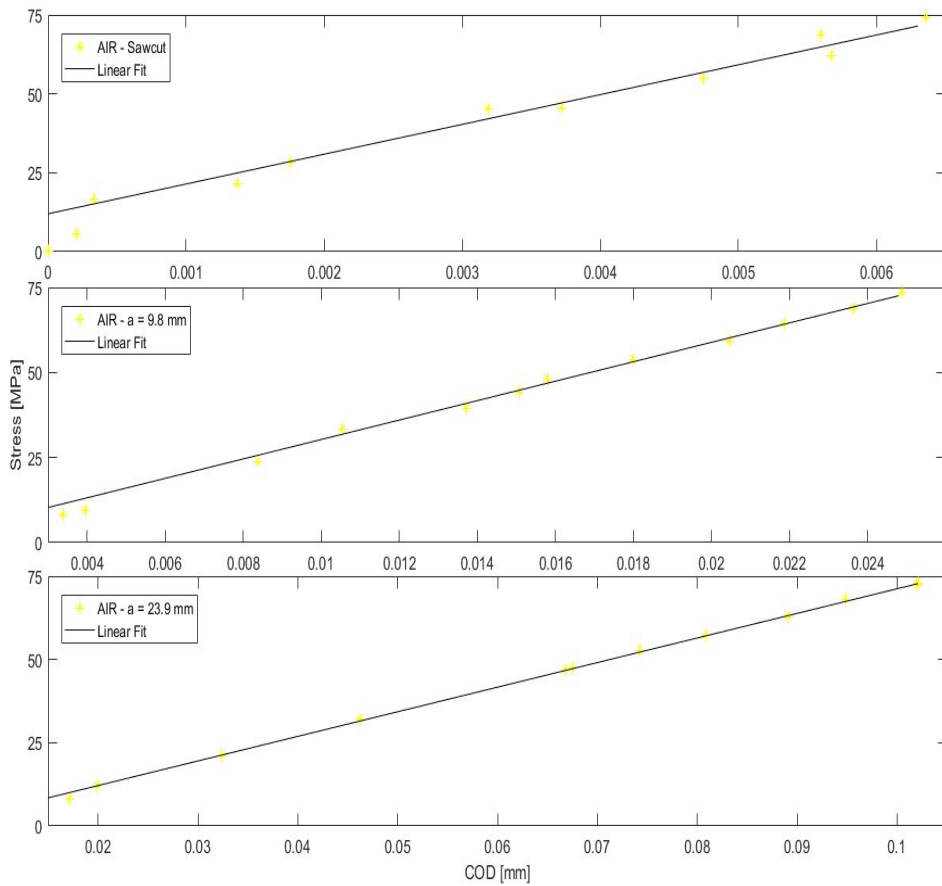
C 13: Load-COD Data of AR01S75 - VIC

APPENDIX C – Load-COD Data
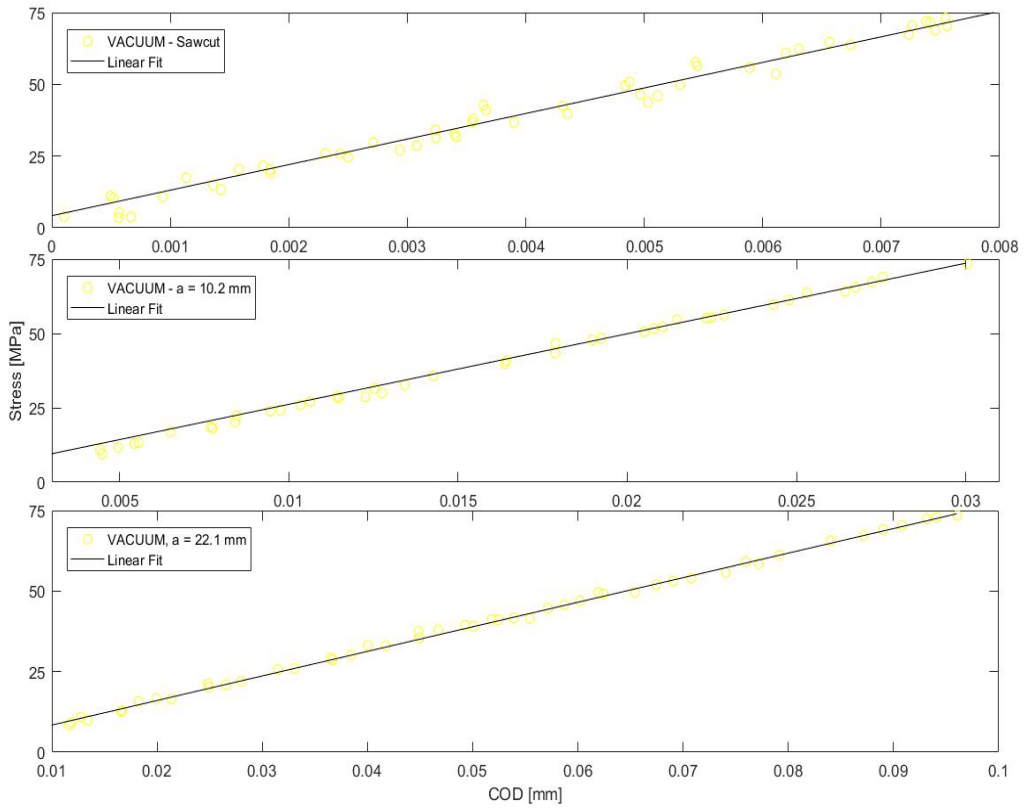
C 14: Load-COD Data of VR01S75 - VIC
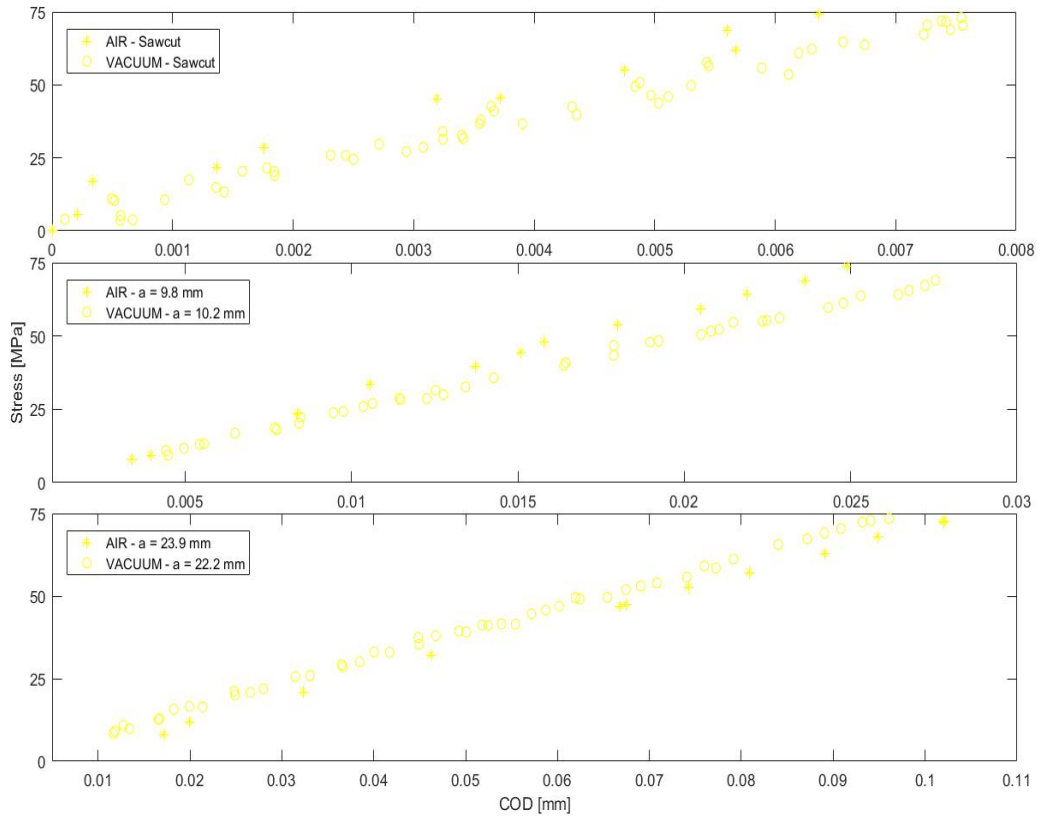
C 15: Load-COD Data of AR01S75 vs VR01S75 - VIC

APPENDIX C – Load-COD Data
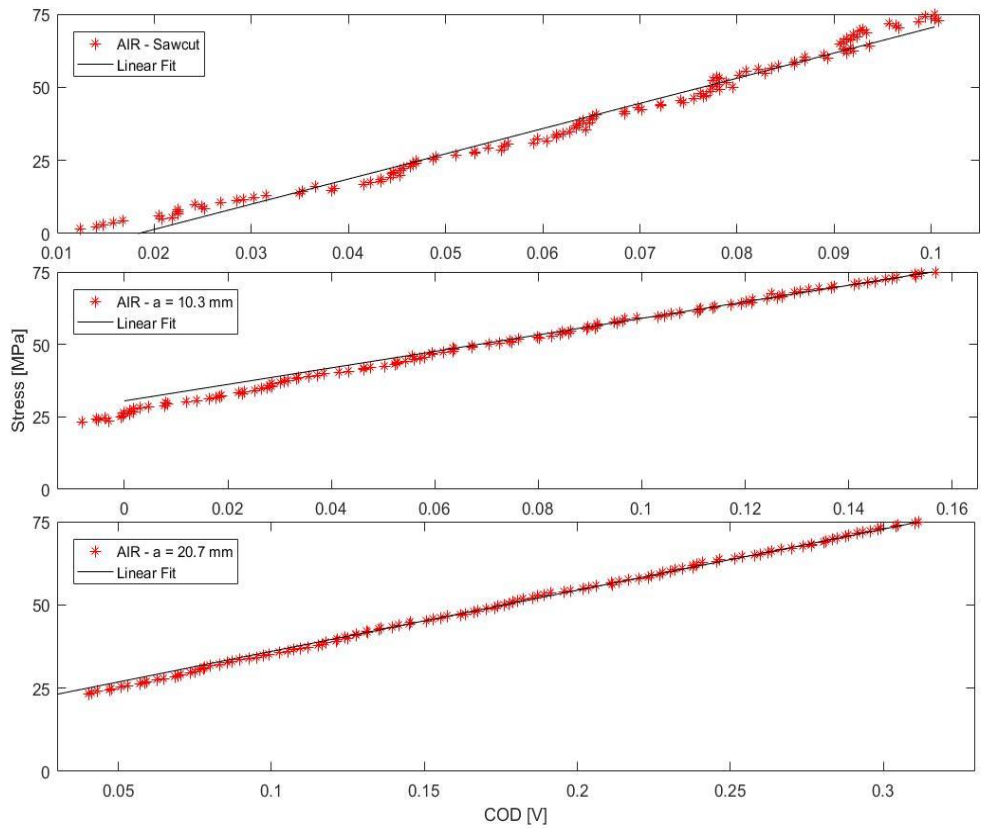
C 16: Load-COD Data of AR03S75 - COD-meter
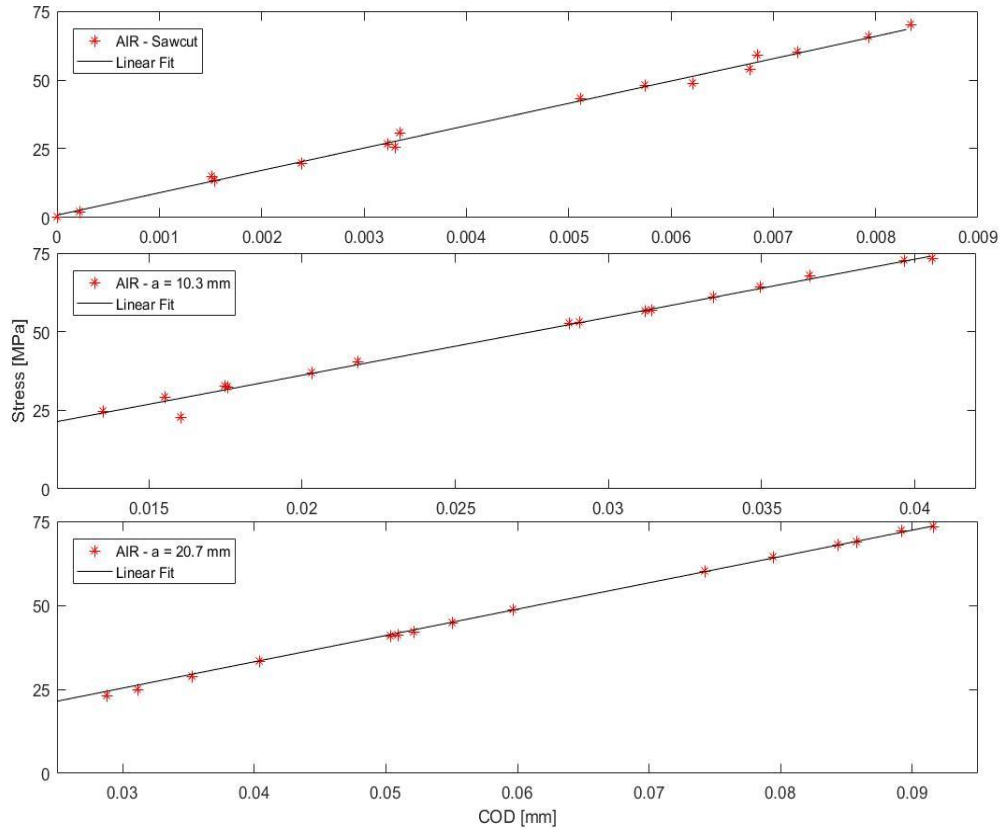
C 17: Load-COD Data of AR03S75 - VIC

APPENDIX C – Load-COD Data
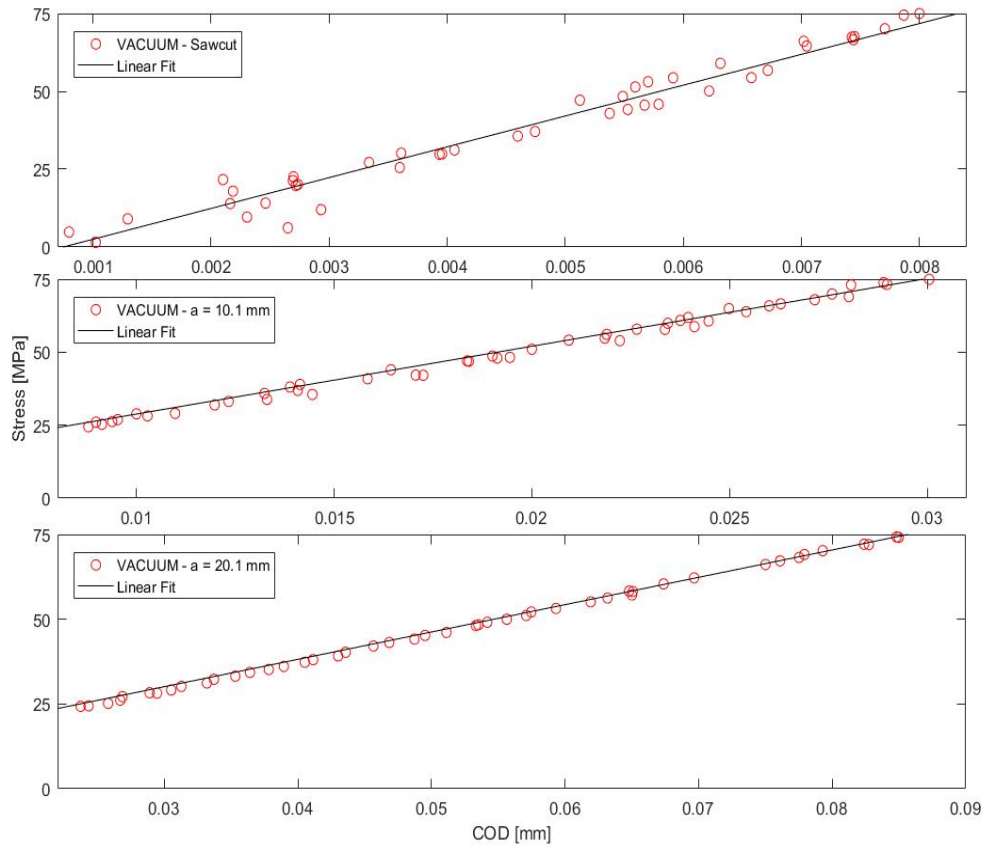
C 18: Load-COD Data of VR03S75 - COD-meter
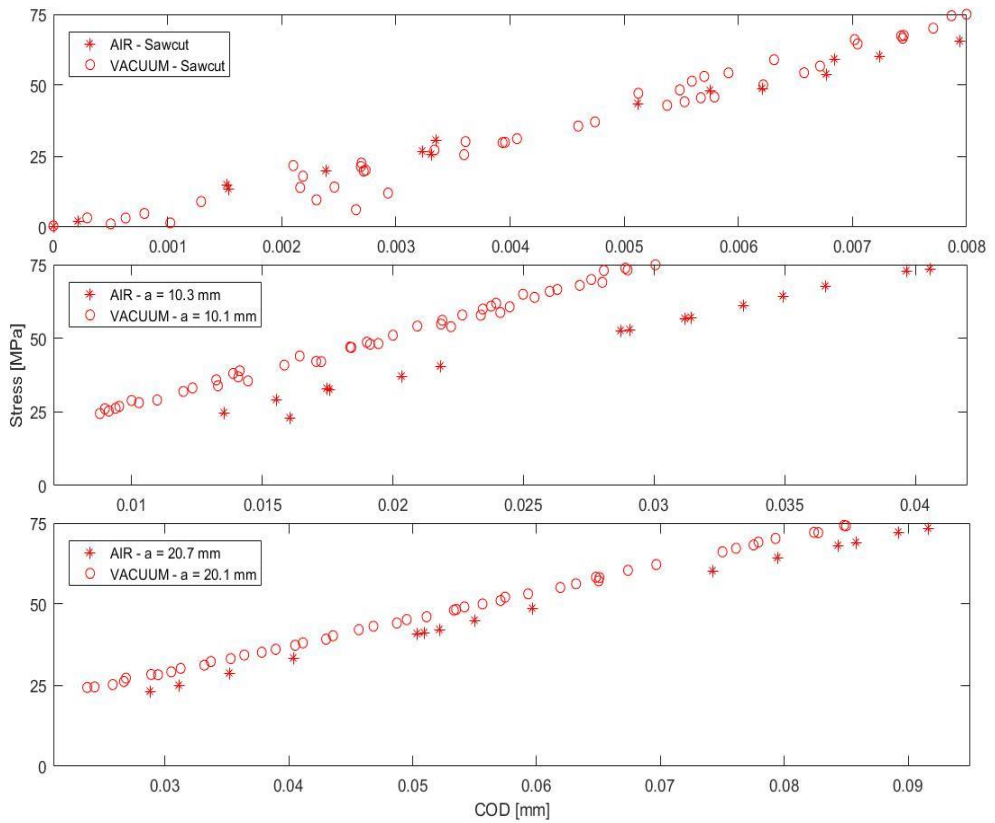
C 19: Load-COD Data of AR03S75 vs VR03S75 - VIC

APPENDIX C – Load-COD Data
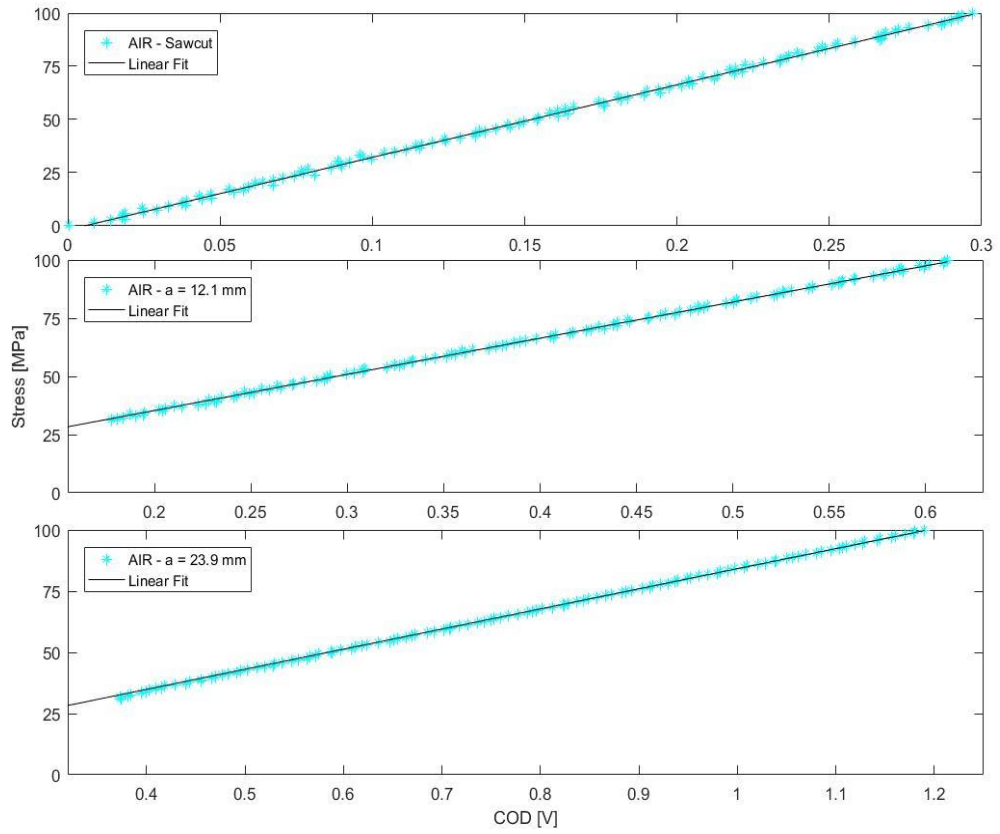
C 20: Load-COD Data of AR03S100 - COD-meter
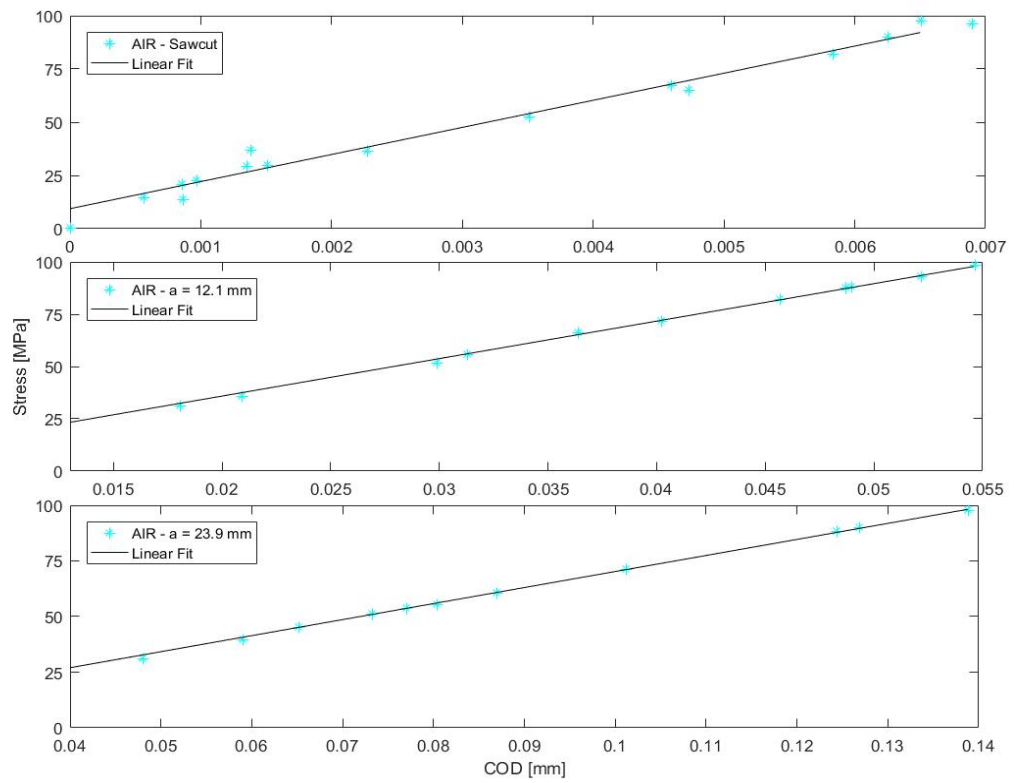
C 21: Load-COD Data of AR03S100 - VIC

APPENDIX C – Load-COD Data
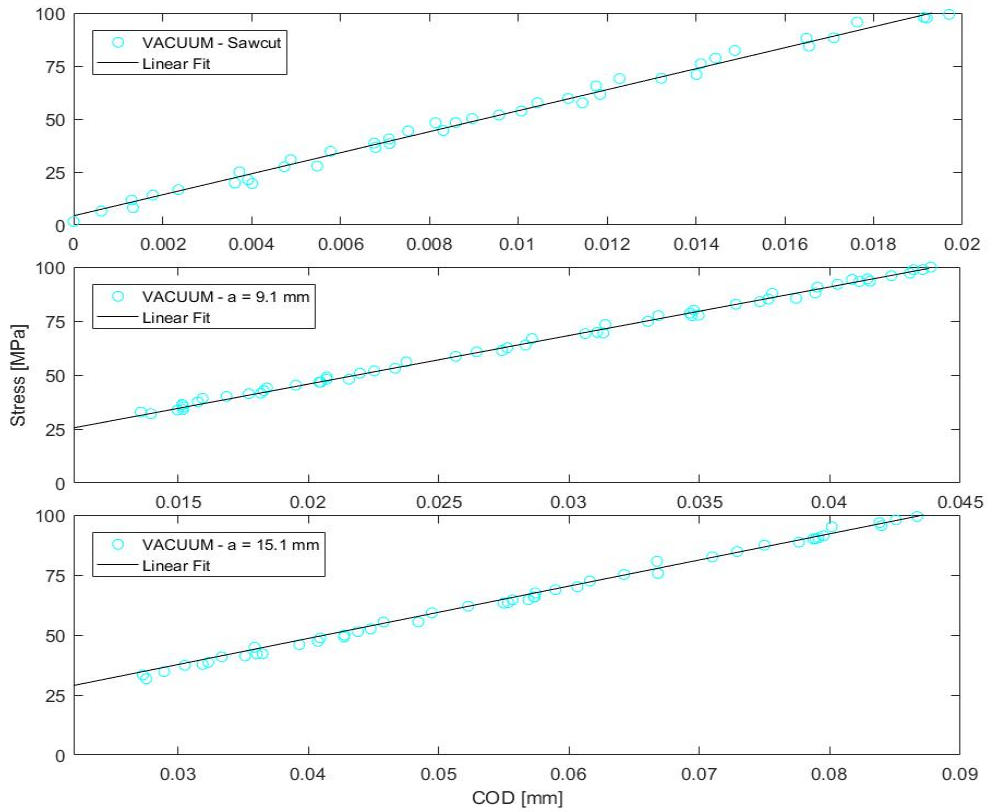
C 22: Load-COD Data of VR03S100 - VIC
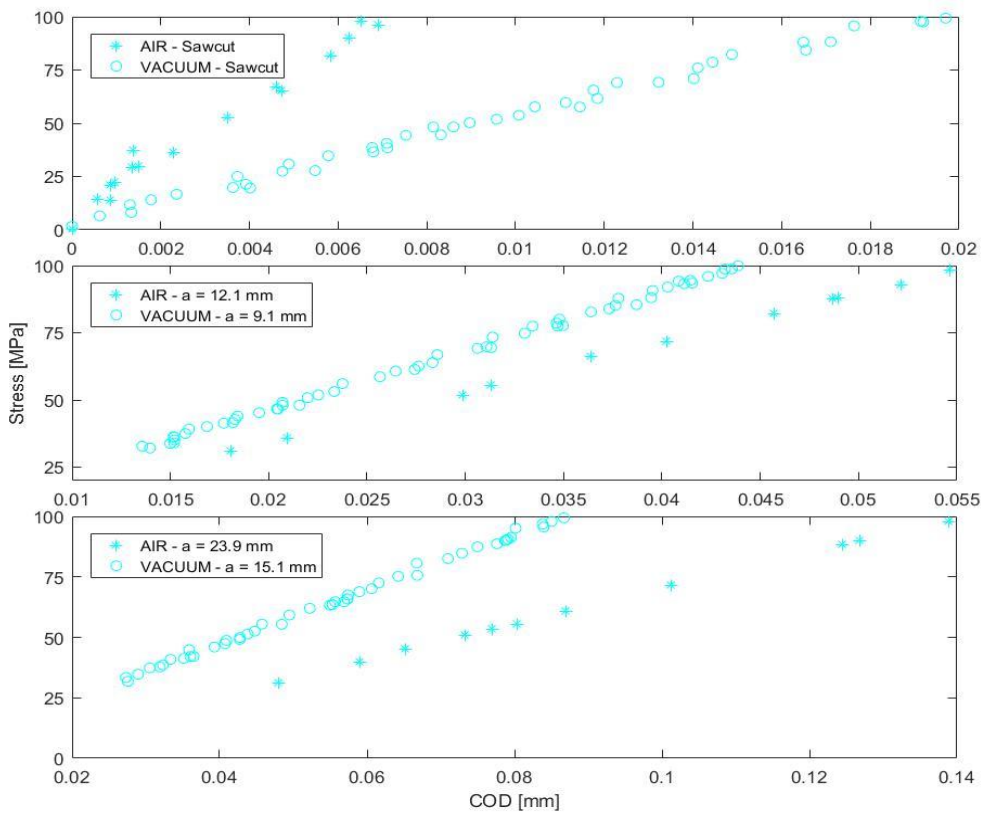
C 23: Load-COD Data of AR03S100 vs VR03S100 - VIC

APPENDIX C – Load-COD Data
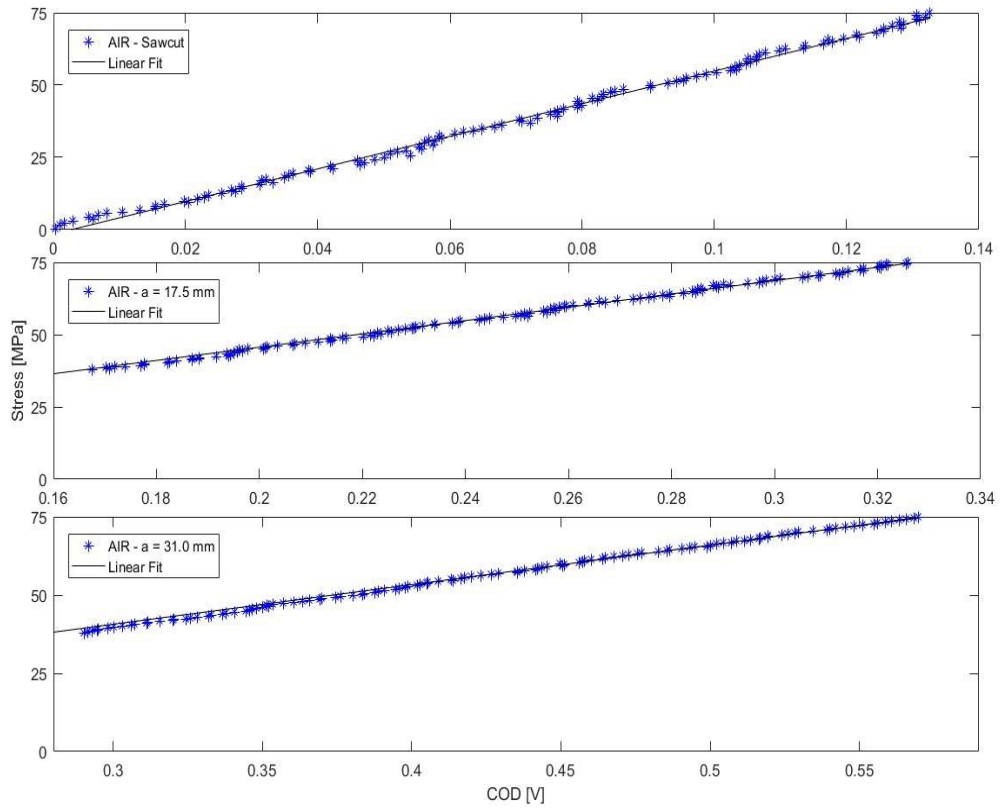
C 24: Load-COD Data of AR05S75 - COD-meter
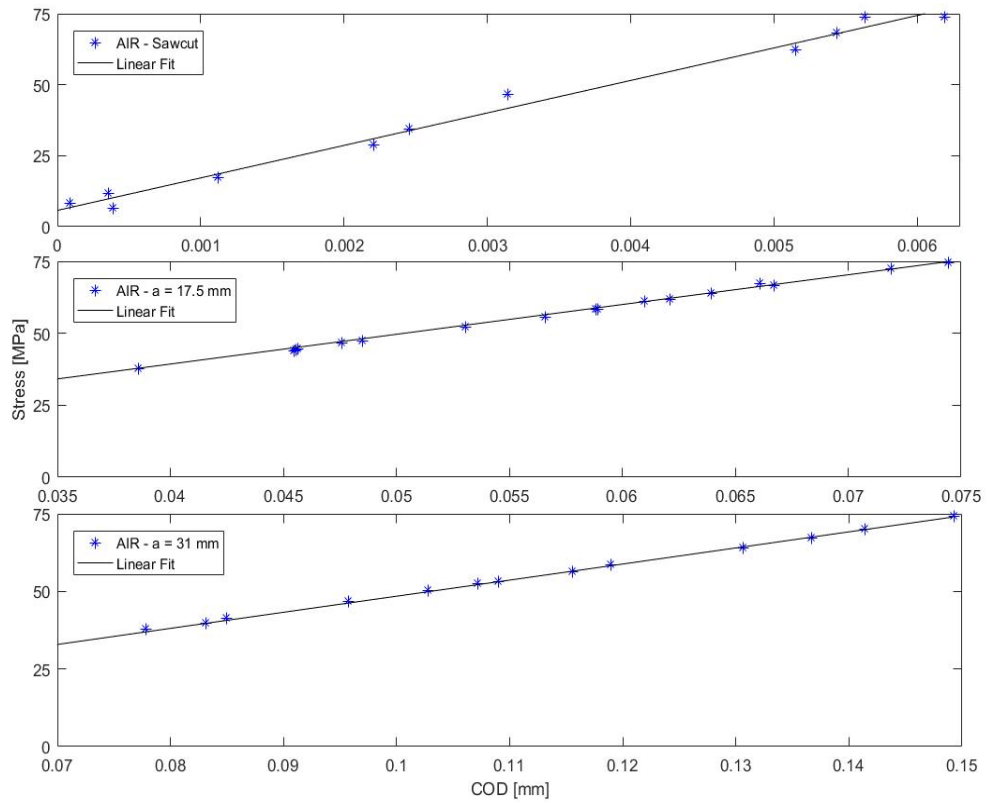
C 25: Load-COD Data of AR05S75 - VIC

APPENDIX C – Load-COD Data
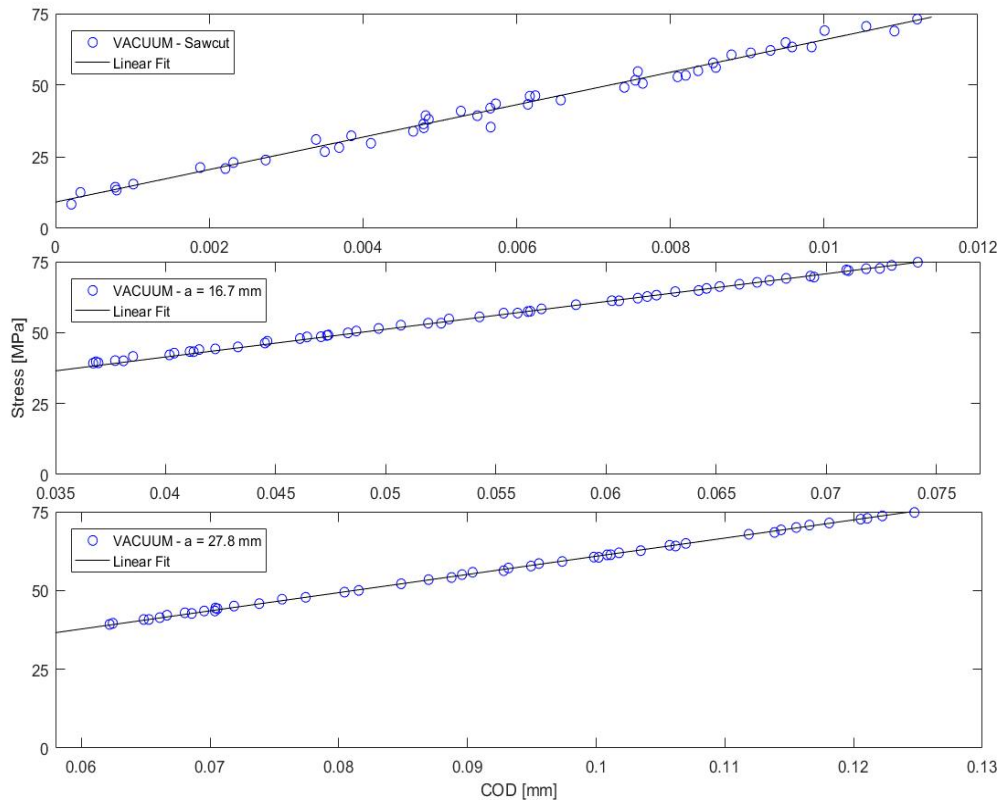
C 26: Load-COD Data of VR05S75 - VIC
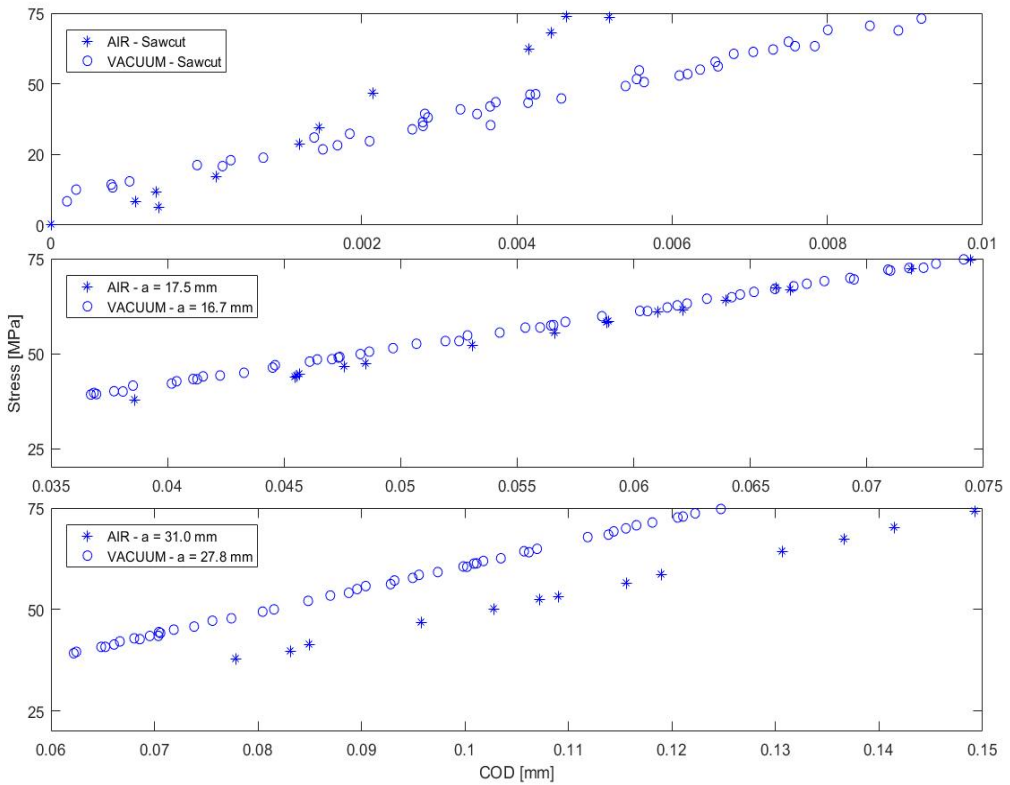
C 27: Load-COD Data of AR05S75 vs VR05S75 - VIC

Appendix D – Load-COD Fits for Cyclic Applied Work Determination

APPENDIX D – Load-COD Fits for Cyclic Applied Work Determination
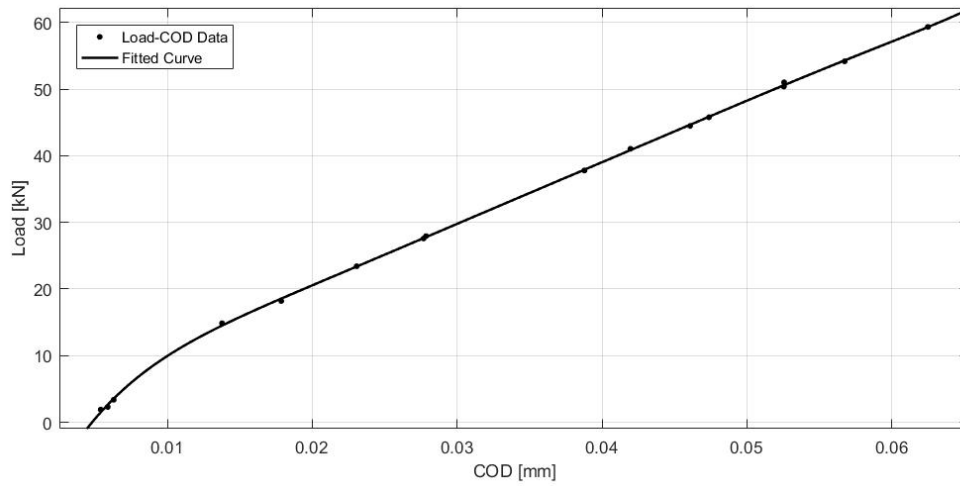
D 1: (Fitted) Load-COD Curve for Specimen AR002S75 at a = 12.8 mm
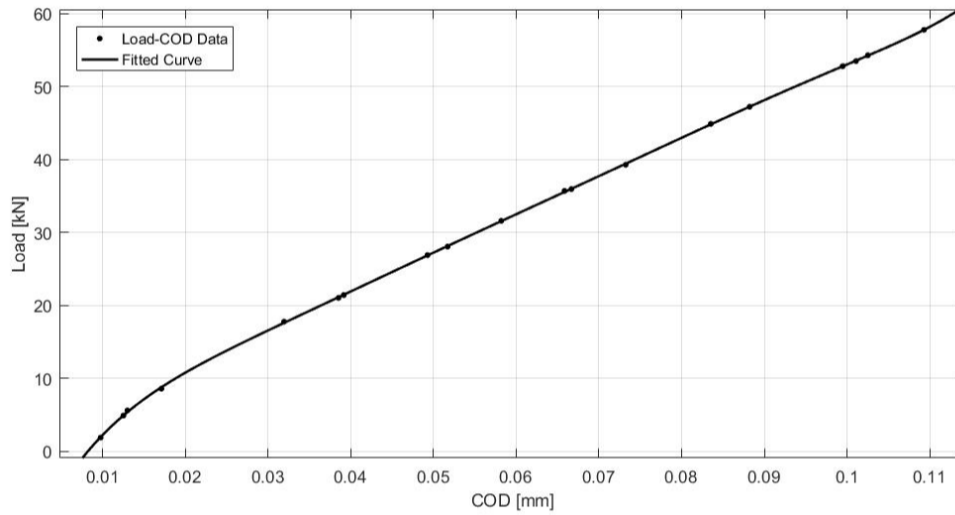
D 2: (Fitted) Load-COD Curve for Specimen AR002S75 at a = 25.8 mm
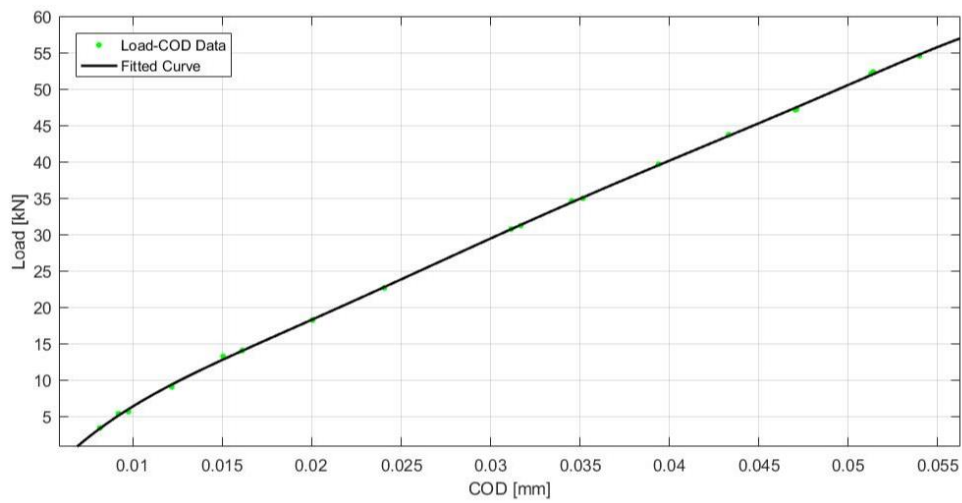
D 3: (Fitted) Load-COD Curve for Specimen AR005S75 at a = 14.4 mm

APPENDIX D – Load-COD Fits for Cyclic Applied Work Determination
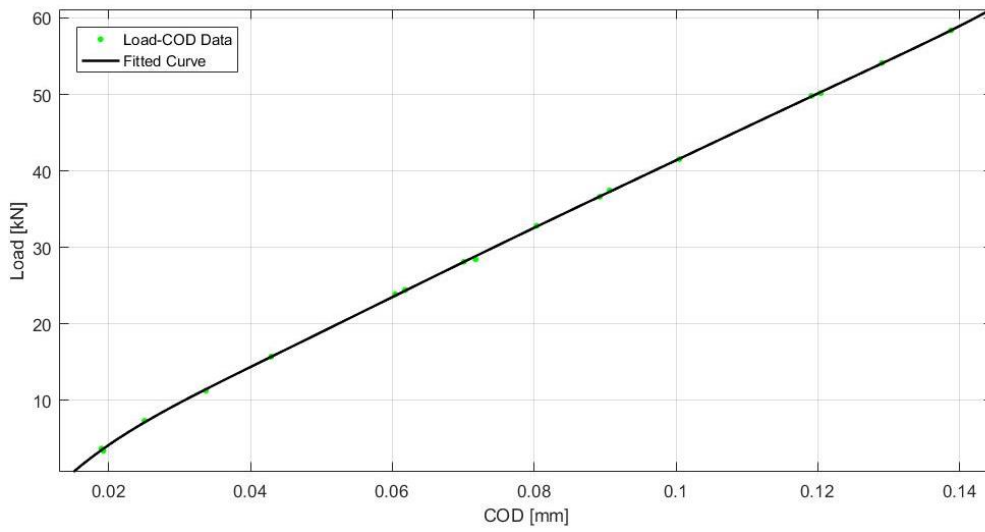
D 4: (Fitted) Load-COD Curve for Specimen AR005S75 at a = 29.0 mm
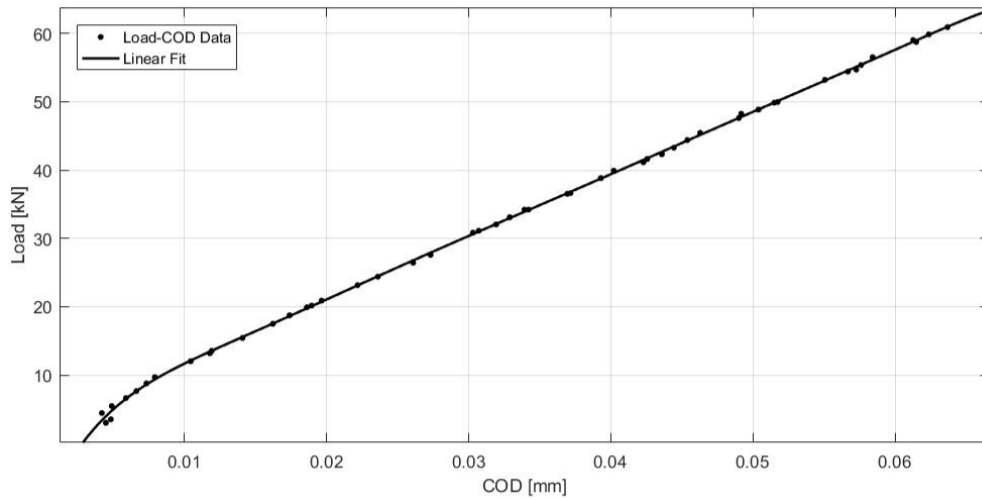
D 5: (Fitted) Load-COD Curve for Specimen VR002S75 at a = 13.7 mm
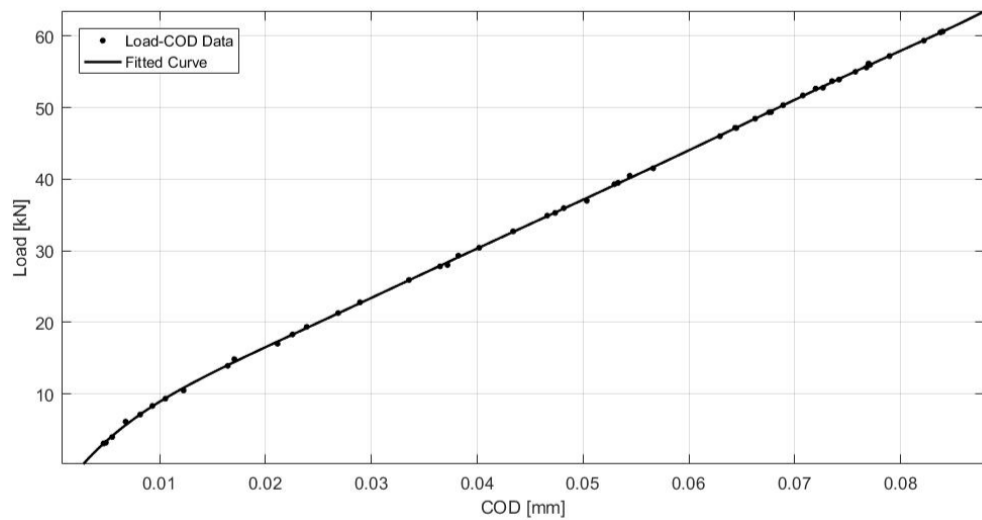
D 6: (Fitted) Load-COD Curve for Specimen VR002S75 at a = 23.6 mm

APPENDIX D – Load-COD Fits for Cyclic Applied Work Determination
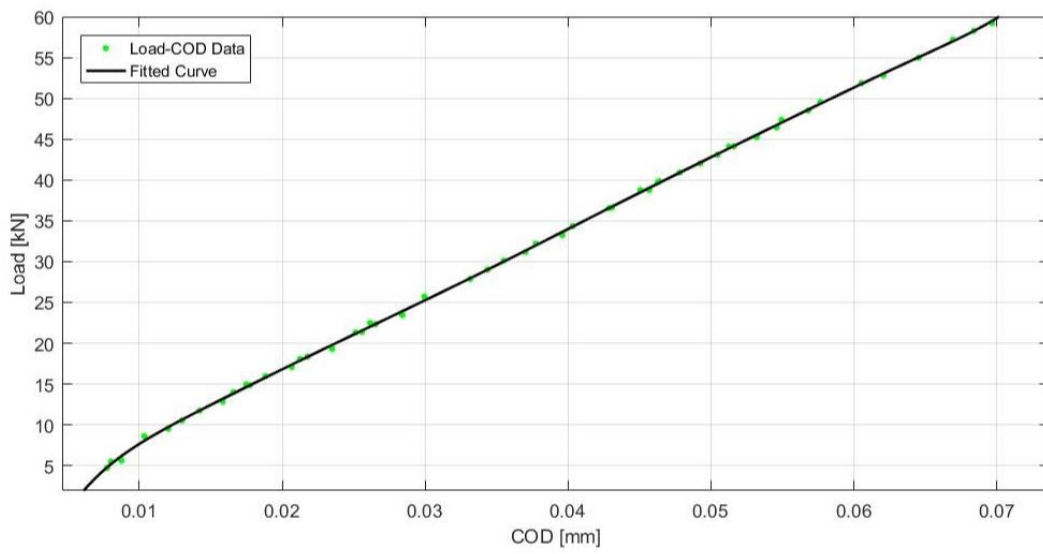
D 7: (Fitted) Load-COD Curve for Specimen VR006S75 at a = 16.4
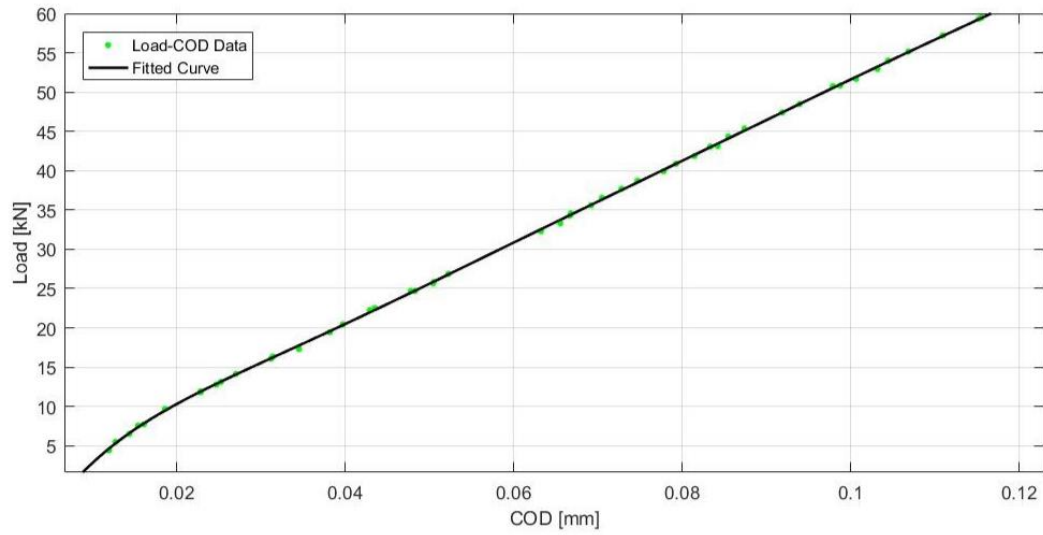
D 8: (Fitted) Load-COD Curve for Specimen VR006S75 at a = 25.6

Appendix E – Elastic-Plastic Behaviour

APPENDIX E – Elastic-Plastic Behaviour
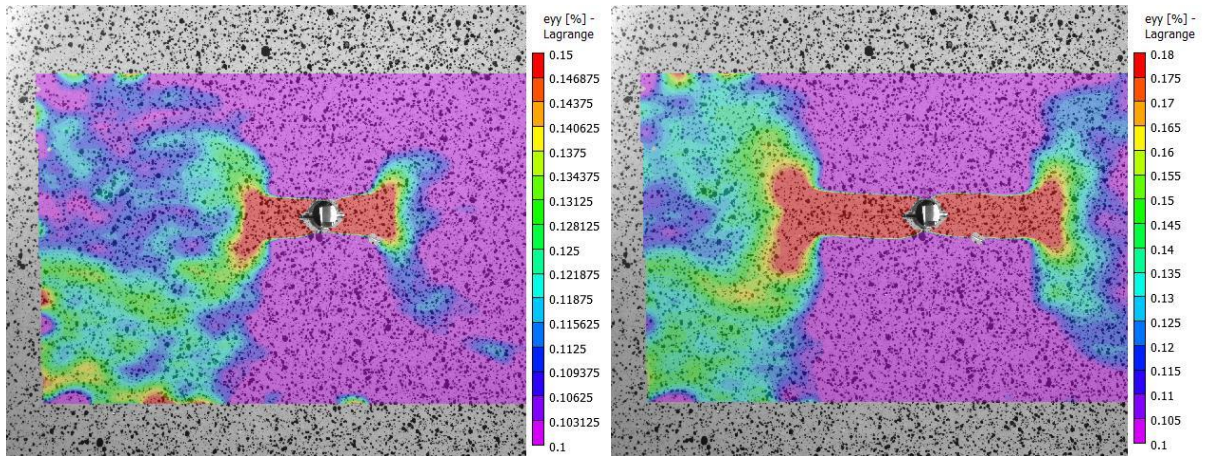
E 1: Elastic-Plastic Zone of Specimen AR002S75. Left: a = 12.8 mm. Right: a = 25.8 mm
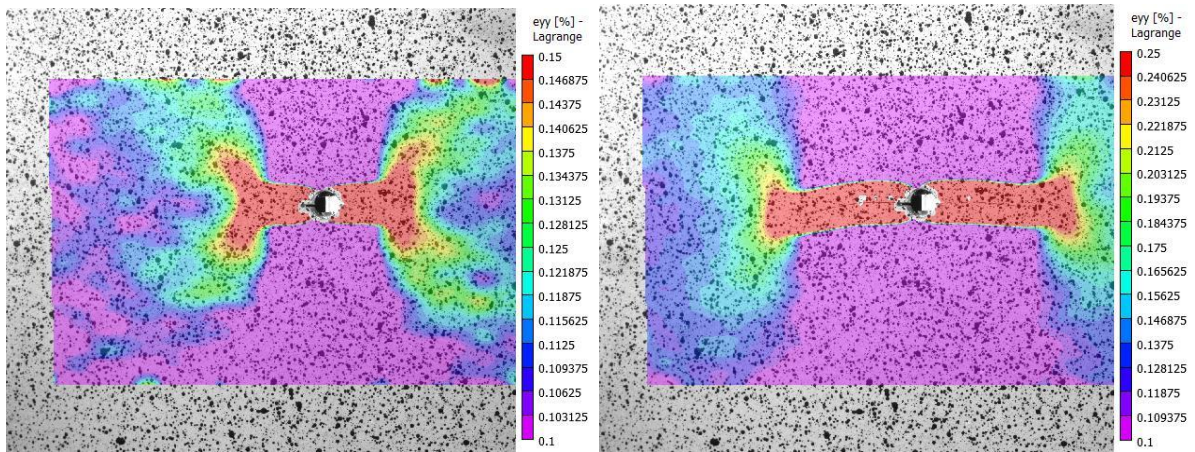
E 2: Elastic-Plastic Zone of Specimen AR006S75. Left: a = 14.4 mm. Right: a = 29.0 mm
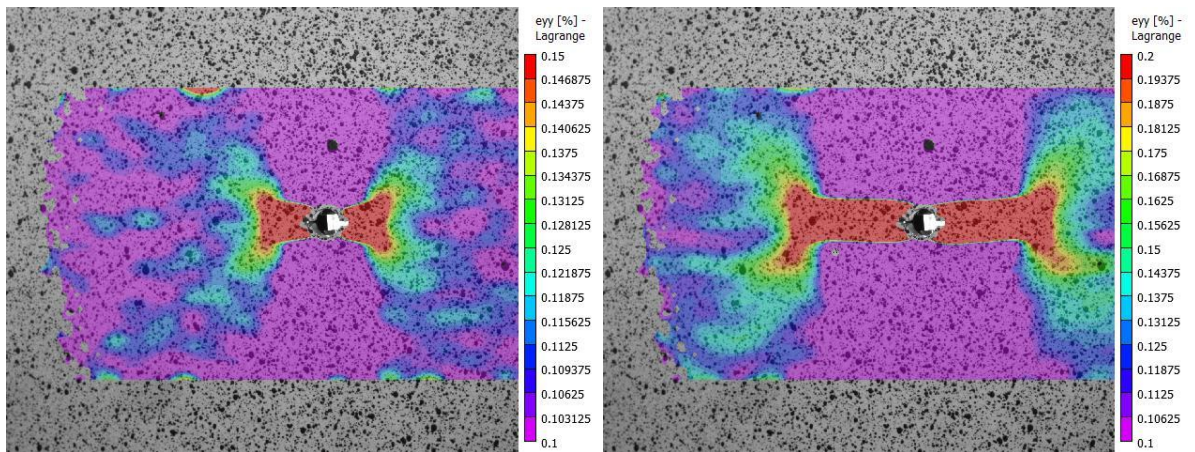
E 3: Elastic-Plastic Zone of Specimen AR01S75. Left: a = 9.8 mm. Right: a = 23.9 mm

APPENDIX E – Elastic-Plastic Behaviour
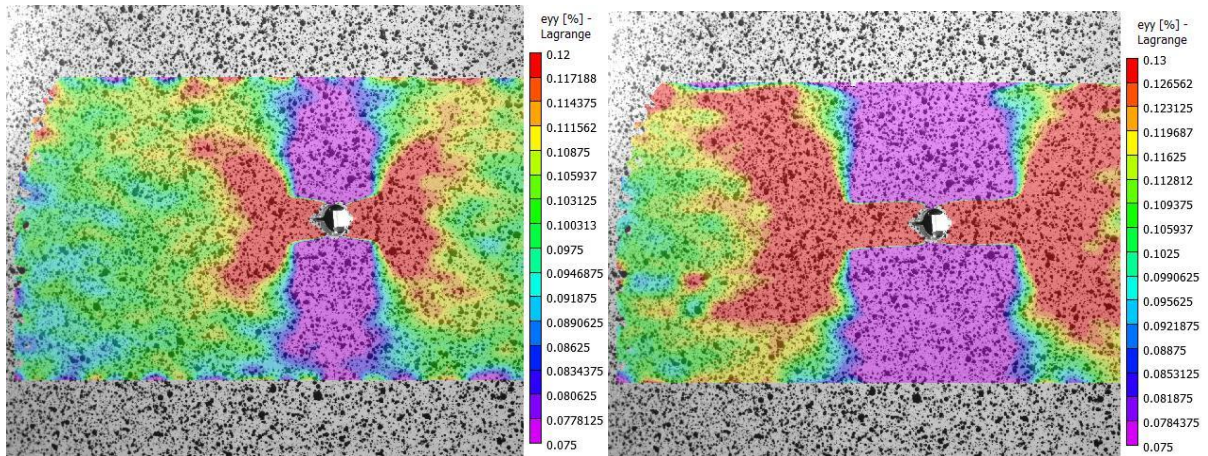
E 4: Elastic-Plastic Zooe of Specimen AR03S75. Left: a = 10.3 mm. Right: a = 20.7 mm
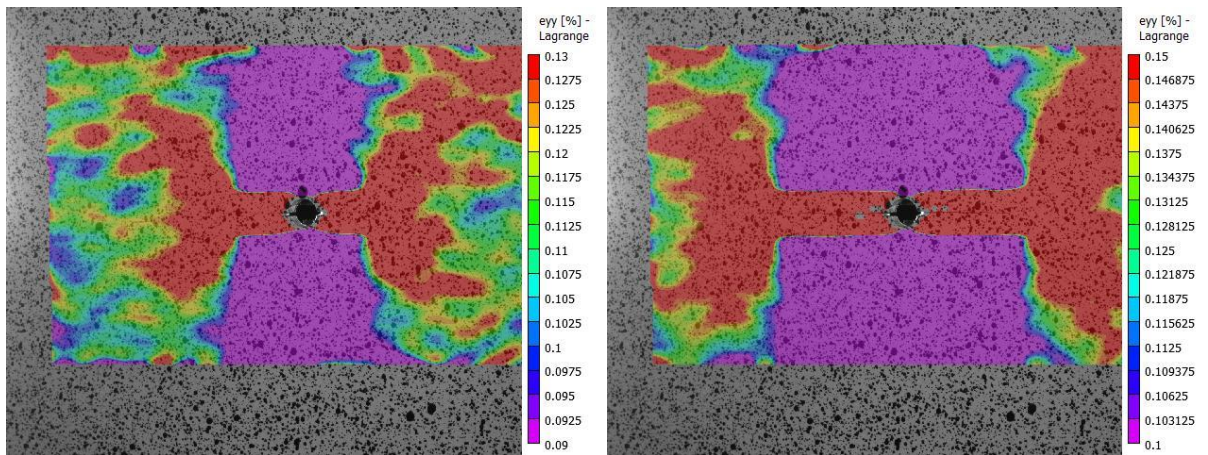
E 5: Elastic-Plastic Zone of Specimen AR05S75. Left: a = 17.5 mm. Right: a = 31.0 mm
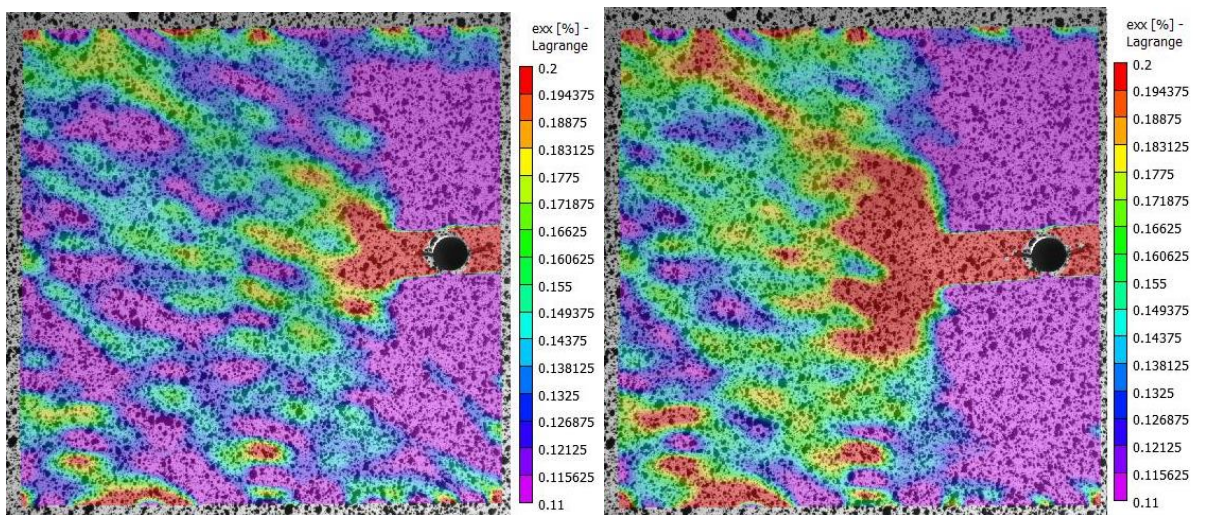
E 6: Elastic-Plastic Zone of Specimen AR006S100. Left: a = 10.3 mm. RIght: a = 19.5 mm.

APPENDIX E – Elastic-Plastic Behaviour
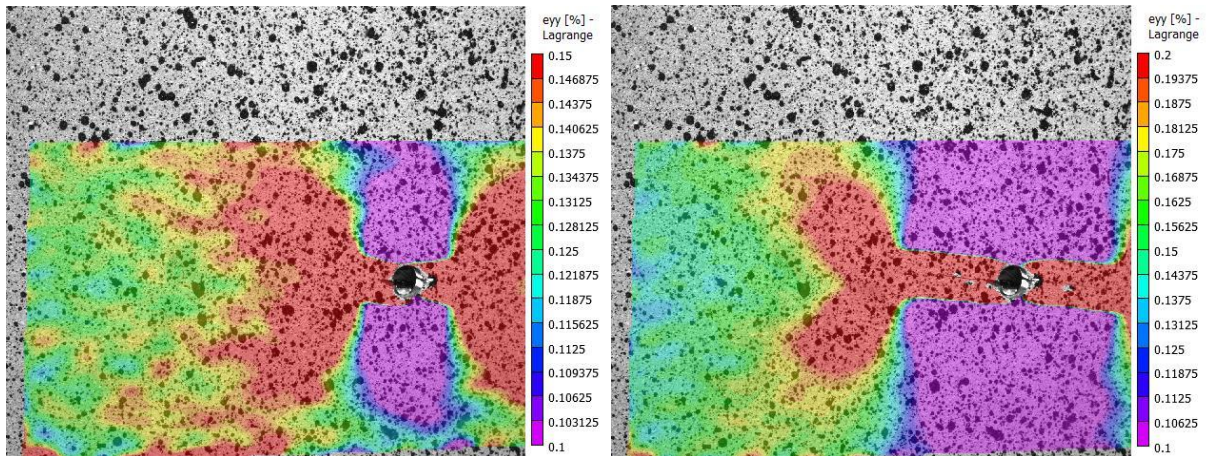
E 7: Elastic-Plastic Zone o Specimen AR03S100. Left: 12.1 mm. RIght: 23.9 mm.
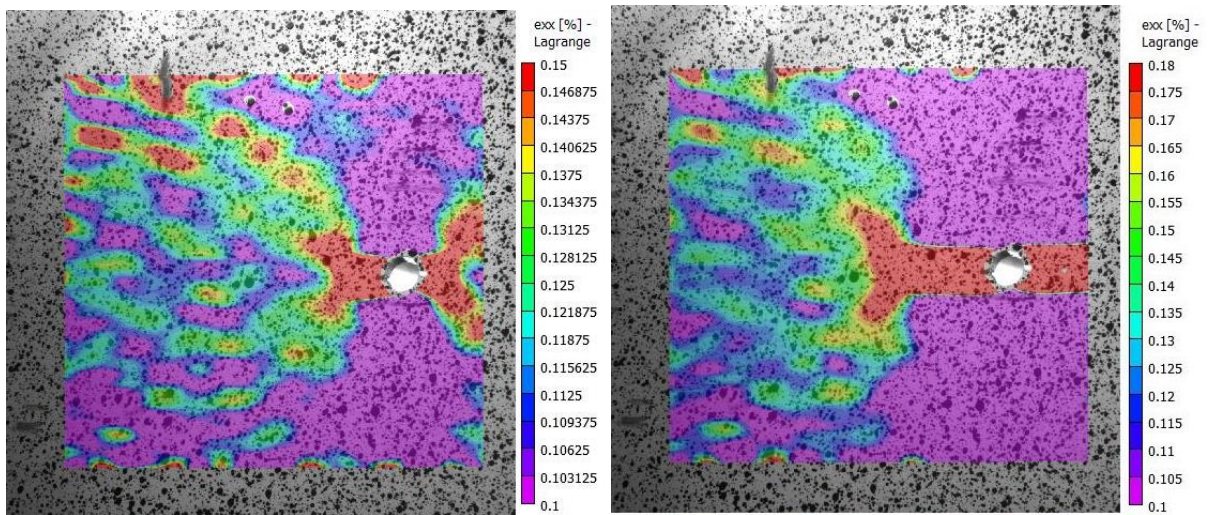
E 8: Elastic-Plastic Zone o Specimen VR002S75. Left: 13.7 mm. RIght: 23.6 mm.
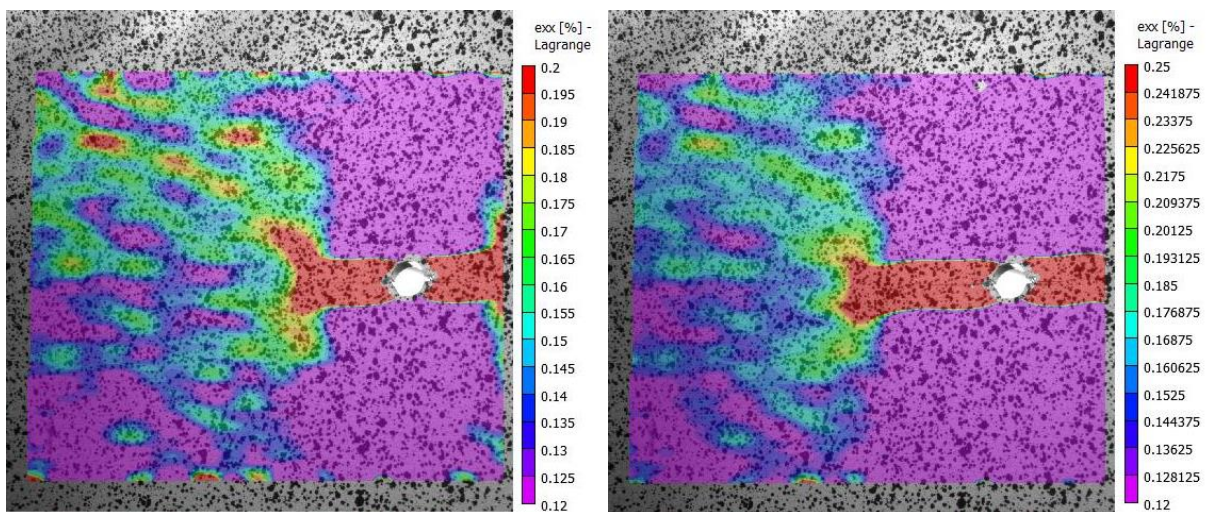
E 9: Elastic-Plastic Zone o Specimen VR005S75. Left: 16.4 mm. RIght: 25.6 mm.

APPENDIX E – Elastic-Plastic Behaviour
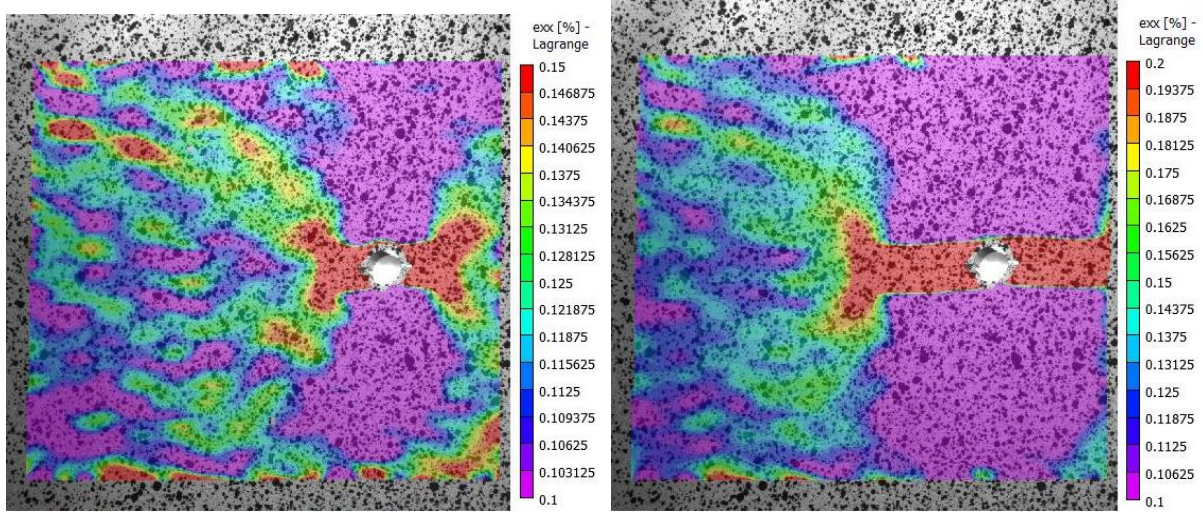
E 10: Elastic-Plastic Behaviour of Specimen VR01S75. Left: a = 10.2 mm. Right: a = 22.2 mm.
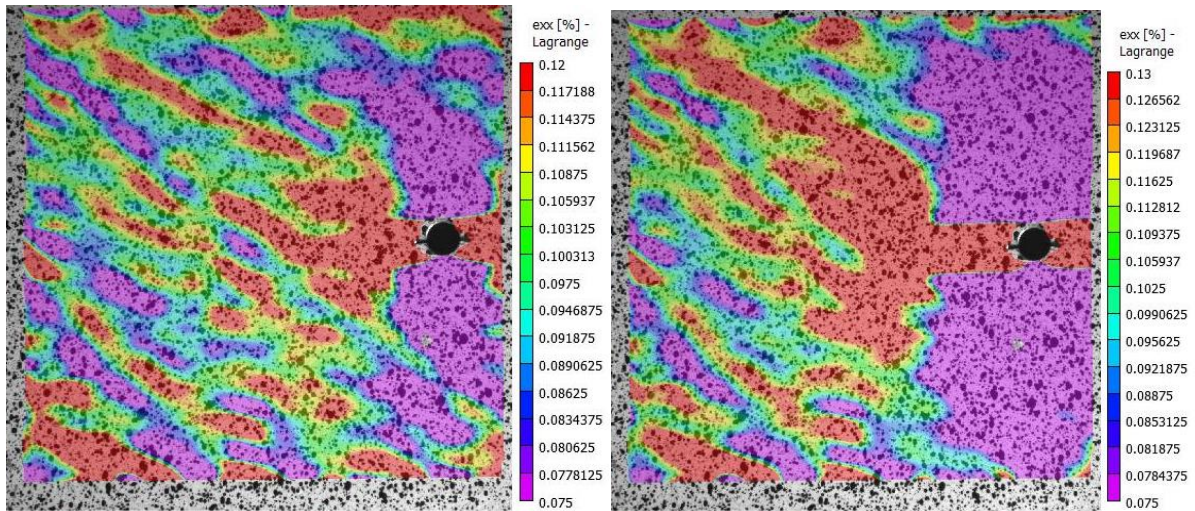
E 11: Elastic-Plastic Behaviour of Specimen VR03S75. Left: a = 10.3 mm. Right: a = 20.7 mm.
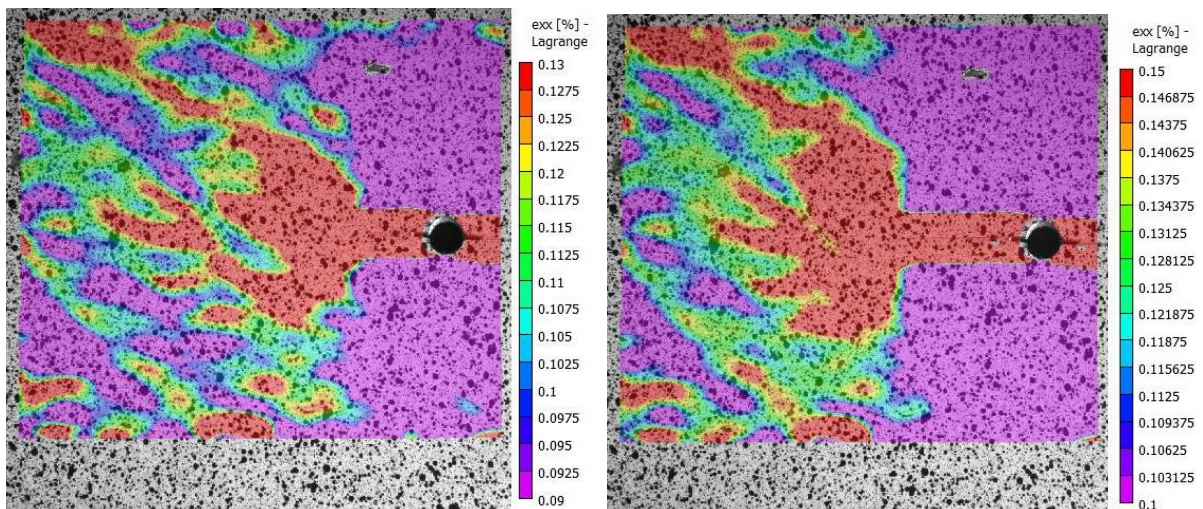
E 12: Elastic-Plastic Behaviour of Specimen VR05S75. Left: a = 16.7 mm. Right: a = 27.8 mm.

APPENDIX E – Elastic-Plastic Behaviour
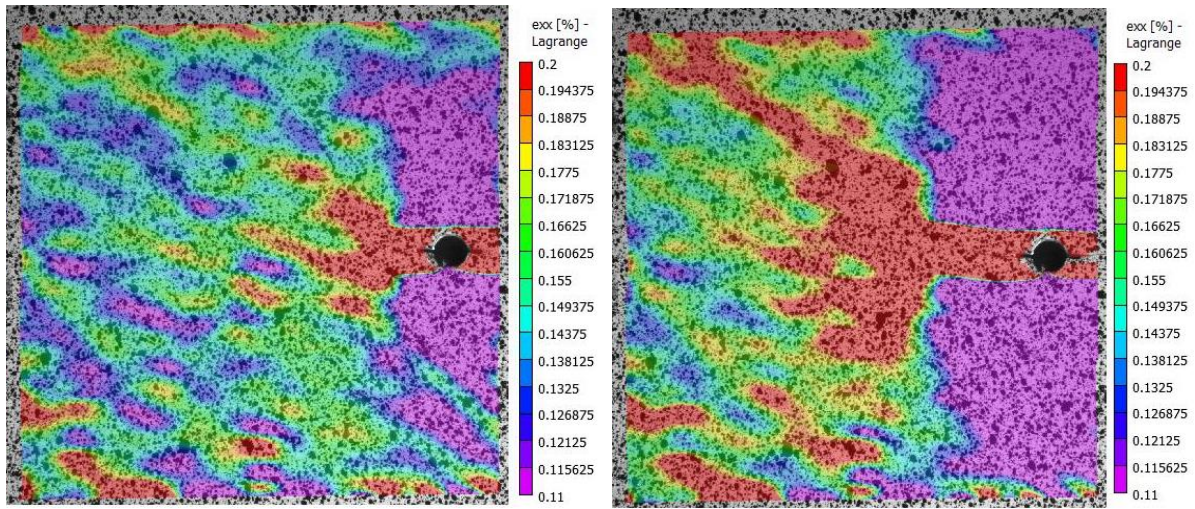
E 13: Elastic-Plastic Behaviour of Specimen VR005S100. Left: a = 10.1 mm. Right: a = 21.7 mm.
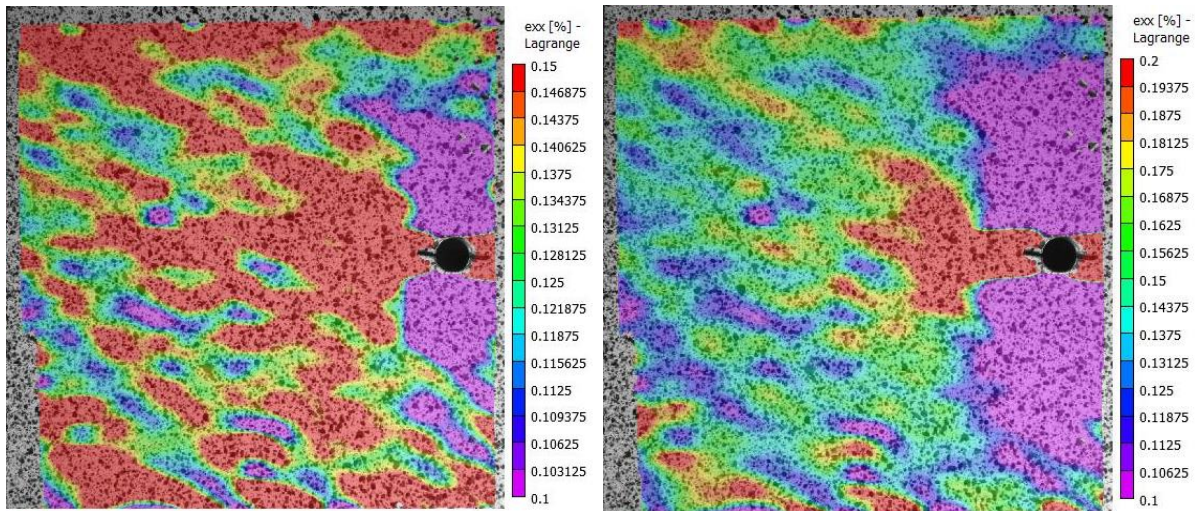
E 14: Elastic-Plastic Behaviour of Specimen VR03S100. Left: a = 9.1 mm. Right: a = 15.1 mm.

Appendix F – Crack Surface Roughness

APPENDIX F – Crack Surface Roughness
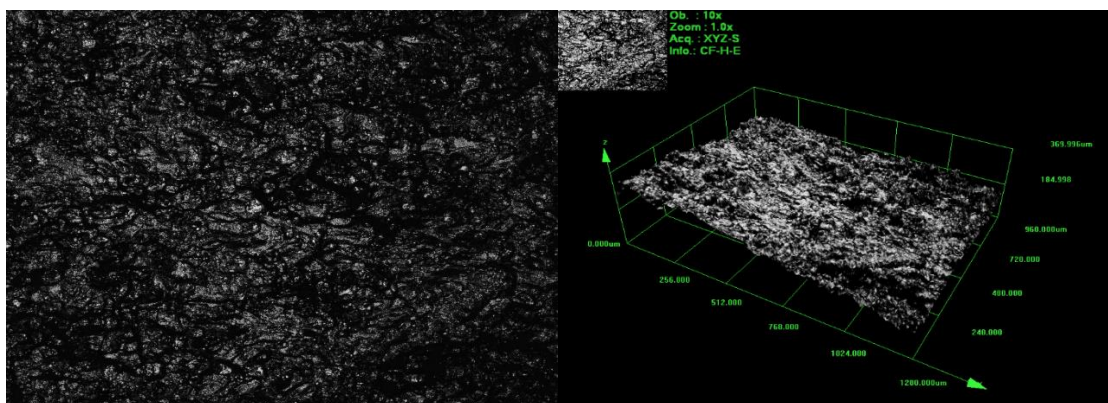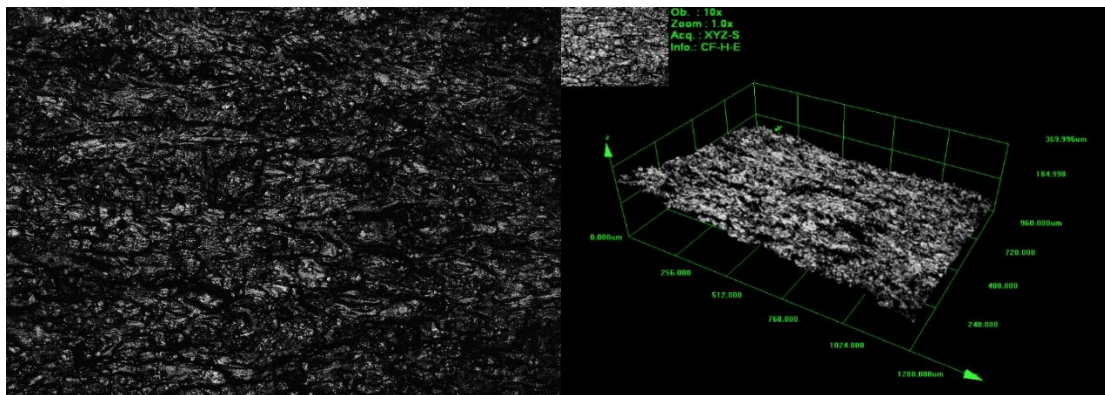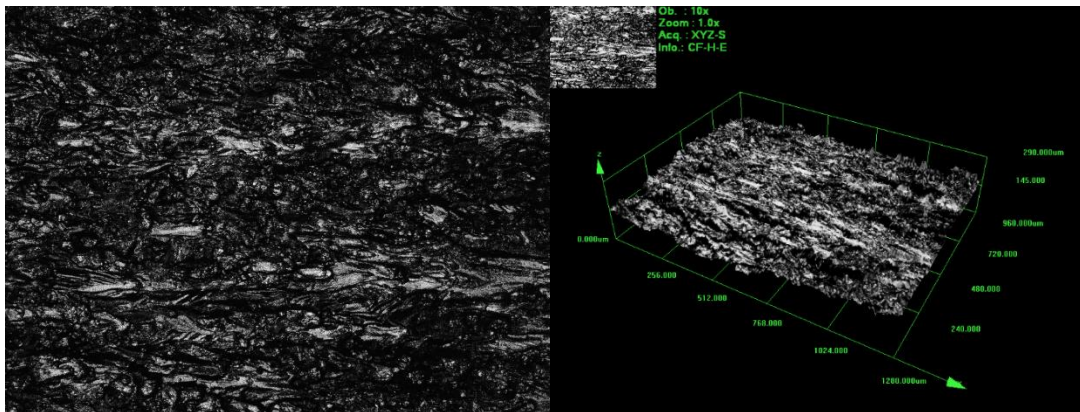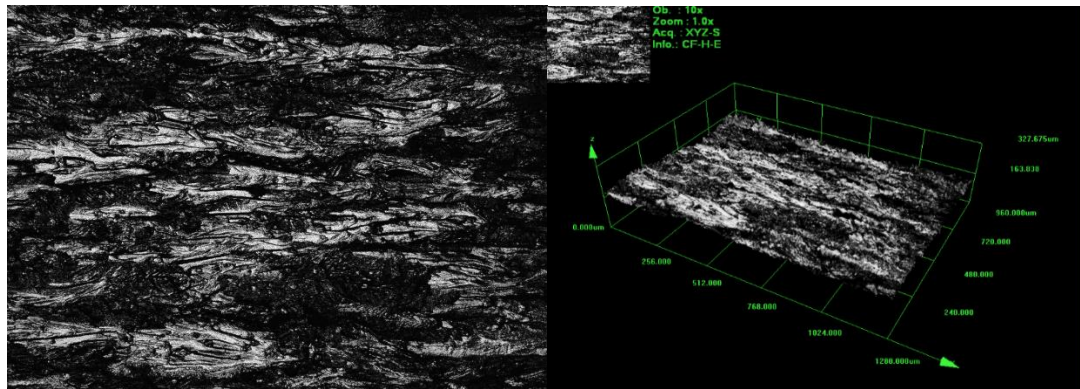
F 1: Crack Surface Roughness (Left: 2D, Right: 3D) of Specimen AR002S75 at a = 1, 11, 21 and 31 mm.
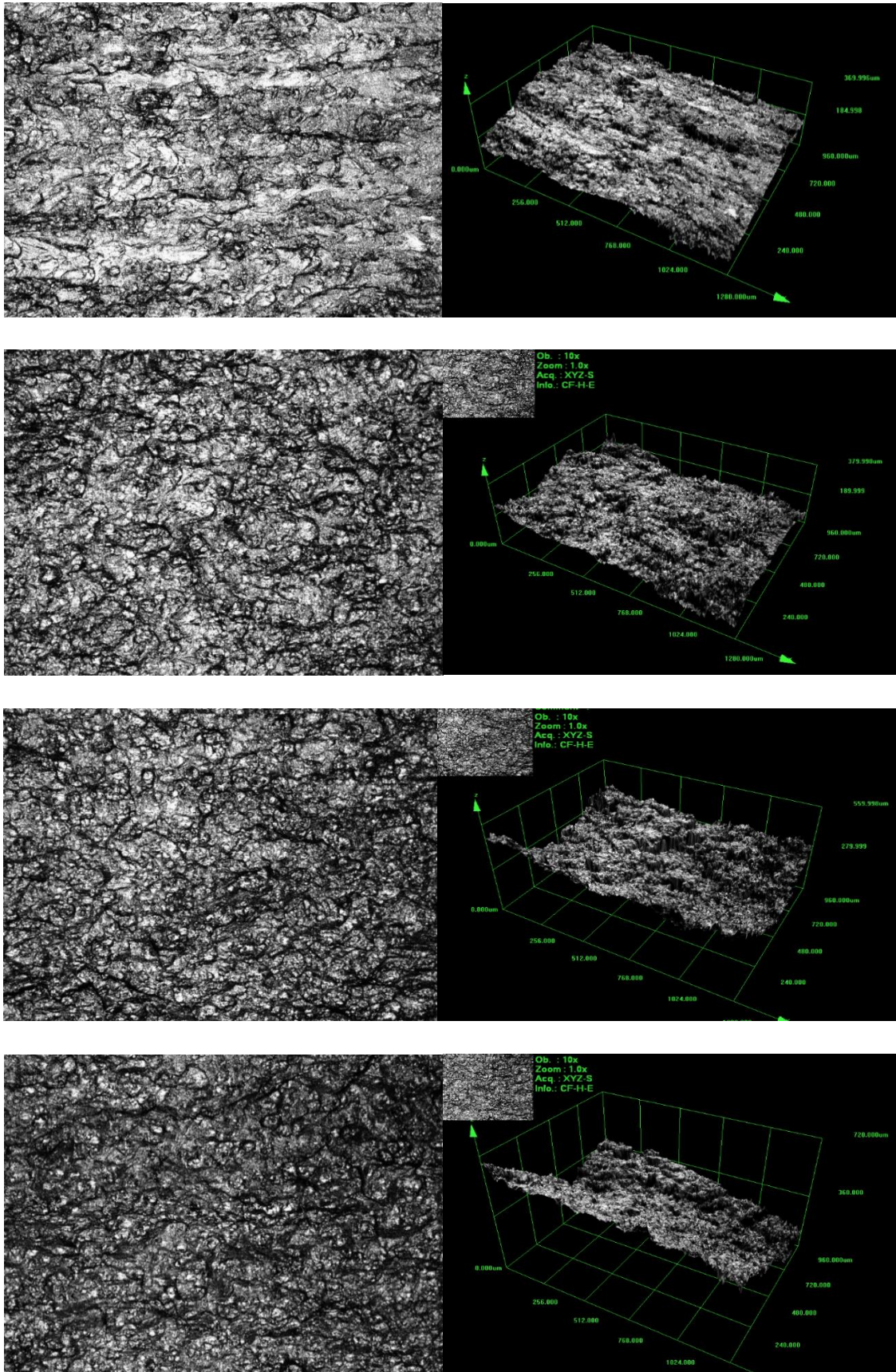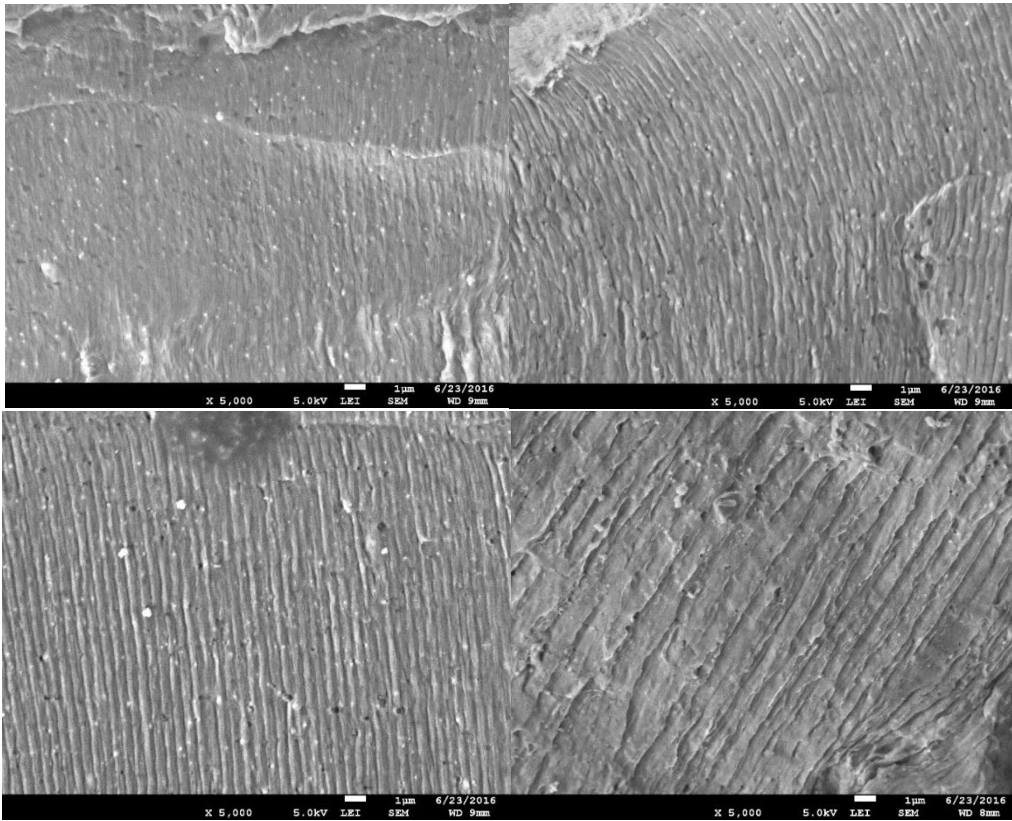
APPENDIX F – Crack Surface Roughness
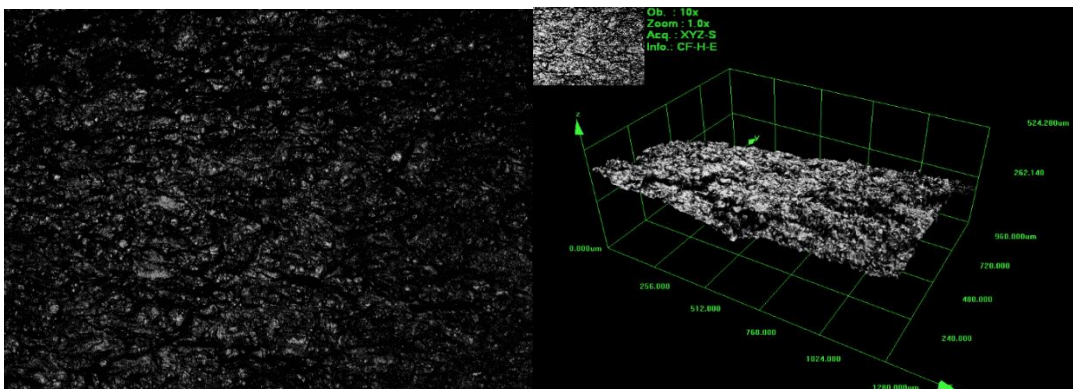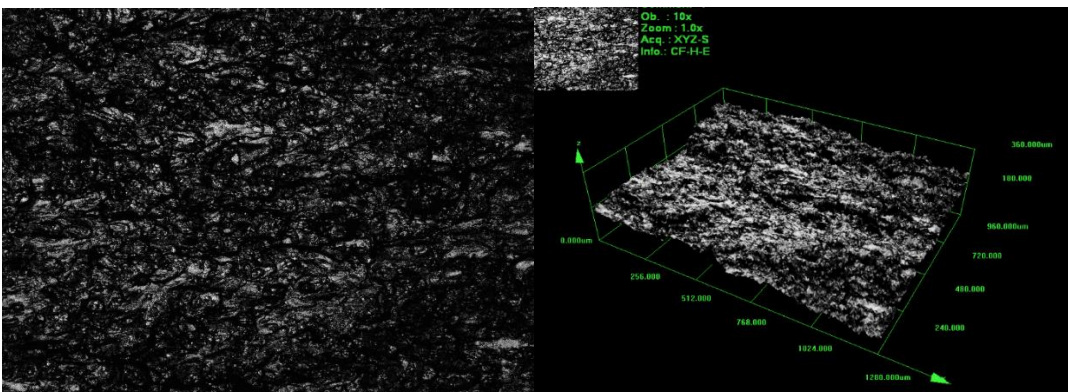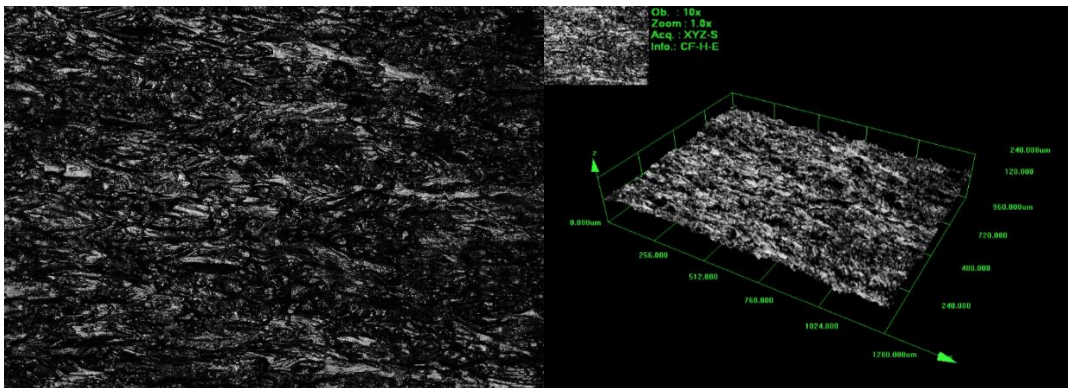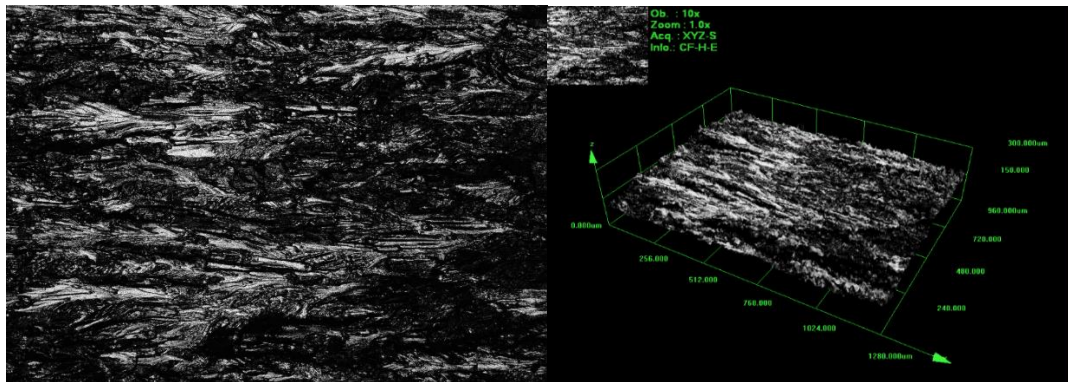
F 2: Crack Surface Roughness (Left: 2D, Right: 3D) of Specimen AR005S75 at a = 1, 11, 21 and 31 mm.
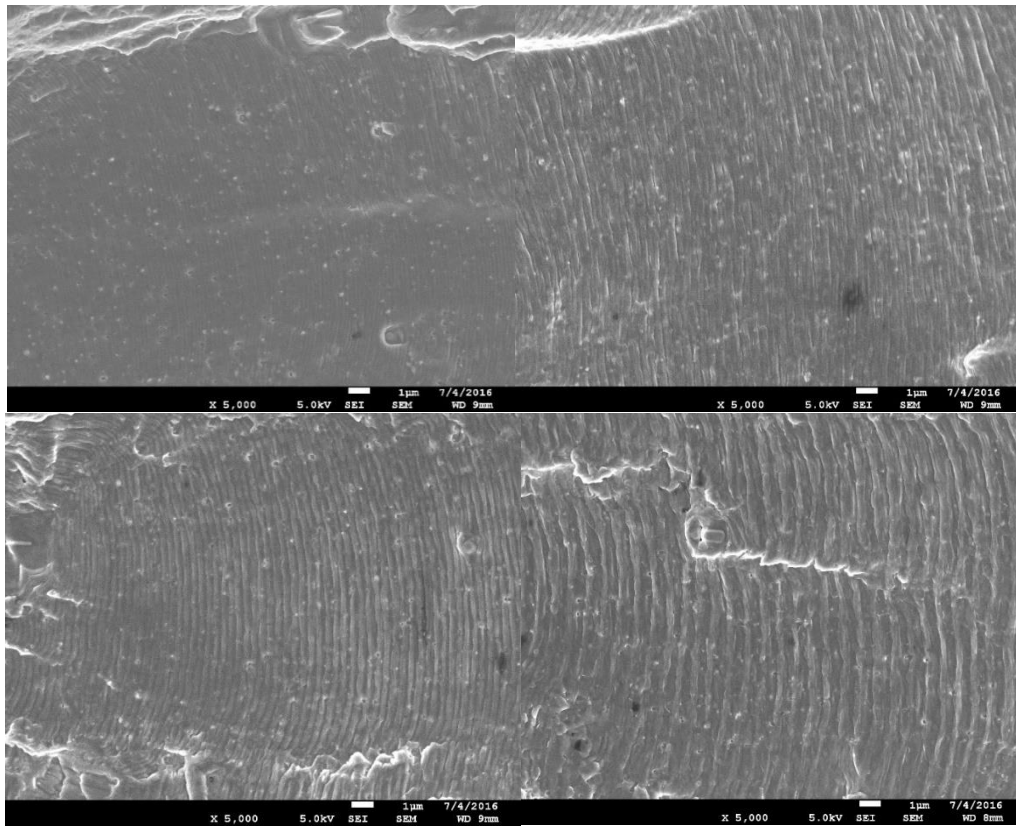
APPENDIX F – Crack Surface Roughness
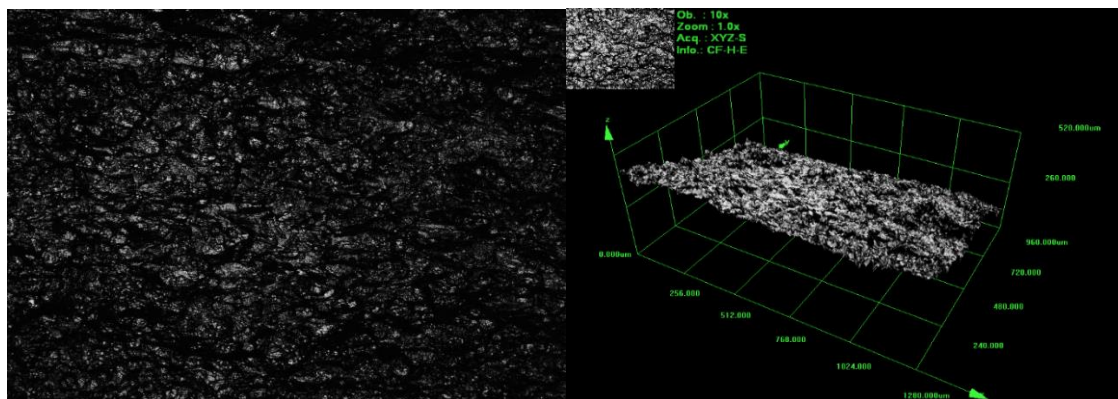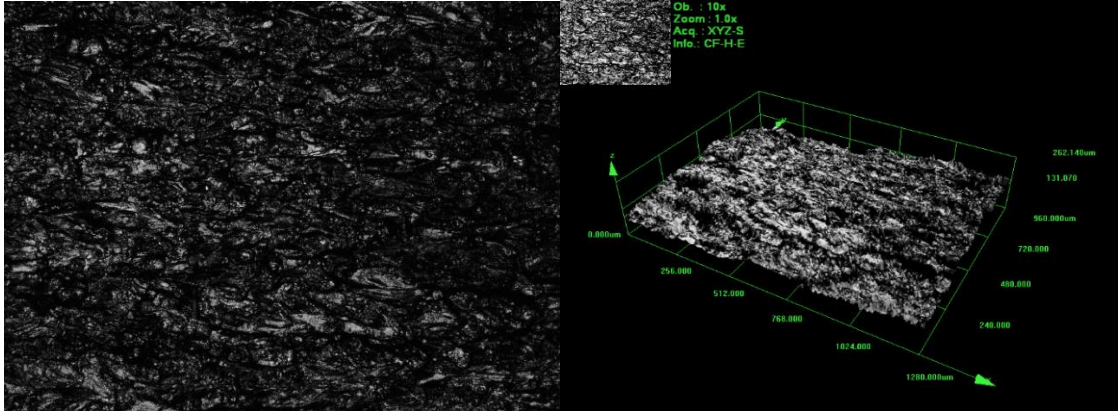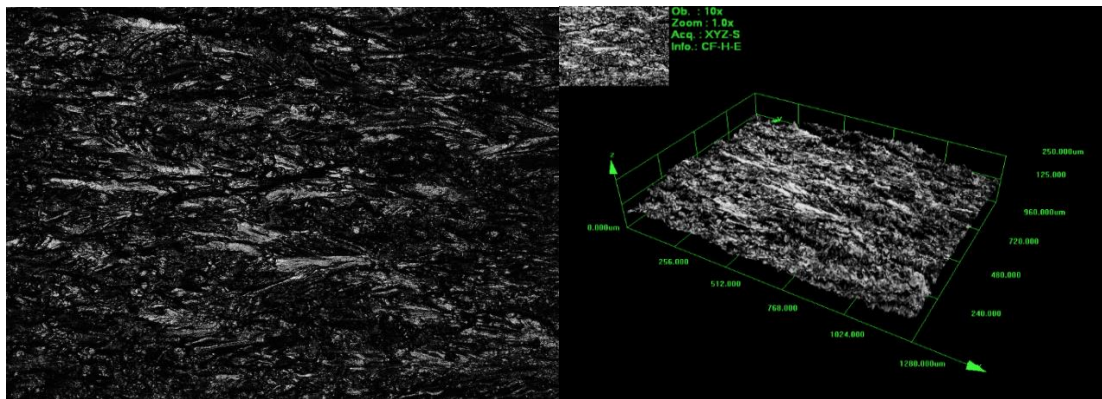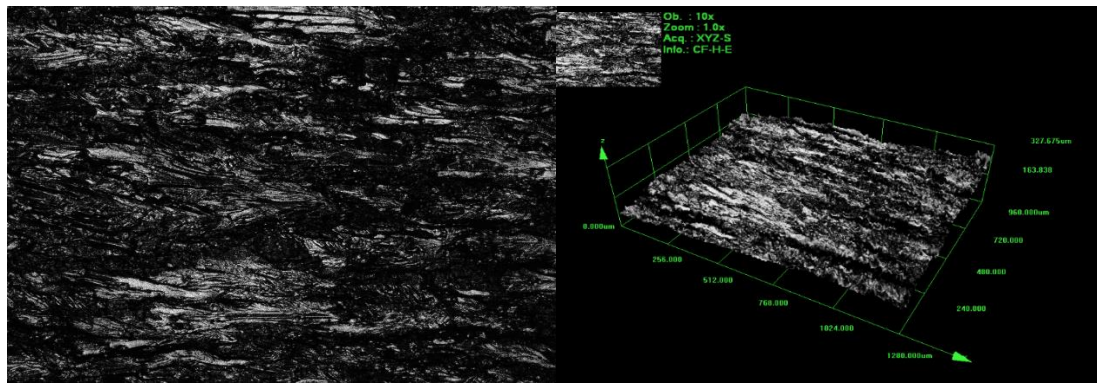
F 3: Crack Surface Roughness (Left: 2D, Right: 3D) of Specimen AR01S75 at a = 1, 11, 21 and 31 mm.
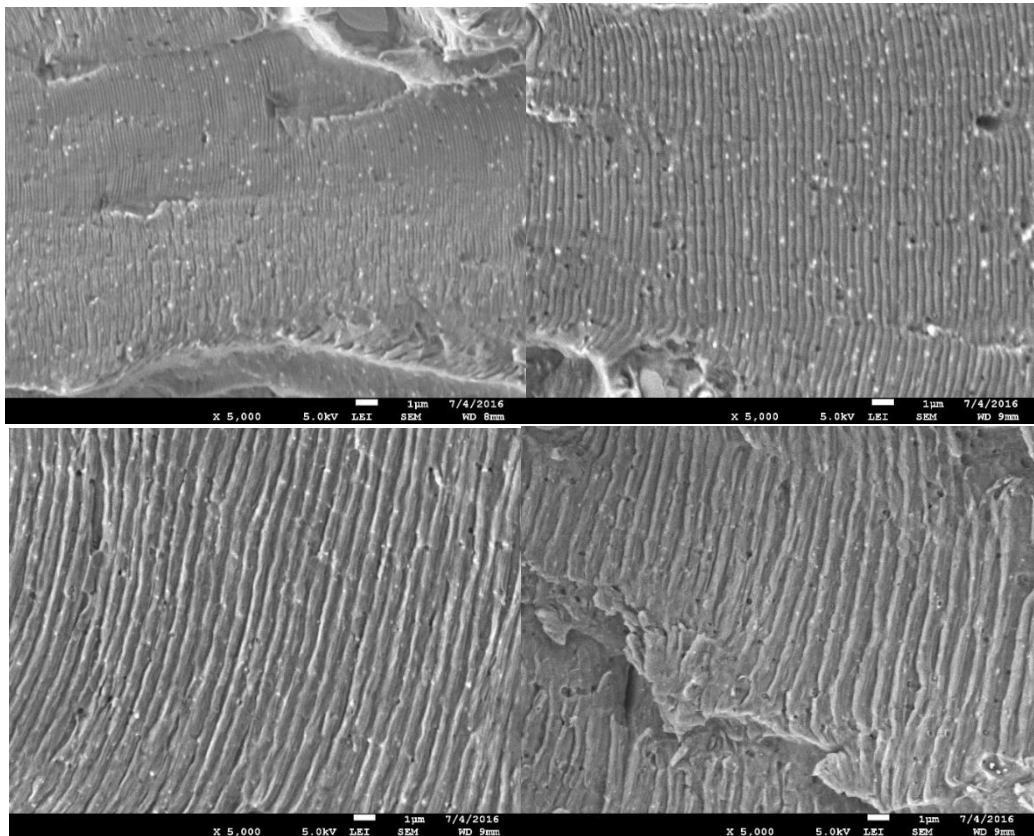
APPENDIX F – Crack Surface Roughness
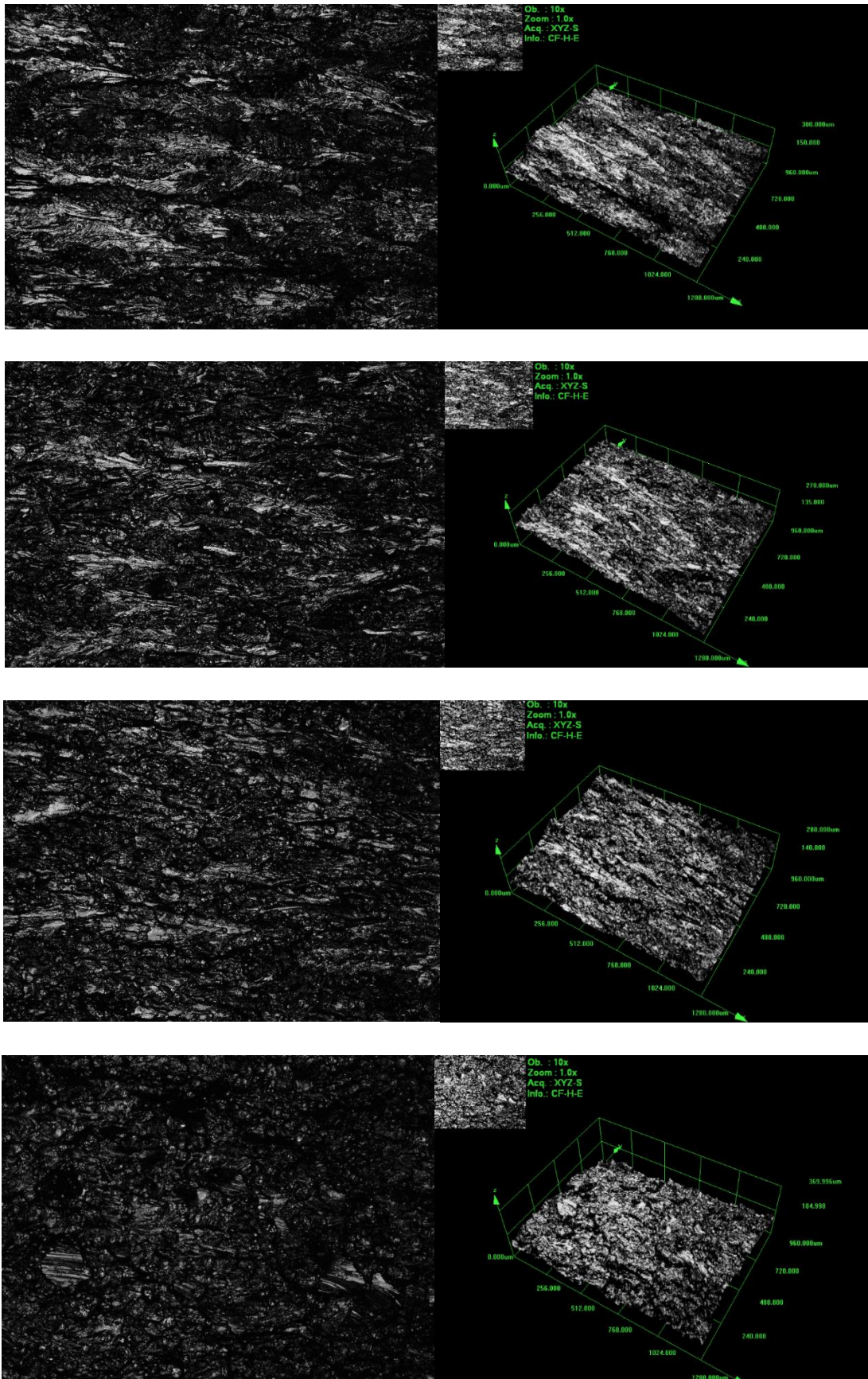
F 4: Crack Surface Roughness (Left: 2D, Right: 3D) of Specimen AR03S75 at a = 1, 11, 21 and 31 mm.

APPENDIX F – Crack Surface Roughness
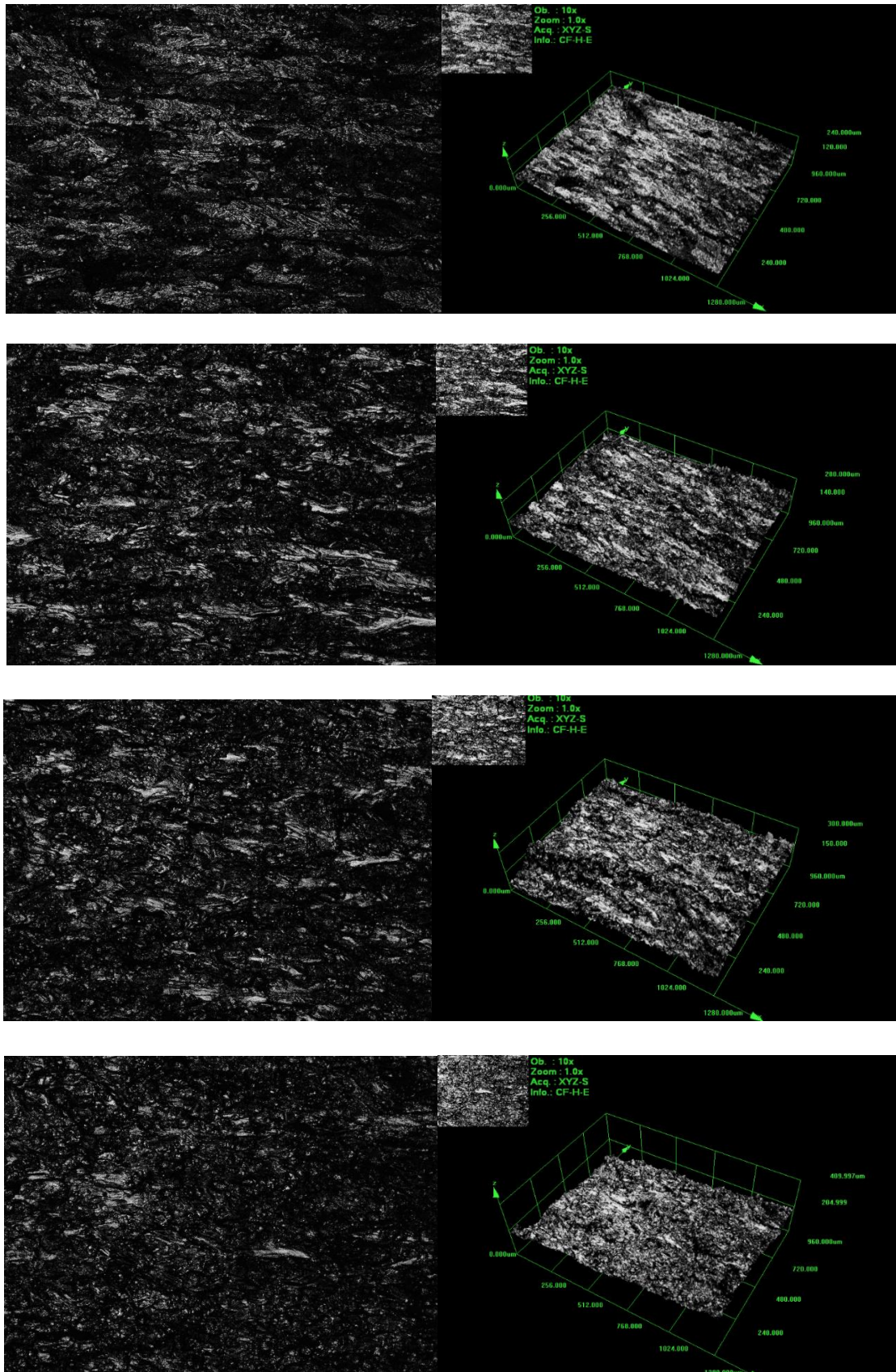
F 5: Crack Surface Roughness (Left: 2D, Right: 3D) of Specimen AR05S75 at a = 1, 11, 21 and 31 mm.

APPENDIX F – Crack Surface Roughness
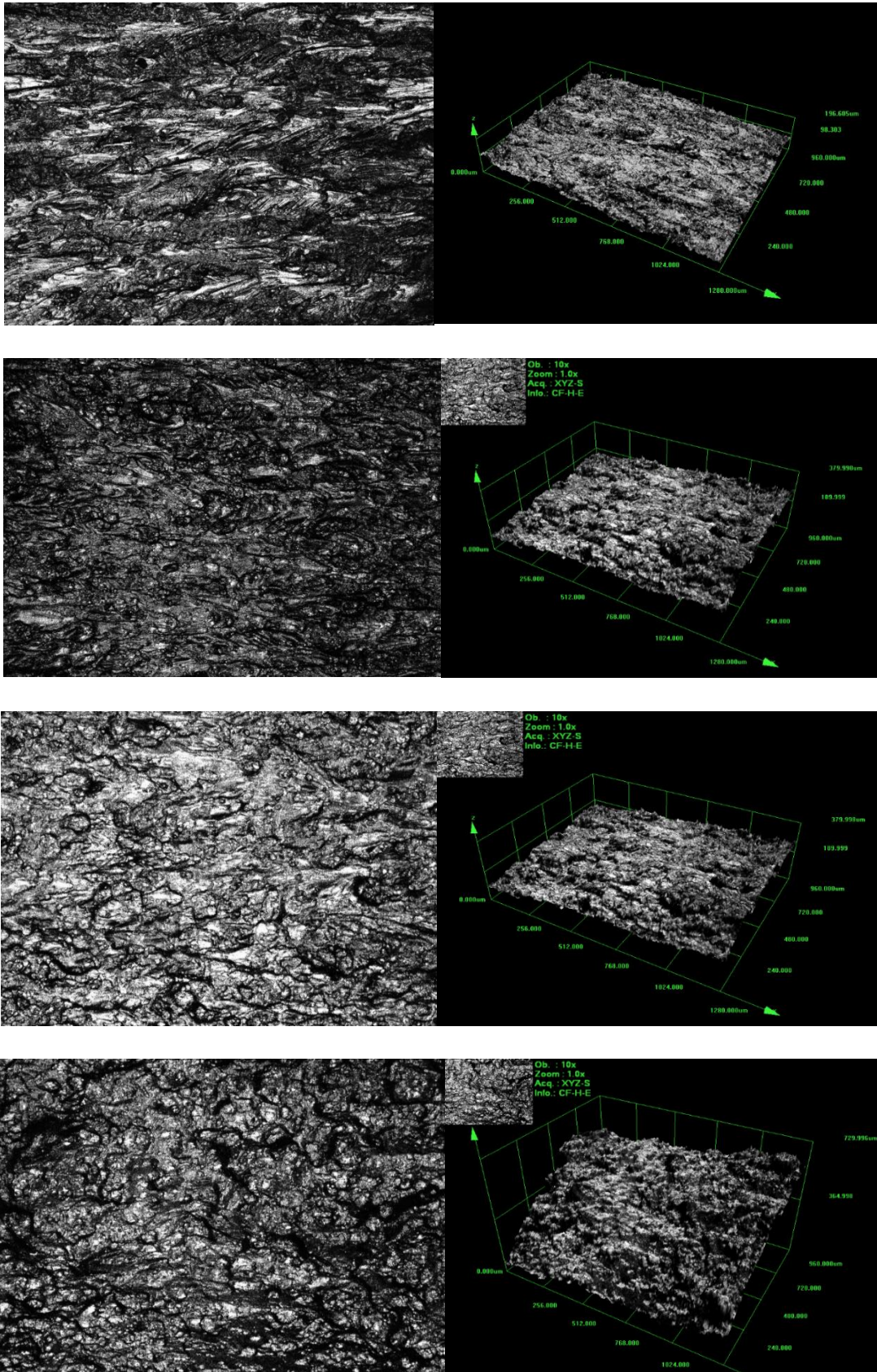
F 6: Crack Surface Roughness (Left: 2D, Right: 3D) of Specimen AR005S100 at a = 1, 11, 21 and 31 mm.

APPENDIX F – Crack Surface Roughness
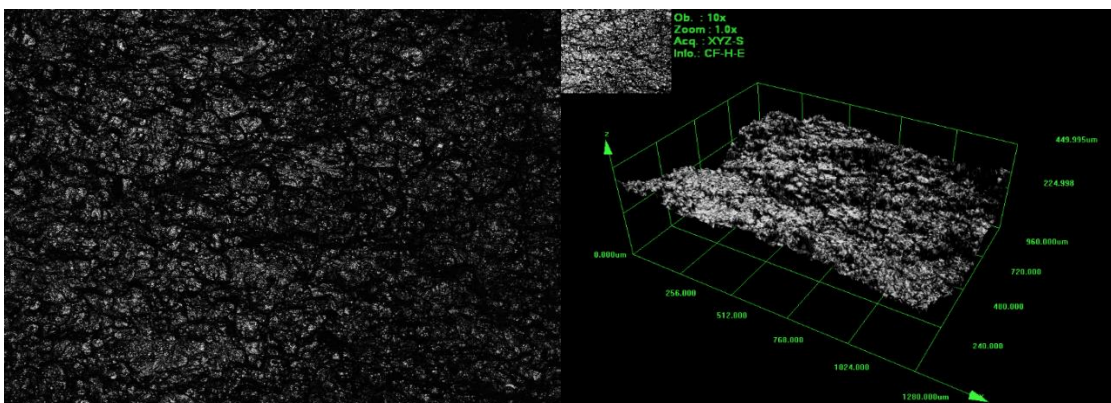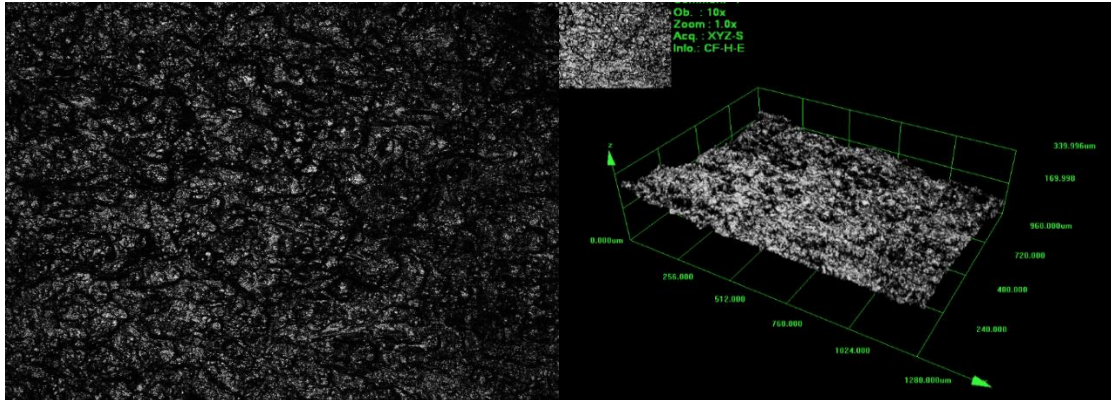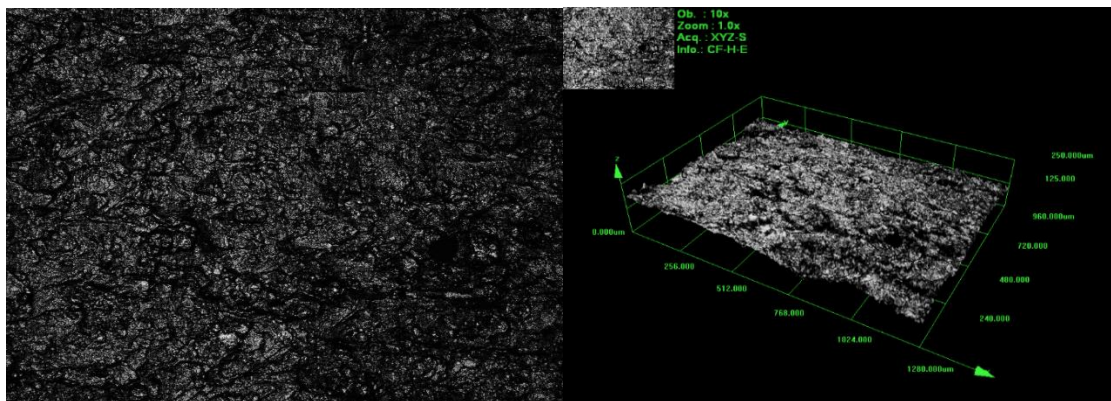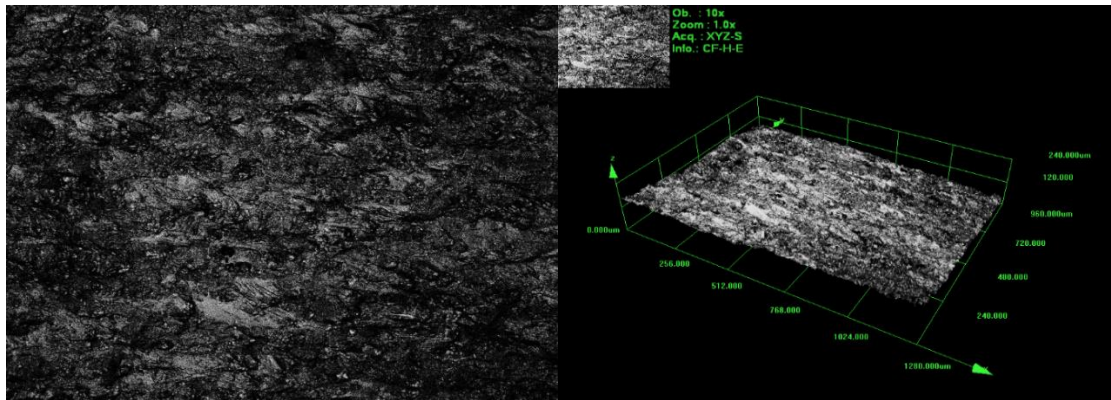
F 7: Crack Surface Roughness (Left: 2D, Right: 3D) of Specimen VR002S75 at a = 1, 11, 21 and 31 mm.
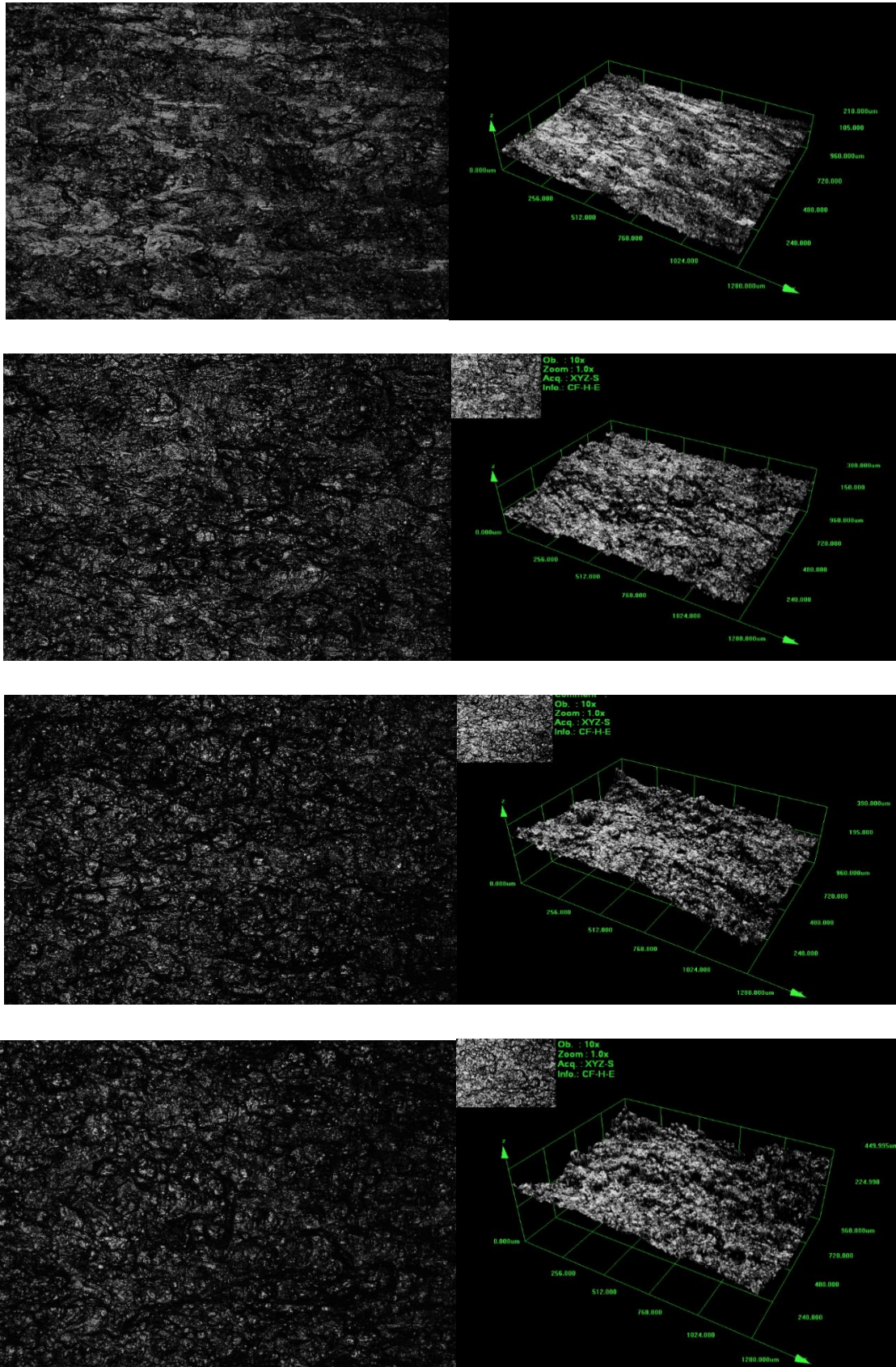
APPENDIX F – Crack Surface Roughness

F 8: Crack Surface Roughness (Left: 2D, Right: 3D) of Specimen VR005S75 at a = 1, 11, 21 and 31 mm.
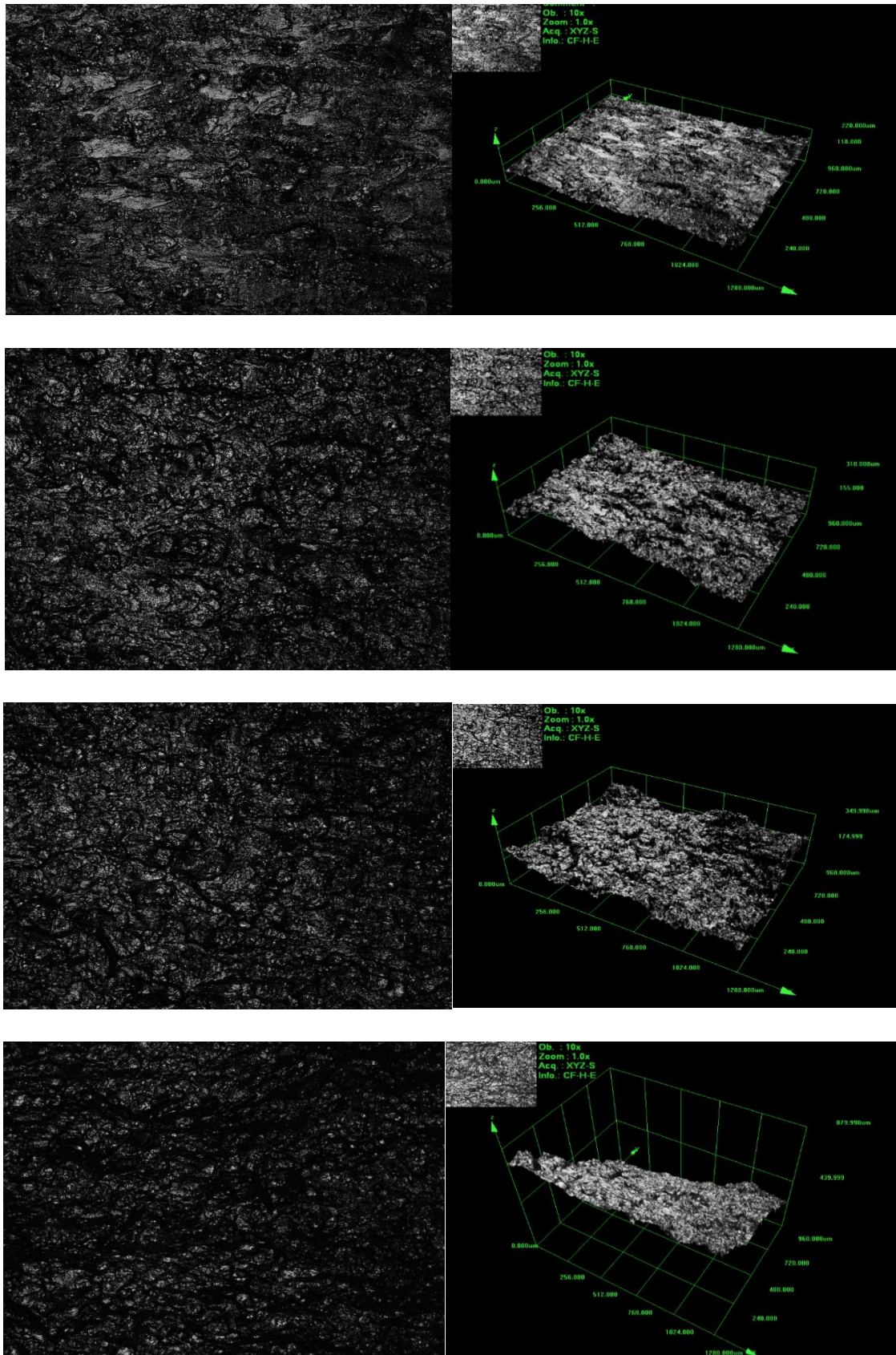
F 9: Crack Surface Roughness (Left: 2D, Right: 3D) of Specimen VR01S75 at a = 1, 11, 21 and 31 mm.

APPENDIX F – Crack Surface Roughness
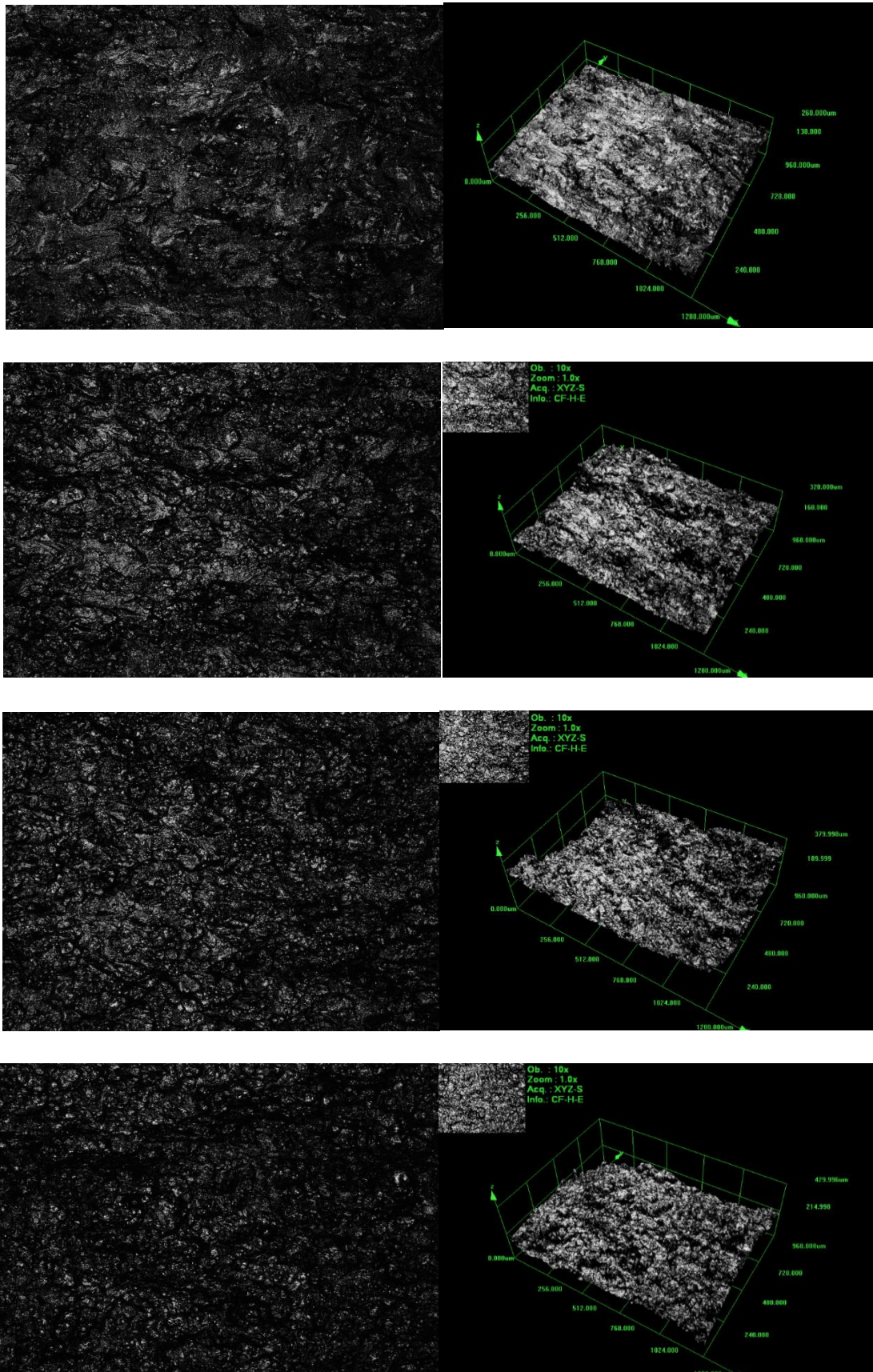
F 10: Crack Surface Roughness (Left: 2D, Right: 3D) of Specimen VR03S75 at a = 1, 11, 21 and 31 mm.

APPENDIX F – Crack Surface Roughness
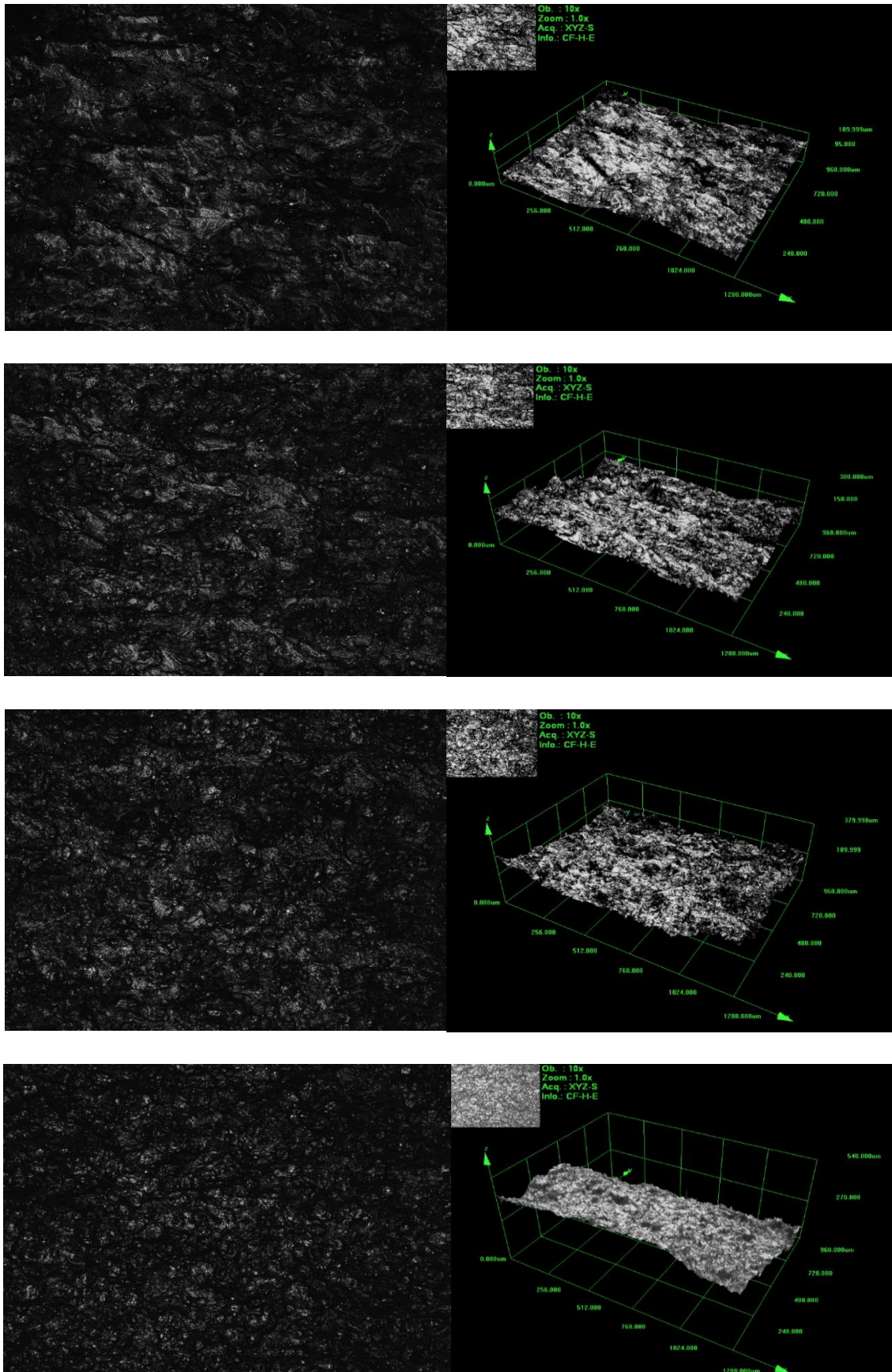
F 11: Crack Surface Roughness (Left: 2D, Right: 3D) of Specimen VR05S75 at a = 1, 11, 21 and 31 mm.

APPENDIX F – Crack Surface Roughness
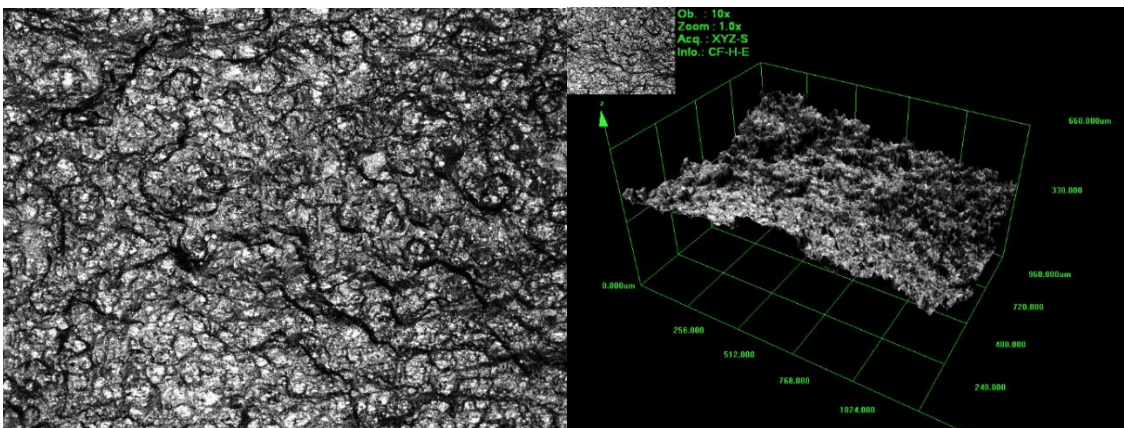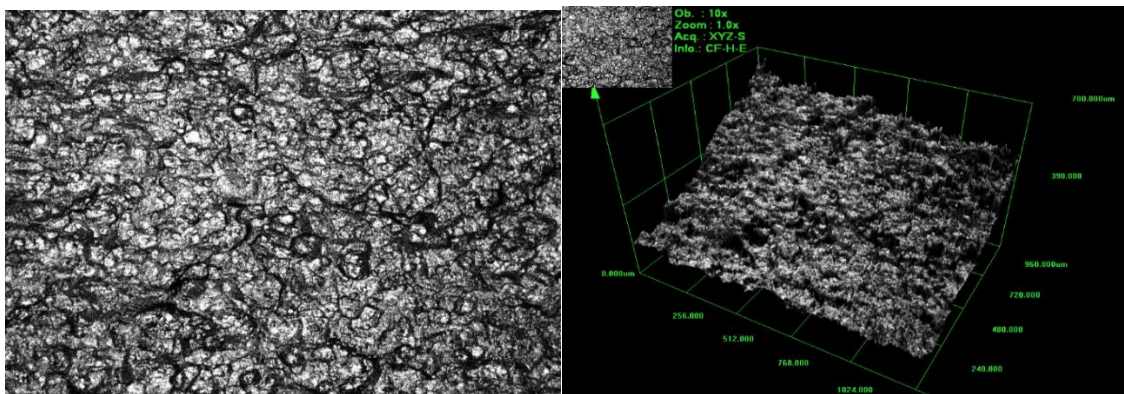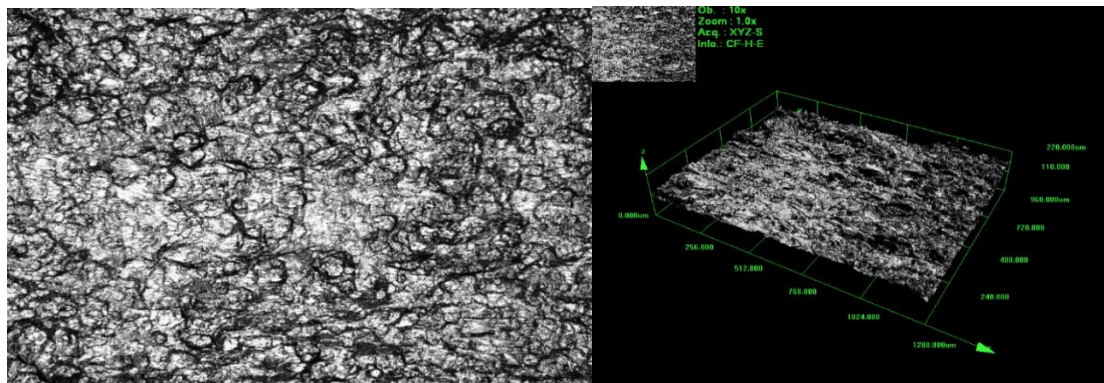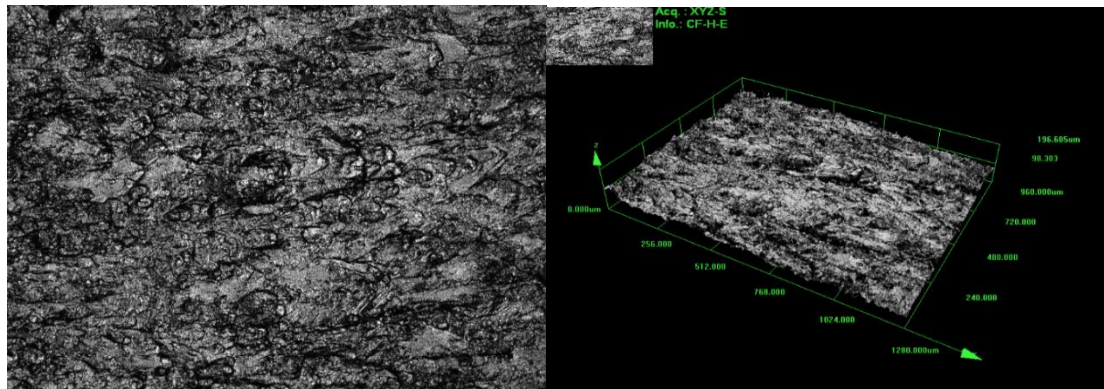
F 12: Crack Surface Roughness (Left: 2D, Right: 3D) of Specimen VR005S100 at a = 1, 11, 21 and 31 mm.

APPENDIX F – Crack Surface Roughness

F 13: Crack Surface Roughness (Left: 2D, Right: 3D) of Specimen VR03S100 at a = 1, 11, 21 and 31mm.
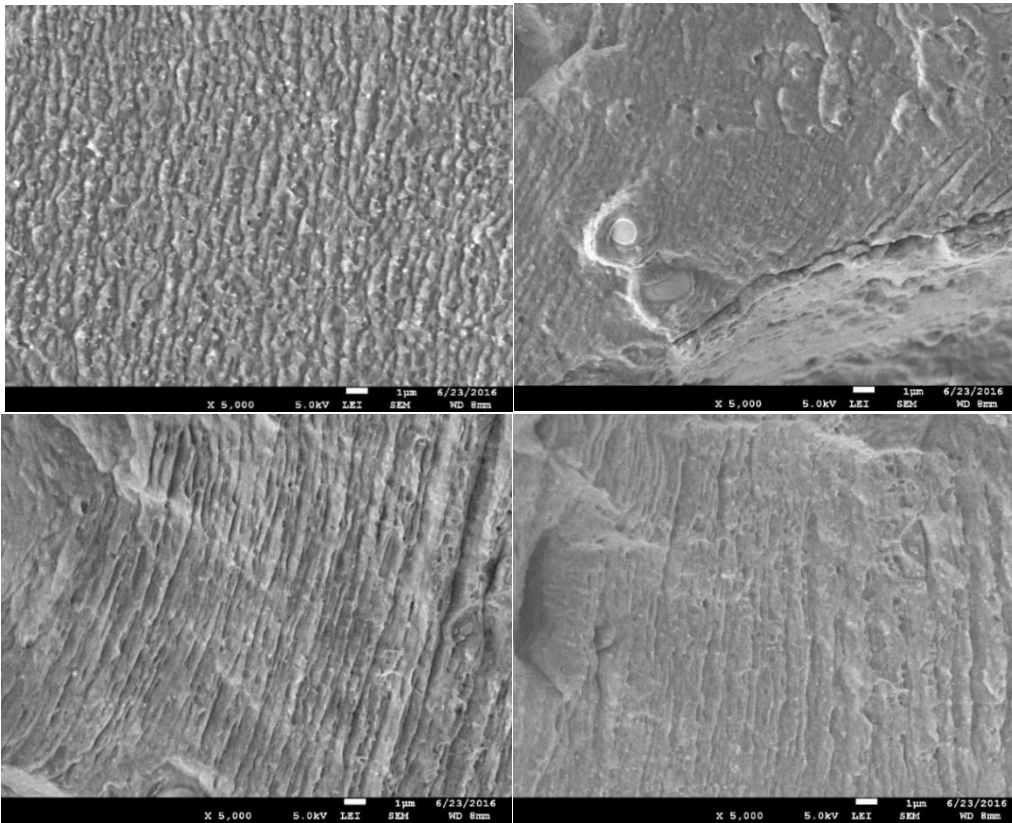
APPENDIX F – Crack Surface Roughness

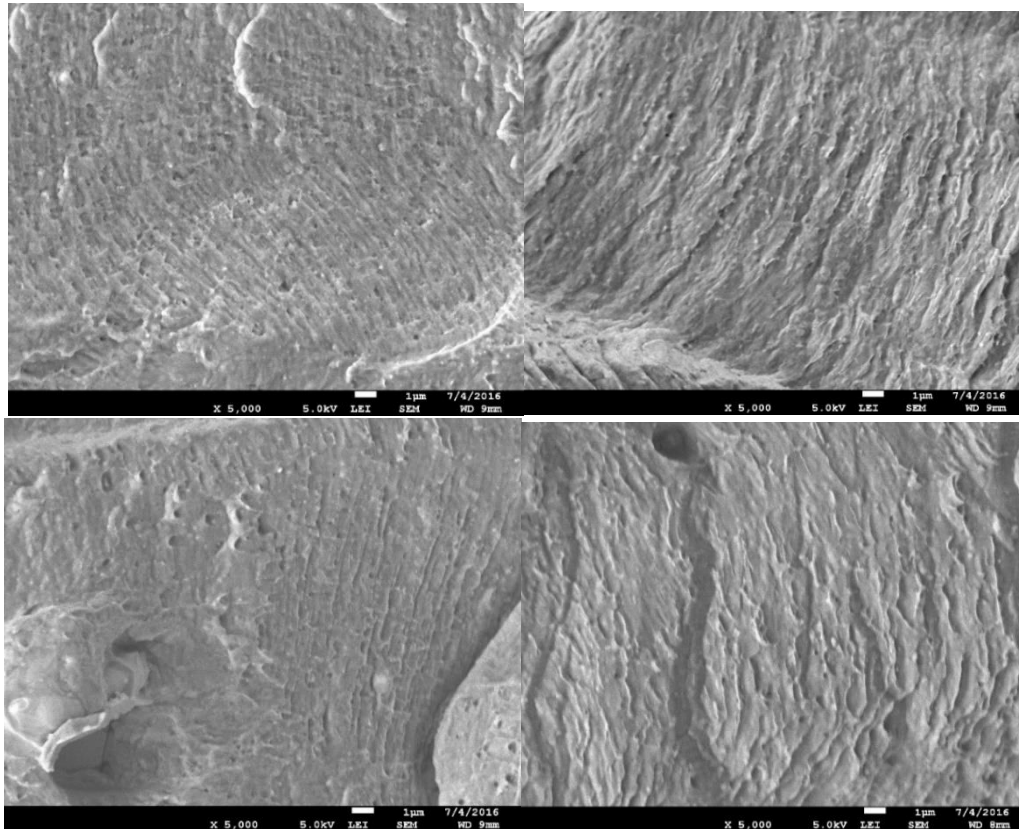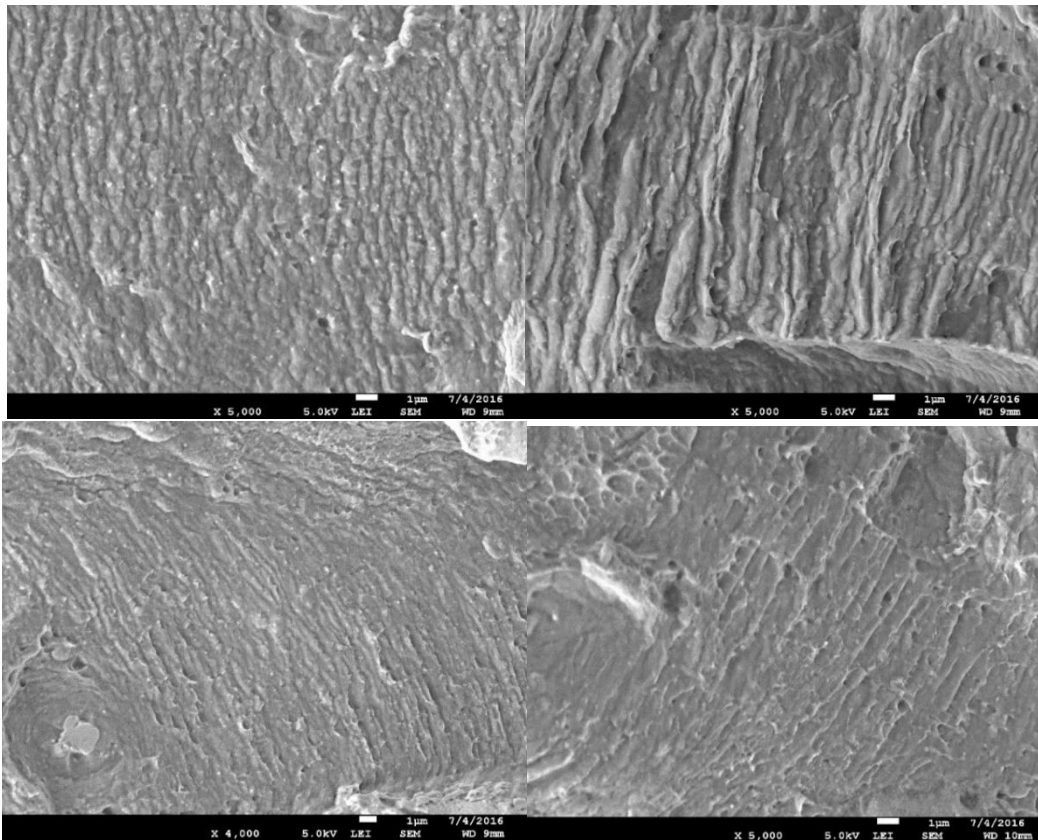*F 14: SEM Photos of Specimen AR002S75. TL: a = 1 mm, TR: a = 11 mm, BL: a = 21 mm , BR: a = 31 mm*

F 15: SEM Photos of Specimen AR005S75. TL: a = 1 mm, TR: a = 11 mm, BL: a = 21 mm , BR: a = 31 mm

APPENDIX F – Crack Surface Roughness

F 16: SEM Photos of Specimen AR01S75. TL: a = 1 mm, TR: a = 11 mm, BL: a = 21 mm , BR: a = 31 mm
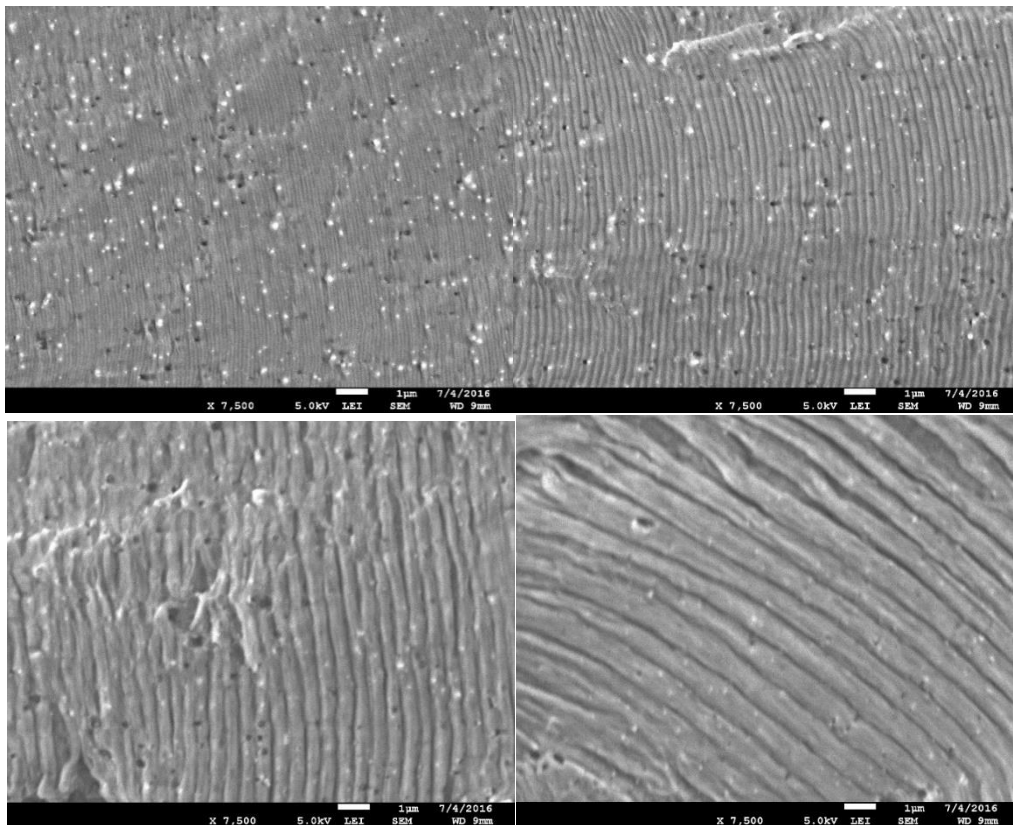
F 17: SEM Photos of Specimen AR03S75. TL: a = 1 mm, TR: a = 11 mm, BL: a = 21 mm , BR: a = 31 mm

APPENDIX F – Crack Surface Roughness
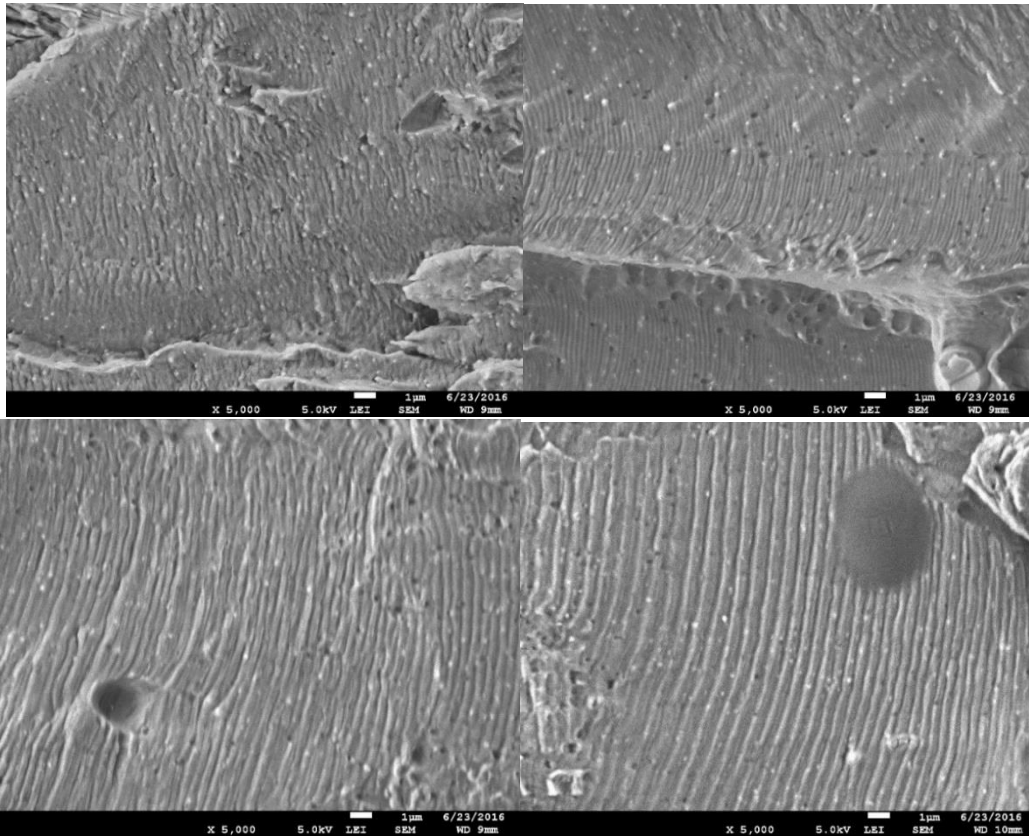
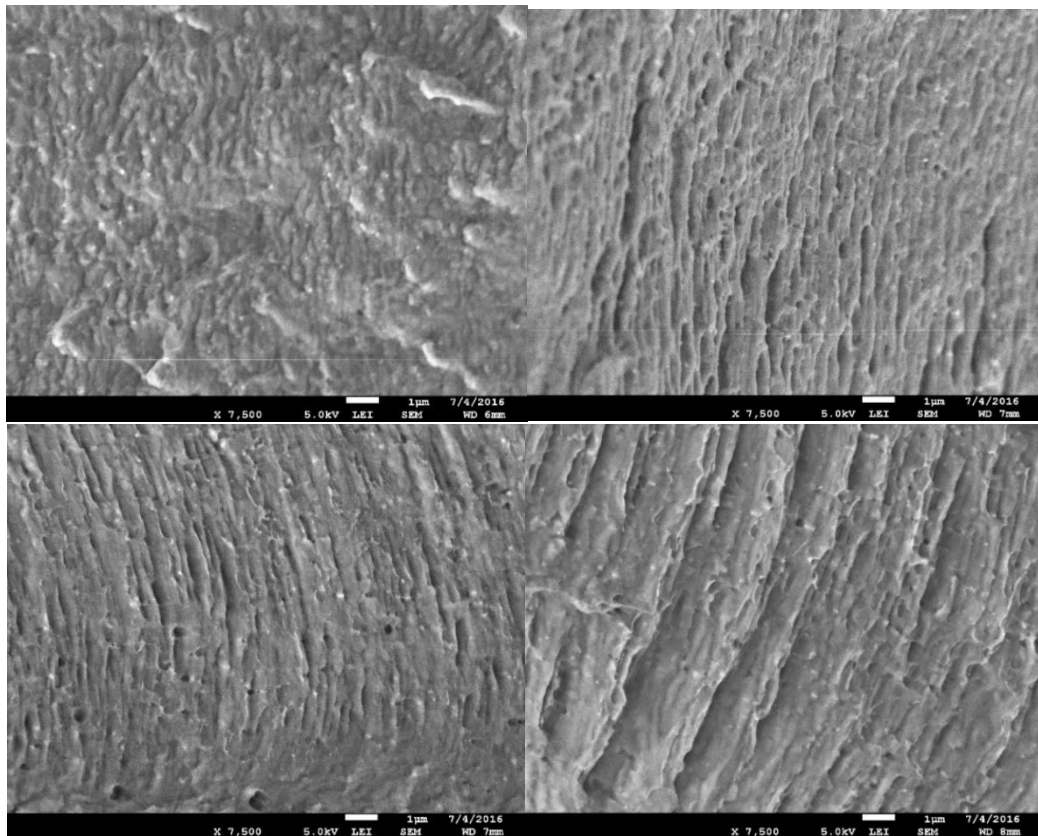*F 18: SEM Photos of Specimen AR05S75. TL: a = 1 mm, TR: a = 11 mm, BL: a = 21 mm , BR: a = 31 mm*
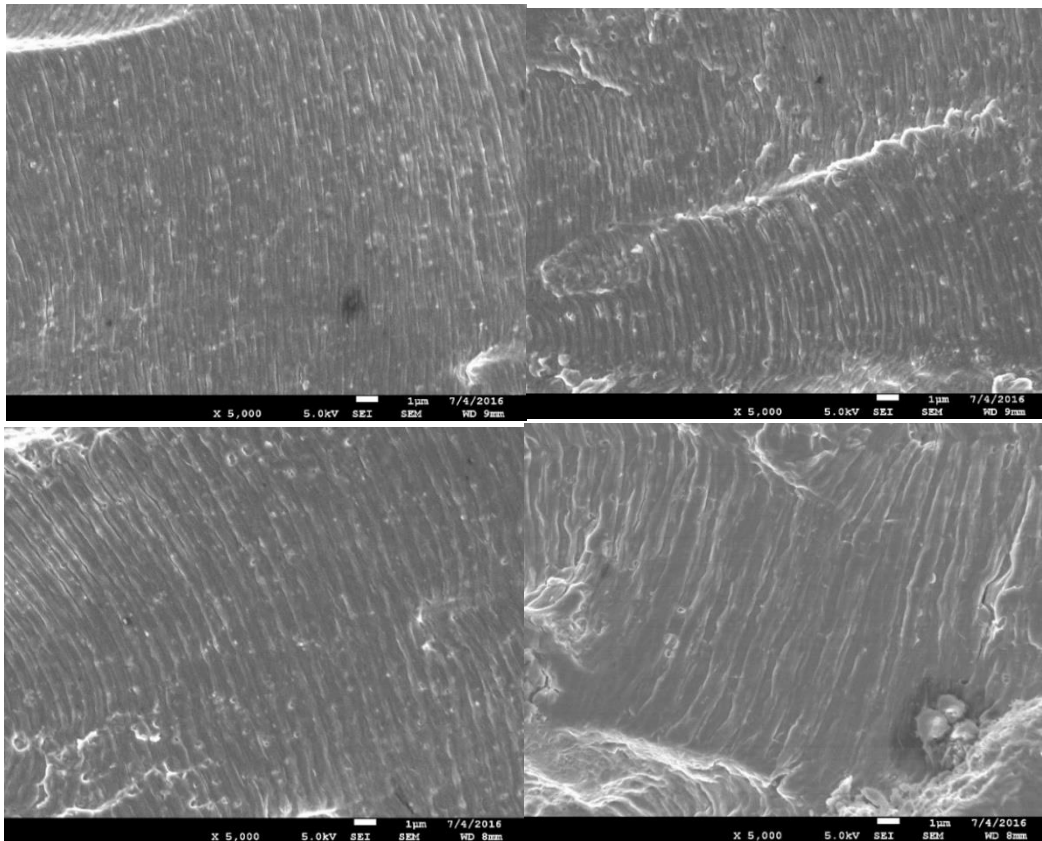
F 19: SEM Photos of Specimen AR005S100. TL: a = 1 mm, TR: a = 11 mm, BL: a = 21 mm , BR: a = 31 mm
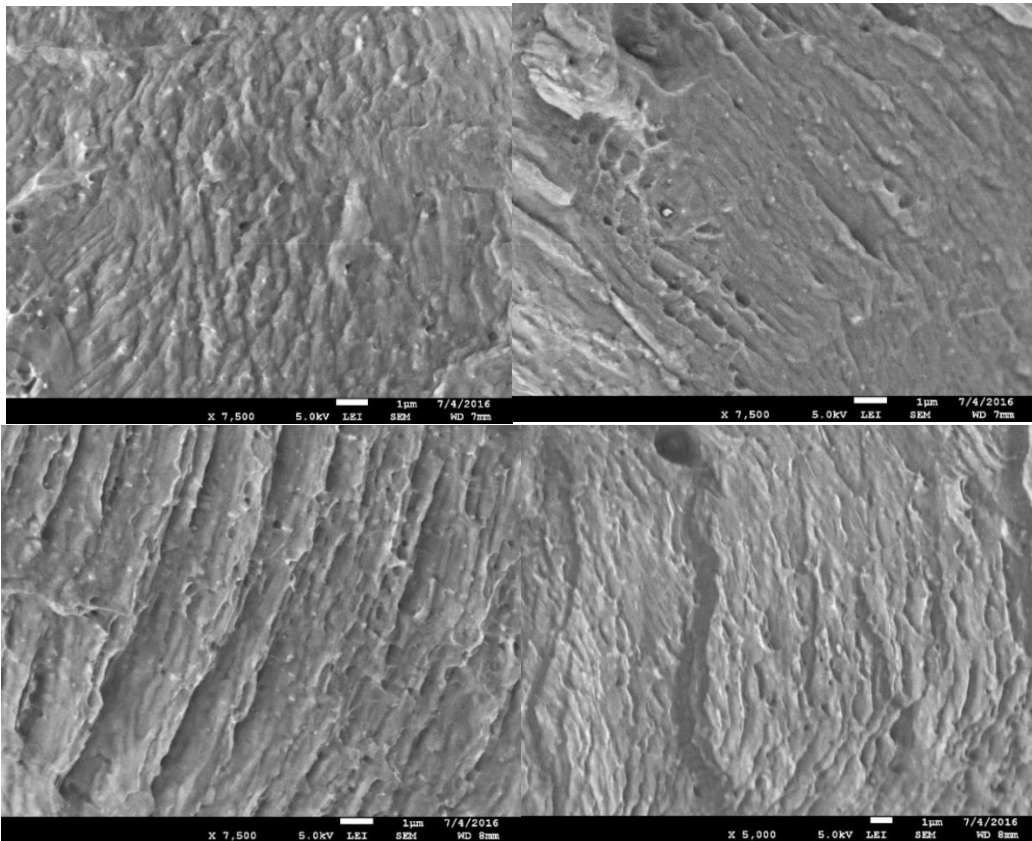
APPENDIX F – Crack Surface Roughness

F 20: SEM Photos of Specimen VR002S75. TL: a = 1 mm, TR: a = 11 mm, BL: a = 21 mm , BR: a = 31 mm

F 21: SEM Photos of Specimen VR005S75. TL: a = 1 mm, TR: a = 11 mm, BL: a = 21 mm , BR: a = 31 mm

APPENDIX F – Crack Surface Roughness

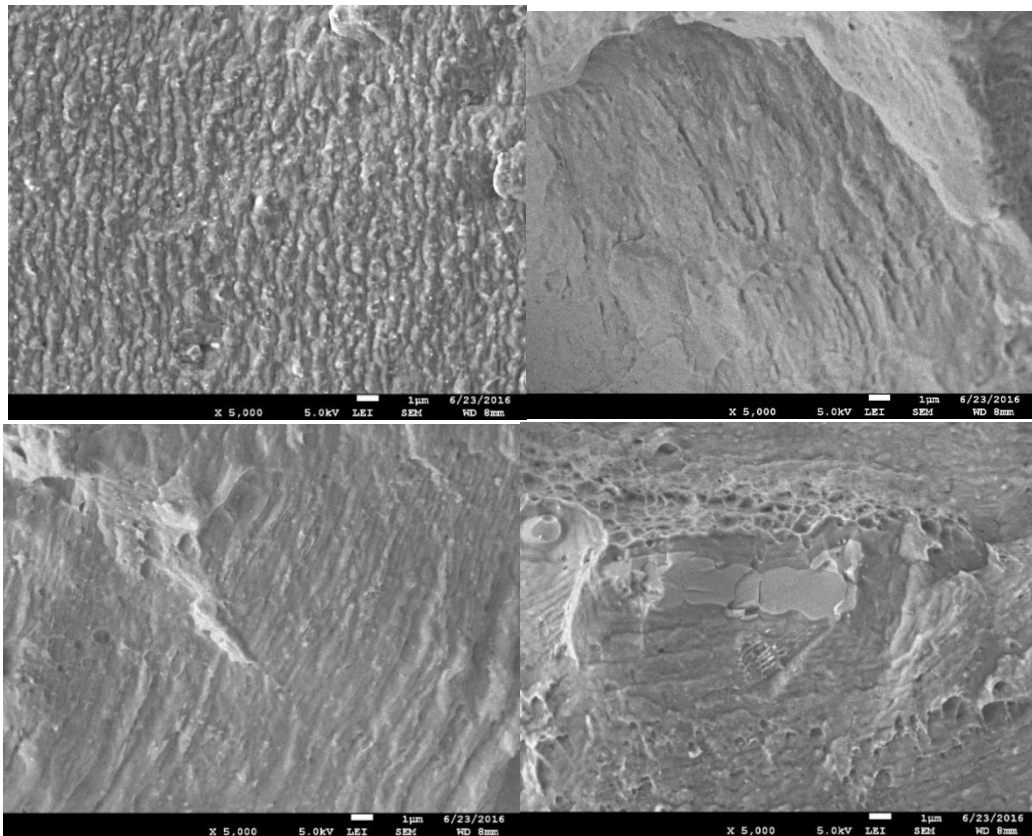*F 22: SEM Photos of Specimen VR01S75. TL: a = 1 mm, TR: a = 11 mm, BL: a = 21 mm , BR: a = 31 mm*

F 23: SEM Photos of Specimen VR03S75. TL: a = 1 mm, TR: a = 11 mm, BL: a = 21 mm , BR: a = 31 mm

APPENDIX F – Crack Surface Roughness

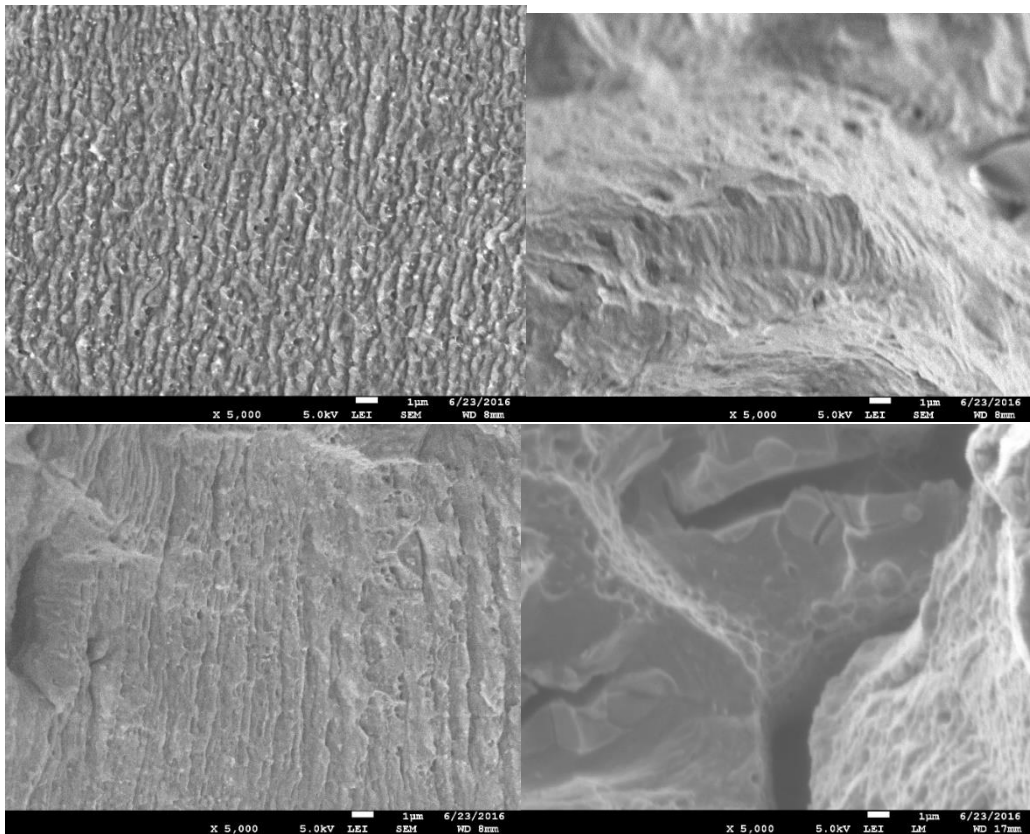*F 24: SEM Photos of Specimen VR05S75. TL: a = 1 mm, TR: a = 11 mm, BL: a = 21 mm , BR: a = 31 mm*

F 25: SEM Photos of Specimen VR005S100. TL: a = 1 mm, TR: a = 11 mm, BL: a = 21 mm , BR: a = 31 mm

APPENDIX F – Crack Surface Roughness

F 26: SEM Photos of Specimen VR03S100. TL: a = 1 mm, TR: a = 11 mm, BL: a = 21 mm , BR: a = 31 mm